2014

A DESIGN PATHFINDER WITH MATERIAL CORRELATION POINTS FOR INFLATABLE SYSTEMS

Jared T. Fulcher
University of Kentucky, jared.fulcher@gmail.com

STUDENT AGREEMENT:

I represent that my thesis or dissertation and abstract are my original work. Proper attribution has been given to all outside sources. I understand that I am solely responsible for obtaining any needed copyright permissions. I have obtained needed written permission statement(s) from the owner(s) of each third-party copyrighted matter to be included in my work, allowing electronic distribution (if such use is not permitted by the fair use doctrine) which will be submitted to UKnowledge as Additional File.

I hereby grant to The University of Kentucky and its agents the irrevocable, non-exclusive, and royalty-free license to archive and make accessible my work in whole or in part in all forms of media, now or hereafter known. I agree that the document mentioned above may be made available immediately for worldwide access unless an embargo applies.

I retain all other ownership rights to the copyright of my work. I also retain the right to use in future works (such as articles or books) all or part of my work. I understand that I am free to register the copyright to my work.

REVIEW, APPROVAL AND ACCEPTANCE

The document mentioned above has been reviewed and accepted by the student's advisor, on behalf of the advisory committee, and by the Director of Graduate Studies (DGS), on behalf of the program; we verify that this is the final, approved version of the student's thesis including all changes required by the advisory committee. The undersigned agree to abide by the statements above.

Jared T. Fulcher, Student

Dr. Suzanne Weaver Smith, Major Professor

Dr. James M. McDonough, Director of Graduate Studies

A DESIGN PATHFINDER WITH MATERIAL CORRELATION POINTS FOR INFLATABLE SYSTEMS

DISSERTATION

A dissertation submitted in partial fulfillment of the requirements for the degree of Doctor of Philosophy in the College of Engineering at the University of Kentucky

By

Jared Terrell Fulcher

Lexington, Kentucky

Co-Directors: Dr. Suzanne Weaver Smith, Professor of Mechanical Engineering

Lexington, Kentucky

and Dr. John R. Baker, Associate Professor of Mechanical Engineering

Paducah, Kentucky

ABSTRACT OF DISSERTATION

A DESIGN PATHFINDER WITH MATERIAL CORRELATION POINTS FOR INFLATABLE SYSTEMS

The incorporation of inflatable structures into aerospace systems can produce significant advantages in stowed volume to mechanical effectiveness and overall weight. Many applications of these ultra-lightweight systems are designed to precisely control internal or external surfaces, or both, to achieve desired performance. The modeling of these structures becomes complex due to the material nonlinearities inherent to the majority of construction materials used in inflatable structures. Furthermore, accurately modeling the response and behavior of the interfacing boundaries that are common to many inflatable systems will lead to better understanding of the entire class of structures. The research presented involved using nonlinear finite element simulations correlated with photogrammetry testing to develop a procedure for defining material properties for commercially available polyurethane-coated woven nylon fabric, which is representative of coated materials that have been proven materials for use in many inflatable systems. Further, the new material model was used to design and develop an inflatable pathfinder system which employs only internal pressure to control an assembly of internal membranes. This canonical inflatable system will be used for exploration and development of general understanding of efficient design methodology and analysis of future systems. Canonical structures are incorporated into the design of the phased pathfinder system to allow for more universal insight. Nonlinear finite element simulations were performed to evaluate the effect of various boundary conditions, loading configurations, and material orientations on the geometric precision of geometries representing typical internal/external surfaces commonly incorporated into inflatable pathfinder system. The response of the inflatable system to possible damage was also studied using nonlinear finite element simulations. Development of a correlated material model for analysis of the inflatable pathfinder system has improved the efficiency of design and analysis techniques of future inflatable structures.

KEYWORDS: Nonlinear Finite Element, Inflatable Structures, Gossamer Space Systems, Photogrammetry Measurements, Coated Woven Fabric

Jared Terrell Fulcher

May 20, 2014

Date

A DESIGN PATHFINDER WITH MATERIAL CORRELATION POINTS FOR INFLATABLE SYSTEMS

By

Jared Terrell Fulcher

Suzanne W. Smith, Ph. D.
Co-Director of Dissertation

John R. Baker, Ph. D.
Co-Director of Dissertation

James M. McDonough, Ph. D.
Director of Graduate Studies

May 20, 2014
Date

This work is dedicated to my father, Terrell Fulcher, who's never wavering support, has allowed me to achieve all that I have achieved; and to the memory of my mother, Donna Fulcher, who taught me to always persevere and to always to do more than what is expected of you.

ACKNOWLEDGMENTS

I would first like to thank my father, who has always supported me, although there were many times were he was worried I would make a career out of just being a student. I would also like to thank the rest of family for all their kind words and encouragement over the last 5 years.

I would like to express my deepest gratitude and respect to my academic advisors Dr. Suzanne Weaver Smith and Dr. John Baker, both of which provided unwavering support and invaluable advice through my graduate academic career. I would like to thank the NASA KY Space Grant Program for providing funding for portions of this work. I would also like to thank the UK Mechanical Engineering Department for providing teaching assistantships throughout my time as a PhD student.

Lastly, I would like to thank the graduate and undergraduate students that I have had the fortune of working with through my time at UK. More importantly, for providing opportunities to play games of skill and analyze the flight dynamics of hand-launched unmanned rotating vehicles to alleviate the stress that is an inherent part of being a graduate student.

TABLE OF CONTENTS

LIST OF TABLES

LIST OF FIGURES

NOMENCLATURE

E_f = elastic modulus in the fill direction, in units of MPa

E_w = elastic modulus in the warp direction, in units of MPa

E_x = modulus found from bias extension tests, in units of MPa

F = magnitude of bi-axial force, in units of N

F_x = x-component of bi-axial force, in units of N

F_y = y-component of bi-axial force, in units of N

G_{wf} = shear modulus in the warp-fill plane, in units of MPa

MAC = modal assurance criterion

n = total number of nodal displacements

t = thickness of nylon fabric

z_{avg} = average displacement for an entire test article, in units of mm

z_i = specific nodal displacement, in units of mm

z_{ij} = nodal displacement with respect to XY, XZ, or YZ plane, in units of mm

Z_{RMS} = root mean square displacement for a test article, in units of mm

v_{wf} = Poisson's ratio

ρ = material density, in units of kg/m^3

CHAPTER ONE INTRODUCTION

1.1 MOTIVATION

Inflatable structures have been increasingly integrated into many aerospace systems over the last half century from the historic Echo balloons (Figure 1.1a) to the more complex Inflatable Antenna Experiment (IAE) (Figure 1.1b). As these structures have evolved, so have their level of complexity. Many applications that use inflatable structures require precise control on internal and external surfaces, such as inflatable antenna, inflatable wings, solar sails (Figure 1.1c), and inflatable radar reflectors. Most inflatable structures are comprised of internal surfaces and pressurized external surfaces. The boundaries and interactions between the internal structures and the external surfaces can be difficult to model. The aim of the current work was defining and resolving challenges in modeling these modern inflatable structures that require high precision internal and/or external surfaces.

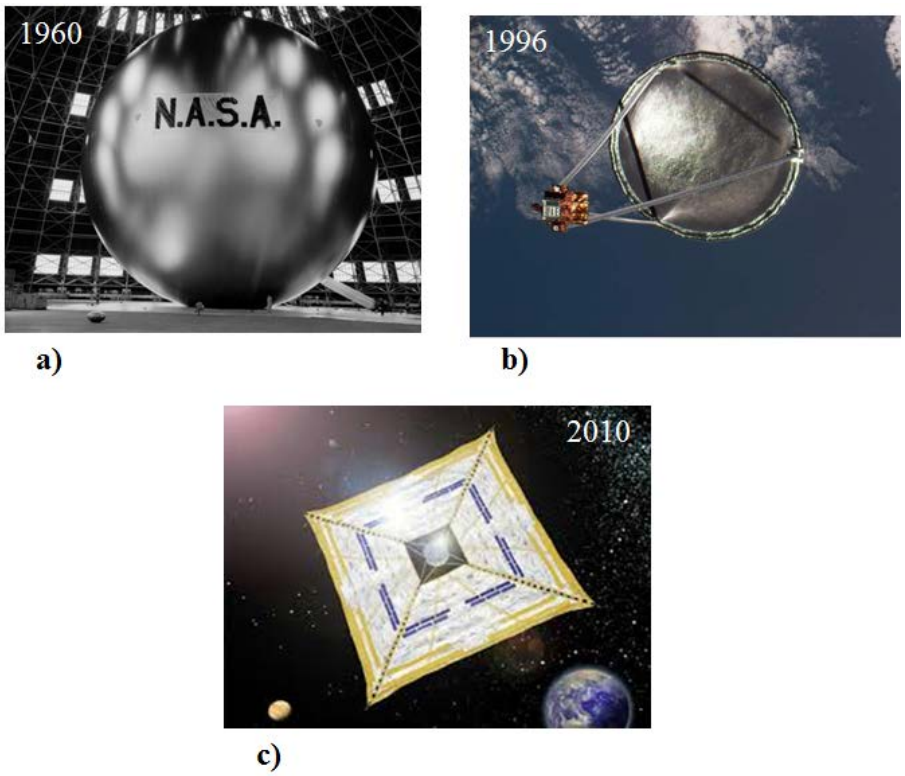

Figure 1.1. a) Echo 1 balloon radar reflector lauched in 1960 (image courtesy of NASA). b) Deployed IAE antenna by L'Grade launched 1996 (image courtesy of NASA). c) Image of JAXA's IKAROS launched 2010.

A majority of inflatable systems are constructed with soft flexible materials, such as coated fabrics. Modeling these inflatable structures presents several problems due to their typically nonlinear macro material properties. Furthermore, some distinct material properties vary with the inflated pressure and the structural geometry of the inflatable. Experimentally determining these properties can be complicated and costly. Research on techniques for the materials common to inflatable systems is advantageous in model verification and design of new inflatable structures.

Accurately modeling canonical geometries that represent the basic structures seen in inflatable systems can lead to a better understanding of the behavior of the entire class of inflatable structures. Furthermore, key factors in designing inflatable structures to control precision surfaces (internal and/or external) can be determined. An advantage of focusing on the canonical geometries is that analytical solutions exist for many of the crucial geometric controls (e.g. flatness). Developing accurate modeling procedures for inflatable structures that require precision surfaces will be predicated on the development of the canonical models proposed in this project.

1.2 OBJECTIVES OF DISSERTATION

Through analyzing canonical geometries with various boundary conditions, loadings, and nonlinear material properties, common to inflatable structures, an understanding of the design factors involved with precisely controlling the geometric surfaces of inflatable systems will be gained. Designing new inflatable systems will be predicated on developing models of structures that comprise inflatable systems. The proposed efforts are an important foundation for future designs.

The current research involved:

1. Developing an understanding of the material behavior of a high-performance coated woven nylon fabric.
    a. Correlate experimental static responses of the coated nylon fabric with non-linear finite element analyses.
    b. Design and develop a test rig for pre-tensioned fabric testing using precision photogrammetry techniques to increase accuracy of measured deflections.

c. Quickly and accurately determine material properties to use in the FE model.

2. Create accurate finite element (FE) models of an inflatable pathfinder system using canonical structures.
    a. Evaluate the effect of boundary conditions, loading, and material properties on geometric controls (i.e. flatness).
    b. Analyze the static response of the inflatable system.
    c. Design the pathfinder system to meet or exceed performance requirements related to radar reflectors and radar decoys.

The inflatable pathfinder system employs only internal pressure to control an assembly of internal membranes. The proposed inflatable system was design to be used as a radar reflector or radar decoy; however the geometries and interfaces considered are universal to the entire class of inflatable structures. This canonical inflatable system will be used as a phased pathfinder system for exploration and development of general understanding of efficient design methodology and analysis of future systems. Canonical structures are incorporated into the design of the phased pathfinder system to allow for more universal insight. Figure 1.2 is a model of the proposed inflatable pathfinder system.

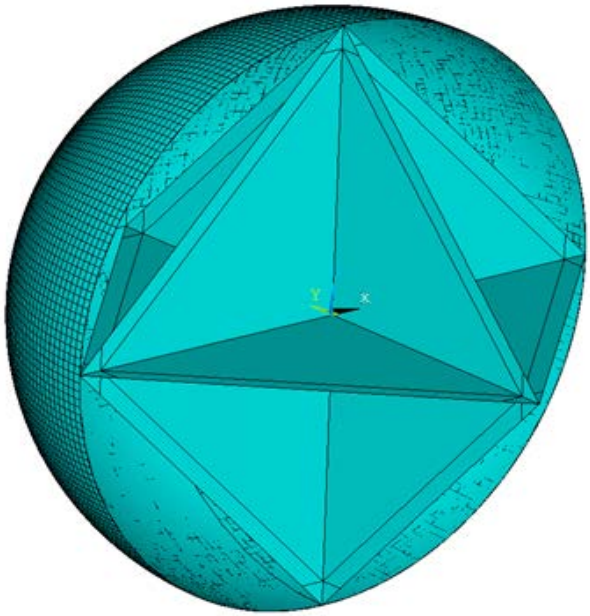

Figure 1.2. Model of inflatable pathfinder system.

A phased approach was taken to the design of the new inflatable system. Figure 1.3 is the development layout for the research conducted in this dissertation. Simulations were performed to establish relationships between specific material properties, the system design (boundary conditions), and the level of geometric precision (i.e. flatness) that can be obtained using the chosen fabric and geometries. Sub-assemblies of the internal membranes of the pathfinder system were studied using nonlinear FE analysis to define the best design. Based upon the analysis of the sub-assemblies, the final iteration of the inflatable pathfinder system was analyzed to compare its performance capabilities with required capabilities of a radar reflector or radar decoy. The final objective of the current work was to determine the effect of damage on the performance of the inflatable pathfinder system. Performance standards for radar reflectors and radar decoys were compared with the static response of the inflatable pathfinder system.

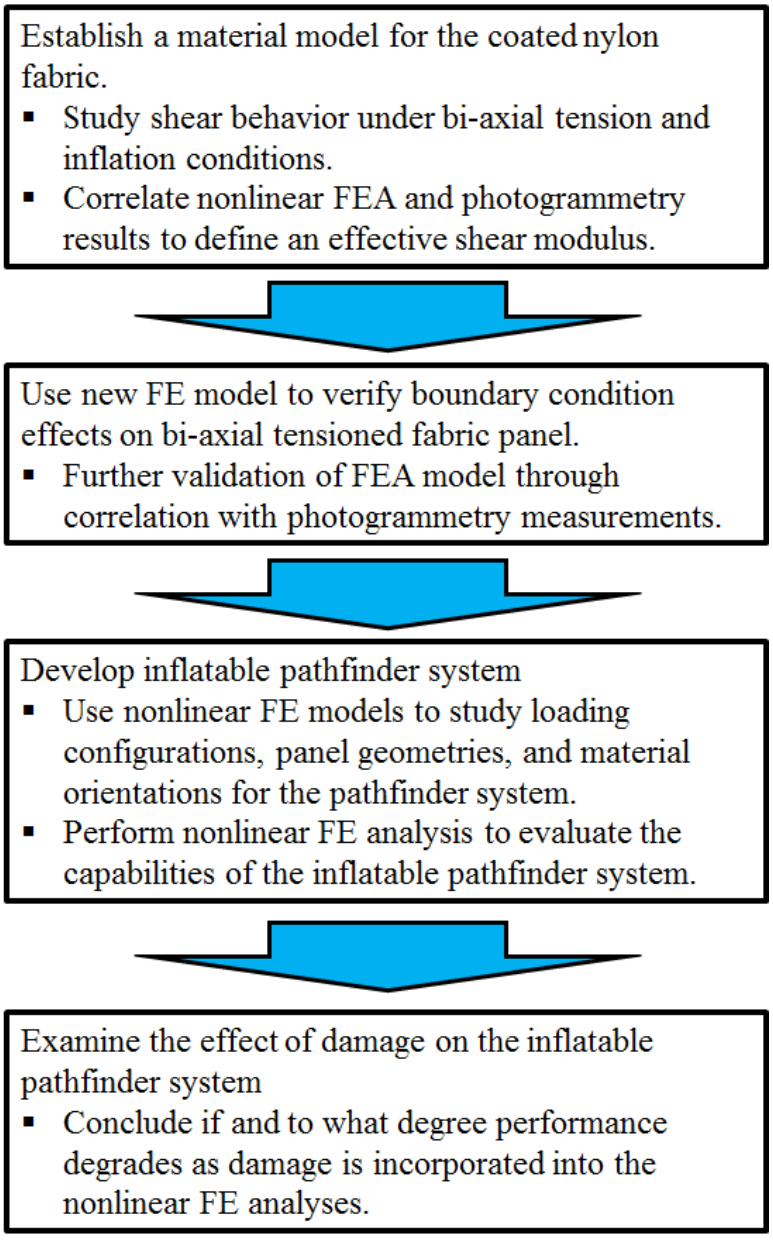

Figure 1.3. Development layout of design and analysis of inflatable pathfinder system.

1.3 ORGANIZATION OF DISSERTATION

Chapter 2 of this dissertation is the review of literatures concerning development of inflatables and modeling the materials used in the construction of inflatable systems. Chapter 3 presents the study of the polyurethane-coated woven nylon fabric under bi-axial tension. This chapter also introduces the shear study for the nylon fabric, and the

final comparison between FE simulations and photogrammetry measurements of static deflections for twelve test cases. Chapter 4 includes the design and development of the test rig for the inflation testing of coated nylon fabric. The techniques for the photogrammetry testing with the inflation chamber are covered, and correlation with FE simulations is also presented. Chapter 5 covers the design and analysis of the inflatable pathfinder system. Chapter 6 presents the analysis of the thread loss study. Conclusions and future works are included in Chapter 7.

CHAPTER TWO REVIEW OF LITERATURE

2.1 INTRODUCTION

Developing ultra-lightweight, deployable, and adaptive systems has become a trend in aerospace and aeronautics over the last two decades. The incorporation of inflatable structures can produce significant advantages in stowed volume and overall weight for many aeronautic and aerospace systems [1-6]. Most inflatable systems are designed to precisely control both internal and external surfaces to achieve a desired response or structure. The static and dynamic structure of inflatable systems is directly related to the geometry, loading, and material of the system [7-12].

Precision inflatables belong to a class of structures referred to as tensile structures. A tensile structure is a membrane-like structure that uses tensile pre-stress to carry externally applied loads. Figure 2.1 is a diagram detailing the classification of tensile structures based upon the mechanism used to produce the pre-tension state. The nature of tensile structures allows for an increase in mechanical packaging efficiency, deployment capability and reliability, small stowed volume, and low weight [7, 8, 13, 14]. Due to these advantages, inflatable structures are ideal candidates for a multitude of engineering applications which are designed to be adaptive and mobile. Inflatable structures in engineering include many structural elements (airbeams), aeronautical systems (inflatable wings and unmanned aerial vehicles), and aerospace systems (antenna, radar reflectors, and solar sails).

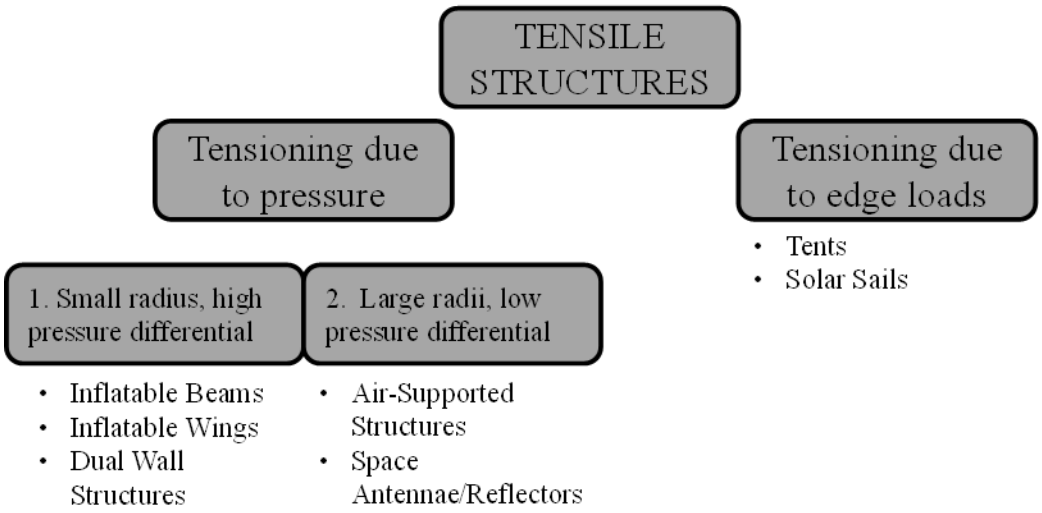

Figure 2.1. Diagram of tensile structures.

2.2 INFLATABLES AS STRUCTURAL ELEMENTS

Over the last four decades air-inflated elements have been used to develop lightweight and deployable structures such as temporary shelters, tents, and temporary bridges. The load bearing members of these structures consist of pressurized fabric tubes, known as airbeams [15, 16]. An over-pressurization is used create stability in these membrane structures [13]. Figure 2.2 shows diagrams of arrangements of membrane structures that have been used to construct various airbeam systems.

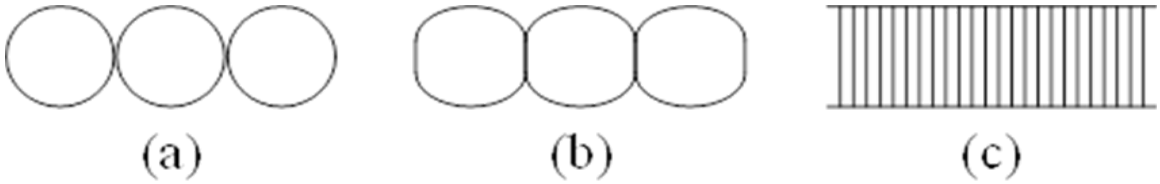

Figure 2.2. (a) Tubular frame arrangement. (b) Dual wall construction. (c) Drop thread construction.

Complex precision inflatable use airbeams are crucial structural elements, thus a large amount of work has been done to develop methodologies to design and analyze airbeams. Thomas and Wielgosz, 2004, developed new deflection equations for overinflated airbeams based upon Timoshenko beam theory. Equilibrium equations were derived from the deformed state as to consider the geometrical stiffness and following forces. A new inflated-beam theory was established that introduces deflection equations for a cantilevered airbeam. Further work was performed to develop an inflated beam finite element. The new finite element considers the non-symmetric compliance matrix. Excellent agreement was seen between the experimental, analytical, and numerical results found by Thomas and Wielgosz [14].

Veldman, 2005, further developed the methodologies for airbeams examining the relationship between geometry, loading, and construction material. Three geometrically identical airbeams constructed of three different materials were tested under large deflection conditions and it was seen that the construction material affects the deflection behavior by altering the load level at which wrinkling occurs. The airbeams were constructed of PolyCarbonate (PC), PolyPhenyleneSulphide (PPS), and PolyEtherImide (PEI), all of which possess linear isotropic material properties. Further work was done to analyze conical beams and an assemblage of three straight beams. Finite element results

were correlated with experimental and analytical results. A FE model for the PPS was created using shell elements and solved using the commercial FEA code ABAQUS. It was seen that agreement was achieved within the linear regime (small deflections), but within the nonlinear regime (large deflection) the finite element modeling overestimated the deflection of both the conical beams and three straight beam assembly [8].

2.3 DEVELOPMENT OF INFLATABLES IN AERONAUTICS

The hot air balloon was the first inflatable structure to be used for manned flight in France during the 1780's. The Mongolfier brothers were the first to take flight with a hot air balloon in 1783. Shortly after that initial flight, Charles (another French balloonist) flew with a hydrogen filled balloon. The hydrogen filled balloon was the precursor to modern airships or blimps [13]. The airship boom ended with the tragedy of the Hindenburg in Lakeburst in 1937. In the mid 1990's interest in airship development began to rise again in Germany and the Netherlands. There are several applications that include advertising, surveillance, transporting heavy loads, and as platforms for high altitude communications [8].

Tensile structures were crucial elements in the first generation of aircraft developed in the early twentieth century. Fabrics were used to create the control surfaces on the wings of the early airplanes. The fabric was stretched across a various numbers of ribs along the wing span. The pre-tension in the fabric was used to resist the aerodynamic loading [17, 18]. Tailoring the material properties of these fabrics was also researched by applying different types and different amounts of coatings [19]. Many of the problems associated with using soft materials in modern applications were defined in some sense during this era. The engineers used rudimentary techniques to simulate the aerodynamic loading and to measure the pre-tension in the fabric membranes. Although they were not inflatable structures, some of the dynamics and nonlinearities studied in early work on fabric wings are relevant to the study of current inflatable structures.

One of the first fully integrated inflatable systems in aeronautics was the Goodyear Inflatoplane constructed in 1956. Testing of the Inflatoplane was carried out for nearly two decades, which lead to the Goodyear Inflatoplane being one of the most successfully developed inflatable aircraft. The plane was developed to be dropped behind enemy lines to downed pilots. The plane could fit into a single container because

both the fuselage and wings were inflatable. However, the landing gear and engine were made from rigid parts. Once deployed, the downed pilot would simply fly the plane out of enemy territory [4, 8, 11, 20]. Figure 2.3 shows a picture of the Goodyear Inflatoplane.

Figure 2.3. Goodyear GA-468 Inflatoplane.

On the success of the Goodyear Inflatoplane, inflatable wings began to be adapted to unmanned air vehicles during the 1970's, with the Apteron developed by ILC Dover (Figure 2.4). The Apteron was flown successfully in testing, but was never put in full production [20, 21].

Figure 2.4. ILC Dover Apteron unmanned air vehicle.

The inflatable wings were seen to actually improve vehicle strength and combat survivability. Also, the inflatable wing allows the UAV to become much more mobile because of the low stowed volume [4, 5, 20-23]. Figure 2.5 shows images of an UAV equipped with inflatable wings. From the figure the difference in volume from the

stowed to the deployed configuration is apparent. Also inflatable wings are dual-wall structures (Figure 2.2) that use the internal pressure to create the desired airfoil shape. Figure 2.6 displays the combination of internal and external surfaces used to create the control surface for the wing when pressurized.

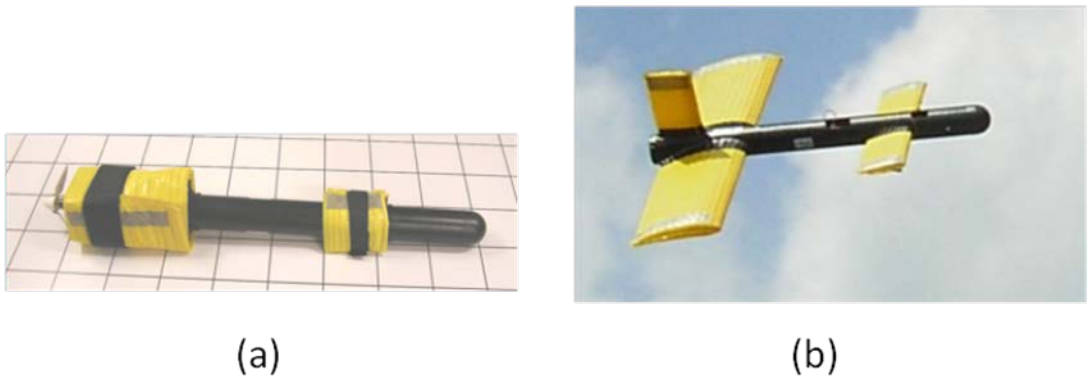

Figure 2.5. (a) Picture of a UAV equipped with an inflatable wing in the stowed configuration. (b) Picture of a UAV equipped with an inflatable wing in the deployed configuration

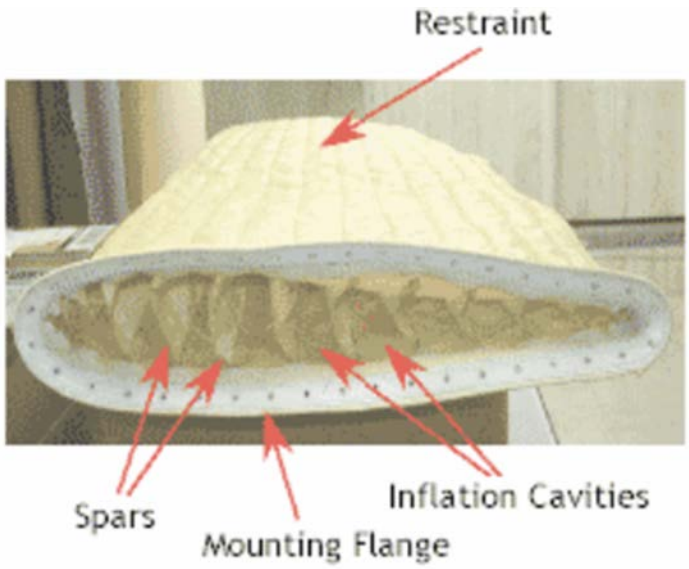

Figure 2.6. Cross section view of inflatable wing with internal spars in the span-wise direction.

In the early 2000's, inflatable/rigidizable wings were the subject of high altitude deployment demonstrations. These classes of inflatable wings use an initial internal pressure to create the airfoil that is fixed by the curing of an epoxy coating that is rigid once exposed to sunlight [24-26]. Inflatable/rigidizable wings have been used in the

development for UAV for high-altitude low-density flight. These UAVs are a possible exploratory vehicle for Mars [27-29]. Upon the success of the rigidizable wing, a purely inflatable wing was desired to further improve the stowed volume, weight, and adaptability. With a purely inflatable wing, wing warping could be used to manipulate the control surfaces of the aircraft. Wing warping would require less power and equipment to activate the control surfaces. Furthermore, wing construction would be simplified and become more robust [20-23].

2.4 INFLATABLES IN SPACE: GOSSAMER SPACECRAFT

Along with applications in aeronautics, high precision inflatable systems have been developed for space applications. Due to the advantages of low stowed volume inflatable structures are a natural selection for space systems that require a significant deployed area. These classes of space structures are referred to as gossamer spacecraft, and include radar reflectors, antennas, solar arrays, and solar sails [1-3, 6, 11, 30-32]. Inflatable structures are often designed to be support structures for the thin precision membranes incorporated in the gossamer systems. The NASA Echo 1 balloon (Figure 2.7), launched August 12, 1960, and was the first generation of these inflatables. The Echo 1 balloon was designed to be a perfectly shaped sphere for radar and antenna calibration. Aluminum was used as the membrane material and the initial inflation pressure was used to plastically deflect the aluminum into the spherical shape. With the

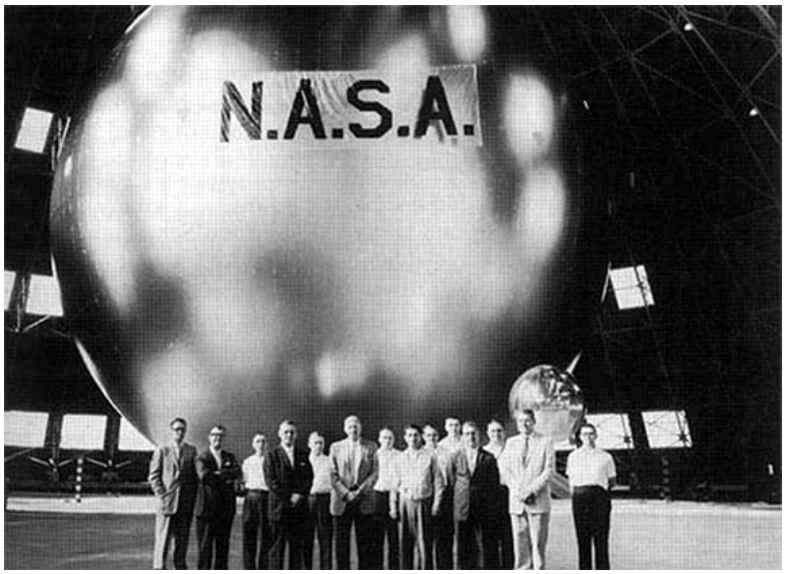

Figure 2.7. NASA Echo 1 Balloon (image courtesy of NASA).

rigidizable design, continuous internal pressure was not needed [1, 3, 11].

The next advancement in gossamer spacecraft was L'Grade's Inflatable Antenna Experiment (IAE) commissioned by NASA. The IAE designed and built an antenna that utilized a combination of several inflatable elements to support a 0.01-inch aluminized Mylar membrane. The antenna was designed to have a surface accuracy of 0.04-inch RMS in comparison to the proposed shape [9, 11]. The IAE was launched in May of 1996. An image of the deployment of the IAE can be seen in Figure 2.8. The deployed antenna had a surface accuracy of 0.08-inch RMS which did not meet the original design goal [33]. However, the experiment demonstrated the robustness of inflatable structures, in addition to showing that inflatable structures were capable of achieving a high level of geometric control.

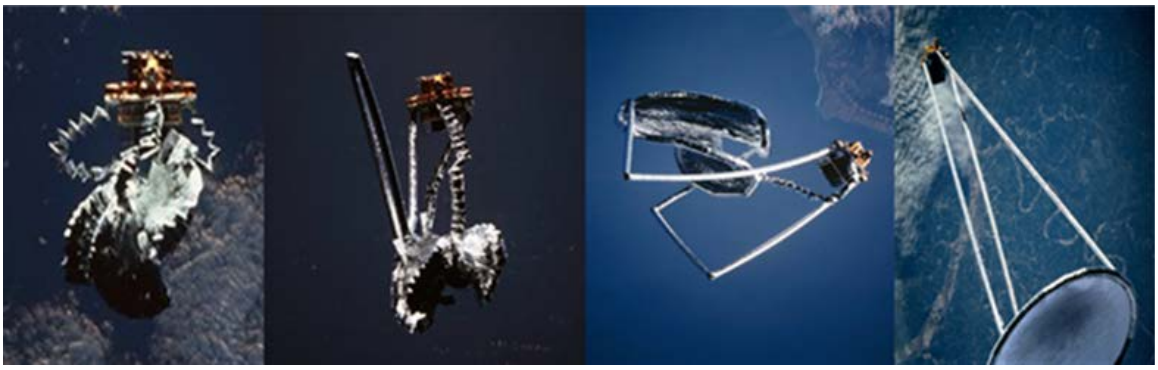

Figure 2.8. Deployment of the IAE (image courtesy of NASA).

Another type of gossamer structures that use inflatable structures to achieve precise geometric control are solar sails. Solar sails are large light-weight structures that provide propulsion through momentum produced by the reflection of photons. Figure 2.9 shows images of L'Garde's development of the Sunjammer solar sail and the Japan aerospace exploration agency's (JAXA) interplanetary kite-craft accelerated by radiation of the Sun (IKAROS), launched May 21, 2010 [34, 35].

Figure 2.9. Left, image of L'Garde's Sunjammer. Right, image of JAXA's IKAROS.

Since the propulsion is proportional to the reflection capability of the sail, the flatness of the sail material is significant [10, 12, 31, 36-40]. Significant work has been done to measure the flatness of the solar sail membrane materials. Photogrammetry and videogrammetry techniques have been used to measure the level of achievable geometric control on the membrane structures. Photogrammetry and videogrammetry are non-contact methods of measuring deflections. Non-contact methods of measurement are preferred in this approach due to the thickness of materials used in solar sails [11, 41-43]. Photogrammetric techniques were used to develop 3-D static response models of the polyurethane-coated nylon under bi-axial tension and inflation.

Another area where inflatable structures have been successfully integrated is in radio frequency (RF) decoys or radar reflectors (Figure 2.10). The first RF decoys were deployable, but were large, rigid, and difficult to build and deploy. Based upon the limitations of the early structural decoys work was done to develop an inflatable RF

Figure 2.10. Images of current inflatable radar reflectors.

decoy. The new inflatable decoy was rapidly deployable, but required complex inflatable structures to adhere to the geometrical precision needed to maintain the needed level of RF performance [44].

In summary, inflatable structures in aeronautics and aerospace require precision geometric surfaces. Inflatable elements are used to tension internal and/or external surfaces to create a desired shape. Table 2.1 presents expected or achieved levels of geometric control for engineered shapes in gossamer structures. For terrestrial radar decoy applications, a flatness of a half wavelength is required for acceptable performance [11]. Terrestrial radar decoys operate in a frequency range of 10 GHz to 40 GHz, so at 40 GHz a half wavelength measures 3.75 mm. For space-based radar reflectors a 2dB loss in transmission is considered to be a practical performance requirement [45]. Thus at an operating frequency of 20 GHz, a RMS deflection of 0.58 mm is required for acceptable performance.

Table 2.1. Summary of expected or achieved surface accuracies for various inflatable systems.

Inflatable System	Geometric Control	Operating Frequency	Expected or Achieved Performance
Terrestrial Radar Reflector [44]	Surface RMS	10 GHz – 40 GHz	Flat within a 0.5 wavelength: 15 mm - 3.75 mm RMS
Space-Based Reflector [45, 46]	Surface RMS	20 GHz – 40 GHz	0.58 mm – 0.17 mm RMS
Antenna [45]	Shape RMS		0.67 mm – 1.3 mm RMS from ideal parabolic shape

2.5 INFLATABLE SYSTEMS: MATERIAL TESTING

The material behavior of the soft materials used in inflatable systems is difficult to model accurately due to material nonlinearities caused by the material's microstructure. Woven fabrics have become the predominant material of choice in inflatable structures. Current woven fabrics used in inflatables are made out of nylon, polyester, glass, or aramid fibers. For many inflatable applications, these woven fabrics

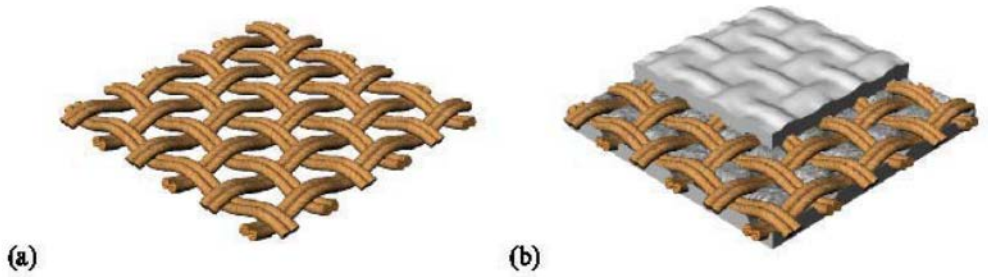

Figure 2.11. (a) Plain woven fabric. (b) Coated woven fabric.

are coated with a polyvinyl, polyurethane, or silicone coating [7]. Figure 2.11 shows a representation of both a plain woven fabric and a plain woven fabric with coating [47].

Plain woven fabrics are usually constructed with two material directions: warp and fill (weft). Each direction corresponds to a yarn and how these yarns overlap define the style of fabric (i.e. woven or braided). Yarn interaction causes the material properties to become functions of orientation and loading of yarns. A significant amount of work has been devoted to define the dependency of material properties to specific loadings. Nonlinearities in the material are caused by the interaction of the yarns in the fabric [48-50]. Shear behavior of the fabrics seems to be more complicated than extension deformation of fabrics [51-56].

Shearing is the main mode of deformation when the fabric is tensioned. Pre-tension of fabric used in tensile structures was of concern in early testing of fabrics [17-19]. Many styles of testing have been developed to accurately measure the mechanical properties of woven fabrics. The warp and fill modulus of woven fabric are traditionally found using bi-axial extension, however, uni-axial tests have been used to measure the moduli of woven fabrics [4, 57-59].

Experimentally determining the shear modulus for woven fabric poses several issues due to its dependence of yarn orientation and loading. Picture frame testing is the accepted method for measuring the shear modulus of woven fabrics. The picture frame test has the fabric in a pre-tensioned condition and measurements are taking of the shear force and the shear angle [60-62]. Galliot and Luchsinger, 2010 presents a review of current technology shear testing for fabrics which include picture frame testing, bi-axial extension, KES-F tester, fabric cylinder shear, T-shaped specimen in bi-axial tension, and bias testing[63]. The advantages and limitations of each type of testing are discussed as

Galliot and Luchsinger develop a new shear testing method using bi-axial extension. The loading is linearly ramped along each edge of the test specimen [63, 64].

Work was performed by Skelton and Freeston, 1971, using the fabric cylinder to explore the shear deformation of plain woven fabric and coated woven fabric. The fabric cylinder shear test is a torsion test that applies torque to an inflatable cylinder, so various inflation pressures and bi-axial loading situations can be applied. The fabric cylinder has become a standard test for experimentally determining the shear properties for inflatables [16, 22, 23]. Skelton and Freeston concluded that the shear deformation depends more on the shear stiffness of the coating material than the properties of the yarns in the fabric [65]. A disadvantage of the fabric cylinder test is the complexity of the testing frame and the requirement for inflation.

2.6 INFLATABLE SYSTEMS: MATERIAL MODELING

Finite element modeling and other numerical analysis of fabrics have used numerous material models. Material models for fabrics used in inflatable systems become complicated due to the dependency on system parameters (i.e. geometry, inflated pressure, and boundary conditions) [15, 16, 22, 23, 66]. Most commonly a "unit cell" approach is applied for plain woven fabrics. These "unit cell" models are defined using many properties that are related to the interaction between the yarns of the fabric [67-70]. The "unit cell" method develops a constitutive law based upon the micro-mechanical behavior of the woven fabric.

Modeling of thin membranes has been increasingly studied in the last decade, with most of the work being done with materials used in solar sails. Significant work has been done in modeling these solar sail materials using finite element software [10, 12, 36-40]. Several key elements for deflection reduction in thin membranes have been developed from these works, one being shear compliant borders [37, 39]. Shear compliant boarders are one of several design parameters that were studied in this project. The material used in most solar sail applications is isotropic, but the material nonlinearities associated with woven fabrics are not. Solar sail geometry can be modeled using membrane theory.

Membrane models are used when bending deformation is not significant in the material behavior. Work has been done to model coated fabrics using membrane theory

[45, 71-74]. Many surfaces in inflatable surfaces can be modeled as membranes. Solar sails, radar reflectors, solar arrays, and antennas require some surfaces to be tensioned so that a high level of flatness is achieved. These elements can be treated as membranes due to the lack of bending deformation. Kyriacou et. al, 1996 and Manach and Rio, 1999 modeled membranes with orthotropic properties. Kyriacou et. al, 1996, created a constitutive model for orthotropic membranes and successfully created a nonlinear finite element code using MATLAB. The new FE code was validated with analytical solution for problems concerning inflation and extension of a long cylinder, biaxial stretching of a rectangular membrane, and inflation of a rectangular membrane [72].

More general techniques for finite element modeling used mainly isotropic material prosperities. Rowe, 2007 performed finite element analysis on inflatable wings at the University of Kentucky. Shell elements and the commercial FEA software ANSYS were used to perform deflection and torsion analyses. Rowe used a 4-node Shell181 element to perform all analyses. Large deflection analysis was performed for both wing tip deflection and torsional deflection. The finite element results were compared to experimental data. Isotropic, orthotropic, and hyperelastic material models were used during the testing. Complications with modeling the material nonlinearities became apparent when the orthotropic and hyperelastic models would not converge. The material Rowe modeled was Vectran and to assure computational convergence the experimentally determined material properties were altered. The shear modulus was reduced to 15% of the warp modulus and for correlation with the experimental testing the warp modulus had to be reduced to 8% of the original modulus. Conclusions were drawn that the FE model was ultimately too stiff. When the warp modulus and shear modulus were reduced, good agreement was found between the FE and experimental results [22, 23].

CHAPTER THREE STATIC RESPONSE OF BI-AXIAL TENSIONED NYLON TRIANGLE SPECIMEN

3.1 PHOTOGRAMMETRY TESTING OF NYLON SPECIMEN

Photogrammetry has been successfully used as a non-contact method of measuring deflections of inflatables and thin membrane materials [11, 36, 41, 74]. Photogrammetry uses triangulation between multiple still images to produce a 3D model of specific points. Scherrer, 2012 used photogrammetry to measure deflections of a thin triangular article of the polyurethane-coated nylon fabric. The aim of the work done by Scherrer was to determine the significant system parameters that would maximize the geometric control (flatness) on the nylon fabric.

In total twelve experiments were performed with various material orientations, loadings, and boundary conditions. The legs of the nylon triangle measured 228.6 mm, with a hypotenuse of 304.8 mm, and a thickness of 0.3 mm. Approximately 170 circular targets were placed on each triangular specimen. PhotoModeler 6 software was used to perform the photogrammetry analysis for each triangular test article. Figure 3.1 shows the experimental setup of the bi-axial tensioned fabric triangle used in Scherrer,

Figure 3.1. Experimental set up for photogrammetry experiments measuring static deflection of coated nylon fabric.

2012.

Bi-axial loading was applied to avoid buckling in the thin nylon fabric. Two magnitudes were considered in the work done by Scherrer, 2012. Figure 3.2 is a diagram of the loading configuration applied to the fabric triangle. Table 3.1 shows the component form of the bi-axial tension and the magnitude of the tension used to test the triangular specimen. The next test variable was material orientation, and for a plain woven fabric there a two main material directions; warp and fill. Two orientations were considered in Scherrer, 2012 and a diagram of the material orientations is shown in Figure 3.3.

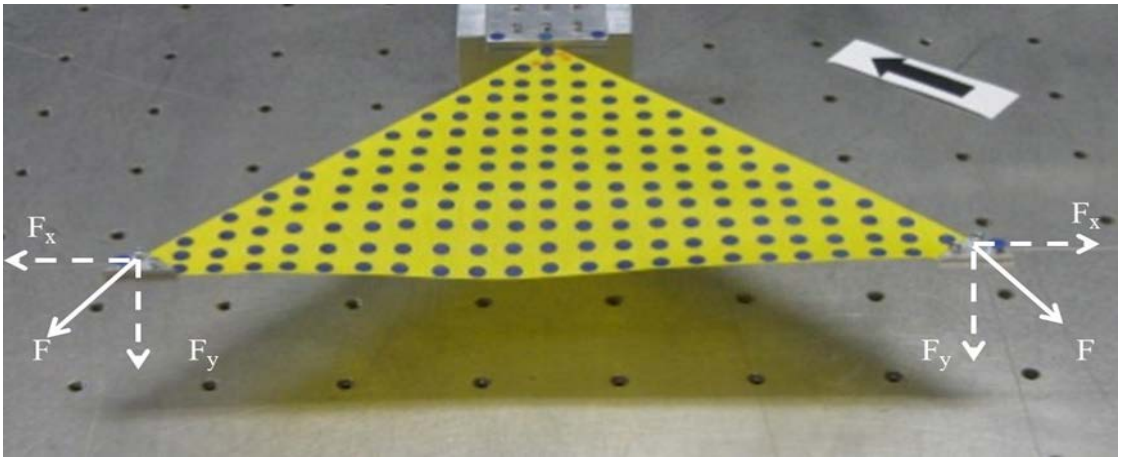

Figure 3.2. Loading diagram for photogrammetry experiments studied in Scherrer, 2012.

Table 3.1. Bi-axial tension by component and resultant magnitude.

	Load Level 1	Load Level 2
F_x, N	3.025	4.359
F_y, N	1.797	1.423
F, N	**3.519**	**4.586**

In Figure 3.4 the clamp to the left is the standard clamp or "triangle" clamp. This clamp was designed to apply a uniform force along both legs of the triangle. The legs of the clamp measured 19 mm and the hypotenuse was 26.9 mm. The shear compliant clamp is shown in the center picture of Figure 3.4. The clamp was designed to reduce the amount of shear stress transferred into the test specimen. The final clamp analyzed was the V-clamp, shown in Figure 3.4. Unlike both the standard and shear compliant clamps,

the V-clamp was designed to only apply forces to the edges of the fabric. A summary table of all the photogrammetry experiments performed in Scherrer, 2012 is given in Table 3.2.

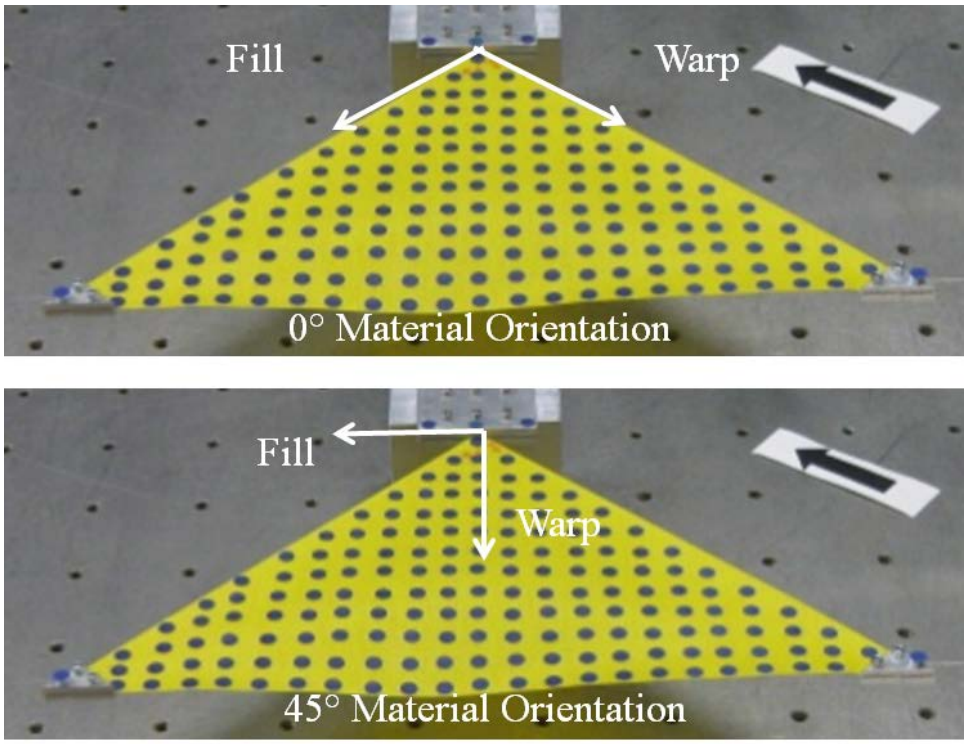

Figure 3.3. Diagram of material orientations studied in Scherrer, 2012.

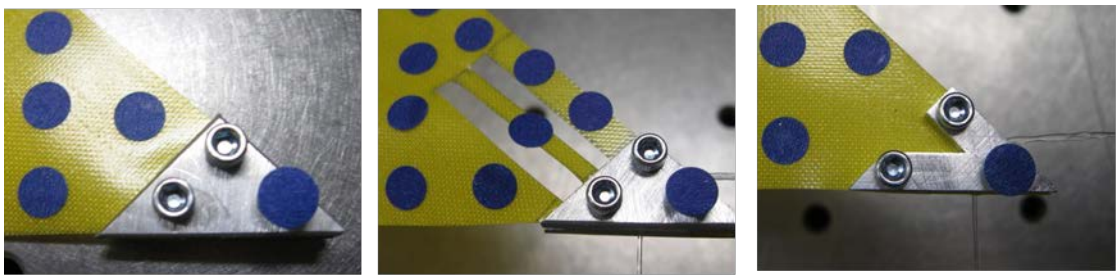

Figure 3.4. Left, picture of standard clamp. Center, picture of shear compliant clamp. Right, picture of the V-clamp.

Table 3.2. Summary of boundary conditions, material orientation, and loading for each experimental case.

Test Case	**F**, N	Boundary Condition	Material Orientation
1	3.519	Standard Clamp	0°
2	4.586	Standard Clamp	0°
3	3.519	Standard Clamp	45°
4	4.586	Standard Clamp	45°
5	3.519	Shear Compliant	0°
6	4.586	Shear Compliant	0°
7	3.519	Shear Compliant	45°
8	4.586	Shear Compliant	45°
9	3.519	V-Clamp	0°
10	4.586	V-Clamp	0°
11	3.519	V-Clamp	45°
12	4.586	V-Clamp	45°

Scherrer, 2012 calculated an error of 0.127 mm for the deflection measurements using the PhotoModeler 6 software. It was noted in Scherrer, 2012 that when clamping the nylon fabric between the clamps, care was taken when tightening bolts to reduce "shifting" of the fabric. This "shifting" would cause unwanted deflection in the fabric article and thus could lead to possible uncertainty in the photogrammetry measurements. Also, uncertainty in the placement of the 170 circular targets adds to uncertainty in the correlation of the photogrammetry measurements to the deflection contours from FE analysis. It should be noted that the error study in Scherrer, 2012 was performed on an optically flat surface. Therefore, more uncertainty than what is present in the current work exists due testing a soft, flexible coated nylon fabric.

3.2 FE Analysis of Nylon Triangle Specimen

Nonlinear FE simulations corresponding to the twelve photogrammetry experiments were performed to evaluate the material model used for the coated nylon fabric. Static deflection contours of the triangular nylon article were simulated and then compared to photogrammetry results for verification of the FE model's response. ANSYS 13.0 FE software was employed to perform all FE analyses. A finite element model of a triangular fabric specimen was created, meshed with SHELL181 elements, which are 4-node elements with six degrees of freedom (DOF) at each node. Gravity

loading was applied perpendicular to the plane of the fabric specimen, and stress stiffening effects were included in the analysis. Nonlinear analyses were performed because the thin nylon fabric specimen cannot be assumed to behave linearly since deflections are large relative to the thickness of the fabric. A mesh convergence study was completed to ensure accuracy and optimization of computational time. Based on the convergence study, a mesh with 2810 quadrilateral elements was chosen for the finite element analysis. The appropriately meshed triangular specimen used for the FE simulations is shown in Figure 3.5. A complete set of the ANSYS APDL batch files used for each test case are given in Appendix A.

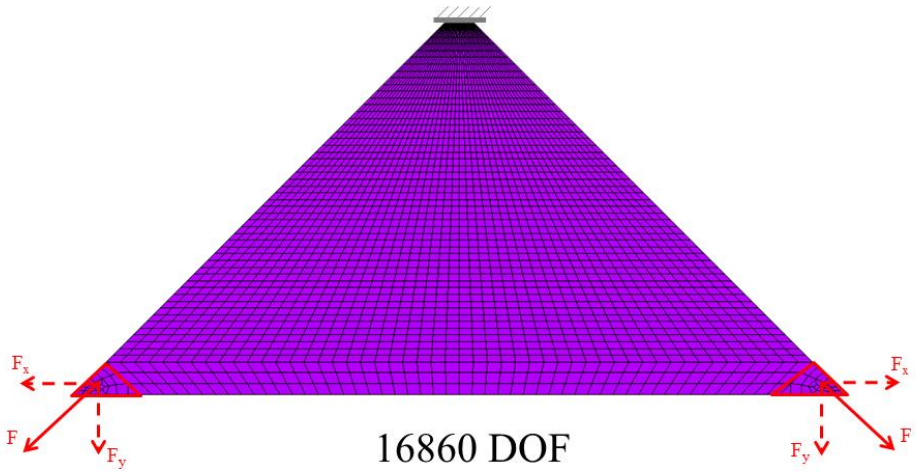

Figure 3.5. Meshed model of triangular fabric panel with boundary conditions and loading applied.

The initial material model incorporated orthotropic properties, with the warp and fill directions of the fabric corresponding to the major material directions. Elastic moduli and Poisson's ratio for the coated nylon fabric are presented in Table 3.3. An effective shear modulus was initially defined to be 15% of the elastic modulus in the warp direction. Shear modulus for inflatable fabric structures is a function of the inflated pressure and structural geometry. In 2007, Rowe et al. used a similar method to define an effective shear modulus for the coated fabric Vectran during bending simulations of inflatable wings [22, 23].

Table 3.3. Material properties used for initial FE model of nylon fabric.

Material Constants	
E_w, MPa	145.17
E_f, MPa	73.65
G_{wf}, MPa	21.78
ν_{wf}	0.3
ρ, kg/m^3	1024.16
t, mm	0.3

Boundary conditions were applied as pseudo clamping areas, as depicted in Figure 3.6. These clamping areas, which are outlined red in Figure 3.6, were modeled with different thicknesses and densities. The clamps were constructed of aluminum and were modeled with a thickness of 6.63 mm and a density of 2625.98 kg/m3 (both the thickness and density take into consideration the nylon being sandwiched by the clamp). The top edge of the triangle as shown in Figure 3.5 was a fixed boundary condition (each node had all DOFs restrained to zero) to simulate the fixed clamp.

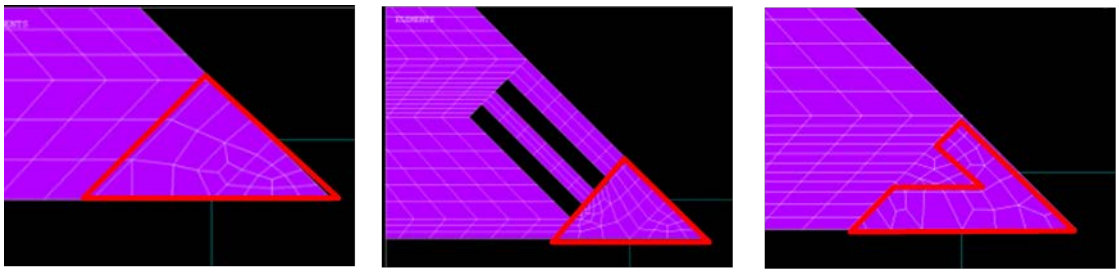

Figure 3.6. Left, FE model of the clamping area of the standard clamp. Center, FE model of clamping area of the shear compliant clamp. Right, FE model of the clamping area of the V-clamp.

The bi-axial force was applied as an x-component and y-component (shown in Figure 3.5) of the force listed in Table 3.1. The nylon fabric material properties were applied in two configurations the 0° and 45° material orientation. These material orientations are diagramed in Figure 3.7. The material orientations were modeled using a local coordinate system based upon a rotation about the global z-axis.

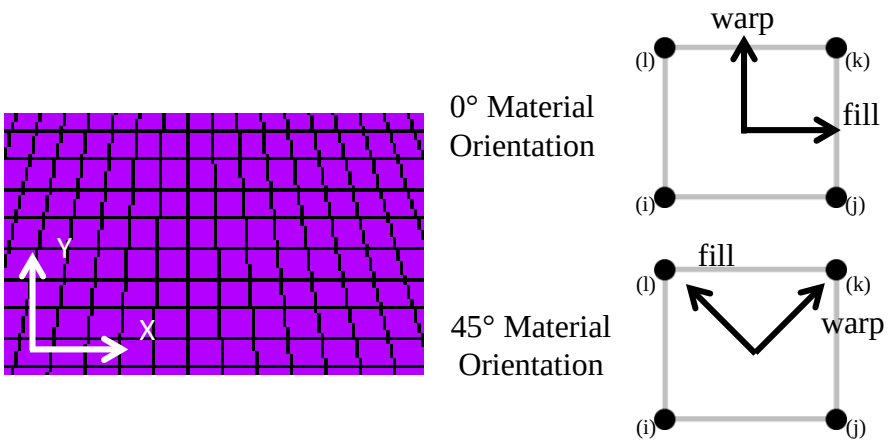

Figure 3.7. Diagram of material orientation used in FE modeling.

3.3 SHEAR STUDY

It was seen that the assumed shear modulus was a significant factor in the static deflection contours of the fabric triangles calculated in the finite element analyses. Focus was put on the shear modulus because the values for the elastic moduli were determined from experimental extension tests. To better define an effective shear modulus for the fabric, various shear moduli were modeled for each of the test cases and the resulting static deflection contours were compared to the photogrammetry results.

The shear study results shown in Figure 3.8 correspond to the fabric having a 0° material orientation and loaded with a 3.519 N force applied using the standard clamp. The effective shear modulus was adjusted until good agreement was reached with the validated static response contour found through photogrammetric measurement. For this specific case the shear modulus was increased from 15% of E_w to 19% of E_w. It was necessary to adjust the shear modulus on a case-by-case basis to achieve the best agreement with the photogrammetry results. The shear studies for each case are shown in Appendix B.

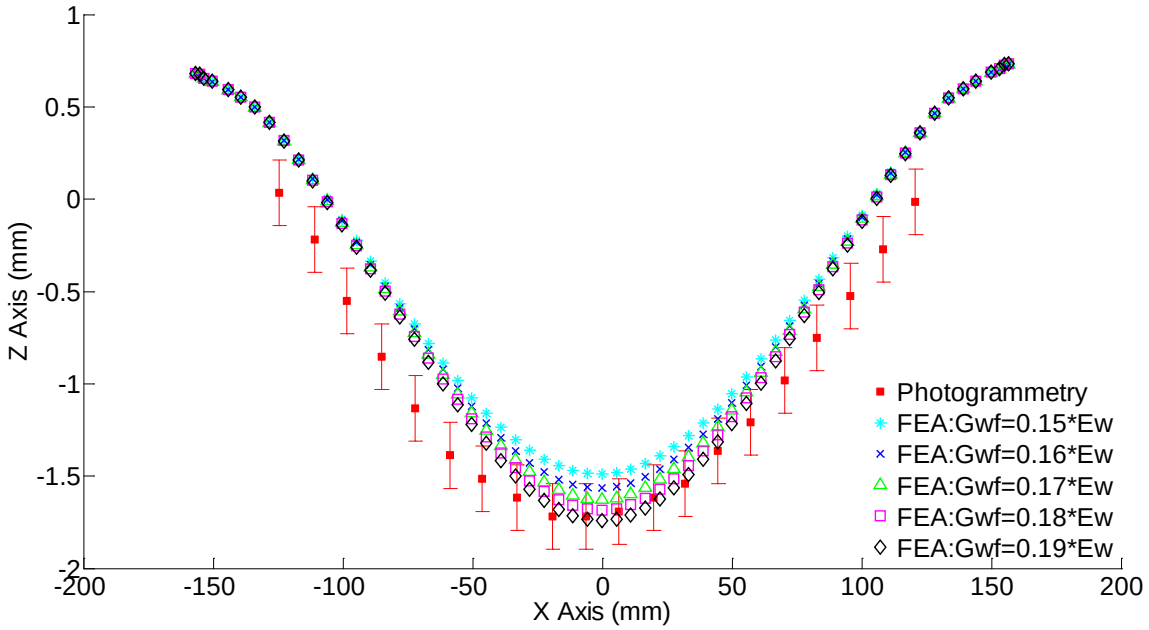

Figure 3.8. Sample shear study plot comparing the deflection profile of the hypotenuse of the triangular specimen.

A shear study was performed for each of the twelve cases to establish a validated-model shear modulus. The shear moduli were defined as a percentage of the elastic modulus in the warp direction based upon work done by Rowe, 2007. The validated-model shear modulus versus experimental boundary condition for the standard clamp (Cases 1-4 from Table 3.2) and V-clamp (Cases 9-12 from Table 3.2) cases are plotted in Figure 3.9. The case number for each set of conditions is labeled along the horizontal axis, with each pair of data points corresponding to different load levels. Thus, each pair of cases shares the same material orientation and boundary condition, but is loaded with different bi-axial loads per the legend.

The plotted results show that identical shear moduli were required for correlated response of the nonlinear FE models for both loading levels in each case included here. But, once the material orientation is changed to the 45° orientation a significantly lower shear modulus is required for correlation. The difference in shear modulus due to material orientation is consistent with previous studies of the fiber interaction in uncoated woven fabric [50, 58]. The material orientation and loading directly affect the level of friction between the fibers of the nylon fabric. However, it can be argued that this material orientation/loading dependence is also a direct result of the polyurethane coating's

hyperelastic behavior. The plot shows that for each boundary condition the shear modulus only depends on material orientation and is independent of the load level, at least for the load level range considered in this study. It is shown that once the material orientation is altered the validated-model shear modulus required for agreement changes. As the material orientation varies, the in-plane stiffness increases or decreases, thus altering the magnitude of the validated-model shear modulus needed for agreement.

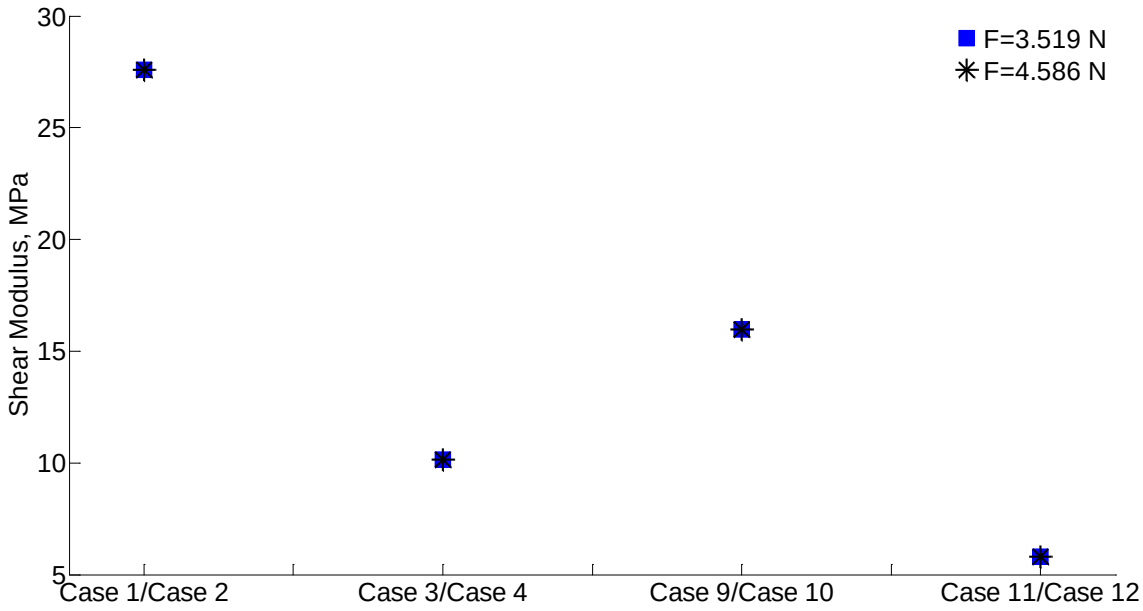

Figure 3.9. Validated-model shear modulus for test cases 1-4 and cases 9-12.

The soft shear compliant boundary (Cases 5-8 from Table 3.2) results do not display the same behavior as the cases above. The validated-model shear moduli for the shear compliant boundary is plotted separately because the required shear modulus increased nearly two orders of magnitude for certain cases. The shear modulus used for the shear compliant boundary simulations are plotted in Figure 3.10, with the case number labeled on the horizontal axis. Again, each pair of cases shares the same material orientation and boundary condition, but was loaded with different bi-axial forces per the legend.

In contrast to the other boundary conditions, when the material orientation is changed to 45°, the effective shear modulus required is seen to increase as the load increases. Thus, results of the shear compliant boundary condition raises many questions

and warrants more work to fully characterize the shear compliant effect on this geometry. The shear compliant boundary was only applied in two orientations for the current work, and further analysis of various orientations of the shear compliant boundary could lead to greater insight. Table 3.4 is a summary of the validated-model shear moduli for the twelve test cases.

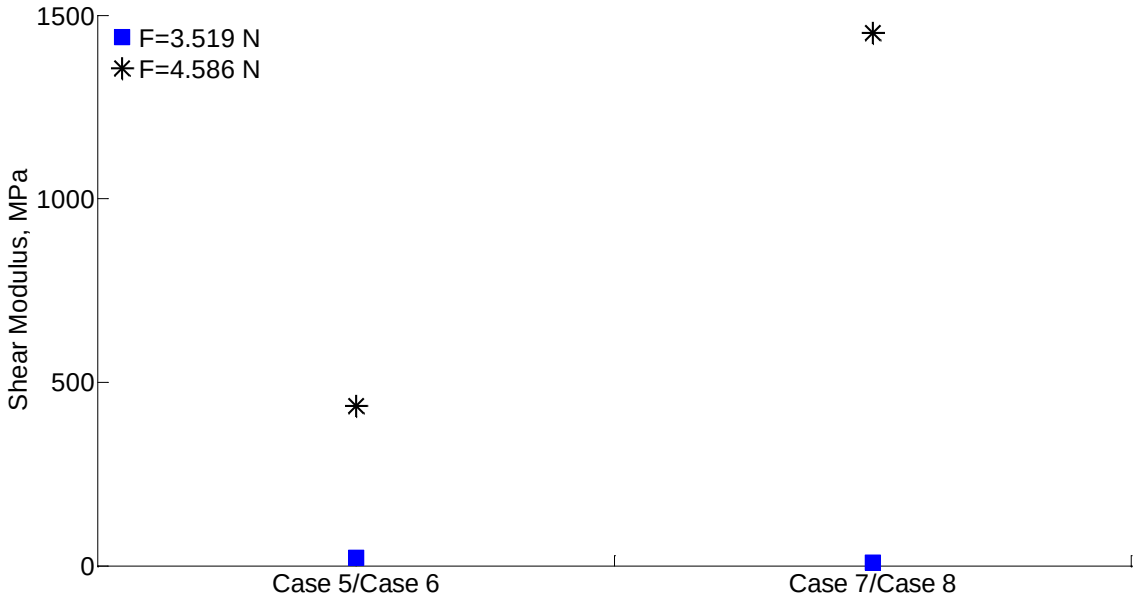

Figure 3.10. Validated-model shear modulus for test cases 5-8.

Table 3.4. Summary of the validated-model shear moduli.

Test Case	G_{wf}, MPa
1	27.58
2	27.58
3	10.16
4	10.16
5	21.78
6	435.51
7	8.81
8	1451.69
9	15.97
10	15.97
11	5.81
12	5.81

To insure that the values determined for the effective shear modulus of the nylon fabric were reasonable, bias extension test data was used to create a range of shear moduli based upon orthotropic lamina theory. Equation (1) determines the shear modulus of an orthotropic lamina using the experimental values E_w, E_f, ν_{wf}, and E_x. The experimental values for these properties are summarized in Table 3.5. Poisson's ratio was not determined during the experiments, but using orthotropic lamina theory an upper bound can be placed on the Poisson's ratio expected from tensile testing and this relationship is given by Equation (2) [75].

$$G_{wf} = \frac{1}{\frac{4}{E_x} - \frac{1}{E_w} - \frac{1}{E_f} + \frac{2\nu_{wf}}{E_w}} \tag{1}$$

Table 3.5. Experimental values for elastic modulus in the warp and fill direction and the bias extension modulus.

Material Constants	
E_w, MPa	145.17
E_f, MPa	73.65
E_x, MPa	57.25

$$\nu_{wf} = \sqrt{\frac{E_w}{E_f}} \tag{2}$$

The upper bound on Poisson's ratio was found to be 1.4 based upon the experimental moduli. To establish the shear modulus range for the nylon fabric Poisson's ratio was varied from 0.001 to 1.5 in Equation (2). Poisson's ratio for composite lamina can be greater than 0.5 due the fact that fibers can relocate under loading with respect to the matrix. By averaging the major (ν_{wf}) and minor (ν_{fw}) Poisson's ratio for a composite lamina an acceptable value (from the standpoint of isotropic materials) should be found.

The resulting range for the shear modulus, Gwf, varied from 14.6 MPa to 20.2 MPa. A shear modulus range from 5.8 MPa to 27.6 MPa was required in the finite element models to produce agreement between analysis and test results for the standard clamp and V-clamp boundary conditions. The orthotropic lamina equations are traditionally used on composite materials which are much stiffer than the nylon fabric.

However, noting that the nylon is a much softer material, the values for the validated-model shear modulus are still within a reasonable proximity to the range defined by the experimental results.

3.4 COMPARISON OF PHOTOGRAMMETRY AND FE SIMULATIONS

Once the validated-model shear modulus was established, nonlinear FE analysis was used to define the correlation between the various boundary conditions and resulting flatness of the bi-axially loaded fabric specimen. To evaluate the geometric control (i.e. flatness) produced by the imposed conditions, an RMS deflection was calculated. Equation (3) is the formula used for the RMS deflection,

$$Z_{RMS} = \sqrt{\frac{1}{n}\sum_{i=1}^{n}\left(z_i - z_{avg}\right)^2} \tag{3}$$

Nonlinear FE simulations were performed to obtain the centerline and hypotenuse deflection profiles. The deflection contours were initially compared to those found experimentally by Scherrer, 2012. Photogrammetric and FE simulation results for the center contour of the triangular test article are presented in Figure 3.12. The deflection contours for the hypotenuse of the triangular test article are presented in Figure 3.11. A comparison of the 3-D static deflection contour is presented in Figure 3.13 and Figure 3.14.

It can be seen that the FE results reasonably correlate to the deflection trend results obtained by photogrammetric measurement for different design options, thus indicating that the modeling approach could be useful in early concept definition trade studies for inflatable structures. The contours shown are for a select set of cases. Center and hypotenuse contours are shown for cases using the standard clamp (Cases 1-4). The 3-D contours consider only Case 1 and Cases 2. A complete set of the center, hypotenuse, and 3-D contour plots for each test case are shown in Appendix B. It should be noted that some of the inconsistencies in the hypotenuse contours were attributed to edge effects and influence of clamp. It was also seen that the hypotenuse edge would curve over because positive deflections once the higher loading was applied in the photogrammetry experiments.

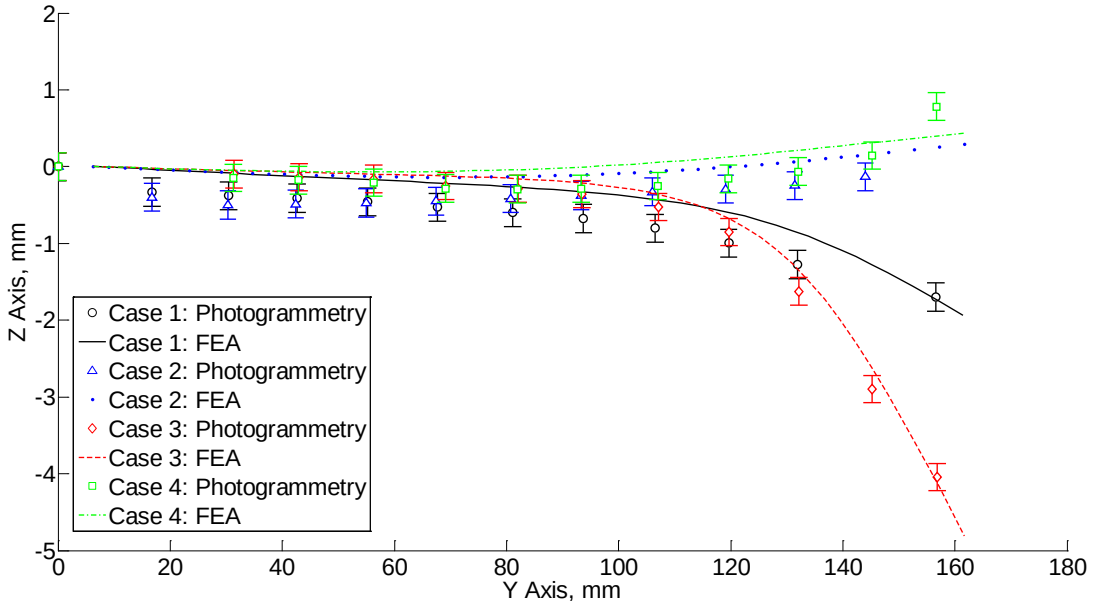

Figure 3.11. Resulting center contours for test cases 1-4.

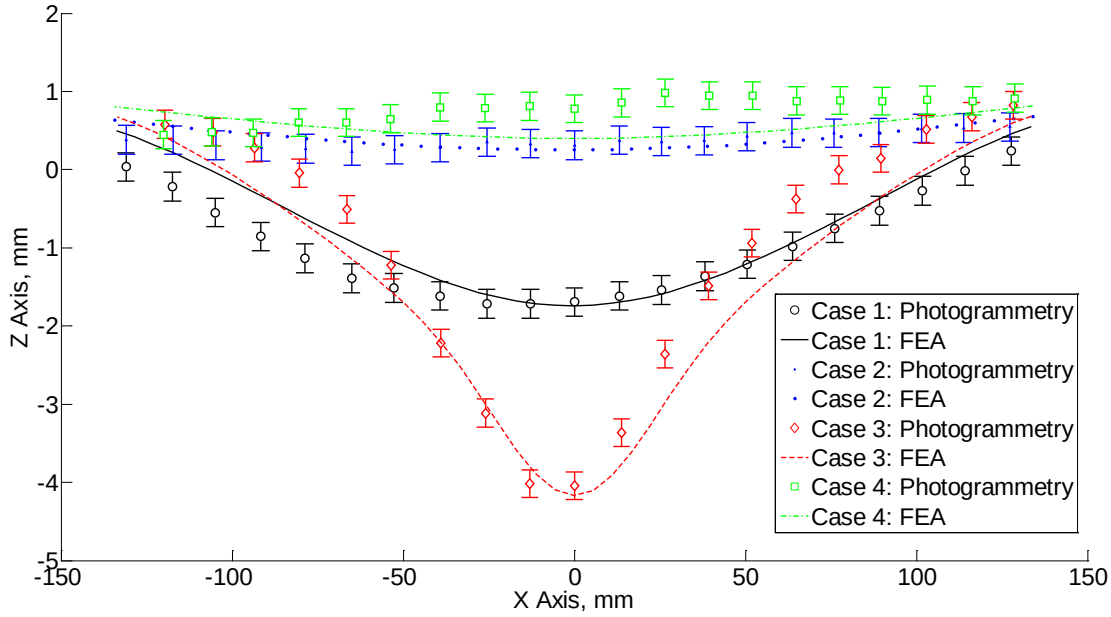

Figure 3.12. Resulting hypotenuse contours for test cases 1-4.

For a more quantitative comparison of the photogrammetry experiments and the FE simulations, RMS deflection was calculated for each test case. The RMS deflections, in the out-plane direction, found using the verified FE models are shown in Figure 3.15 and Figure 3.16. For further validation of the modeling procedure, RMS deflection results from Scherrer, 2012 are also plotted. Performance requirements for terrestrial and space-based radar reflectors are plotted as benchmarks for flatness of the triangular fabric panel. Terrestrial radar decoy applications require a flatness of a half wavelength acceptable performance [11]. Terrestrial radar decoys operate in a frequency range of 10 GHz to 40 GHz, so at 40 GHz a half wavelength measures 3.75 mm. For space-based radar reflectors a 2dB loss in transmission is considered to be a practical performance requirement. Thus at an operating frequency of 20 GHz, a RMS deflection of 0.58 mm is required for acceptable performance [45].

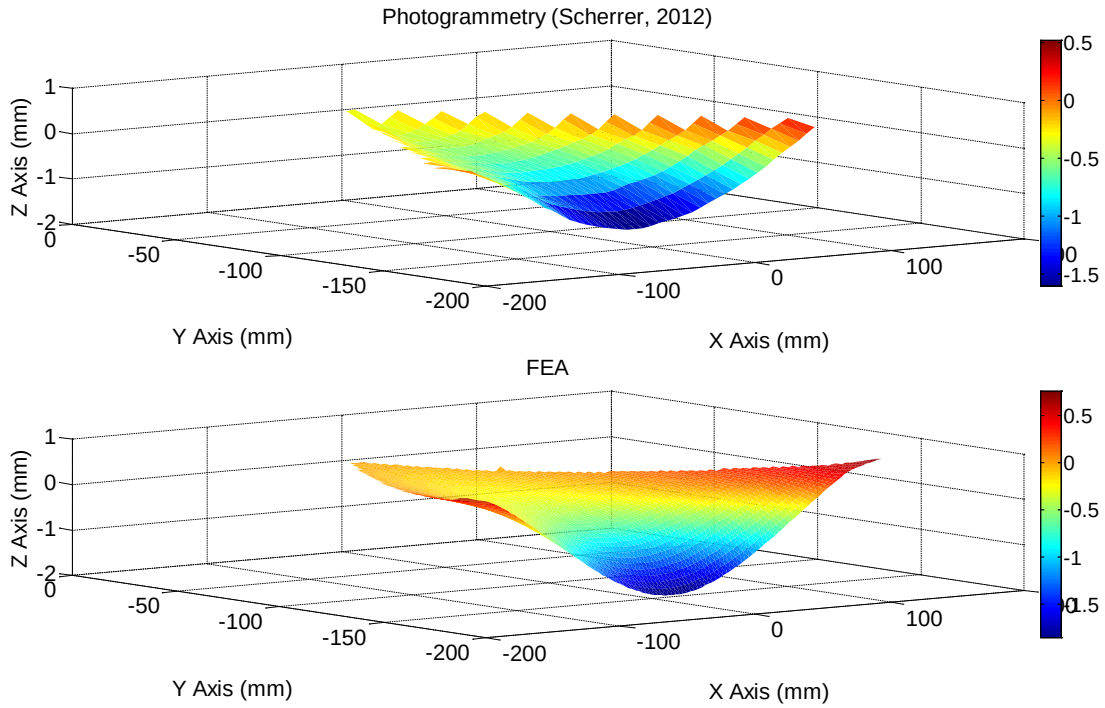

Figure 3.13. Resulting 3-D contour for Test Case 1.

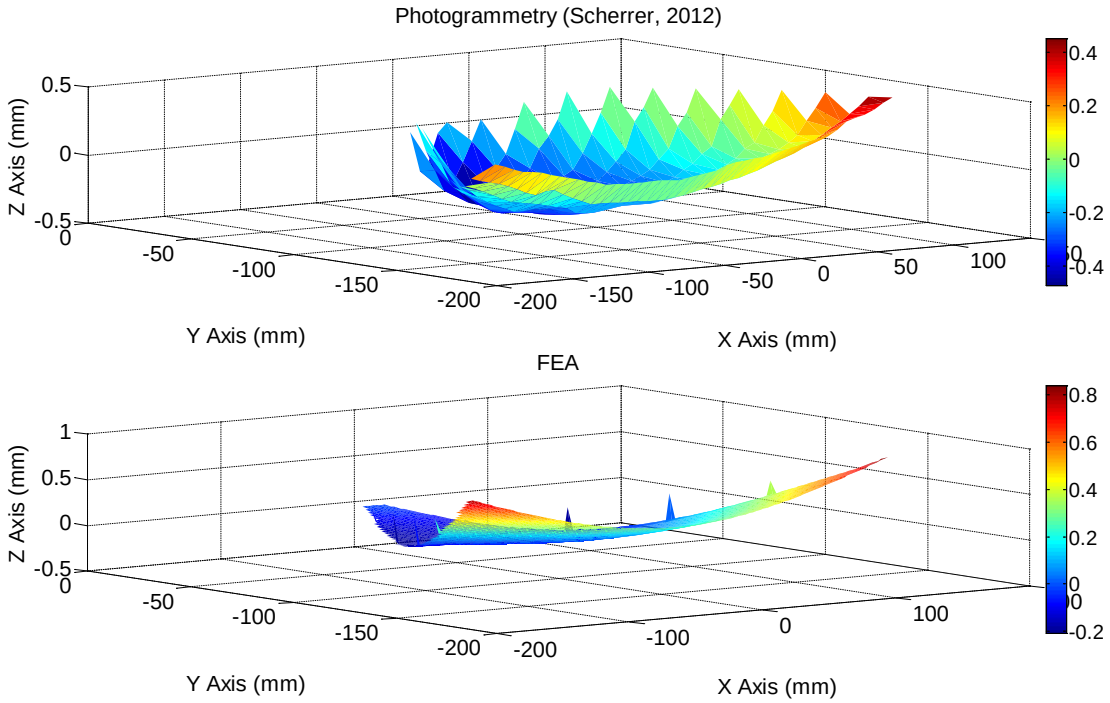

Figure 3.14. Resulting 3-D contours for Test Case 2.

Figure 3.15 presents the RMS deflections for the standard clamp and V-clamp test cases. It can be seen that FEA results correlate to the photogrammetry measurements for the majority of cases. Further the majority of cases achieves or exceeds performance requirements for the radar reflector. Figure 3.16 shows the RMS deflections for the shear compliant boundary test cases. The shear compliant boundary is only in good agreement with the photogrammetry measurements for one of the four test cases. However, the performance of the shear compliant boundary still exceeds the requirement for the terrestrial radar reflector. The overall trends seem to agree for all the test cases, and the majority of the test cases correlate well with the photogrammetry results. It can be seen that both the FE simulations and photogrammetric measurements indicate that Case 2 provides the greatest level of geometric control on the fabric surface. Case 2 uses the standard clamp, 0° material orientation, and the higher bi-axial load.

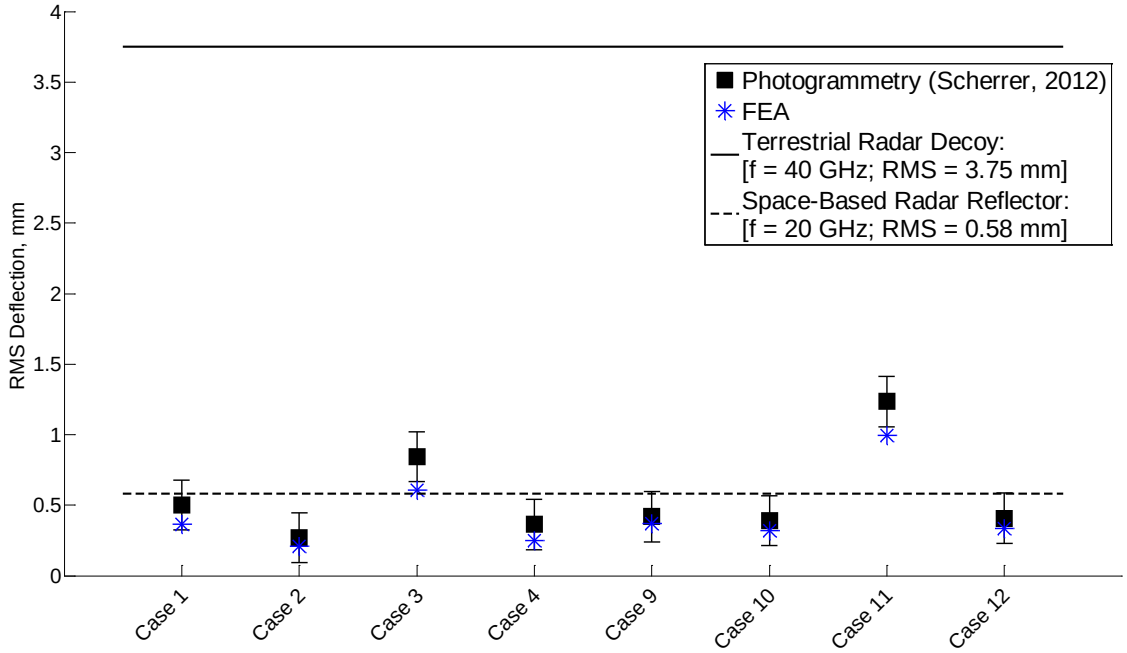

Figure 3.15. RMS deflection comparison for cases with the standard clamp and V-clamp.

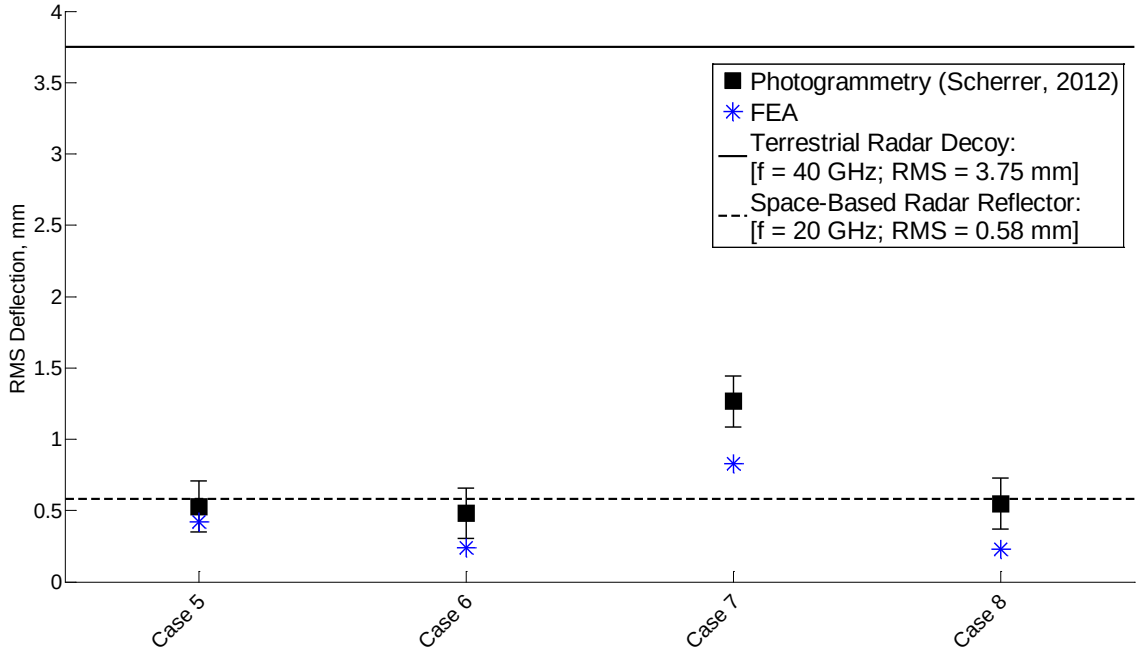

Figure 3.16. RMS deflection comparison for the shear compliant clamp.

3.5 CHAPTER SUMMARY

Photogrammetric results were used to validate the finite element modeling of the nylon fabric article. A linear orthotropic material model was used for the finite element simulations. However, large deflection nonlinearities and stress stiffening effects were included in the finite element analyses. It was found that a key factor to the fabric response was the shear modulus. The shear modulus of the fabric was seen to depend on the material orientation, boundary conditions, and loading. Once a validated-model shear modulus was found for each experimental case, a final simulation was performed to produce deflection profiles for each case. From the deflection profiles a RMS deflection was calculated and compared to the photogrammetry measurements and performance requirements for current engineering systems. The overall trends agree for all the test cases, and the majority of the test cases correlate well with the photogrammetry results.

Furthermore, the majority of the FE results met or exceeded geometric control requirements of terrestrial and space-based radar reflectors. Thus, the linear orthotropic material model was successfully used to model the response of the coated woven nylon. An acceptable accuracy was achieved for each analysis, when considering the level of uncertainty inherent to flexible, nonlinear materials. The results for the shear compliant boundary raise many questions. The current shear compliant boundary was designed to be parallel to the line of loading. Various other shear compliant boundary designs could be much more beneficial, so due to the limited treatment of the shear-compliant boundary, future work is warranted to better define the effect of this boundary condition. The nonlinear finite element simulations were found to agree with the findings of Scherrer, 2012. In both studies it was seen that increasing the magnitude of the biaxial-tension was the largest factor in decreasing the root mean square deflection of the fabric article.

CHAPTER FOUR STATIC INFLATION RESPONSE OF NYLON CIRCULAR SPECIMEN

4.1 DESIGN OF INFLATION CHAMBER

To further evaluate the material model developed for the polyurethane-coated nylon fabric, an inflation chamber was designed for static deflection testing of fabric over a range of inflation pressures. The chamber was designed to inflate a circular area of a fabric sample. Static inflation response was measured using the same photogrammetry techniques discussed earlier. A schematic of the experimental setup is shown in Figure 4.1. Loading and geometries of this experiment are similar to the canonical structures of the inflatable pathfinder system. Further, this study extends the understanding of how boundary conditions affect the coated nylon fabric previously examined in Scherrer, 2012. The results of this analysis will be used to develop the FE model for the pathfinder system.

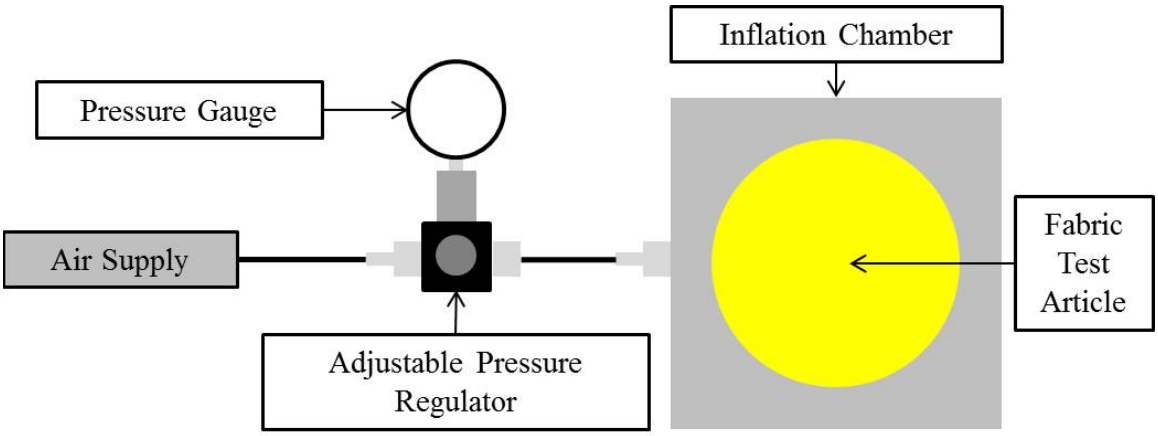

Figure 4.1. Schematic of inflation testing using the photogrammetry.

Design of the inflation chamber was based upon an existing test fixture, but the existing fixture had a square hole. It was decided that a circular chamber would be more beneficial because of its relation to the geometries being modeled in the inflatable pathfinder system. The inflation chamber was designed to apply even clamping along the circumference of the circular nylon article. A thick plate of clear cast acrylic was used to create the main pressure chamber. Aluminum plates were used to enclose the chamber and clamp the fabric test article in place. The dimensions were such that an 8-inch

diameter circular area would be inflated. A 3-D model of the inflation chamber is shown in Figure 4.2.

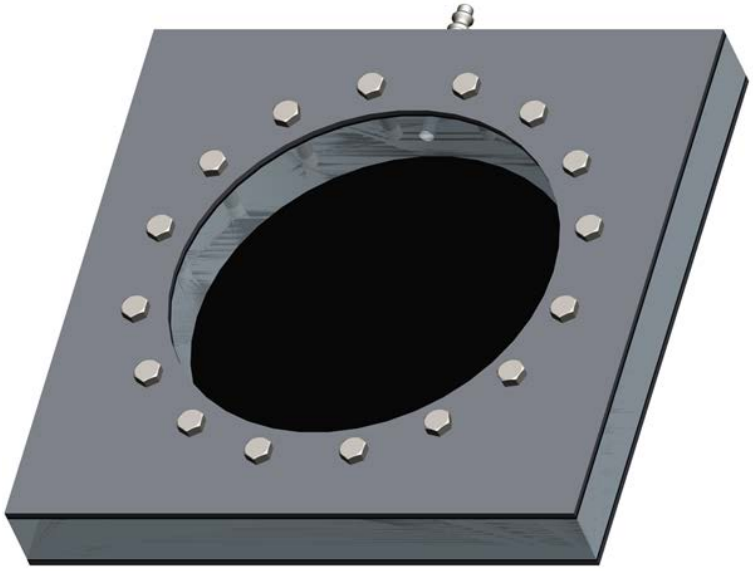

Figure 4.2. Model of inflation chamber created with Creo Element 2.0/Pro Engineer Wildfire 5.0.

An exploded assembly of the inflation chamber is presented in Figure 4.3. The hardware used to clamp the assembly together was 5/16-inch hex head bolt with hex nuts. A Buna-N rubber material was used to create an airtight seal between the aluminum plates and acrylic chamber. Fabric test articles were placed between the acrylic plate and the top rubber gasket. An Industrial male hose coupling designed per the National Fluid Power Association (NFPA) standard was installed on one side of the inflation chamber. The male coupling allowed for the inflation chamber to be portable and adaptable to any lab setting.

A detailed construction drawing of the inflation chamber is shown in Figure 4.4. The bolt pattern was designed to provide even clamping around the circumference of the fabric test specimen. Sixteen bolts were placed in concentric circle with diameter of 9.25-inches. Bolts were spaced at even intervals around the circumference to provide optimal clamping. The even spacing also insured that an airtight seal was created around the fabric test article.

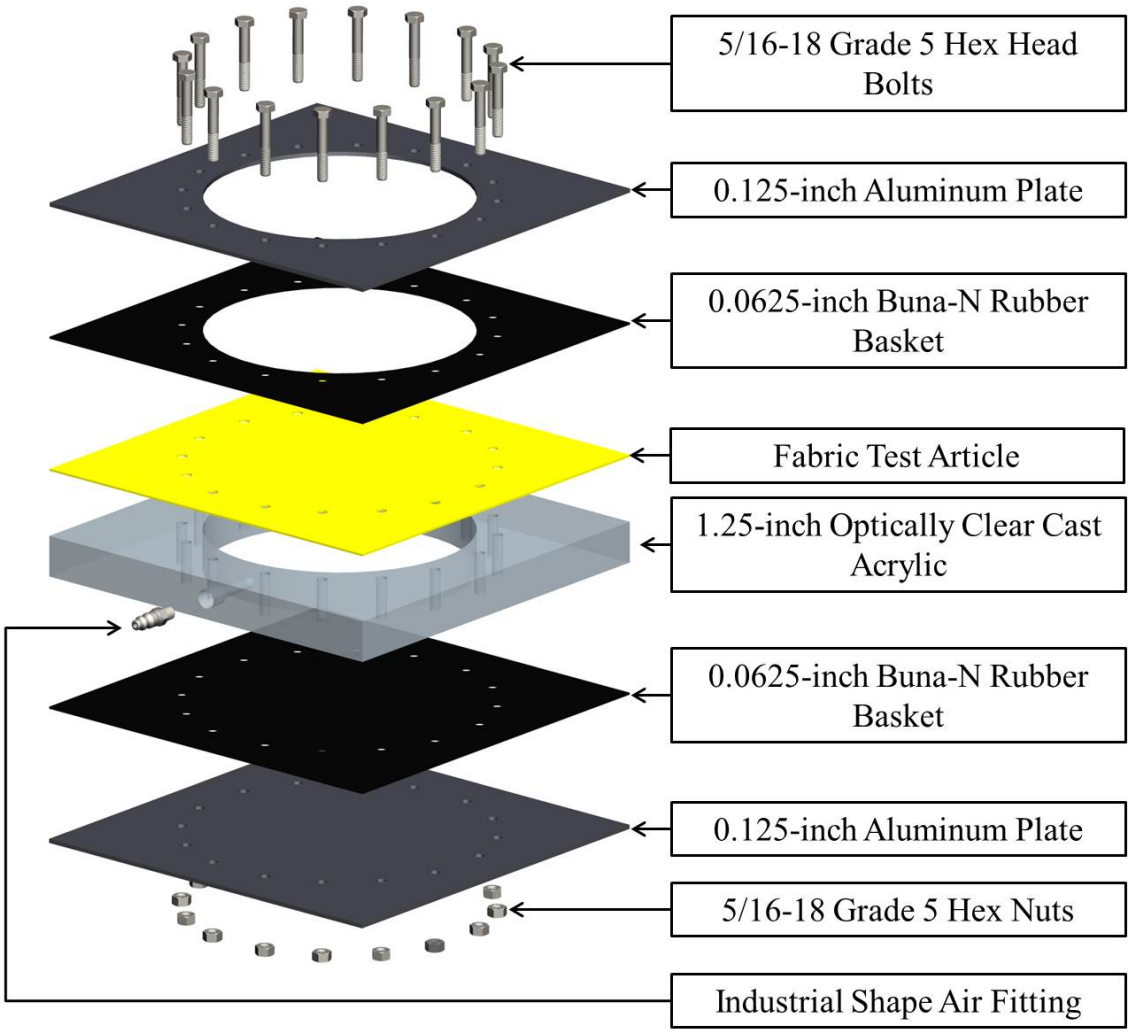

Figure 4.3. Exploded assembly of inflation chamber created with Creo Element 2.0/Pro Engineer Wildfire 5.0.

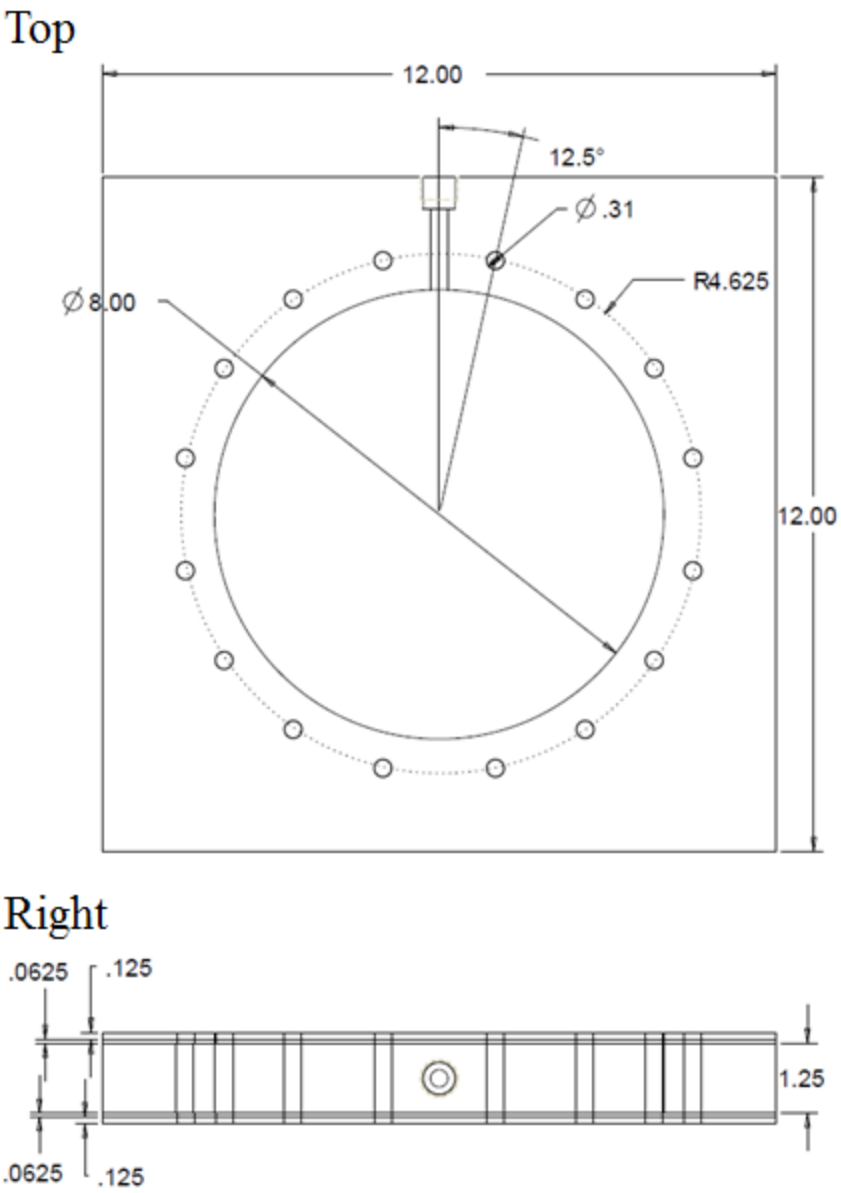

Figure 4.4. Construction drawing of inflation chamber created with Creo Elements 2.0/Pro Engineer Wildfire 5.0. All dimensions are inches.

4.2 PHOTOGRAMMETRY TESTING OF NYLON FABRIC

Based upon work performed in Scherrer, 2012, photogrammetry experiments were performed to capture the static deflection response of a circular piece of the polyurethane-coated nylon fabric. An annotated photograph of the experimental setup for the inflation chamber is shown in Figure 4.5. All photogrammetry experiments were analyzed using PhotoModeler 6 software.

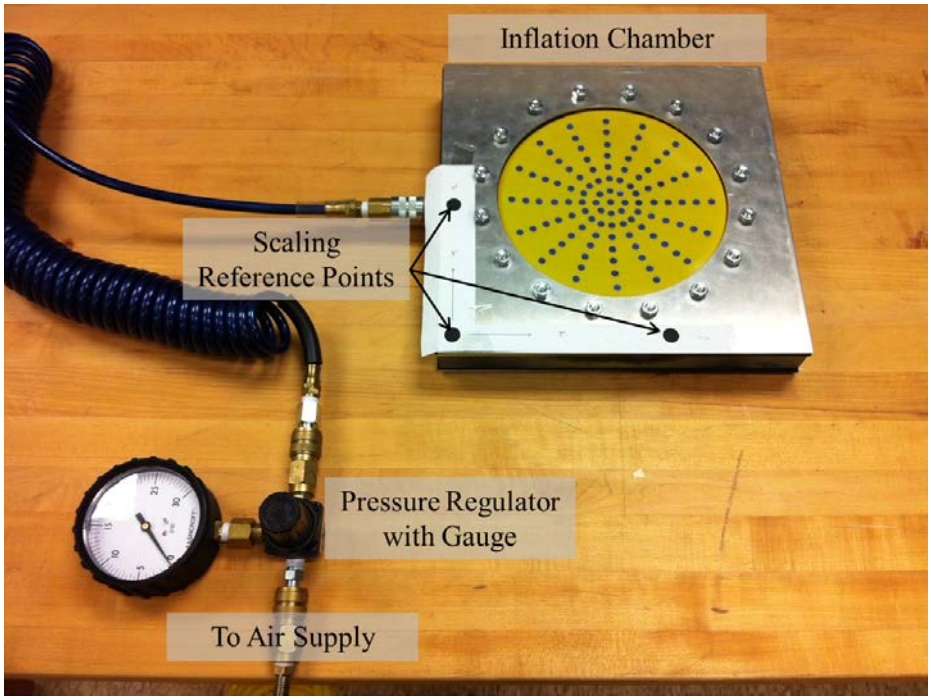

Figure 4.5. Diagram of experimental setup for inflation chamber.

The study done by Scherrer, 2012 involved analyzing the static deflection contour of a triangular piece of the polyurethane-coated nylon fabric subjected to bi-axial tension. It was determined that four photos provided enough accuracy to capture the response of the geometry considered in Scherrer, 2012. However, for the current study it was found that four photos were insufficient and could not capture the large curvature of the inflated circular membrane.

Eight photos were needed to accurately model the response of the inflated circular membrane. The clamped boundary conditions and internal pressure loading caused large deflections with curvature. Figure 4.6 is a photograph of the current geometry (inflated

circular specimen) with targets. From the photograph the large curvature caused by the inflation loading can be seen.

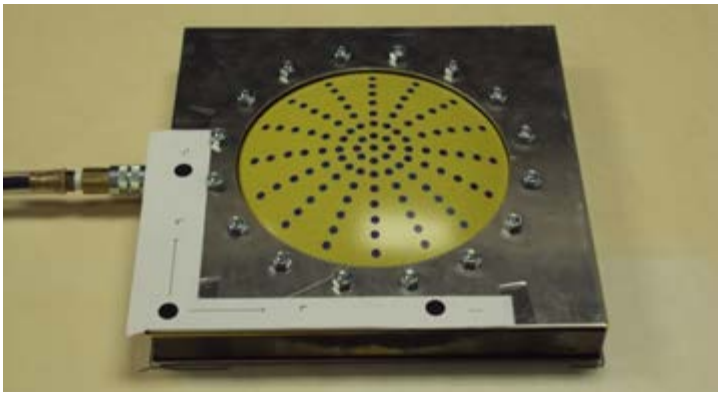

Figure 4.6. Picture of inflated circular nylon specimen.

Sample images from locations of the eight camera locations are shown in Figure 4.7. The camera locations are marked by a number and are circled in black. A University of Kentucky logo is placed in the center of the square to provide reference for the orientation of the camera locations. The camera was held at 45° angle down from the vertical.

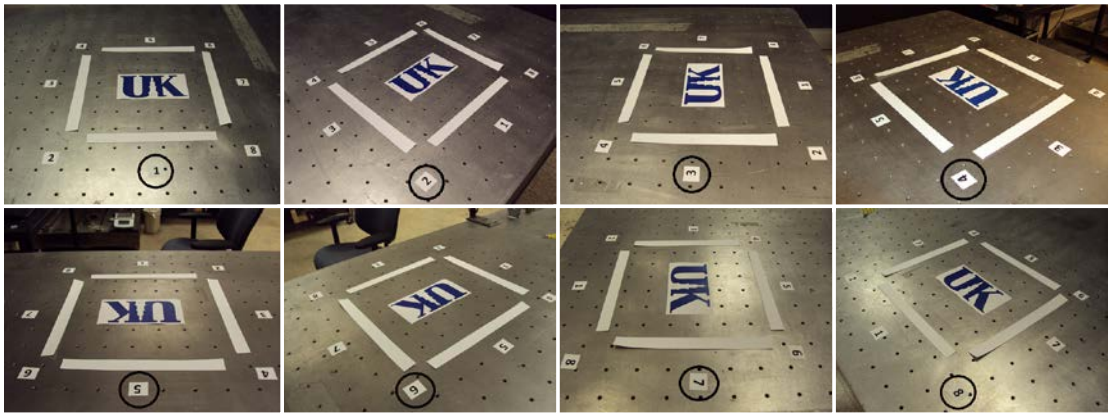

Figure 4.7. Diagram of the camera locations for all photogrammetry tests.

An example of the 3-D model created by the PhotoModeler 6 software is shown in Figure 4.8. White points in the PhotoModeler 3-D model correspond to the blue targets on the circular nylon specimen. The eight camera locations are also depicted in Figure 4.8. Reference points are chosen to define axes and scale of the model. Three reference points were used for this analysis, and these points are defined in Figure 4.5.

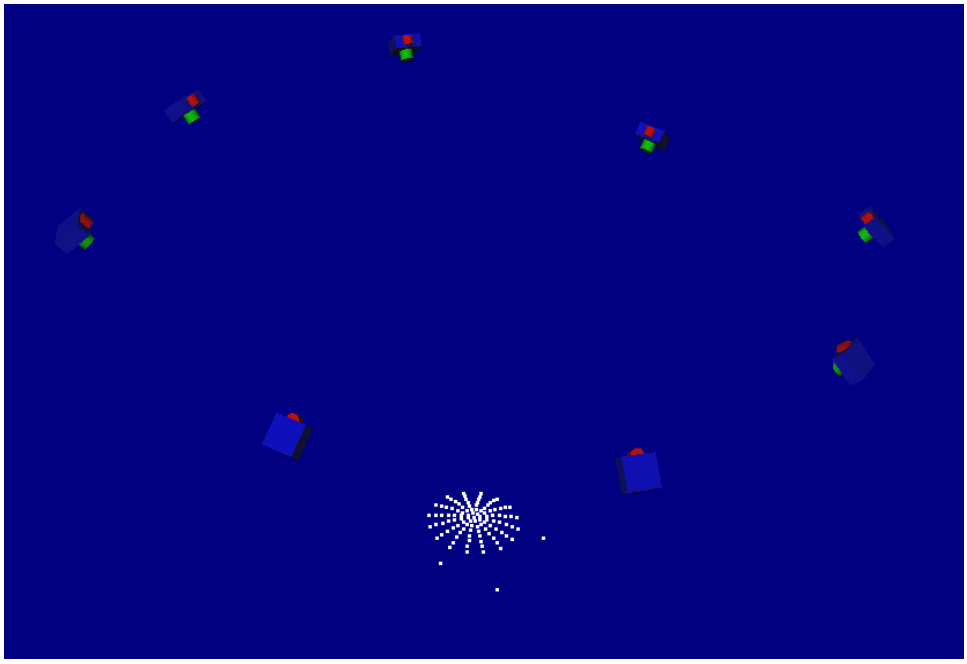

Figure 4.8. Example of 3-D model created using the PhotoModeler 6 software with the eight camera locations shown.

4.3 PHOTOMODELER 6 AUTO-REFERENCING STUDY

Significant influence on the results of the photogrammetry process is seen with the amount of auto-referencing used in the PhotoModeler 6 software. The PhotoModeler 6 software orients a set of photographs based upon reference points the user manually defines across each photograph. Once a sufficient number of reference points that are manually selected, the software can estimate the location of all remaining points through triangulation. This process is called auto-referencing. To examine the influence of auto-referencing, a study was performed varying the amount of manual referencing. This study also considered the selection of the manual reference points. Figure 4.9 is a plot of the percent difference of the maximum deflection for various levels of manual referencing with a 100% manual referencing case being the accepted true value.

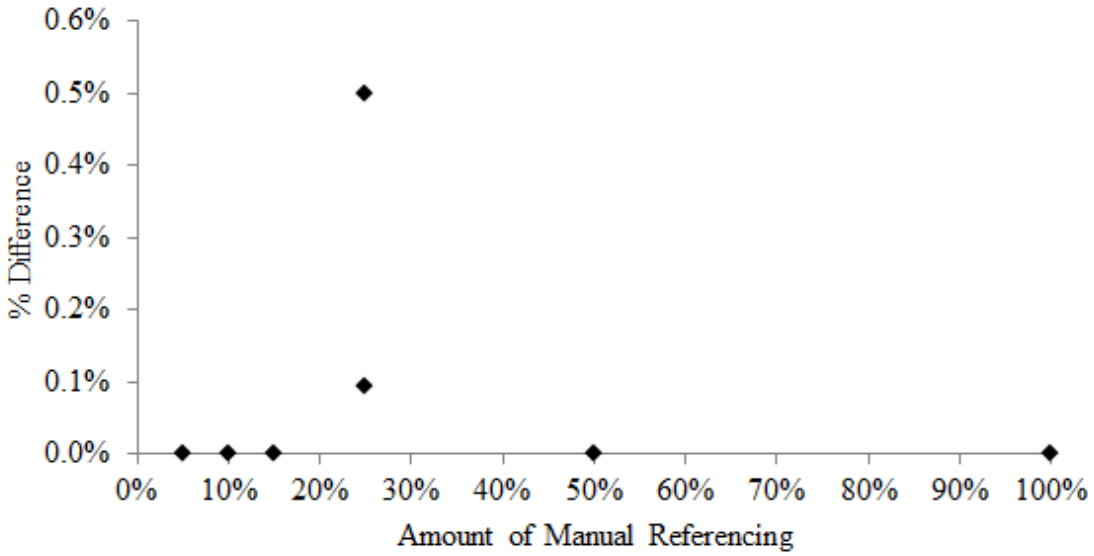

Figure 4.9. Plot of manual-referencing study.

The percent difference between the auto referenced results and the 100% user defined results was negligible for many of the auto-referencing subsets. However, the location of the points used for the referencing can greatly affect the results of the photogrammetry tests. Two different sets of points were used for the 25% manual (75% auto) referenced tests. The first set consisted of only points near the center of the circle which resulted in a 0.1% difference (Figure 4.10a). The second set was defined by manually referencing a quadrant of the circle; this resulted in the highest percent difference (0.5%) of the study (Figure 4.10b). It was concluded that for the best results reference points should be chosen over the entire test article, and increased manual referencing should be used in areas where targets are placed close together. For all subsequent tests at least 15% of the targets were manually referenced, and a selection pattern was defined that included the main horizontal, vertical, and diagonal lines and the outer ring of targets on the nylon test article (Figure 4.10c).

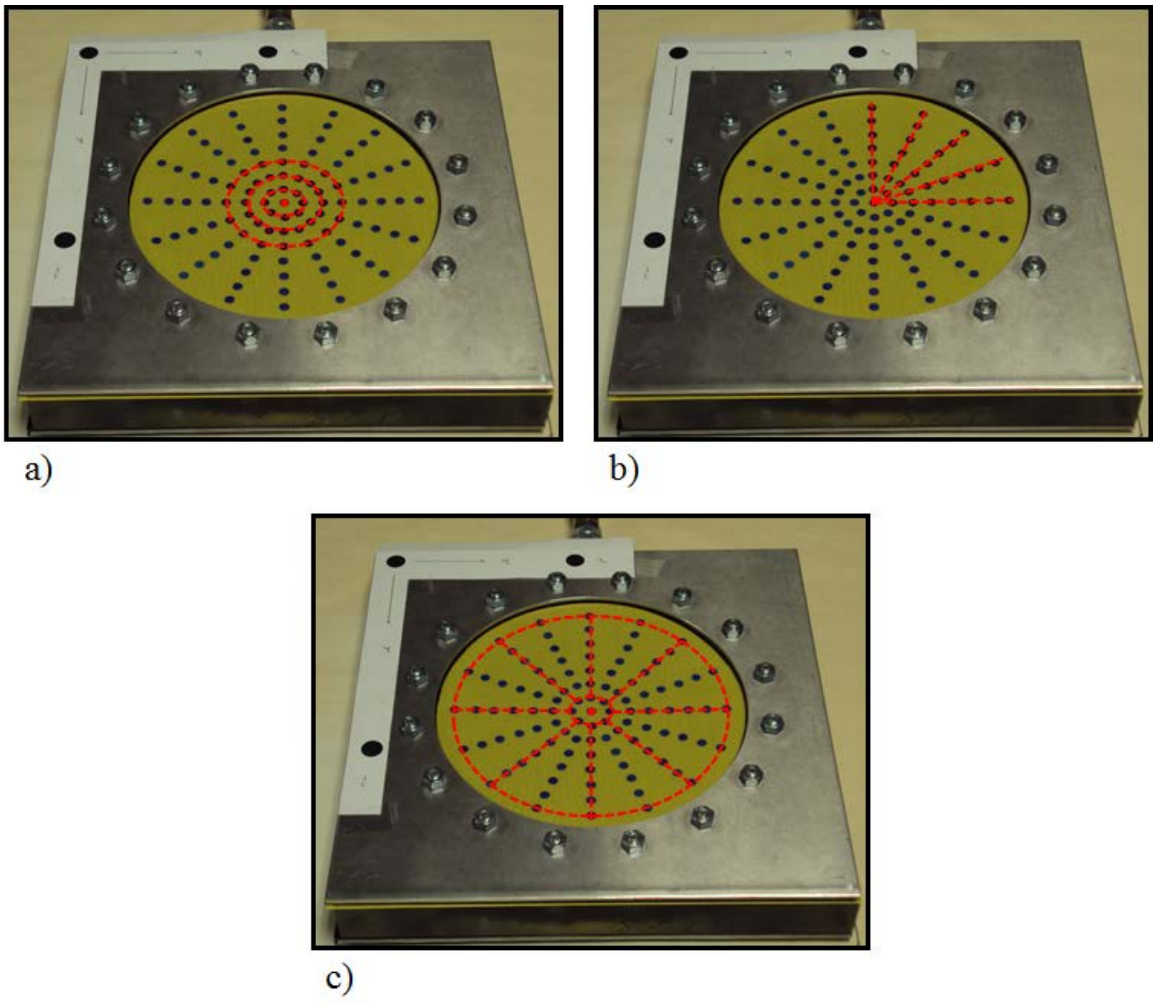

Figure 4.10. a) Points manually referenced around center of test article. b) Points manually referenced for quadrant of test article. c) Final manual reference pattern used for all test.

4.4 Error Analysis of Photogrammetry Experiment

To establish the sensitivity of the photogrammetry testing procedure and resulting baseline variability, a study was performed with six repetitions of the nylon specimen being installed, but without inflation pressure applied. Deflections of the fabric were thus due to gravity loading only. Thus, error associated with installation and photogrammetry measurement would be determined through this analysis.

Establishing variability was done by calculating error of the deflection of targets located near the center of the fabric article. Nine targets' deflections for each of the six

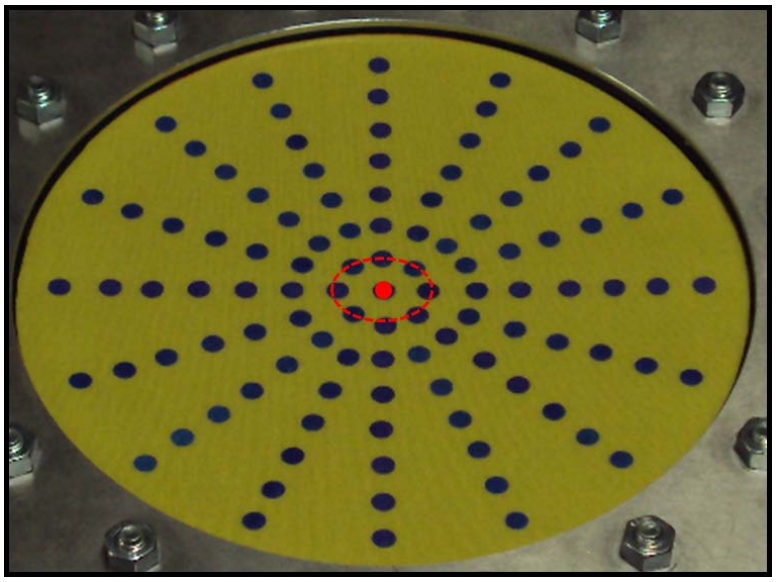

Figure 4.11. Diagram of targets selected for error analysis.

installations were considered for a total of 54 data points for the error analysis. A diagram of the targets considered in the error analysis is shown in Figure 4.11.

4.4.1 INSTALLATION ERROR

Scherrer, 2012, observed that installation of the nylon fabric into testing fixtures can make a significant impact on the results of the photogrammetry measurements. Therefore, it was important to establish an accurate process for installing the nylon fabric into the inflation chamber. Care had to be taken when installing the fabric test article because over tightening the nut and bolt would cause the fabric to "shift" in a similar manner described in Scherrer, 2012. Each bolt and nut was hand-tightened with an additional quarter to half turn to minimize "shifting" in the fabric during installation.

Figure 4.12 plots the absolute value of the deflections for all six repetitions of the installation study. An average of the 54 deflections is also plotted for reference. Installation error was defined as being the difference in a target's deflection from zero. Ideally, the fabric panel should have zero deflection without pressure applied, but due to "shifting" of the fabric non-zero deflections existed. An error of 3.28 mm was determined for installation of fabric into the inflation chamber. It should be noted that the error defined in this section has both installation and photogrammetry error components. The next section determines the photogrammetry component of the error.

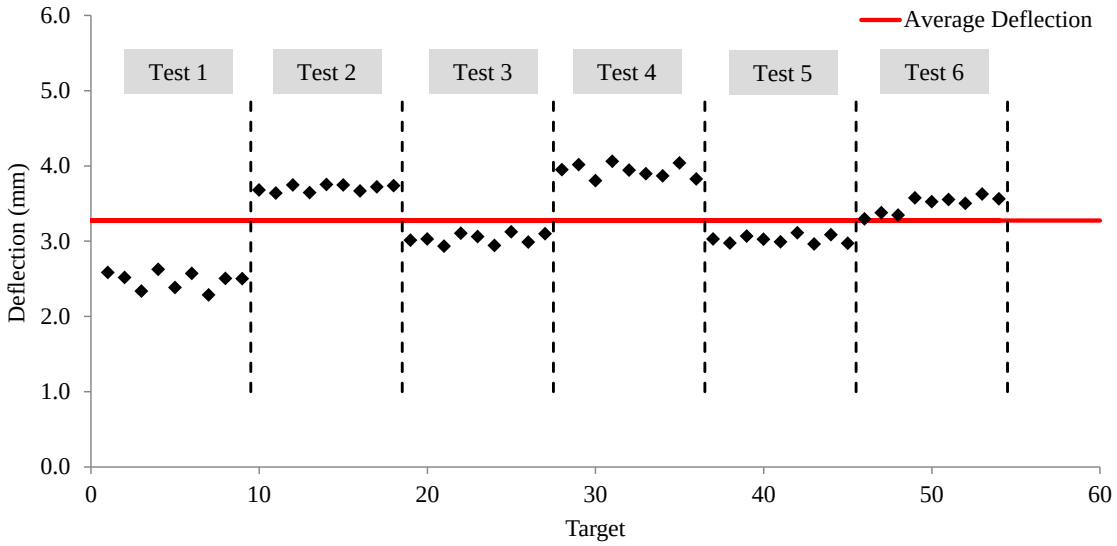

Figure 4.12. Plot of target deflections of all six installation tests.

4.4.2 PHOTOGRAMMETRY ERROR

Error associated with photogrammetry measurement was defined through comparison of the same six installation tests. A normalization of the 54 target deflections was performed. An average of the six center target deflections was used to normalize each of the remaining 48 target deflections near the center. The error for photogrammetry measurement was defined as the absolute difference of each target's deflection to the normalized center target deflection.

Figure 4.13 plots the absolute value of deflection with respect to the normalized center target deflection average for all six tests. The average deflection is plotted for reference, and this value of 0.44 mm was used as the error associated with the photogrammetry process. It should be noted that the error calculated for the photogrammetry inflation experiments (0.44 mm) is nearly 2.5 times larger than the uncertainty found from Scherrer, 2012 (0.18 mm). This was to be expected because Scherrer measured an optical surface to define the accuracy of photogrammetry measurement. Error calculated from the current work is more representative of the level of uncertainty associated with testing of flexible, nonlinear materials.

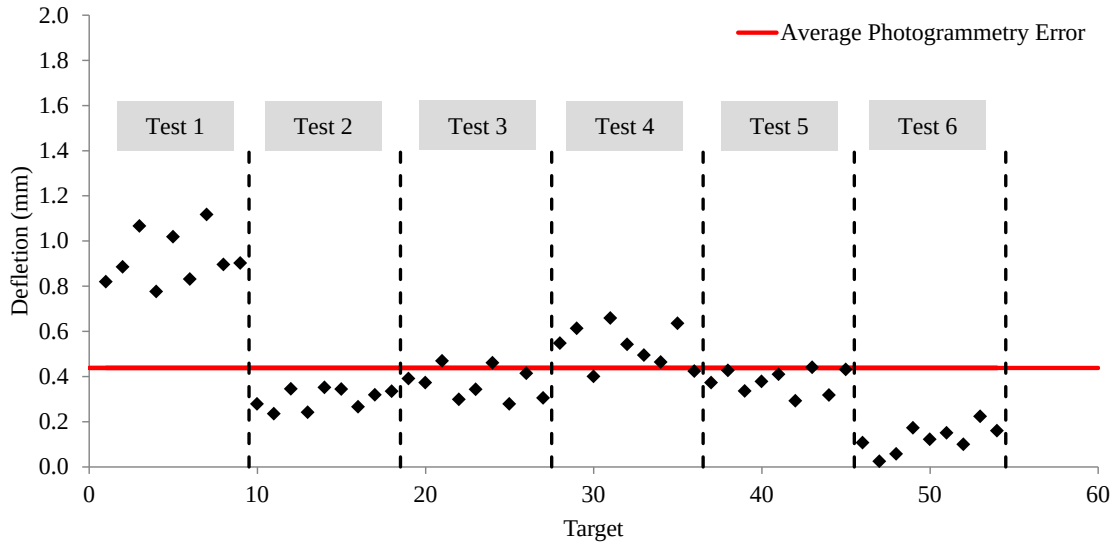

Figure 4.13. Plot of deflections normalized to average center target deflection for all six installation tests.

4.5 PHOTOGRAMMETRY TESTING OF INFLATED FABRIC PANEL

With the photogrammetry testing technique developed and refined, inflation testing of the circular nylon fabric specimen was performed. Three separate nylon articles were prepared and used for the testing. Each nylon article was installed into the inflation chamber, and then inflated to pressure and deflated. This process was repeated for each test article three times at each pressure level. Each test article was re-installed prior to high pressure testing to ensure the same amount of pre-tension was applied to the fabric panel.

The inflation experiments were carried out at two pressure levels; 8.6 kPa and 21.5 kPa. In total, 9 photogrammetry models were created for each pressure level. Figure 4.14 is the deflection contour for the main horizontal set of targets which align with the warp material direction of the nylon fabric inflated at 8.6 kPa. The deflection contour for the same set of points with the nylon fabric article inflated at 21.5 kPa is shown in Figure 4.15. Deflection in the fabric panel increased with pressure level, with maximum deflection being an average of 18.91 mm for the 8.6 kPa pressure level and 23.93 mm for the 21.5 kPa pressure level. The maximum deflection increase 5.02 mm when the pressure is increased approximately 13 kPa.

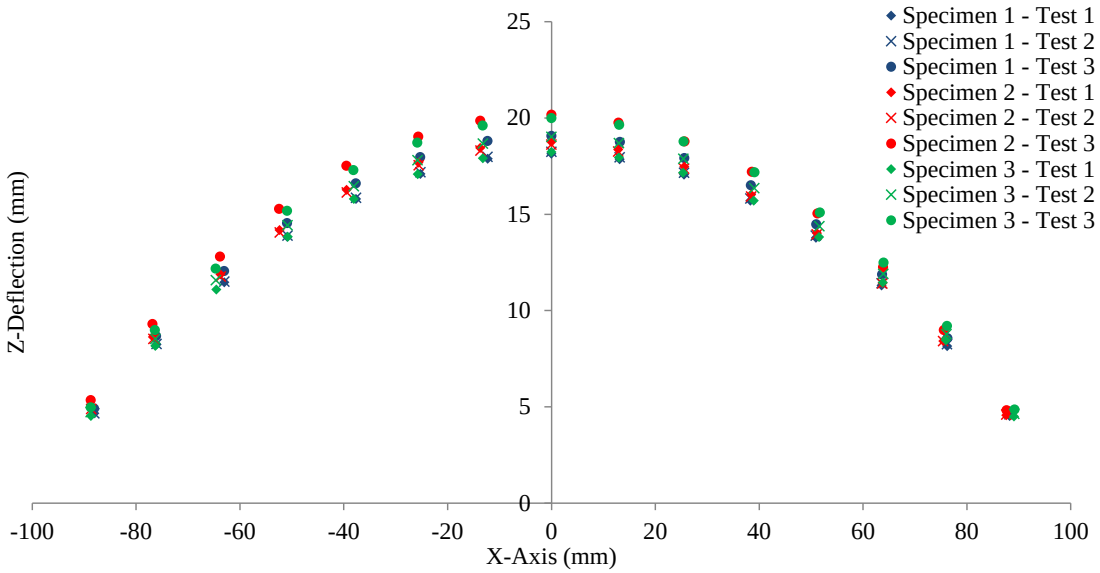

Figure 4.14. Deflection contour of main horizontal set of targets that align with the warp material direction. Tested under an 8.6 kPa inflation pressure.

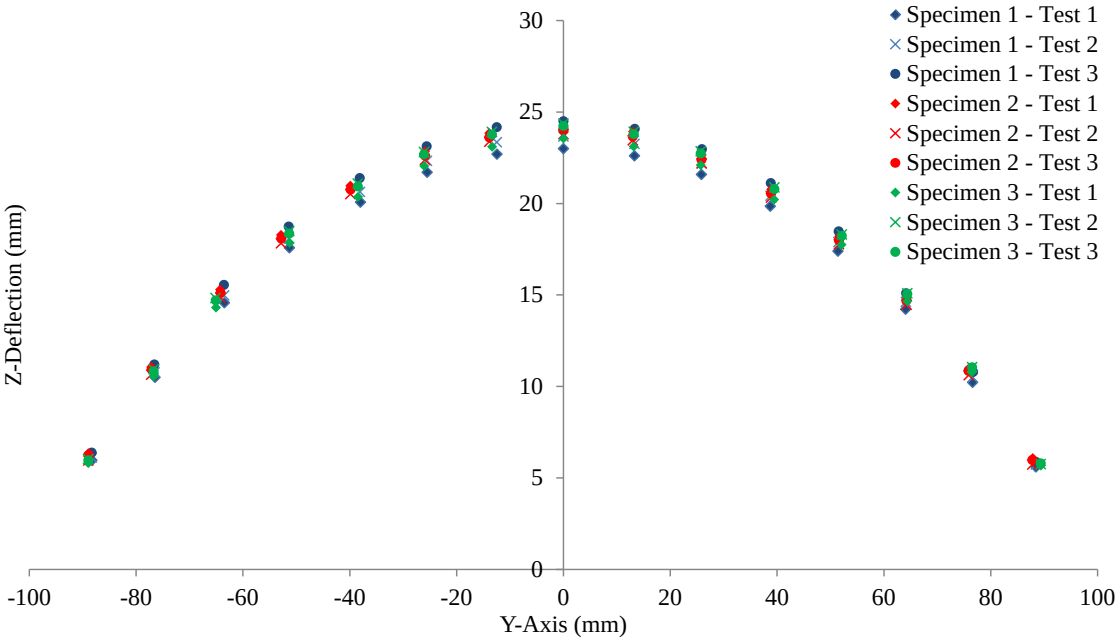

Figure 4.15. Deflection contour of main horizontal set of targets that align with the warp material direction. Tested under an 21.5 kPa inflation pressure.

The maximum deflection increased for each test specimen as it was uninflated and then re-inflated. An average increase of 0.73 mm was seen for the 8.6 kPa pressure level and an average increase of 0.52 mm was seen for the 21.6 kPa pressure level. This phenomenon was believed to be a relaxation in the clamping interface. As the fabric was inflated a "slipping" occurred between the fabric and the gasket material because a true clamped boundary condition is difficult to create in any physical experiment. Another factor for the increase of deflection is that under the inflation loading the threads and/or coating could have naturally deflected or exhibited "creep" behavior. To minimize the impact of these factors, an average of the nine deflection contours for each pressure was used for comparison with FE simulations.

4.6 FE Analysis of Nylon Fabric

With photogrammetry measurements available for comparison, further verification of the material model created for the polyurethane-coated nylon fabric was done. ANSYS 13.0 FE software was used for all FE simulations. A linear orthotropic material model as defined in Table 3.3 was used. SHELL 181 elements were used to create the FE model. Again, a mesh convergence study was performed to determine the most effective mesh for the inflated circular nylon specimen. Figure 4.16 shows the appropriately meshed FE model of the nylon fabric article used in all FE simulations. A fixed boundary condition was applied to the entire circumferential edge of the model to simulate the clamp condition. Gravity loading was applied perpendicular to the plane of the circular fabric test article. Nonlinear analyses were performed because the deflection of the nylon fabric was large with respect to its thickness. The ANSYS APDL batch file used for analysis is included in Appendix A.

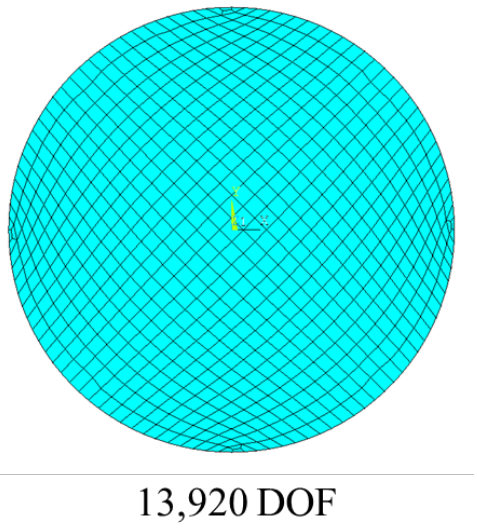

Figure 4.16. Meshed model of inflated circular nylon specimen.

The shear modulus was again the main interest for comparing the photogrammetry measurements and the FE analysis. Greater insight was gained on the behavior of the shear modulus with respect to loading and

boundary conditions through analysis of the inflated nylon fabric article. The effective shear modulus was initially estimated as 10% of the elastic modulus in the warp direction of the coated nylon fabric, and adjusted in the same manner as described in Chapter 3. Figure 4.17 shows the shear study for an inflation pressure of 8.6 kPa. The results of the shear study for an inflation pressure of 21.5 kPa are shown in Figure 4.18. Error bars are included with the photogrammetry results. As establish earlier in this chapter, an error of 3.28 mm was determined for the photogrammetry testing.

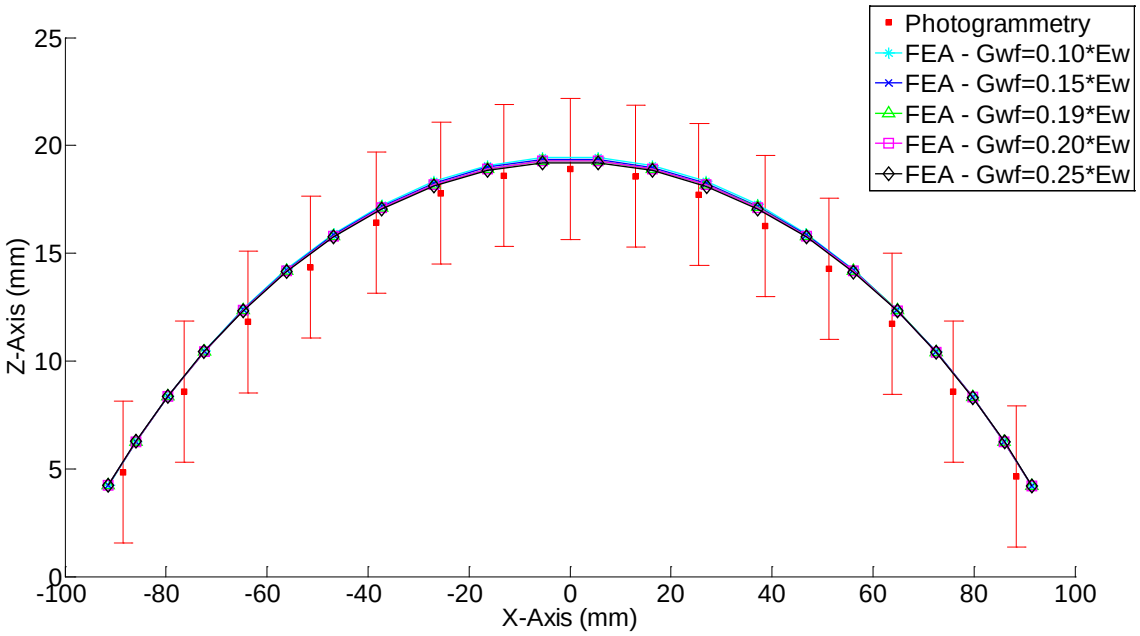

Figure 4.17. Shear study for the circular nylon specimen inflated at 8.6 kPa.

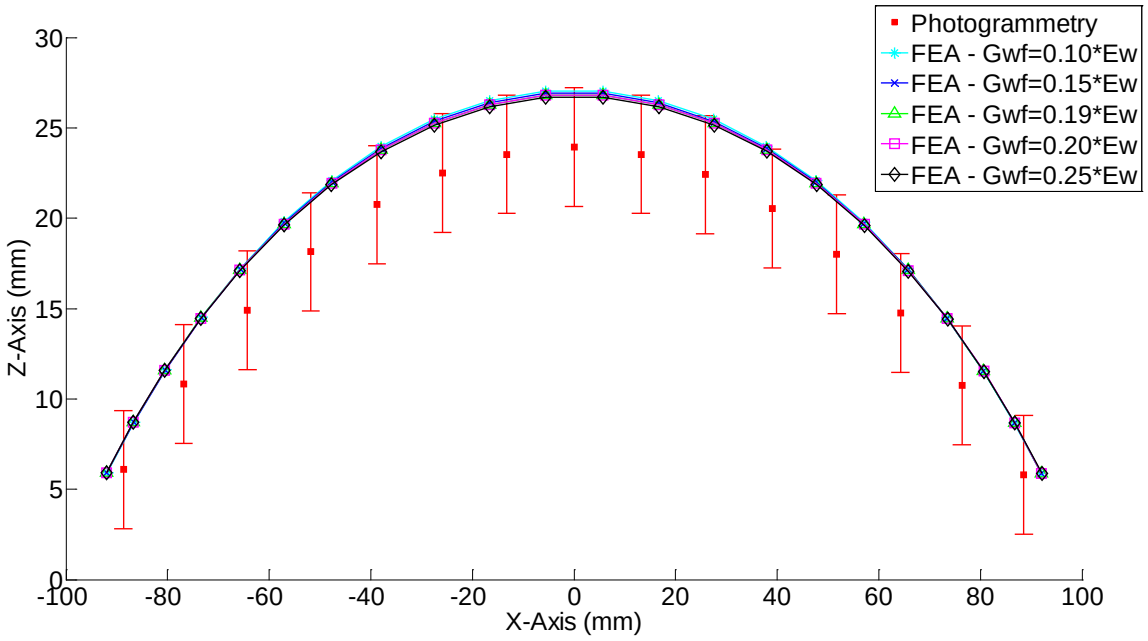

Figure 4.18. Shear study for the circular nylon specimen inflated at 21.5 kPa.

It can be seen from the plots that varying the effective shear modulus did not significantly change the response of the FE model. In the previous study involving the bi-axial tensioned piece of nylon, the response of the nylon was more dependent on the effective shear modulus. Thus it is thought that the inflation loading and clamped boundary condition creates a higher degree of in-plane stiffness in the fabric due to shear locking. Shear locking refers to the phenomenon of threads no longer slipping or moving within a fabric. The in-plane stiffness becomes constant once a certain level of shear locking is reached in a fabric. Individual thread behavior is not accounted for in the current FE model. Thus, the FE model was thought to be less stiff than the possibly shear-locked fabric resulting in the higher deflections form FEA.

It is thought that FEA and photogrammetry results match well at the lower pressure (maximum deflections were within 2% of each other), but differ at the higher pressure (maximum deflections were with 12% of each other). For both pressures, the shape and deflection trends agree. An effective shear modulus of 29.0 MPa (20% of the elastic modulus in the warp material direction) was chosen as the validated-model shear modulus for the inflation chamber experiments.

Once the effective shear modulus was established 3-D deflection models were created using the updated FE model. A comparison of the 3-D FE model and

photogrammetry 3-D model inflated at 8.6 kPa is shown in Figure 4.19. Figure 4.20 is a comparison of the 3-D deflection contours of the circular piece of coated nylon inflated at 21.5 kPa. The plots show that the deflection response of the coated nylon is successfully captured by the FE model using the validated-model shear modulus. It should be noted that the resolution of the FEA results is finer than the photogrammetry results. Resolution was based upon meshing of the FE model and number of targets placed on test articles for the photogrammetry tests. FEA results contained 2,320 nodes and photogrammetry experiments were analyzed with 105 targets.

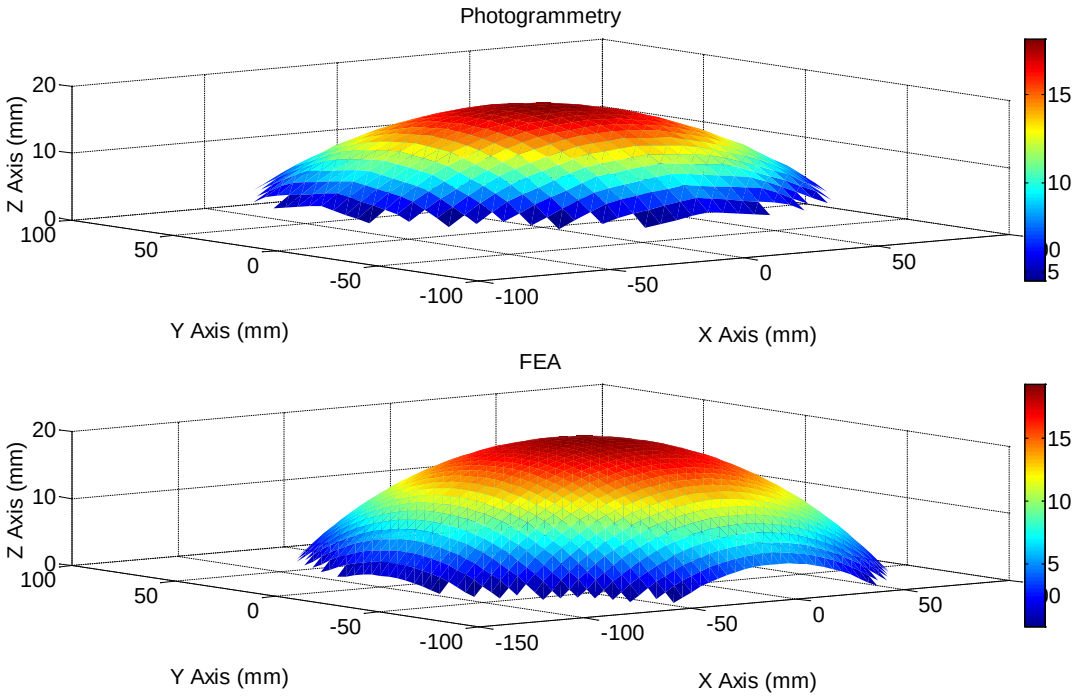

Figure 4.19. 3-D deflection contours of the circular nylon fabric inflated at 8.6 kPa.

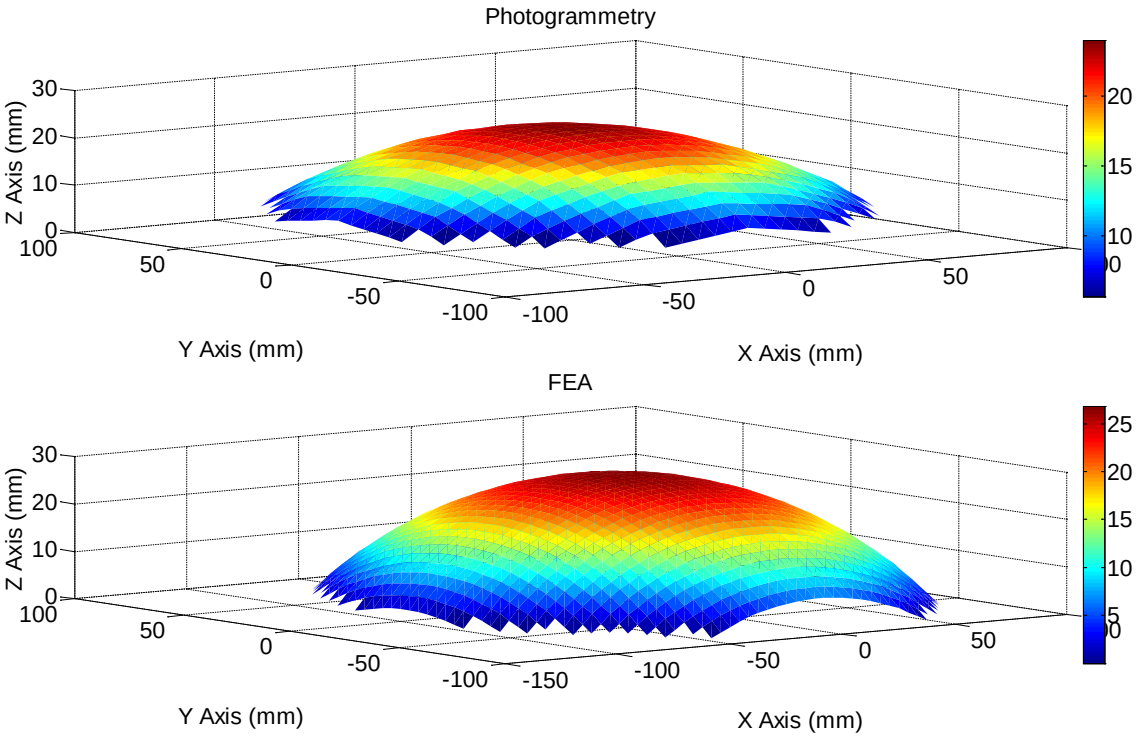

Figure 4.20. 3-D deflection contours of the circular nylon fabric inflated at 21.5 kPa.

4.7 CHAPTER SUMMARY

Through testing the polyurethane-coated woven nylon inflated at certain pressures insight was gained into the behavior of the fabric. The shear behavior of the fabric was the focus of the analysis, and an effective shear modulus was established and verified through correlation of FE simulation and photogrammetry measurements.

Initially, studies were performed to establish variability in photogrammetry measurement of an inflated fabric panel. Influence of auto-referencing in PhotoModeler 6 was analyzed through varying the amount of manually referenced targets that are used to define the auto-referencing scheme in PhotoModeler 6. It was found that a broad selection of points was best. However, in areas that have a high density of targets, manually referencing these targets is best.

An error analysis was also done to examine the error associated with installing the fabric panel and photogrammetry measurement. Six fabric panels were installed and left un-inflated. 3-D photogrammetry models were made for each installation test and the resulting deflections were used to establish the variances in install and the

photogrammetry process. A combined error of 3.28 mm was calculated for the photogrammetry testing of the fabric panel. From the combined error an error 0.44 mm was determined as being the error associated with photogrammetry measurement. The photogrammetry error established in this study is more representative of error associated with testing soft, flexible structures. However, more un-quantified uncertainties exist, these include: uncertainty in the pressure gauge reading and positioning the targets on the test article. Also, it should be noted that the deflections measured using photogrammetry are for the top surface of the fabric, and deflection results from FE analysis are with respect to the mid-plane of the element. This difference is thought to be minimal, but could still contribute to some uncertainty in comparing results.

Through correlation between the FE model and photogrammetry measurements a validated-model shear modulus was defined as 20% of the elastic modulus in the warp material direction or 29 MPa. It was found, however, that varying the effective shear modulus did not affect the deflection response of the FE model to the same degree seen in the finite element analysis of the bi-axial tension experiments. It is thought that the pressure loading and clamped boundary condition created a higher level of shear locking in the fabric, and although the FE model does account for individual thread behavior it does reflect the possible results of this phenomenon. 3-D FEA and photogrammetry results were seen to agree, thus the validated-model shear modulus established in this study will be used in the subsequent analysis of the inflatable pathfinder system.

CHAPTER FIVE DESIGN OF INFLATABLE PATHFINDER SYSTEM

5.1 INFLATABLE SYSTEM CONCEPT

A goal of this project is to design an inflatable pathfinder system which employs only internal pressure to control an assembly of internal membranes. Figure 5.1 is a model of the proposed inflatable pathfinder system. This canonical inflatable system will be used as a phased pathfinder system for exploration and development of general understanding of efficient design methodology and analysis of future systems. Canonical structures are incorporated into the design of the phased pathfinder system to allow for more universal insight.

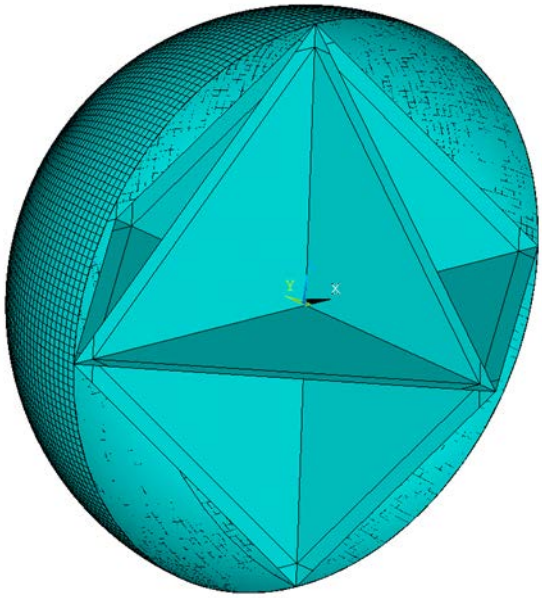

Figure 5.1. Model of proposed inflatable pathfinder system.

The geometries involved in this study are designed to be supported within an inflated sphere. This analysis focuses on different designs of the internal membranes supported by the inflated sphere. In this chapter, initially, loading schemes were examined to determine the most efficient scheme for performance and ease of manufacturing. Once the support connection design was finalized, variations in the fabric panel geometry were considered. The variation in geometry concerned removing material from the center of the fabric panel. These free center geometries have been designed into several solar sail systems including; the Japan aerospace exploration

agency's (JAXA) interplanetary kite-craft accelerated by radiation of the Sun (IKAROS) launched May 21, 2010 (Figure 2.9) and L'Garde's development of the Sunjammer solar sail (Figure 2.9). Variations in loading and material orientation were also examined to determine the optimal system design to achieve the greatest amount of geometric precision.

5.2 FE MODELING AND SIMULATED PRESSURE LOADING FOR TRI-LATERAL CORNER

All FE simulations were carried out using ANSYS 13.0 FE software. Finite element models of the fabric elements were created and meshed with 4-node shell elements (SHELL181), which have six degrees of freedom (DOFs) at each node. Gravity loading was applied perpendicular to the plane of the fabric panel, and stress stiffening effects were included. Large deflection nonlinear analysis was used to solve for the deflection profiles of the model. A complete of set of all ANSYS APDL batch files is included in Appendix A.

The material model used for the entirety of this phase incorporated linear orthotropic properties. Table 5.1 presents the linear orthotropic material properties used for the current analysis. An effective shear modulus was defined to be 20% of the elastic modulus in the warp direction, as was concluded from the analysis from Chapters 4.

Table 5.1. Material constants used for linear orthotropic material model.

Material Constants	
E_w, MPa	145.17
E_f, MPa	73.65
G_{wf}, MPa	29.0
ν_{wf}	0.3
ρ, kg/m^3	1024.16
t, mm	0.3

For verification of modeling procedure, an eighth symmetry FE model of a sphere was created without internal structures and isotropic aluminum properties were used to define the material model. The response of this FE model was compared to analytical equations for radial deflection and stress. Agreement was found within 0.008% for both

the radial displacement and stress, and thus the eighth symmetry FE modeling procedure was verified.

Initially, an approximation of the pressure loading was determined using an isotropic model of the inflated sphere with internal membranes. This isotropic model was used to define boundary condition force estimation. The material properties used for the isotropic model are shown in Table 5.2. Lines bounding the fabric sections and meshed model of the inflated sphere are shown in Figure 5.2. An eighth-symmetry model was used to predict the radial deflections at the corners of the internal panels in response to internal pressure in the sphere.

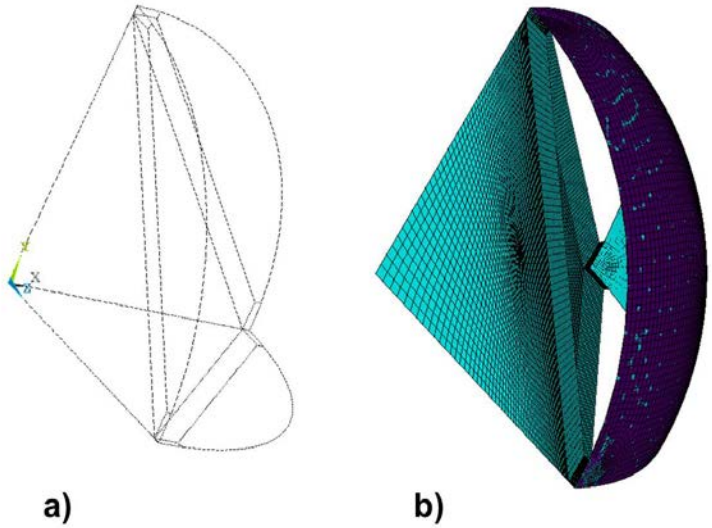

Figure 5.2. a) Line model of eighth-symmetry model of spherical assembly. b) Meshed model of spherical assembly.

Table 5.2. Material constants for linear isotropic material model.

Material Constants	
E_{avg}, MPa	109.41
ν_{wf}	0.3
ρ, kg/m^3	1024.16
t, mm	0.3

Radial displacements occurring along the boundary areas (highlighted in red in Figure 5.3) were averaged for each of the pressure levels: 7 kPa, 35 kPa, and 70 kPa. These averaged deflections were imposed as defined radial displacements on the same

loading boundaries of the fabric panel to simulate the pressure loading. The averaged displacements used were 0.143 mm (7 kPa), 1.336 mm (35 kPa), and 4.311 mm (70 kPa). These simulated pressures are used throughout the current analysis, however, it is to be noted that these approximated deflections would change as the geometry and/or loading scheme are changed. The variation in simulated deflection due to change in geometry and/or loading scheme was considered to be minimal with respect to the overall response of the system.

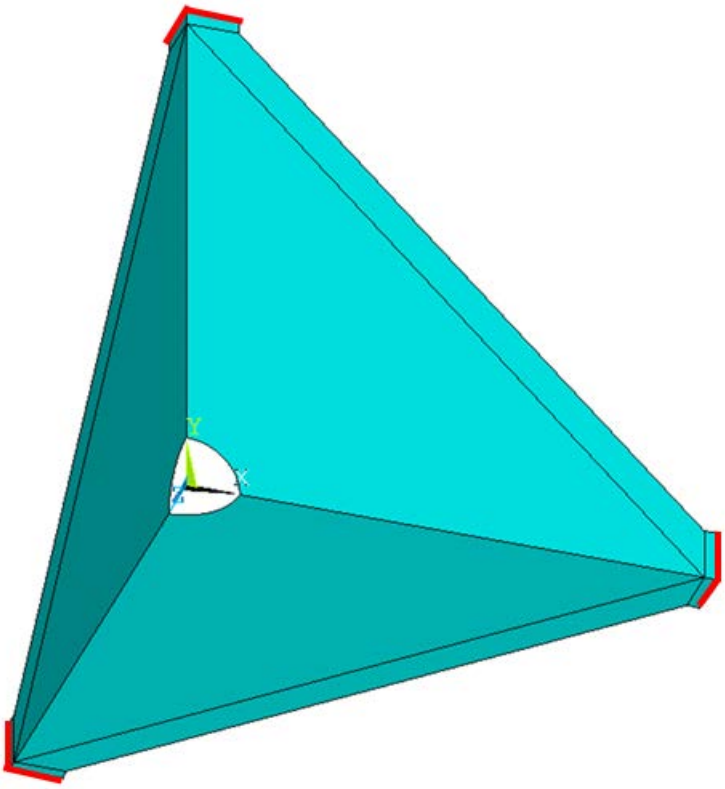

Figure 5.3. Diagram highlighting the loading boundaries were radial deflections were averaged.

With the simulated pressure loading defined, the panel geometries could be analyzed. It was found that a quarter-symmetry model of the planar geometry would be computationally advantageous. To verify the accuracy of the quarter-symmetry model, the deflection contour of the full geometry model was compared with the corresponding plot for a quarter symmetry model (Figure 5.4). It can be seen that the quarter-symmetry model accurately captures the response of the full fabric panel geometry. Minimum displacement for both the quarter symmetry model and full model was -2.45 mm. Further

consistency exists in the deflection along the hypotenuse edge; where a slight dip occurs at the minimum displacement

With a verified quarter symmetry model created, nonlinear FE simulations were performed to define the correlation between the various boundary conditions and resulting flatness of the multiple geometries and loadings. To evaluate the geometric precision produced by the imposed conditions, again a RMS deflection was calculated using Equation (3).

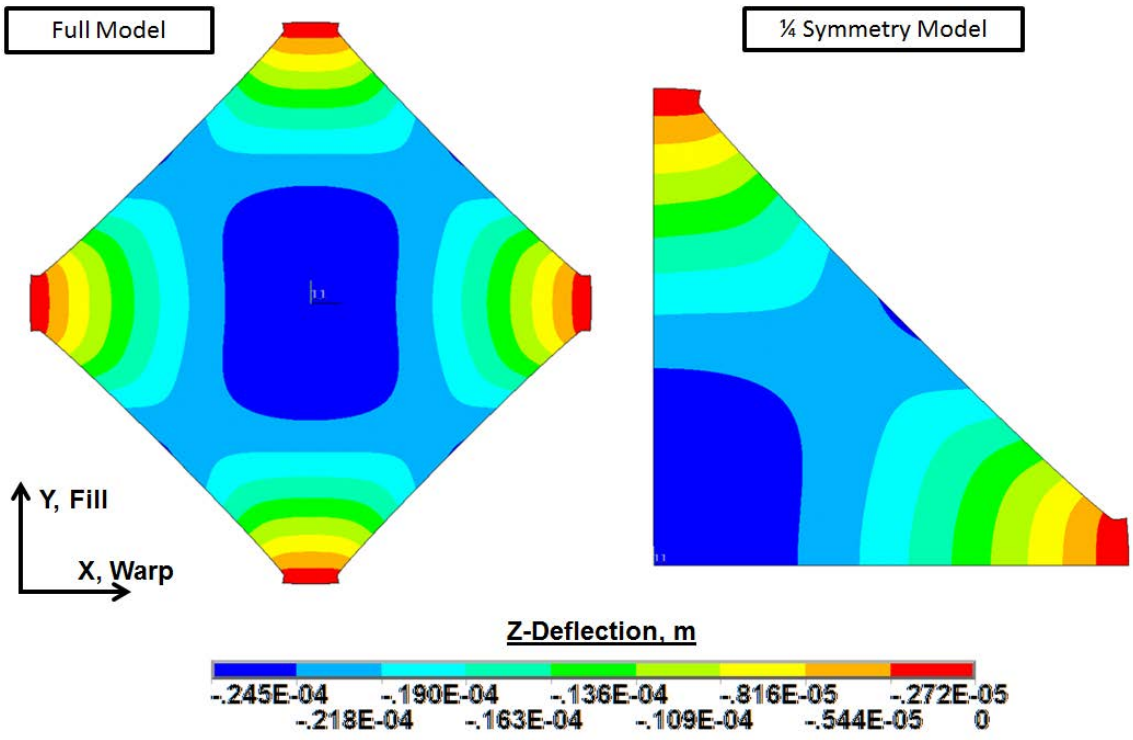

Figure 5.4. Left, ANSYS FEA deflection contour for the full model of the fabric panel. Right, ANSYS FEA deflection contour for the 1/4 symmetry model of the fabric panel.

5.3 LOADING GEOMETRY DESIGN FOR TRI-LATERAL CORNER

This study examined the influence of support connections on the flatness of the fabric panel under the approximated pressure loading. Figure 5.5 presents appropriately meshed models of the fabric panel with four support connections and eight support connections. To analyze the effect of support connections on the flatness of the fabric panel the out-of-plane deflections were examined where the out-of-plane deflections are due to gravity loading. Analysis involved varying the number of connections between the panel and sphere to determine the effect of connections on flatness.

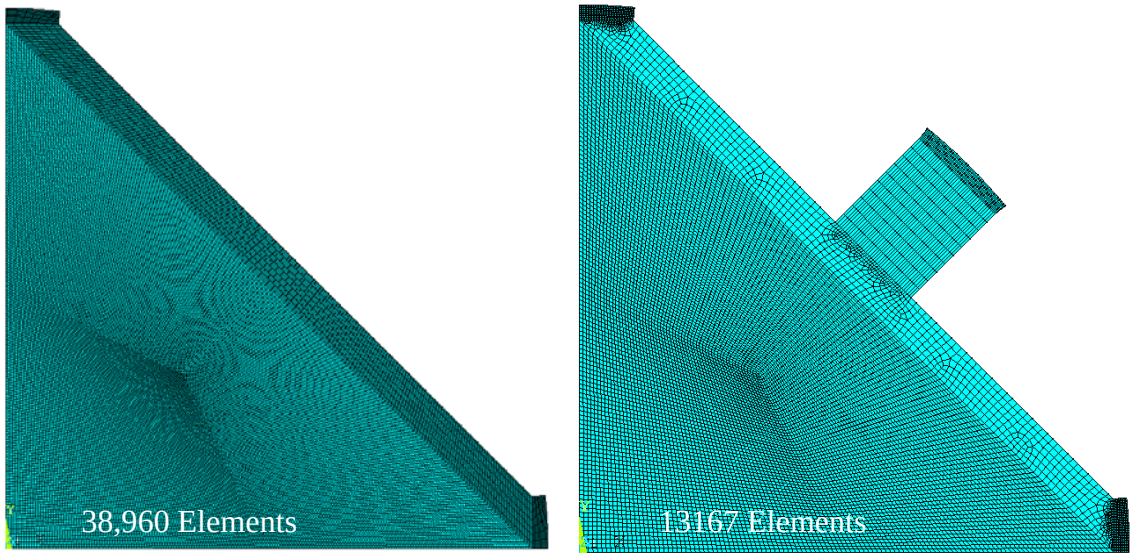

Figure 5.5. a) Meshed model of fabric panel with 4 loading connections. b) Meshed model of fabric panel with 8 loading connections.

The Resulting deflection contours were used to evaluate the response of each of the geometries at the three pressure levels (7 kPa, 35 kPa, and 70 kPa). The out-of-plane deflection contours for the fabric panel with four total connections are shown in Figure 5.6 and the contours for the fabric panel with eight total connections are shown in Figure 5.7.

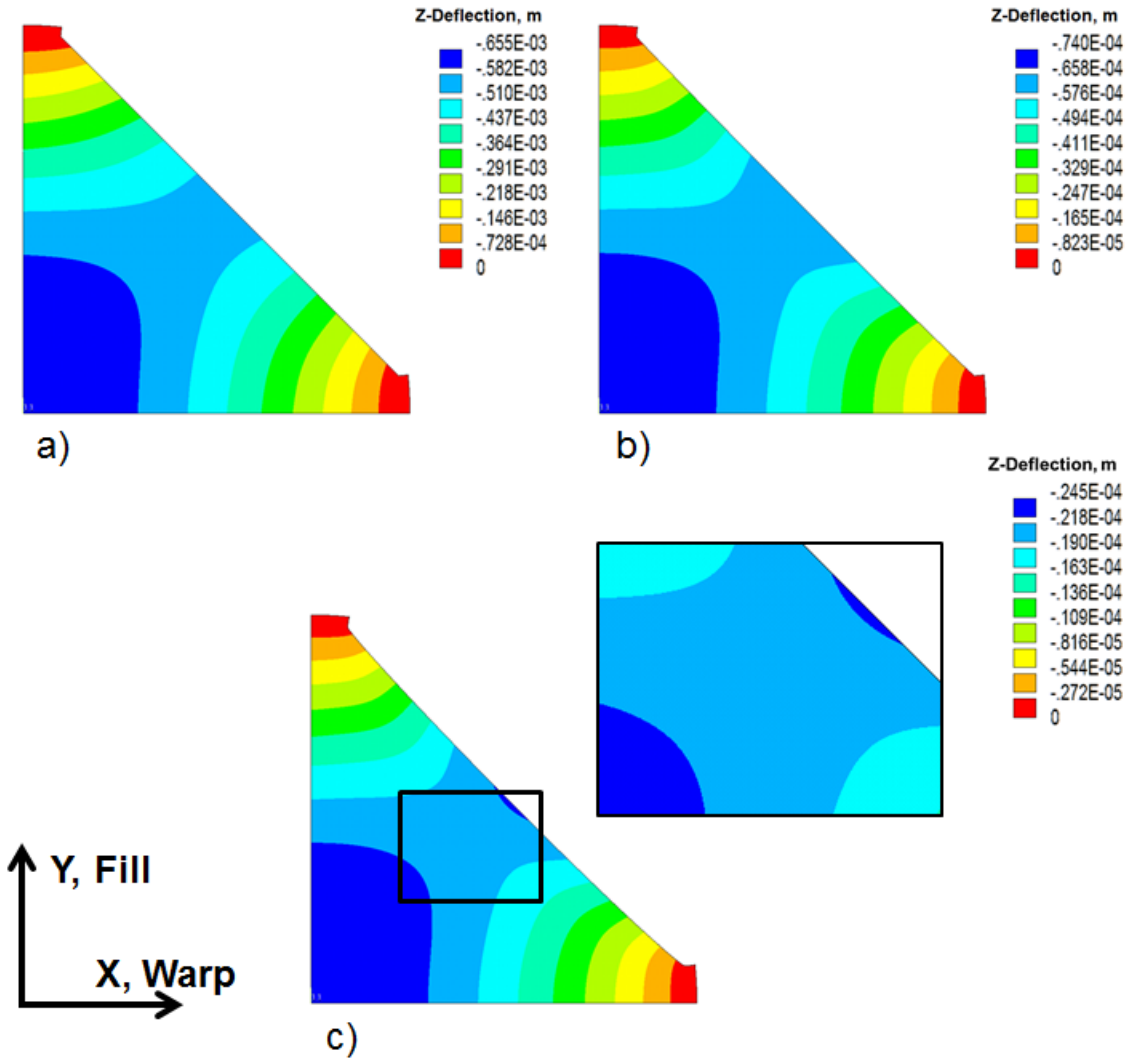

Figure 5.6. ANSYS FEA z-deflection contour plot of the fabric panel with 4 support connections loaded at the pressure levels a) 7 kPa, b) 35 kPa, and c) 70 kPa. The wrinkling area is defined for the 70 kPa pressure level.

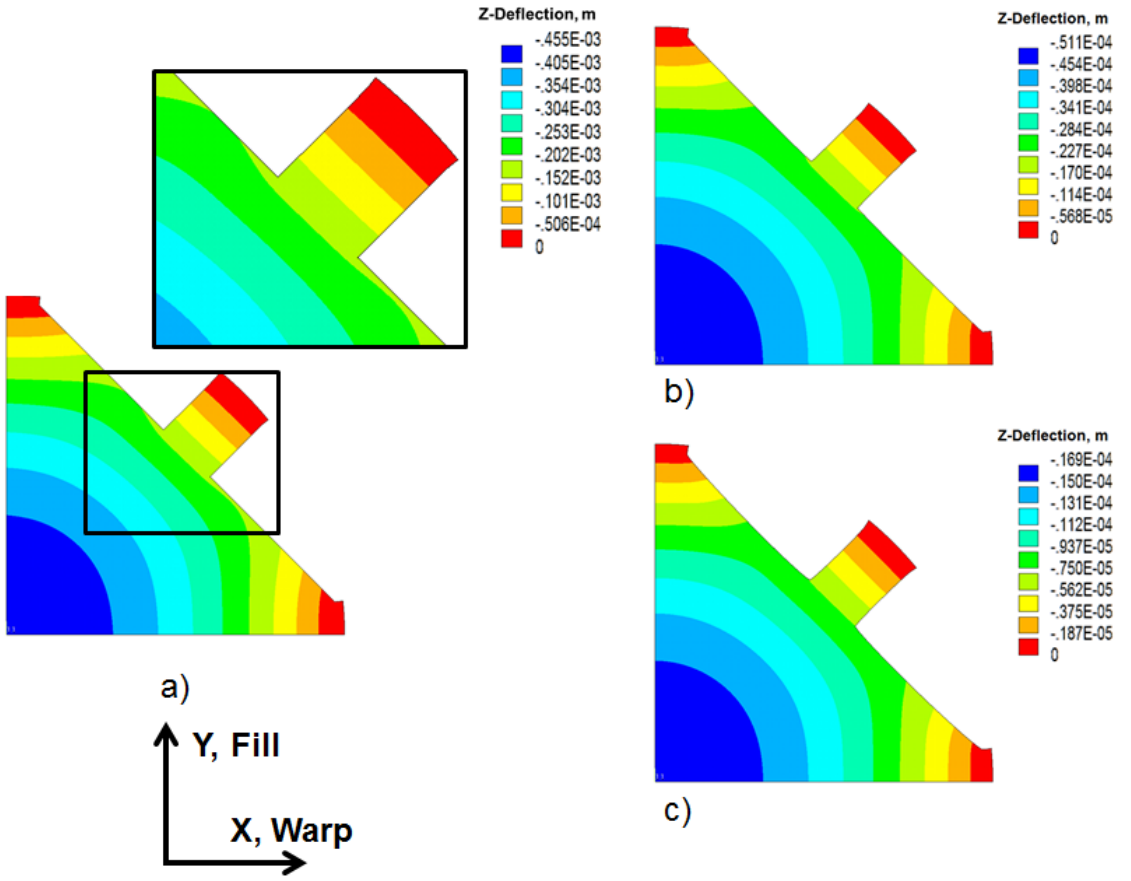

Figure 5.7. ANSYS FEA z-deflection contour plot of the fabric panel with 8 support connections loaded at the pressure levels a) 7 kPa, b) 35 kPa, and c) 70 kPa. The wrinkling area is defined for the 7 kPa pressure level.

It was seen that a wrinkle began to form in the fabric panel with four connections as the pressure level increased. Due to the level of loading the deflection scales for panel are all negative. It should be noted that wrinkling occurs in areas were the deflection transitions from most negative to less negative and back to a larger negative value. In contrast, the presence of wrinkling decreased as the pressure level increased in the fabric panel with eight connections. The height of the wrinkle developed using for support connections is 5.5 µm. The eight support connections reduced the wrinkling at higher loading (wrinkle height of 3.75 µm), although wrinkles were still present. Wrinkling patterns and magnitudes for the fabric panel did not correspond to those of materials traditionally used in large aerospace inflatables (such as Kapton with wrinkle amplitudes on the order of millimeters), but that was expected because the polyurethane-coated

nylon has different material properties. For further evaluation, the RMS out-of-plane deflections were compared in Figure 5.8.

As expected, the RMS deflection decreased for each simulated pressure loading as the number of support connections increased. A large difference (0 .0314 mm) was seen between the RMS deflections for the four connections versus the eight connections at the lower loading levels. The difference in RMS deflection decreased as the pressure level increased. At the higher loading level the difference in RMS deflection (0.0012 mm) became significantly less. Within standard operating pressures for this system (55 kPa to 83 kPa) the increase in performance becomes negligible. Furthermore, eight connections would add significant complexity to the manufacturing of the inflatable system. It appears that the four support connections are probably the most efficient scheme for supporting the fabric panel. It is to be noted that numerous schemes exist for supporting geometry such as this. The two loading schemes considered in this study were the two most straightforward with respect to manufacturing.

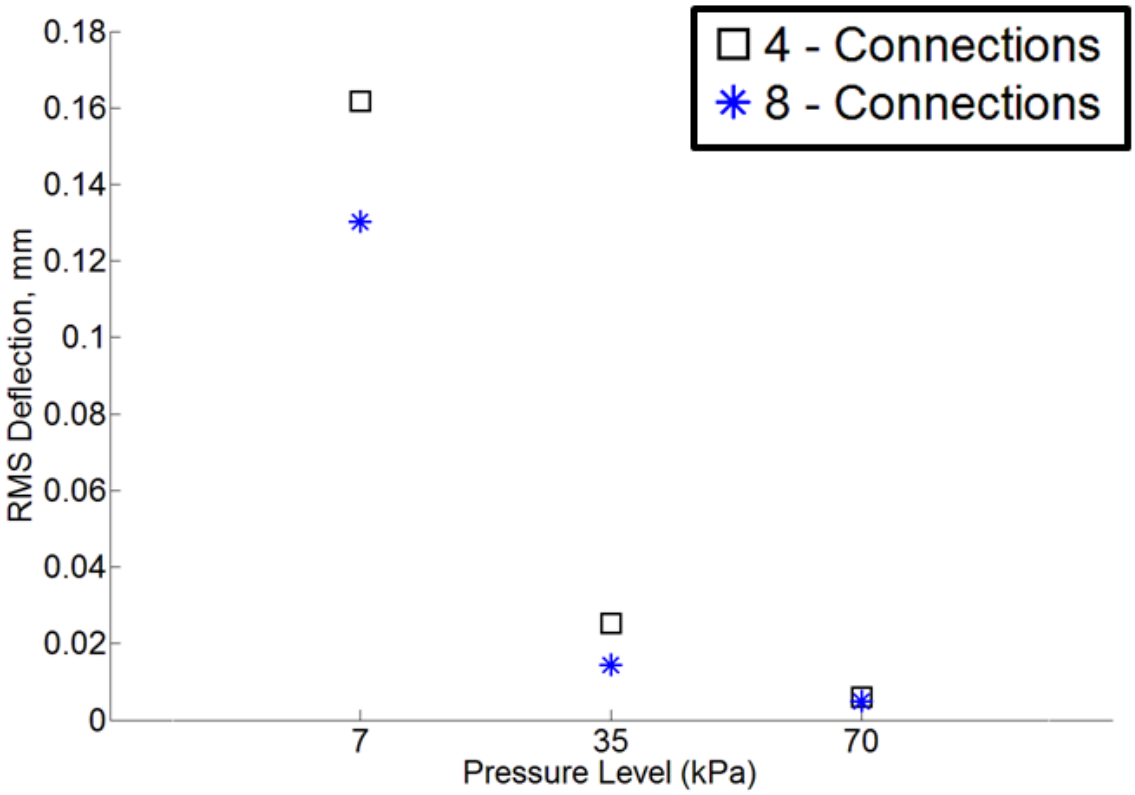

Figure 5.8. RMS deflections of the fabric panel comparing 4 total connections and 8 total connections.

5.4 PANEL CENTER GEOMETRY DESIGN FOR TRI-LATERAL CORNER

Next, based upon the most efficient loading scheme, variations in the fabric panel geometry were considered. Figure 5.9 shows the various fabric panel geometries considered for this study. Two main ideas for the fabric panel geometry were considered: complete-center geometry and free-center geometry. In turn, the free center design incorporated three different options: square, diamond and circular (Figure 5.9).

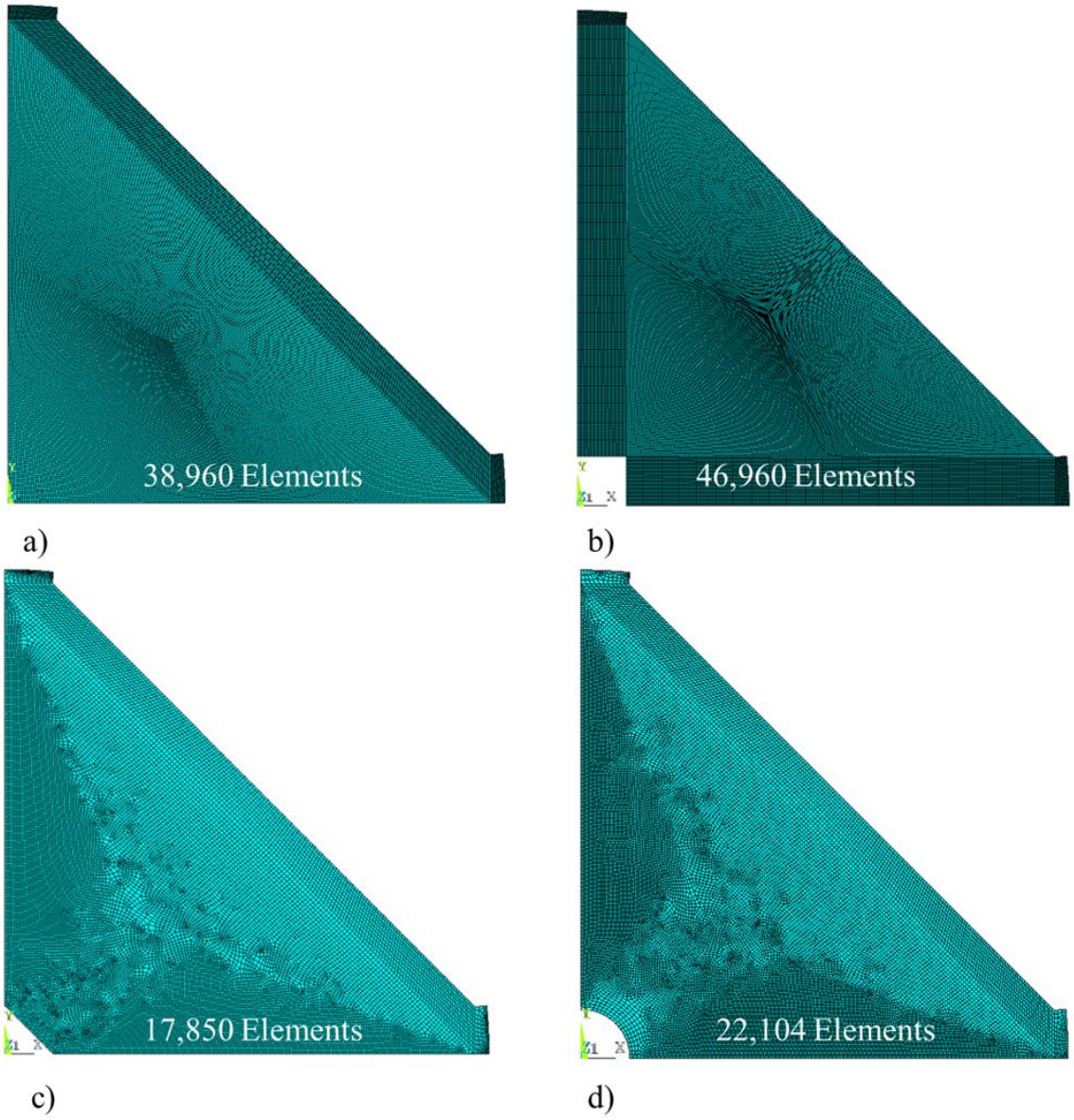

Figure 5.9. a) Meshed model of complete center geometry. b) Meshed model of the square free center geometry. c) Meshed model of the diamond free center geometry. d) Meshed model of circular free center geometry.

To compare design performance, each of the fabric panel geometries was analyzed under the 70 kPa pressure level and the 0° material orientation, and the resulting out-of-plane deflection contours, First Principal Stress contours, and out-of-plane RMS deflections were considered. Further analyses were performed to evaluate the influence of material direction on the achievable geometric control. Figure 5.10 shows a diagram of the material orientations considered for this analysis. The material orientations were the same as those considered in Chapter 3 of this dissertation. These orientations were applied in the FE models as diagramed in Figure 3.7.

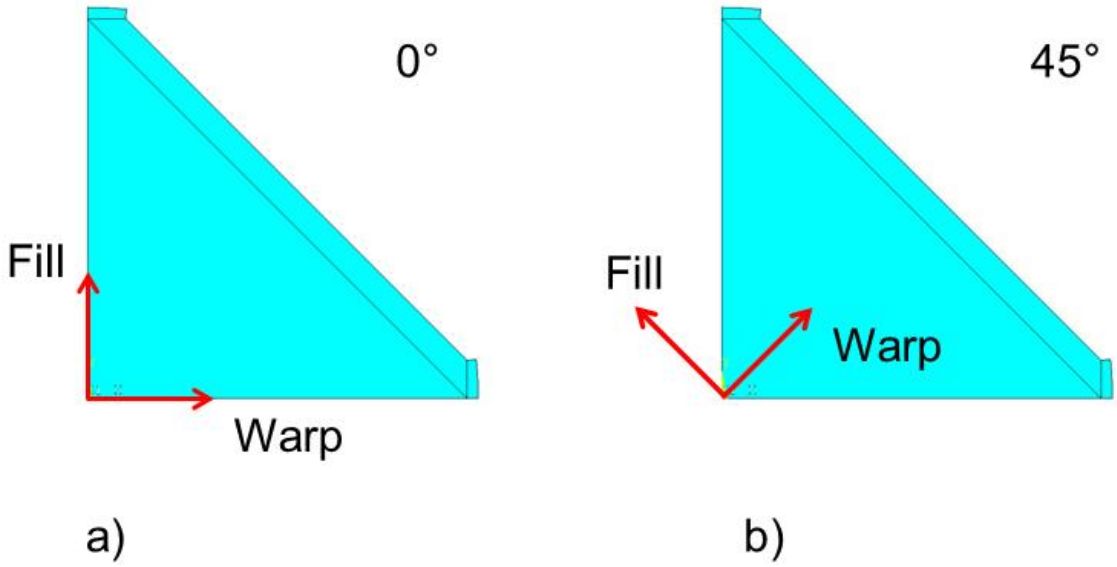

Figure 5.10. a) Diagram of the warp and fill material directions for the 0° material orientation. b) Diagram of the warp and fill material directions for the 45° material orientation.

First, a design study was performed to evaluate the effect of center geometry size on the response of the fabric panel. The center geometries were varied based upon a percentage of the overall radius, R, of the inflated sphere supporting the fabric panel. A radius of R=125 mm was used throughout the current study. Figure 5.11 presents the RMS deflections for each of the free center geometries as the characteristic length was changed.

The RMS deflections converged to the complete center model (RMS=0.0059 mm) once the characteristic length was below 6.25 mm. The RMS deflections of the diamond

and square geometries began to increase drastically once their characteristic lengths became larger than 25 mm. The circular geometry was seen to be more stable than the other free center geometries for the entire range of characteristic lengths; furthermore, it improved upon the response of the complete center model at larger characteristic lengths. The circular free center model achieved a RMS deflection of 0.0047 mm at a characteristic length of 25 mm and a RMS deflection of 0.0054 mm at a characteristic length of 50 mm. Once the characteristic length was increased past 12.5 mm the response for the majority of the free center geometries became unstable. Thus, the characteristic length of 12.5 mm was an upper bound on the stability of the geometry, and with a length less than 12.5 mm manufacturing issues may arise.

Next, the Z-deflection contours and First Principal Stress contours were examined to further evaluate the free center geometries. Each of the geometries was analyzed with a characteristic length of 12.5 mm, and the fabric panel had the 0° material orientation and was loaded under the 70 kPa pressure level. Figure 5.12 presents the Z-deflection contours for the various fabric panel geometries. The First Principal Stress contours are presented in Figure 5.13.

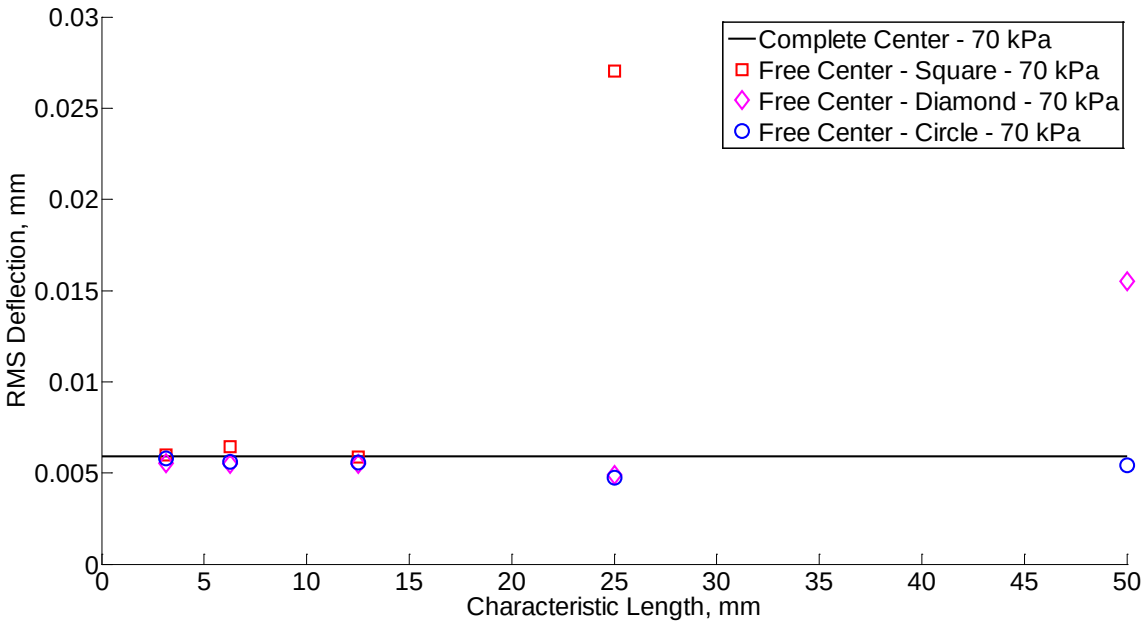

Figure 5.11. RMS deflections of the three free center geometries considered. The RMS deflections are plotted against the characteristic length of each of the geometries in terms of the overall radius of the fabric panel.

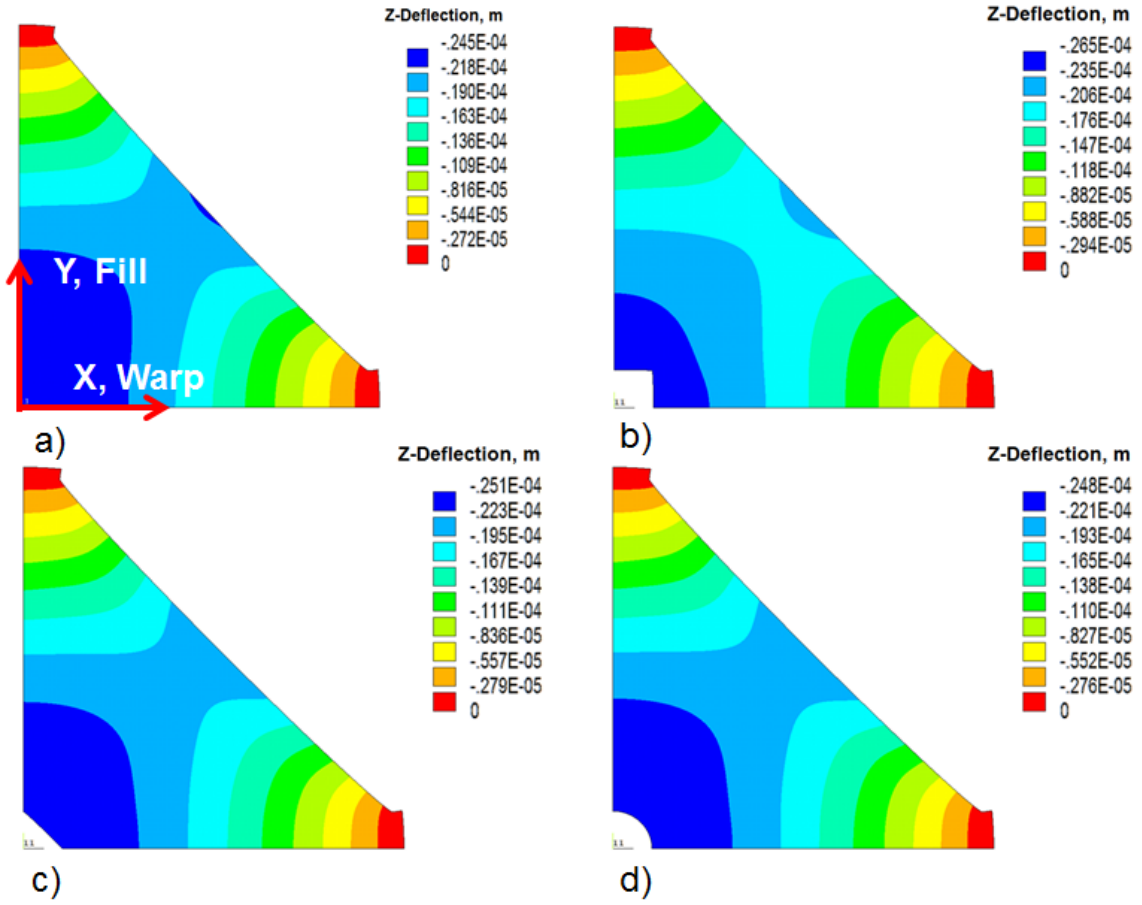

Figure 5.12. ANSYS FEA z-deflection contours comparing the complete center geometry (a) to the free center geometries; square center (b), diamond center (c), and circular center (d).

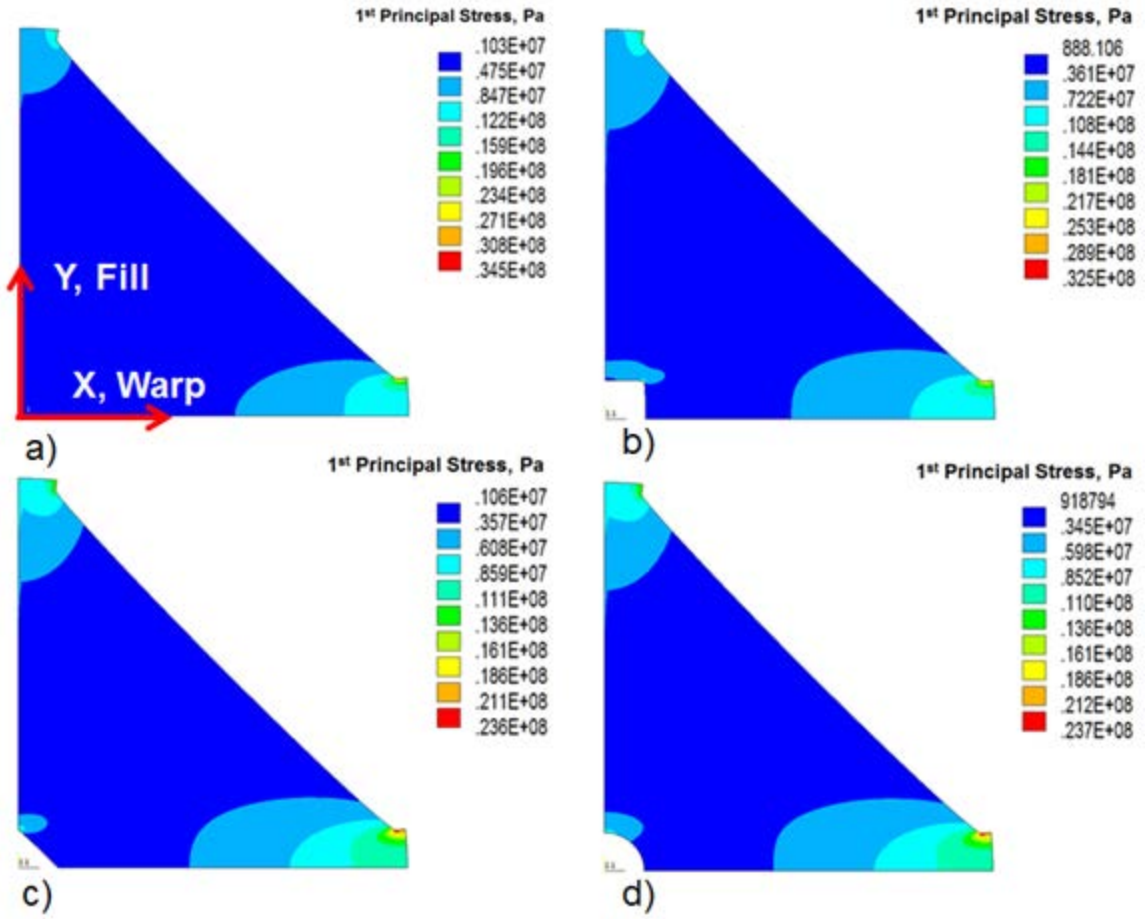

Figure 5.13. ANSYS FEA First Principal Stress contours comparing the complete center geometry (a) to the free center geometries; square center (b), diamond center (c), and circular center (d).

The on-set of wrinkling became more apparent near the center in the square free center geometry. However, the onset of wrinkling was less pronounced in the diamond and circular free-center geometries. The stresses were seen to decrease in each of the free center geometries compared to the complete center, however additional stress concentrations developed along the corners of each of the center geometries. It is also noted that the anti-symmetric stress contours of each of the geometries were attributed to orthotropic material properties of the coated woven nylon fabric. Based upon the analysis of the deflection and stress contours, the circular free center geometry presented the most desirable response.

For further understanding, the circular free center and complete center geometries were used to examine the influence of material orientation on the response of the fabric

panel. The out-of-plane RMS deflection was used to analyze the effect of material orientation, and the results for this analysis are shown in Figure 5.14. The label "CC" refers to the complete-center geometry, and the label "CIR" refers to the circular free-center geometry.

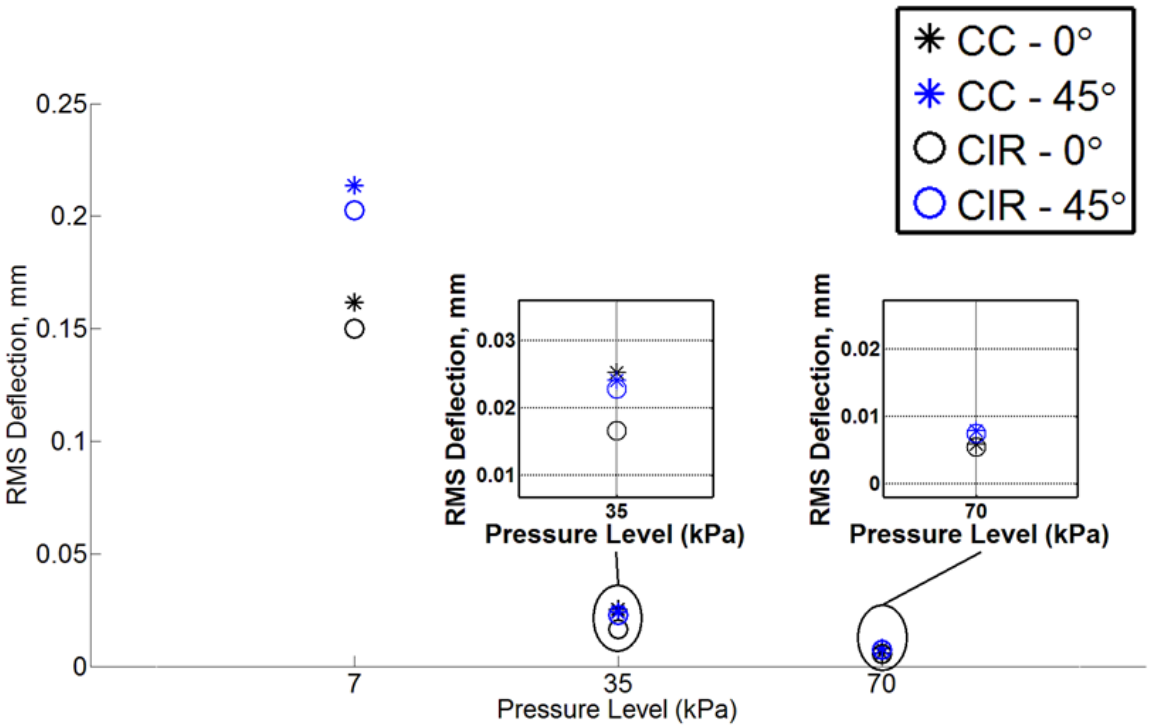

Figure 5.14. RMS deflections for complete and circular free center geometries. The points plotted correspond to changes in loading and material orientation of the fabric panel.

It was seen that the 0° material orientation reduced the out-of-plane deflection for both geometries at each loading level. However, as the loading level increased the variation in response between the 0° and 45° material orientations became minimal. In Scherrer, 2012 and Fulcher et al., 2013 photogrammetry and FEA analysis were performed on a single triangular panel of the same fabric, and it was also seen that as loading increased the influence of material orientation became negligible. Furthermore, as the loading was increased the difference in response between the free-center and complete center geometry became less.

5.5 FINAL PANEL GEOMETRY FOR TRI-LATERAL CORNER DESIGN

The greatest amount of geometric control was achieved using the circular free center geometry, 0° material orientation, and 70 kPa pressure level. Figure 5.15 presents a comparison of the final results of the current study to deflection/flatness requirements of both terrestrial and space-based engineered systems. For terrestrial radar decoy applications, a flatness of a half wavelength is required for acceptable performance [11]. Terrestrial radar decoys operate in a frequency range of 10 GHz to 40 GHz, so at 40 GHz a half wavelength measures 3.75 mm. For space-based radar reflectors a 2dB loss in transmission is considered to be a practical performance requirement [45]. Thus at an operating frequency of 20 GHz, a RMS deflection of 0.58 mm is required for acceptable performance. It is also noted here that if a spaced-based radar reflector operated at 40 GHz the RMS requirement would become 0.17 mm. The system designed (RMS=0.0056 mm) meets or exceeds all of the above mentioned performance requirements for terrestrial or spaced-based applications.

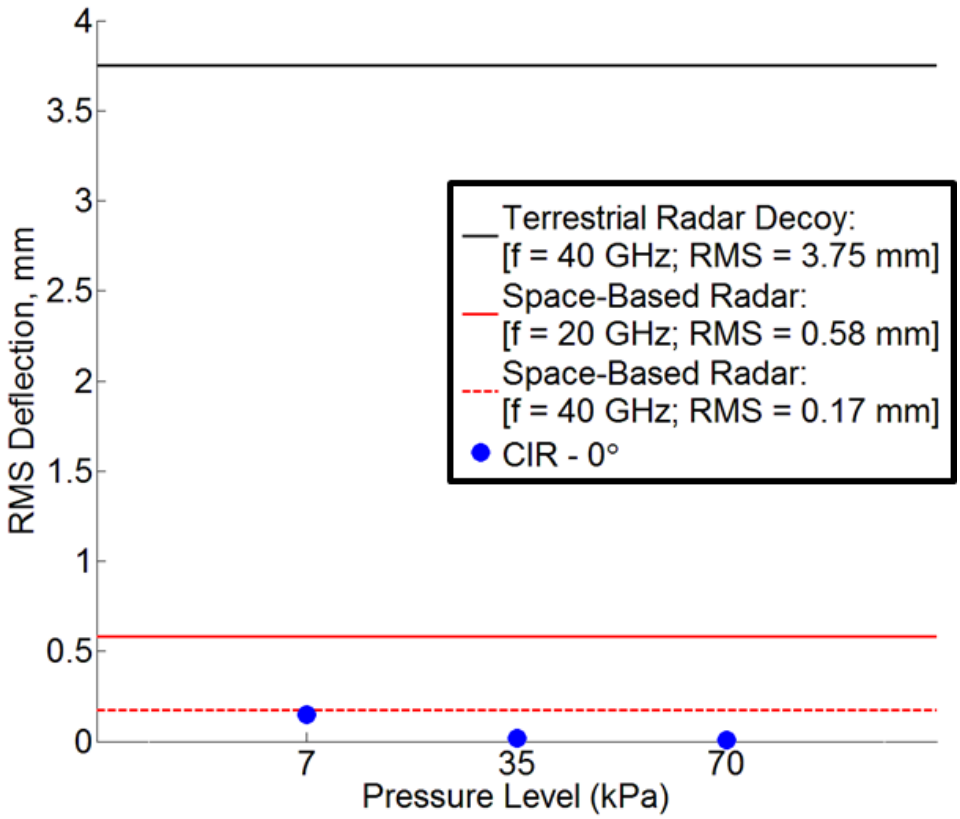

Figure 5.15. RMS deflection for the circular free center geometry versus the flatness requirement for a terrestrial radar reflector.

Using the modeling methodology from the previous chapters of this dissertation, a design was developed for the internal tri-lateral corner geometry. The final design of the tri-lateral corner is shown in Figure 5.16. Also the proposed octahedral set of tri-lateral corners is shown in Figure 5.16.

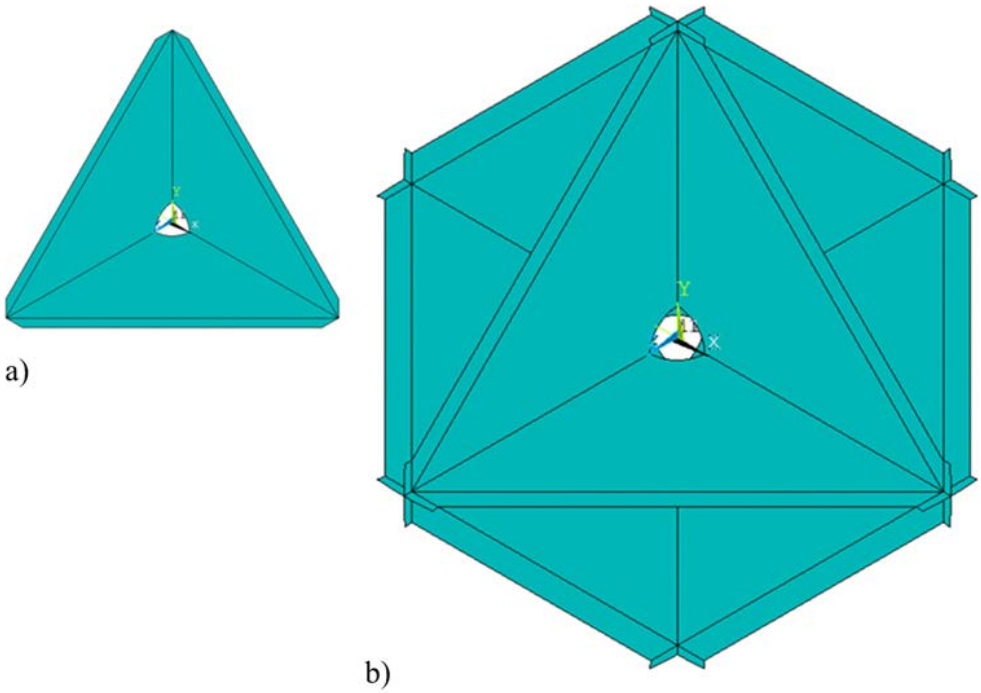

Figure 5.16. a) Single tri-later corner incorporating proposed geometry from design analysis. b) An octahedral set of tri-lateral corners that will be supported by the inflated sphere.

5.6 ANALYSIS OF THE PATHFINDER INFLATABLE SYSTEM

After the design of the internal structure was finished, the new inflatable system was analyzed. A range of internal pressure was imposed and calculated deflections were compared to expected performance requirements. Figure 5.17 is a model of the pathfinder inflatable system with a portion of the outer sphere removed so the internal structure can be seen. The pathfinder system integrates canonical structures that are common to many inflatable systems. This full model was used to verify the analyses performed on the individual components.

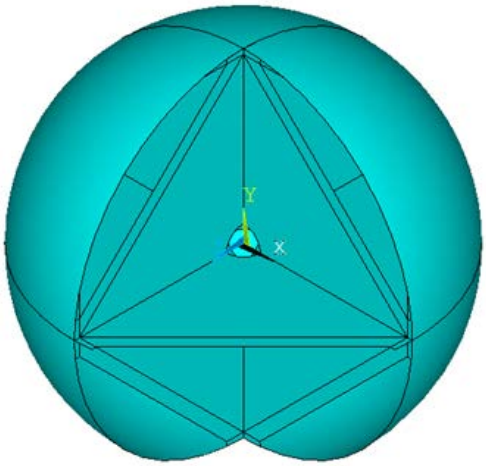

Figure 5.17. Model of the pathfinder inflatable system.

FE simulations were carried out using ANSYS 13.0 FE software. Finite element models of the inflatable system were created and meshed with 4-node shell elements (SHELL181), which have six degrees of freedom (DOFs) at each node. Gravity loading was applied perpendicular to the plane of the fabric panel, and stress stiffening effects were included. Large deflection nonlinear analysis was used to solve for the static deflection response of the pathfinder system. The material model described in Table 5.1 was again used for the FE simulations. A meshed model of the pathfinder system is shown in Figure 5.18. The ANSYS APDL batch files for the inflatable pathfinder system are included in Appendix A.

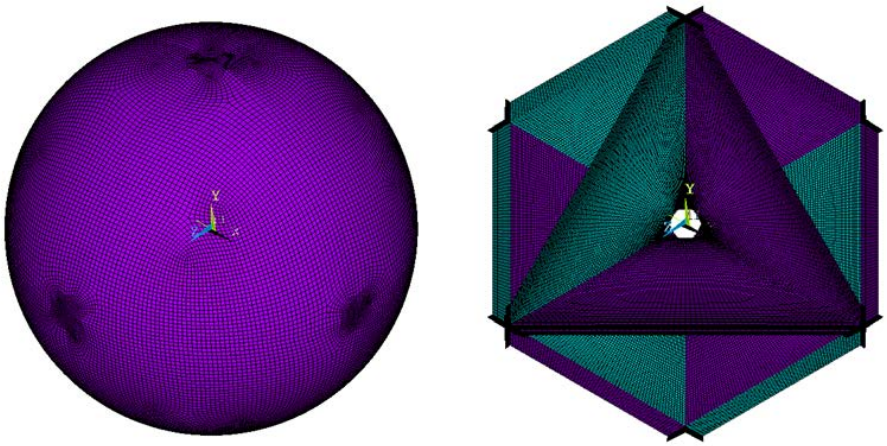

Figure 5.18. a) FE model of pathfinder system showing the meshed outer sphere. b) FE model of pathfinder system showing the meshed internal structure. The model incorporated 76,673 elements.

Simulations were performed for different levels of inflation pressure varying from 7 kPa to 70 kPa. With gravity loading applied, the greatest amount of deflection occurs in the panels that are perpendicular to the gravity field. Thus, the deflection response of the panels perpendicular to the gravity field was the focus of the analysis. Considering these panels allowed for a direct comparison to results from the previous study of the single panel geometry. Through comparison with the single panel results, it was seen that the single panel response correlated well with the full model simulations. So, for many purposes, a single panel model should suffice.

5.6.1 MATERIAL MODEL COMPARISON FOR OUTER SPHERE

The inflatable pathfinder system was initially computed for a range of inflation pressures (7 kPa – 70 kPa). Through this analysis, correlation was established between the response of the full model of the system and the single panel model studied earlier. However, issues with convergence occurred when the outer sphere of the pathfinder system was inflated above the 48 kPa pressure. Figure 5.19 presents the out-of-plane deflection contours for the pathfinder model analyzed with the linear orthotropic material model presented in Table 5.1.

A large wrinkle begins to form along the hypotenuse edge of the panel above a pressure of 30 kPa. The propagation of this wrinkle toward the lower leg of the panel, as seen in the 30 kPa and 40 kPa subplots of Figure 5.19, was thought to be the cause of the convergence problem. As the wrinkle becomes larger the deflection begins to increase along the corners of the loading boundary. The behavior of the loading boundaries affects the response of the model, and with the creation of these high-deflection areas inconsistent values were introduced into the FE solver. Again, as noted previously in this chapter, wrinkling areas are areas where deflection begins most negative then becomes less negative and then becomes more negative. Also included on these plots are areas were the deflection goes from negative to positive and these areas are also location of possible wrinkling. A full set of out-of-plane deflection contours can be found in Appendix B.

An isotropic material model for the outer sphere was used to overcome the problem with convergence. Table 5.2 presents the linear isotropic sphere model considered for the comparison study. The linear isotropic sphere model was defined

using the average of the elastic modulus in the warp direction and the elastic modulus in the fill direction. For each pressure level the RMS deflection (Equation (3)) of a panel corresponding to the panel that was studied in the single panel analysis was calculated. Figure 5.20 plots the RMS deflection results for each of the material model analyses.

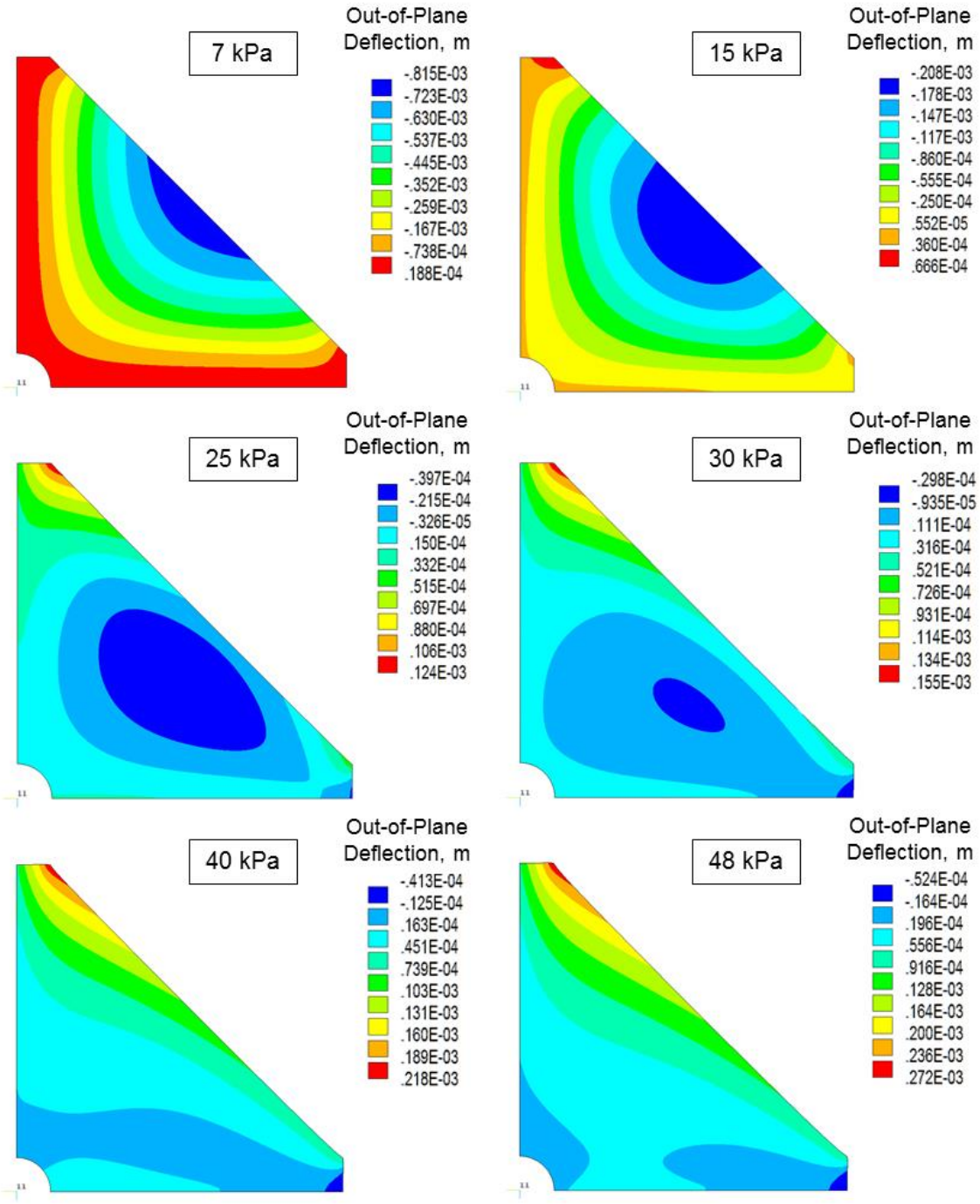

Figure 5.19. Out-of-plane deflection contours for the inflatable pathfinder system modeled with linear orthotropic material model.

The RMS deflections for the orthotropic outer sphere steadily decrease as the pressure is increased until a pressure of 30 kPa is reached. As was discussed earlier a large wrinkle begins to propagate at this pressure and the RMS deflection verifies the effect of the wrinkle on the response of the pathfinder system. After a pressure of 30 kPa is reached the RMS deflection begins to increase for each pressure level until convergence became a problem at a pressure level of 48 kPa. It can be seen that the pathfinder system model with the isotropic material model for the outer sphere and the single panel model converge together above a pressure level of 25 kPa. Thus, the response of the single panel is seen to be correlated to the response of the inflatable pathfinder system.

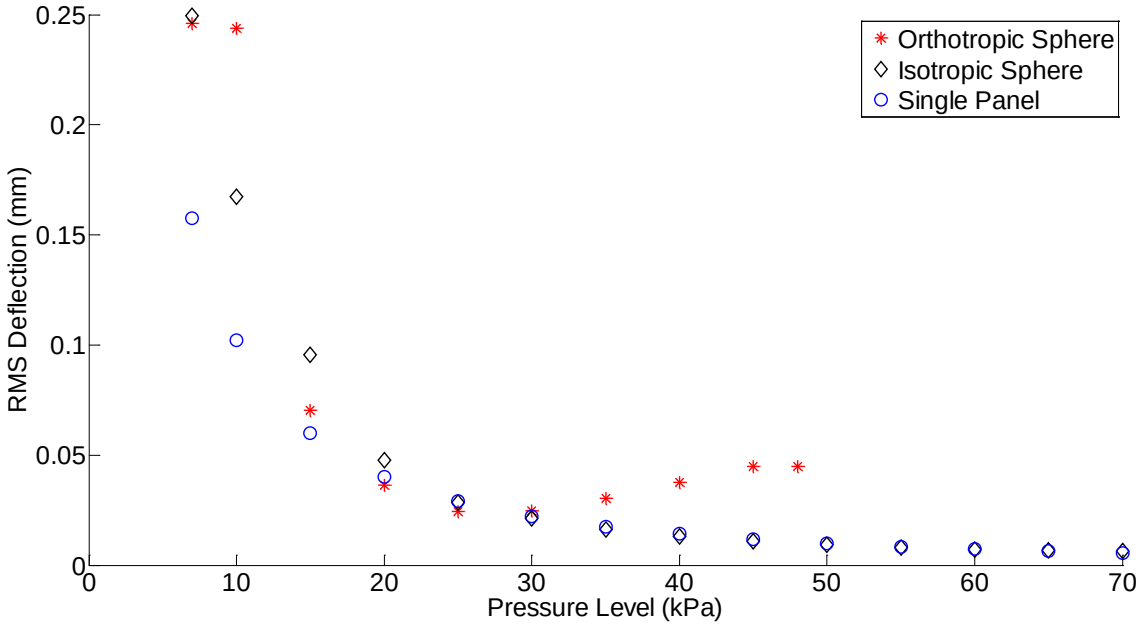

Figure 5.20. RMS deflections for comparison analysis.

5.6.2 ORTHOGONALITY OF TRI-LATERAL CORNER

Upon verification using an isotropic material model for the outer sphere, further analysis could be carried out to examine the performance of the inflatable pathfinder system. Since the original concept of the pathfinder system was to act as a radar reflector, there are two primary considerations. First, the levels of flatness that can be achieved for each panel of the tri-lateral corner, and second, the orthogonality of each

panel in the tri-lateral corner. Each panel should be perfectly perpendicular to each of the other panels for optimal radar performance.

The modal assurance criterion (MAC) was used as a metric for the orthogonality of a tri-lateral corner in the octahedral set supported in the pathfinder system. Equation (4) was used to calculate the MAC number for each set of panels in a tri-lateral corner.

$$MAC = \frac{\left([z_{ij}]^T[z_{ji}]\right)^2}{[z_{ij}]^T[z_{ij}][z_{ji}]^T[z_{ji}]} \qquad \text{for i,j = X, Y, or Z} \qquad (4)$$

The MAC number establishes consistency and orthogonality between modal vectors. For the purposes of this work the MAC number will be used to establish the orthogonality between the out-of-plane deflection vectors of each of adjacent set of panels in a tri-lateral corner. The closer the MAC number is to unity the better the level of consistency and orthogonality between the two vectors [76]. Figure 5.21 presents the MAC number for each of set of adjacent panels in the tri-lateral corner that had the greatest amount of deflection with respect to the complete octahedral set. Three sets of MAC numbers are plotted, each set represents a set of adjacent panels (i.e. the XY-XZ set

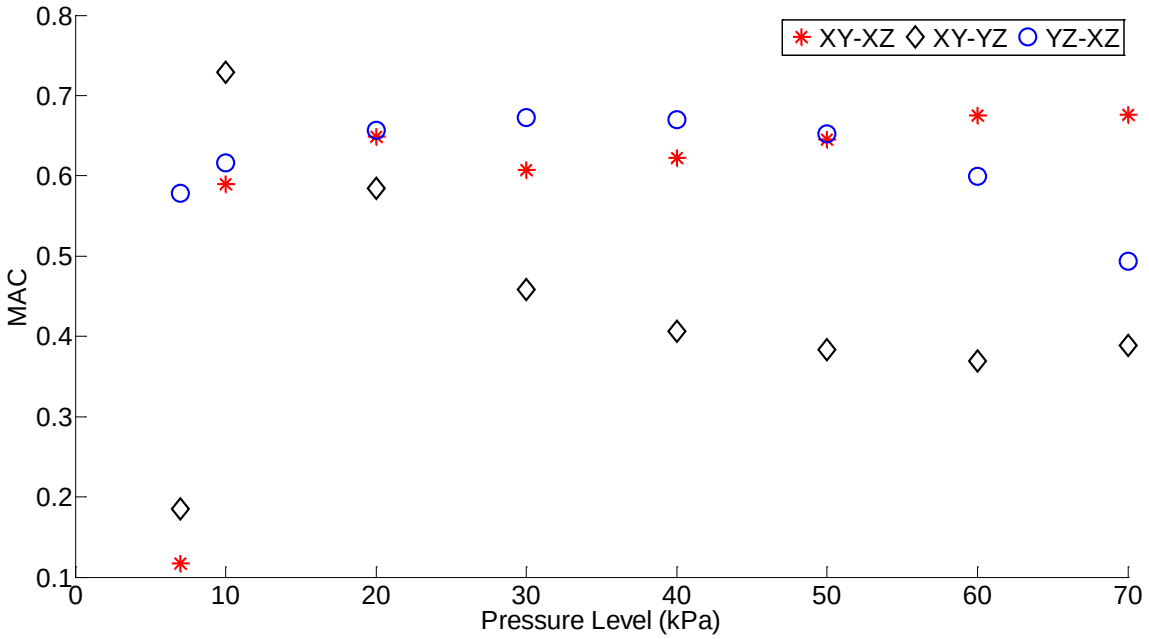

Figure 5.21. Plot of MAC number versus inflation pressure.

compares the orthogonality of the panel in the XY plane and the panel in the XZ plane).

It can be seen that the XY and XZ planes become more orthogonal as the pressure is increased. For the majority of pressures the MAC numbers for the XY-XZ comparison are between 0.6 and 0.7. Orthogonality of XY and YZ planes was seen to initially increase to above a MAC number of 0.6, but for highest pressure the MAC number is below 0.5. Orthogonality becomes worse for the set of panels that consider the panel in the YZ plane for nearly all higher pressures. To further examine what was physically occurring in each panel, deflection contours were created for each panel in the tri-lateral corner under 7 kPa, 20 kPa, and 70 kPa inflation pressures. The out-of-plane deflection contours for each panel of the tri-later corner are shown in Figure 5.22 (7 kPa), Figure 5.23 (20 kPa), and Figure 5.24 (70 kPa). Gravity loading is applied parallel to the Y-direction for this analysis.

Examining the contours, the panels in the XY and XZ planes have a constant deflection pattern although the magnitude of deflections changes. However the deflection pattern of the panel in the YZ plane varies for each of the pressure levels. The panel in the YZ plane has a more consistent deflection pattern when inflated at 20 kPa which explains why the MAC number is optimized at that pressure level. Also, the deflection pattern becomes more varied at the 70 kPa pressure level. The higher level of variance in the deflection pattern at higher pressures caused the decrease in orthogonality for the adjacent panels that include the YZ panel. For radar performance the orthogonality at intersections of the panels has the most influence on reflectivity. Further efforts, beyond the scope of the current work, could apply radar analysis tools to evaluate the orthogonality of the geometries in more detail.

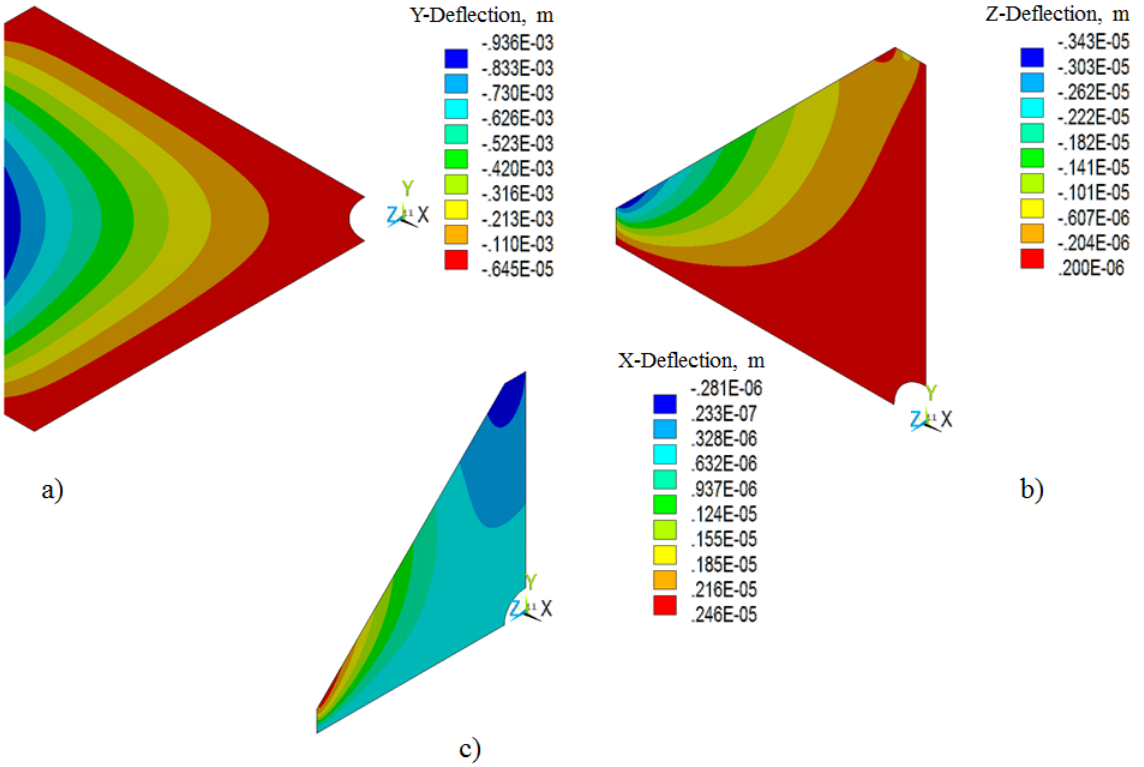

Figure 5.22. a) Out-of-plane deflection contour of the panel in the XZ plane. b) Out-of-plane deflection contour for the panel in the XY plane. c) Out-of-plane deflection contour for panel in the YZ plane. All contours are for an inflation of 7 kPa.

.

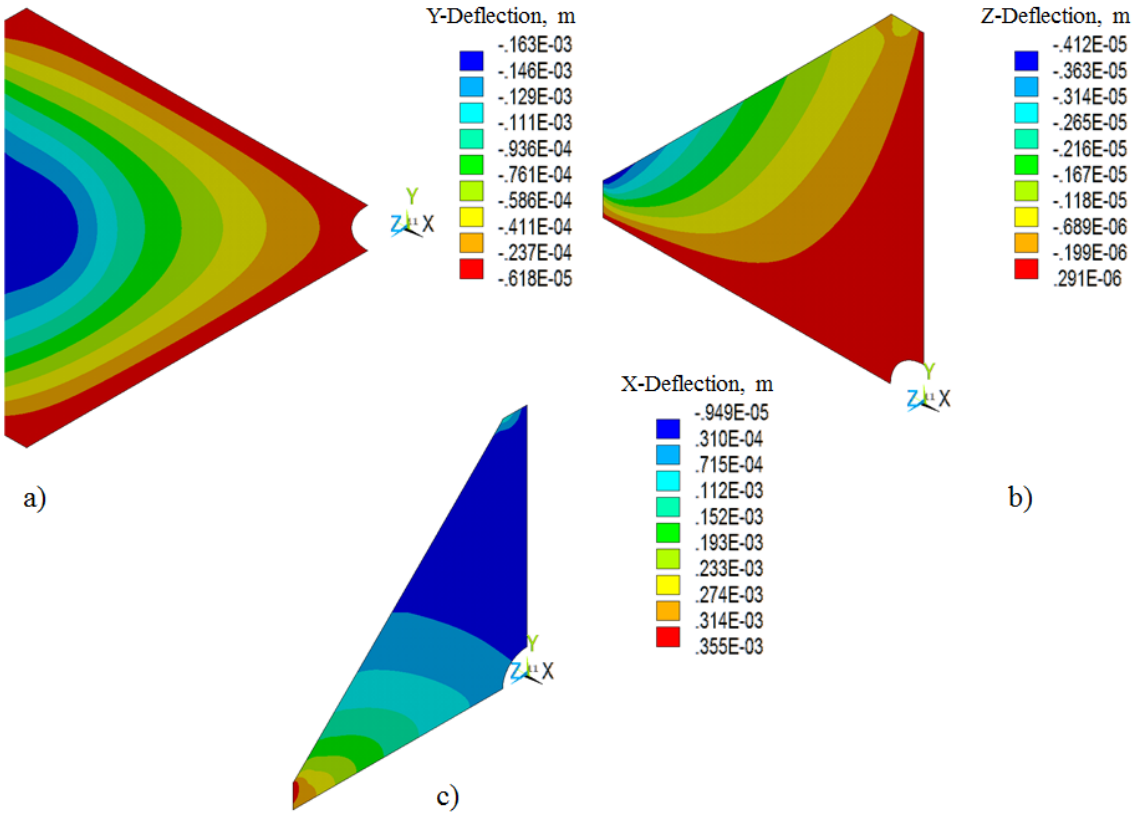

Figure 5.23. a) Out-of-plane deflection contour of the panel in the XZ plane. b) Out-of-plane deflection contour for the panel in the XY plane. c) Out-of-plane deflection contour for panel in the YZ plane. All contours are for an inflation of 20 kPa.

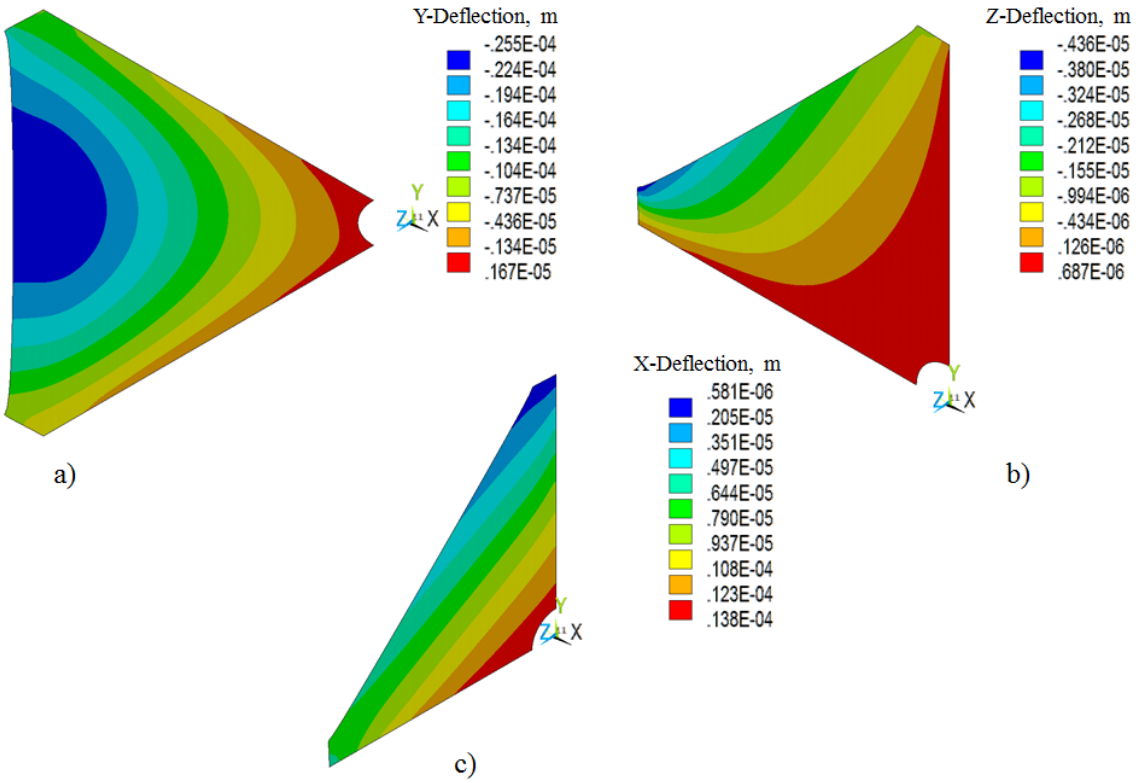

Figure 5.24. a) Out-of-plane deflection contour of the panel in the XZ plane. b) Out-of-plane deflection contour for the panel in the XY plane. c) Out-of-plane deflection contour for panel in the YZ plane. All contours are for an inflation of 70 kPa.

5.7 CHAPTER SUMMARY

The material model developed in the second and third chapters of this dissertation was successfully used in the design and analysis of the new inflatable pathfinder system. The new inflatable pathfinder system incorporated canonical structures so the analysis could give insight in a phenomenological sense for the entire class of inflatables. The pathfinder system was designed in phases. Each phase considered a more complex geometry with the final phase being analysis of the entire pathfinder system.

A single panel was the first geometry analyzed, and imposed radial displacement were applied along the loading the boundaries. The radial displacements were defined through FE analysis of an isotropic eighth symmetry model of the pathfinder system. Two design studies were performed using the single panel model; first the number of loading connections, and the second was the geometry of the center area of the panel. It was found that having four supporting connections was the most efficient from both a

performance and manufacturing standpoint. Several center geometries were studied including a circular, rectangular, and diamond shaped center geometry. The circular free center geometry proved to be the best geometry based upon performance and stability.

With the panel geometry finalized the next step was to analyze the inflated sphere with the octahedral set of tri-lateral corners. The circular free center geometry and four loading connections were incorporated into the final design of the inflatable pathfinder system. Since the original concept for the pathfinder system was to be developed as a radar reflector both the RMS flatness and orthogonality are important benchmark measurements. The RMS deflection was calculated for a single panel that had gravity loading applied perpendicular to the plane of the panel, since this was where the maximum out-of-plane deflection would occur.

An issue developed with convergence of the FE solutions when the linear orthotropic sphere model was used above a pressure of 48 kPa. An isotropic sphere model was then developed for the outer sphere to solve the convergence issues. Also with the isotropic material model applied for the outer sphere, the RMS deflections converged to those for the single panel model, thus verifying the use of the single panel model in the design of the pathfinder system. The MAC number was then calculated for each adjacent pair of panels in a tri-lateral corner. It was seen that the deflection pattern of the panel in the YZ plane, which was parallel to the gravity loading, affected the level of orthogonality (MAC number) the most. An optimal pressure of 20 kPa was seen to provide the best orthogonality between panels.

CHAPTER SIX DAMAGE ANALSYIS FOR SINGLE PANEL OF TRI-LATERAL CORNER

6.1 POSSIBLE MODES OF DAMAGE

In many applications, the effect of damage could be important. The pathfinder system was used to understand the sensitivity of the current geometry to imposed damage. Insight into effects of several forms of damage can be obtained by analysis of this pathfinder system, types of damage include: puncture of outer sphere, possible thread loss between panels stitched together, and creasing and wrinkling from being packed. In this chapter, the effect of loss of thread between panels stitched together in the pathfinder system will be studied. Figure 6.1 is a depiction of a single panel of the inflatable pathfinder system. The single panel consists of four separate quadrants stitched together to form the panel. Dashed lines are drawn where the seams would be. For the current study analysis was performed to examine the effect of thread loss on the achievable

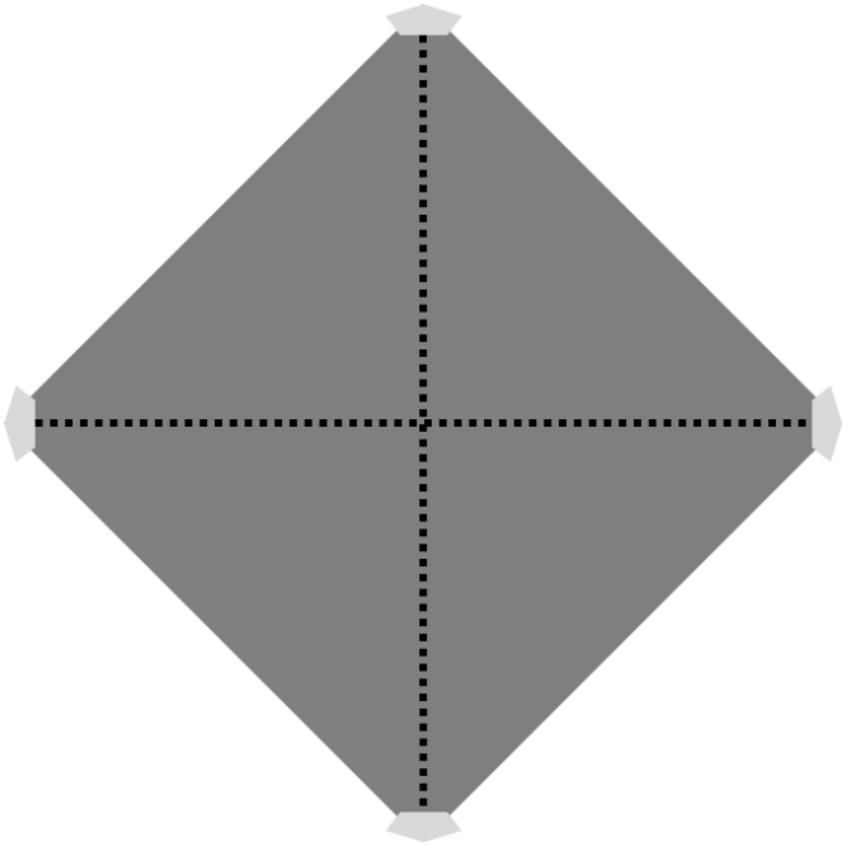

Figure 6.1. Schematic of proposed stitched assembly of single panel.

geometric control (i.e. flatness) of the single fabric panel.

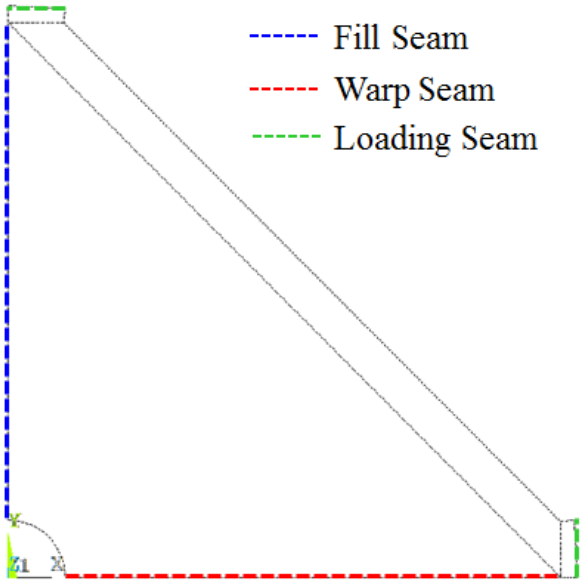

Figure 6.2. Diagram of seams considered in thread loss study.

Three seams were considered to be of the most interest (Figure 6.2) for the thread loss study; the seam along the warp direction of the fabric, the seam along the fill direction of the fabric, and the seam that connects the internal structure to the outer sphere or the loading seam. FE simulations were used for the analysis of the effect of thread loss.

6.2 Analysis of Possible Thread Loss

FE simulations were carried out using ANSYS 13.0 FE software. Finite element models of the fabric elements were created, as in earlier analyses; the models were meshed with 4-node shell elements (SHELL181), which have six degrees of freedom (DOFs) at each node. Gravity loading was applied perpendicular to the plane of the fabric panel, and stress stiffening effects were included. Large deflection nonlinear analysis was used to solve for the deflection profiles. The material model used for the entirety of this study incorporated linear orthotropic properties, with the warp and fill directions of the fabric corresponding to the major material directions.

Table 6.1 presents the linear orthotropic material properties used for the current analysis. A meshed model of the geometry used for the thread loss study is shown in Figure 6.3.

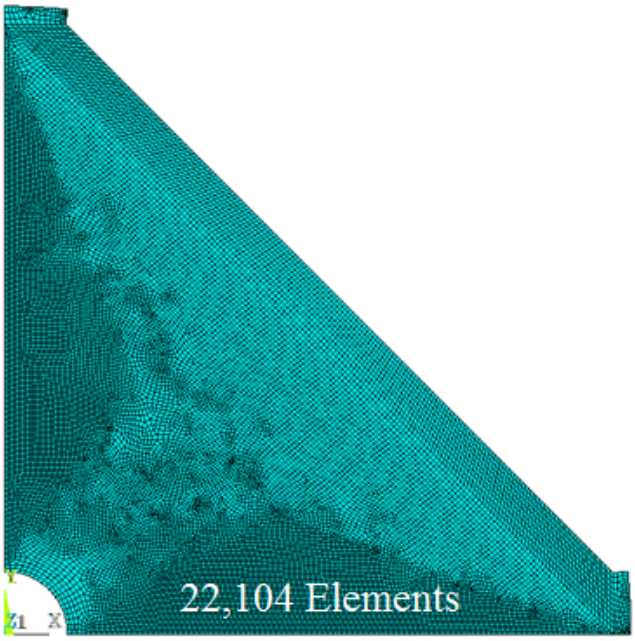

Figure 6.3. Meshed FE model of geometry used for thread loss study.

Table 6.1. Linear orthotropic material model constants.

Material Constants	
E_w, MPa	145.17
E_f, MPa	73.65
G_{wf}, MPa	29.0
ν_{wf}	0.3
ρ, kg/m^3	1024.16
t, mm	0.3

Initially the fill and warp seams had boundary conditions applied to allow only motion in the radial direction. To simulate the thread loss along each of the seams, the boundary conditions for a portion of each seam were freed. The boundary conditions were freed along each seam based upon a percentage of the total seam length. A range of 10% to 100% thread loss was studied for the fill and warp seams. A diagram defining the percentage and direction of thread loss along the fill and warp seam is presented in Figure 6.4. Further analysis was performed to see the effect of thread loss along the loading

seams. The loading seam is the area where the internal panels are stitched to the outer sphere. Again a range of 10% to 100% thread loss was examined and Figure 6.5 shows the orientation for the thread loss along the loading seams. To evaluate the effect of thread loss the RMS deflection (Equation (3)) was calculated.

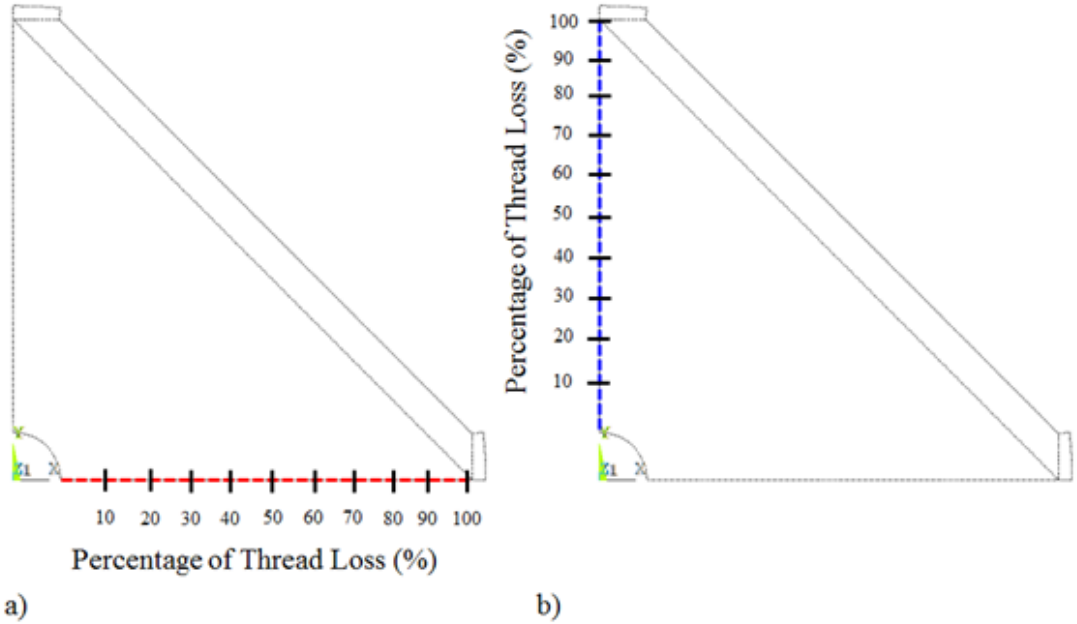

Figure 6.4. a) Diagram of thread loss definition along warp seam. b) Diagram of thread loss definition along fill seam.

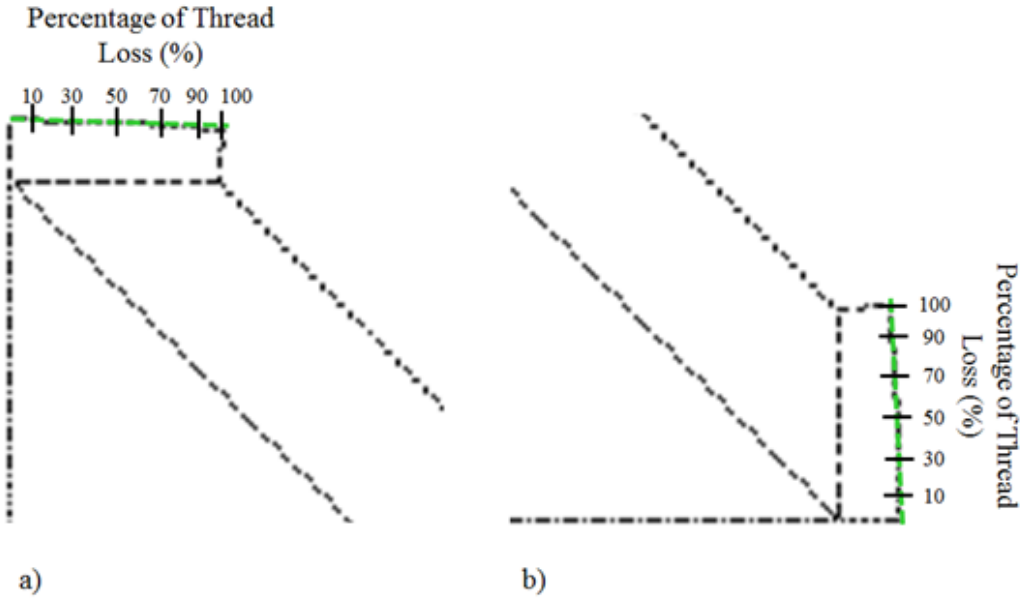

Figure 6.5. a) Diagram of thread loss definition for the loading seam associated with the fill direction. b) Diagram of thread loss definition along the loading seam associated with the warp direction.

6.3 RESULTS OF THREAD LOSS STUDY

Analyses were performed to define the effect of thread loss along important seams on the flatness of the fabric panel. Deflection contours and RMS deflections were found to evaluate the performance of the fabric panel under the possible thread damage. Deflection contours were examined to see how the wrinkling patterns evolved as thread loss was introduced. The RMS deflections were used to quantify the effect of thread loss on the performance capabilities of the fabric panel.

Out-of-plane (Z-direction) contours for thread loss occurring along the fill seam are shown in Figure 6.6. It can be seen that a large wrinkle develops around 50% thread loss, but that same wrinkle dissipates above 70% thread loss. The large out-of-plane displacement along the hypotenuse of the triangular panel is seen to decrease as the thread loss is increased. The maximum out-of-plane displacement moves from occurring along the hypotenuse of the triangular element to the corner of the center. This phenomenon was expected since, as thread loss increases, the support along the fill seam was removed. Once thread loss was higher than 90% the wrinkling dissipates and the maximum out-of-plane displacement occurs at the corner of the circular center.

The deflection contours for thread loss occurring along the warp seam are shown in Figure 6.7. Again analyzing the out-of-plane deflection contours illustrates the propagation of wrinkling in the fabric panel. From the contours it was noted that as thread loss was increased above 50% wrinkles began to form and the maximum out-of-plane deflection along the hypotenuse began to decrease. A large wrinkle forms at 70% thread loss and the maximum out-of-plane deflection occurs at the corner of circular center. At 90% thread loss, the wrinkle has its largest magnitude and the maximum out-of-plane deflection is the wrinkle. Above 90% thread loss, a second wrinkle propagates and the maximum out-of-plane deflection again occurs at the corner of the circular center.

Comparing the response of the fabric panel to thread loss along the fill and warp seams, it was seen that the propagation and magnitude of wrinkling is greater when thread is lost along the warp seam. The static deflection response of the fabric panel was seen to be more sensitive to the loss of thread along the seam in-line with warp material direction.

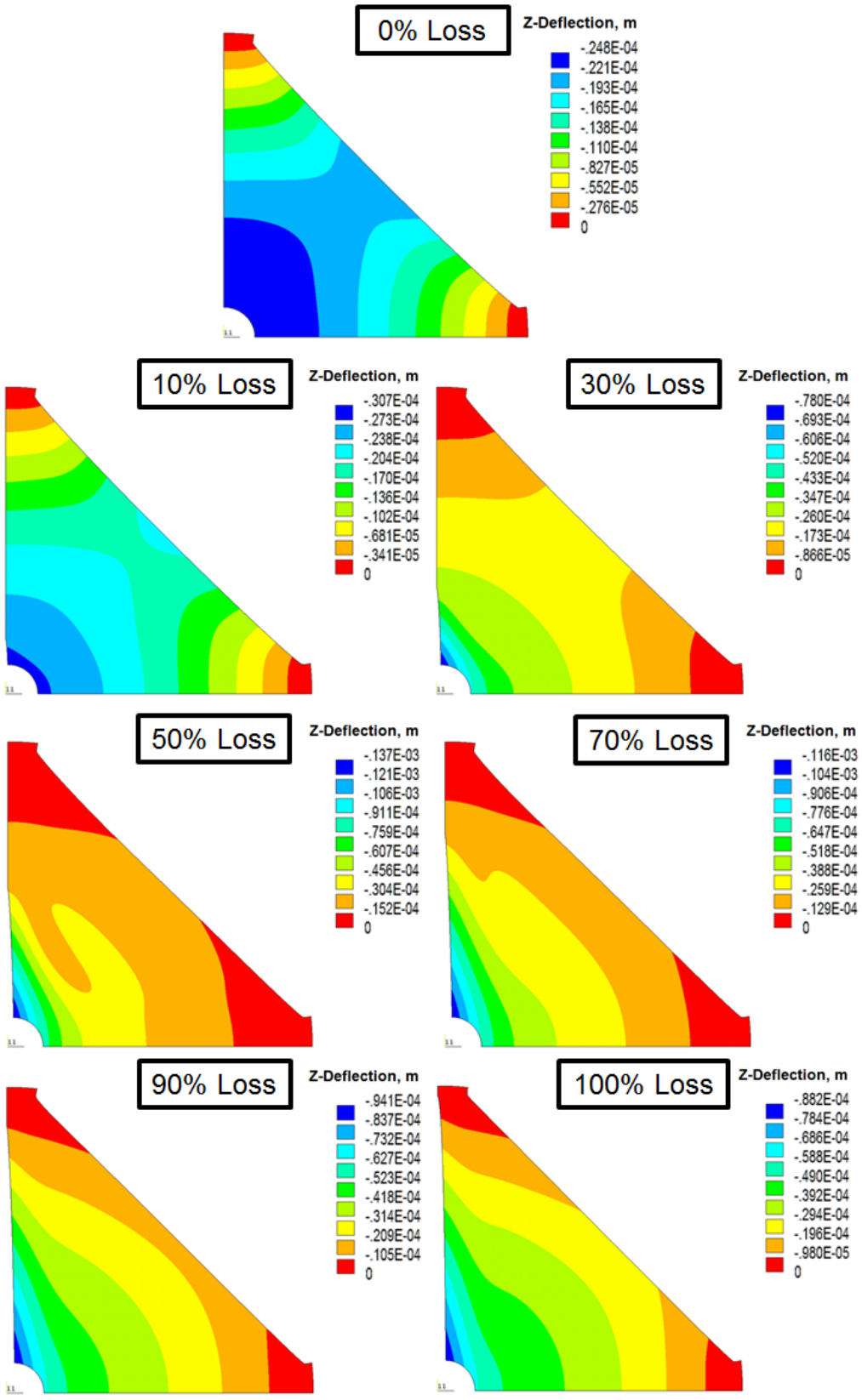

Figure 6.6. Z-deflection contours for thread loss along the fill seam.

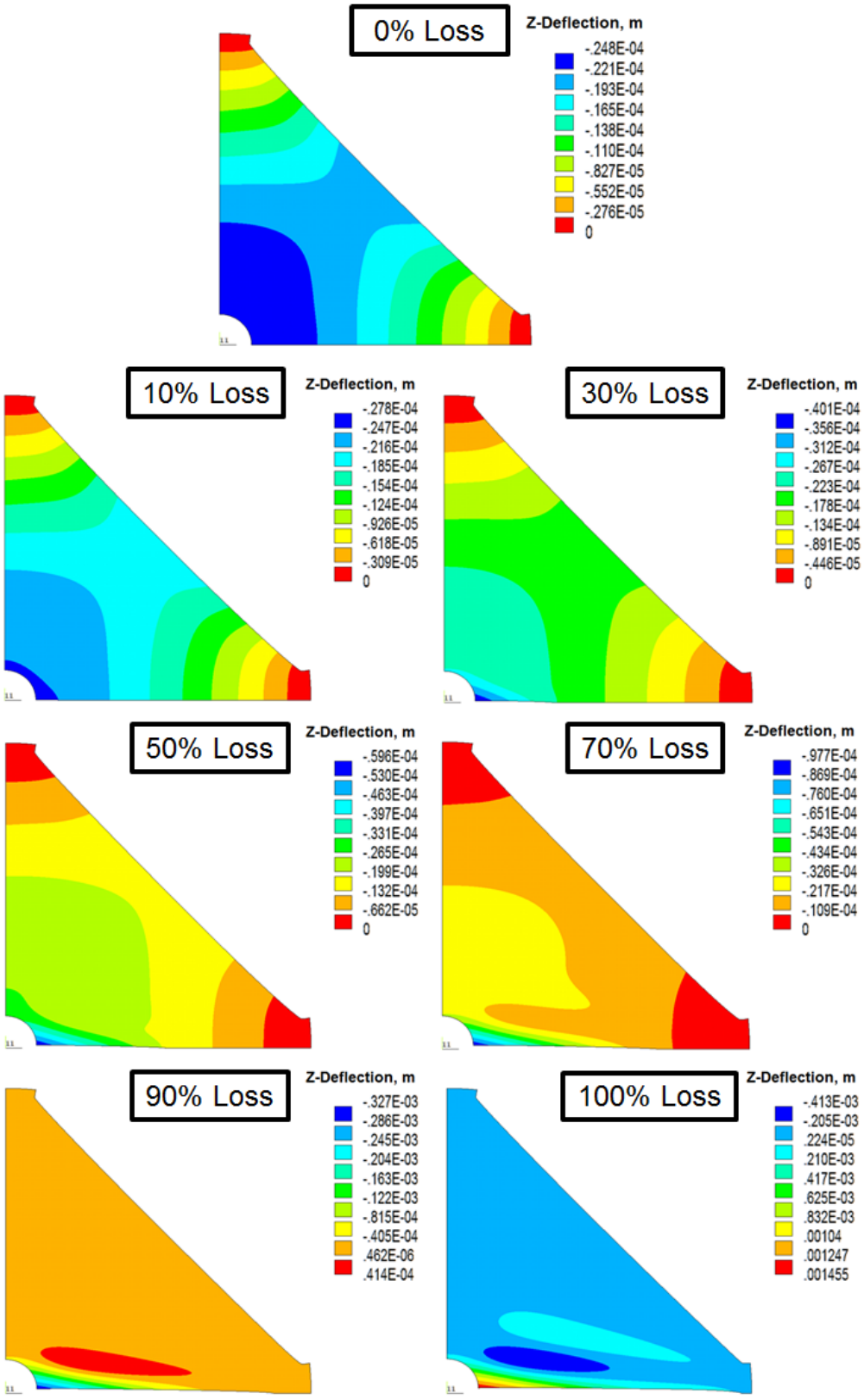

Figure 6.7. Z-deflection contours for thread loss along the warp seam.

The effect of thread loss along the loading seams was also examined. The loading seams connect to the outer sphere. Again out-of-plane deflection contours were used to illustrate the effect of thread loss along the loading seams. Unlike the thread loss along the fill and warp seams, once 100% thread loss was reached, the FE simulations became un-converged.

The out-of-plane deflection contours for thread loss along the loading seam associated with the fill direction (as diagramed in Figure 6.5) are shown in Figure 6.8. It was seen that the static out-of-plane deflection response of the fabric panel was not significantly affected by the loss of thread until a level of 70% thread loss was reached. Above 70% thread loss, the maximum out-of-plane deflection occurring along the hypotenuse of the triangular specimen begins to increase. Also above 90% thread loss, a wrinkle begins to form in the center of the fabric panel. Figure 6.9 presents the out-of-plane deflection contours for thread loss along the loading seam associated with the warp direction (as shown in Figure 6.5). The response of the fabric panel remains relatively unchanged as thread is lost along this loading seam. Above 50% thread loss the deflection along the hypotenuse of the triangular article is decreased and the onset of wrinkling is also dissipated. For both cases of thread loss along loading seams, as the amount of thread loss increases, the maximum overall out-of-plane deflection in the fabric panel increases.

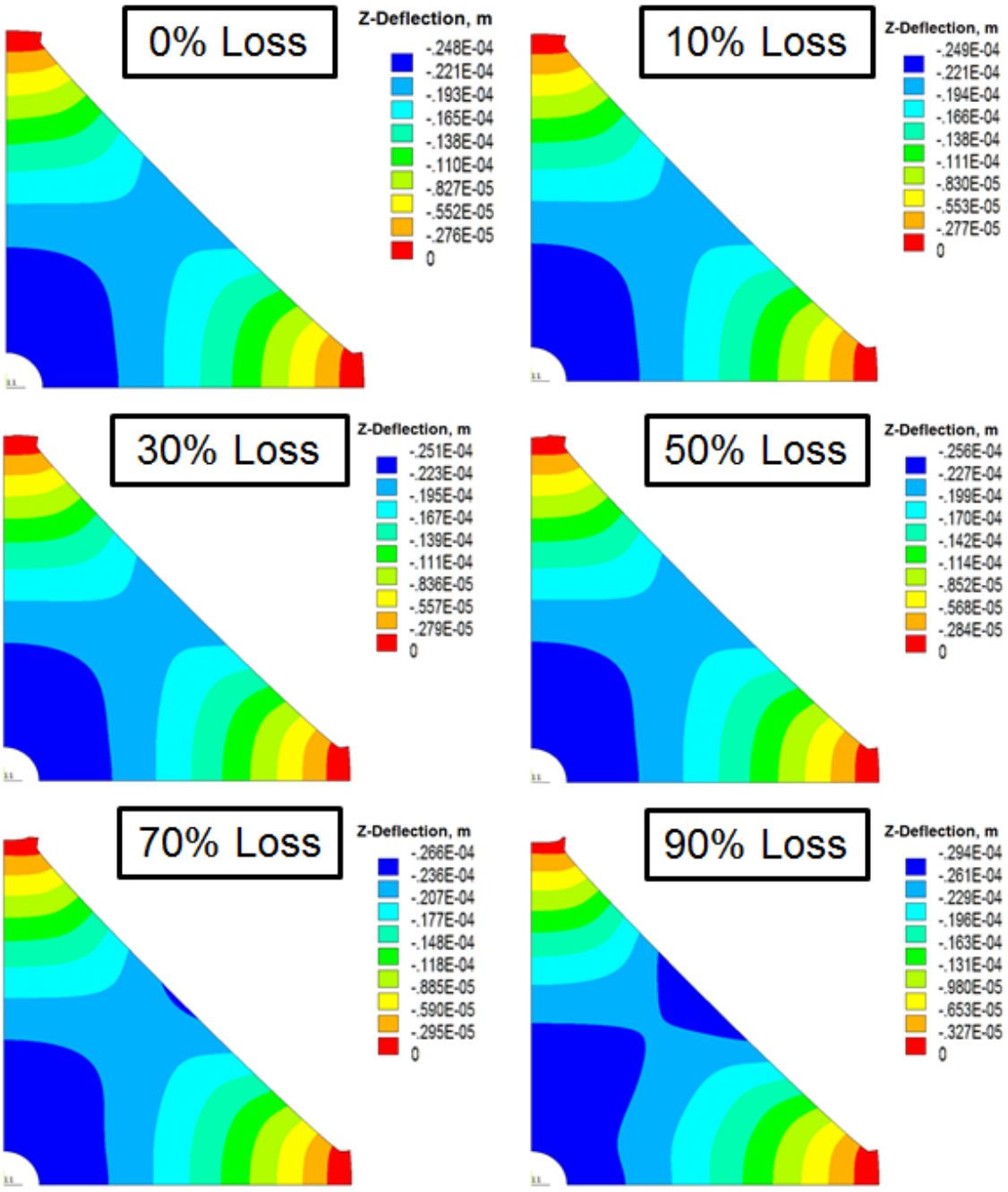

Figure 6.8. Z-deflection contours for thread loss along the loading seam associated with the fill direction.

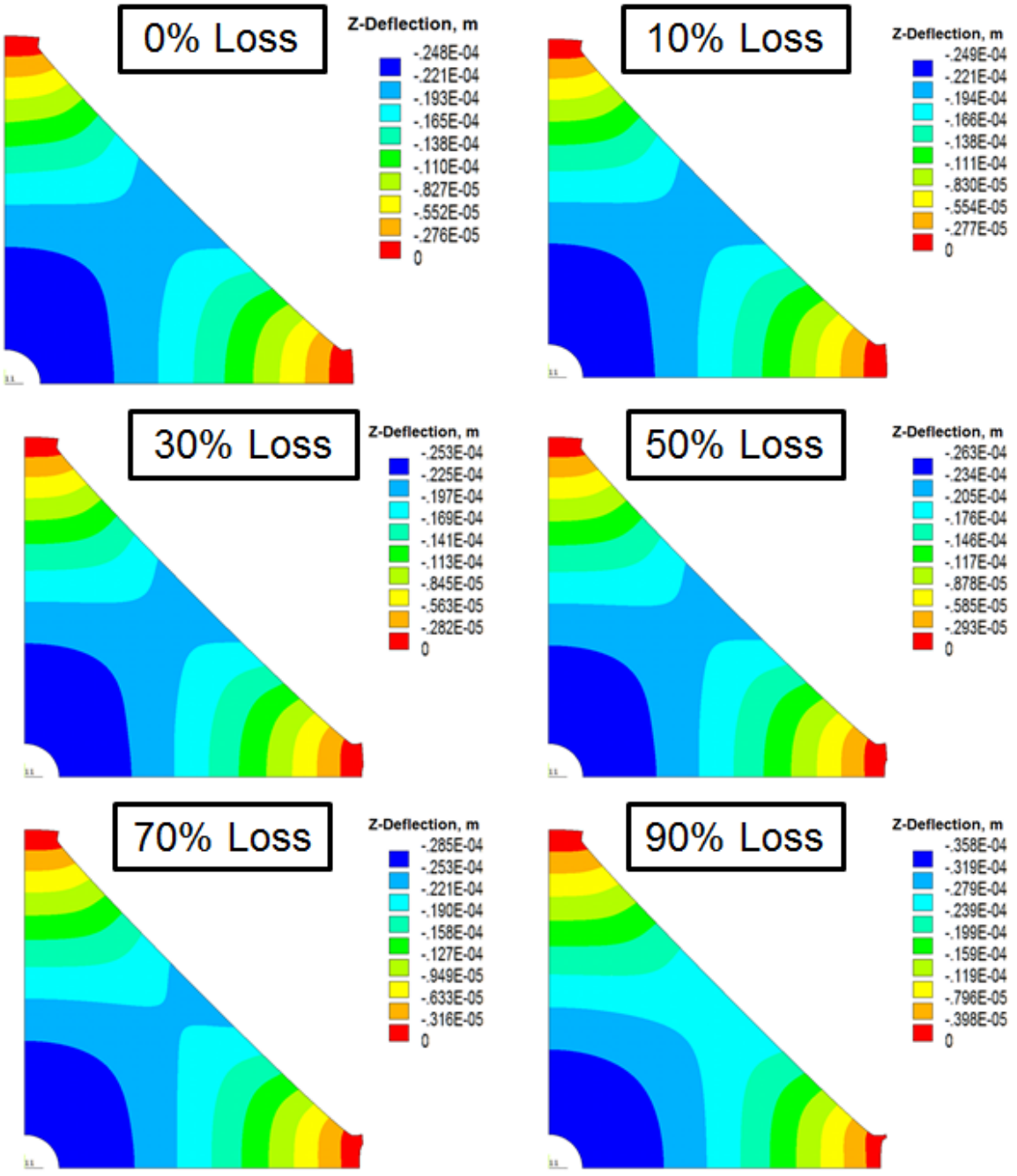

Figure 6.9. Z-deflection contours for thread loss along the loading seam associated with the warp direction.

For a more quantifiable measure of performance loss due to the possible thread loss between panels, the RMS deflections were calculated. A summary plot of the out-of-plane RMS deflections for each thread loss study is shown in Figure 6.10 with the 0% thread loss case plotted for comparison. The performance of the fabric panel was unchanged until the thread loss was increased above 10%. Once the loss of thread was above 10% the RMS deflection increased to various levels based upon which seam was damaged. The losses of thread along the loading seams were the most stable modes of thread loss for the entire study. It is shown that the loss of thread along the seam aligned with the warp material direction had the greatest impact on the RMS deflection of the fabric panel.

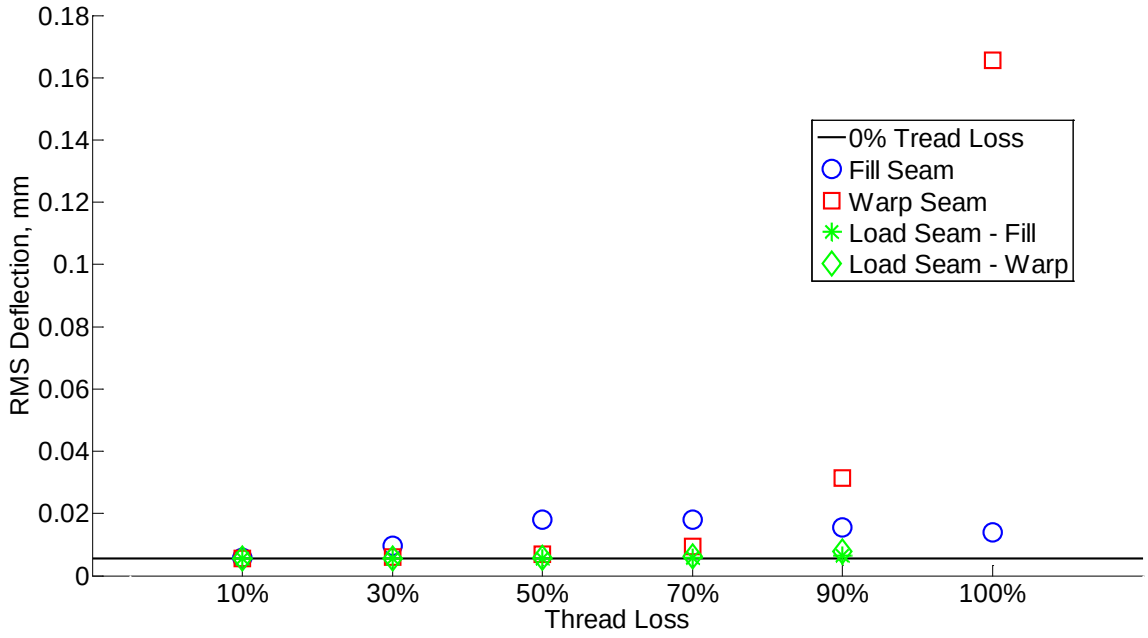

Figure 6.10. RMS deflections for the thread loss study.

To better examine the effects of thread loss on the performance of the fabric panel expected performance requirements for radar reflector and radar decoy applications were plotted with the RMS deflections from the thread loss study. Figure 6.11 presents the RMS deflections for the thread loss study concerning the seams aligned with the fill and warp material directions. The flatness meets or exceeds all of the performance requirements up to 100% thread loss along the warp direction seam. Figure 6.12 shows

the thread loss along the loading seams and expected performance requirements. For all levels of thread loss studied the flatness still exceeds the performance standards. Thus, losing threads along the seams supporting the internal panels affects the response of the fabric panel more than losing thread along the loading boundaries.

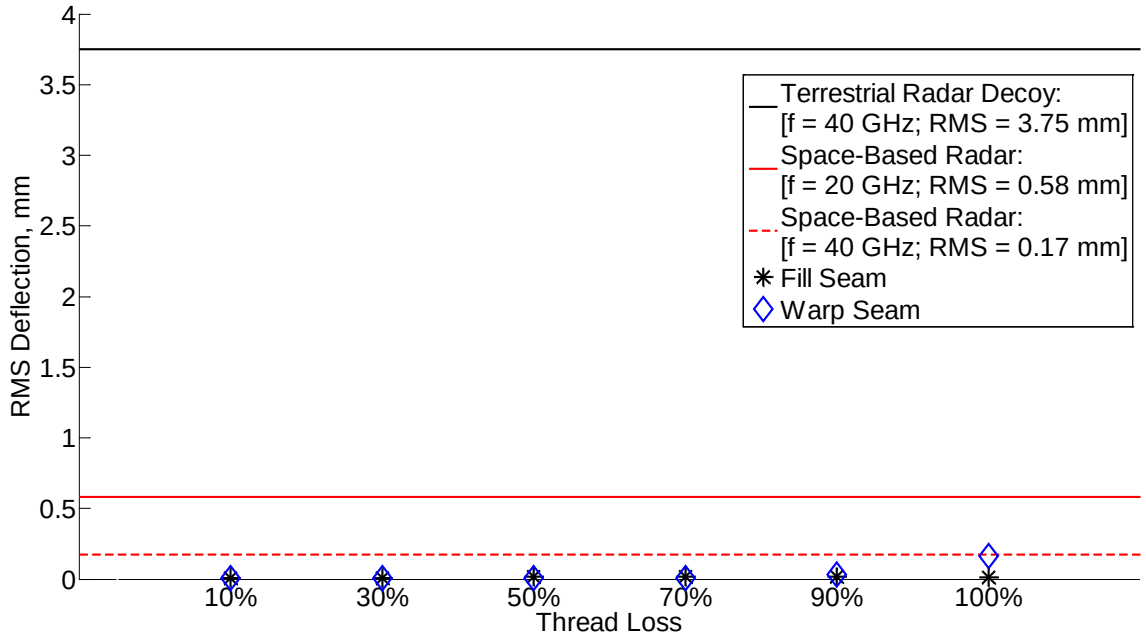

Figure 6.11. RMS deflections for thread loss along the warp and fill seams with expected performance requirements.

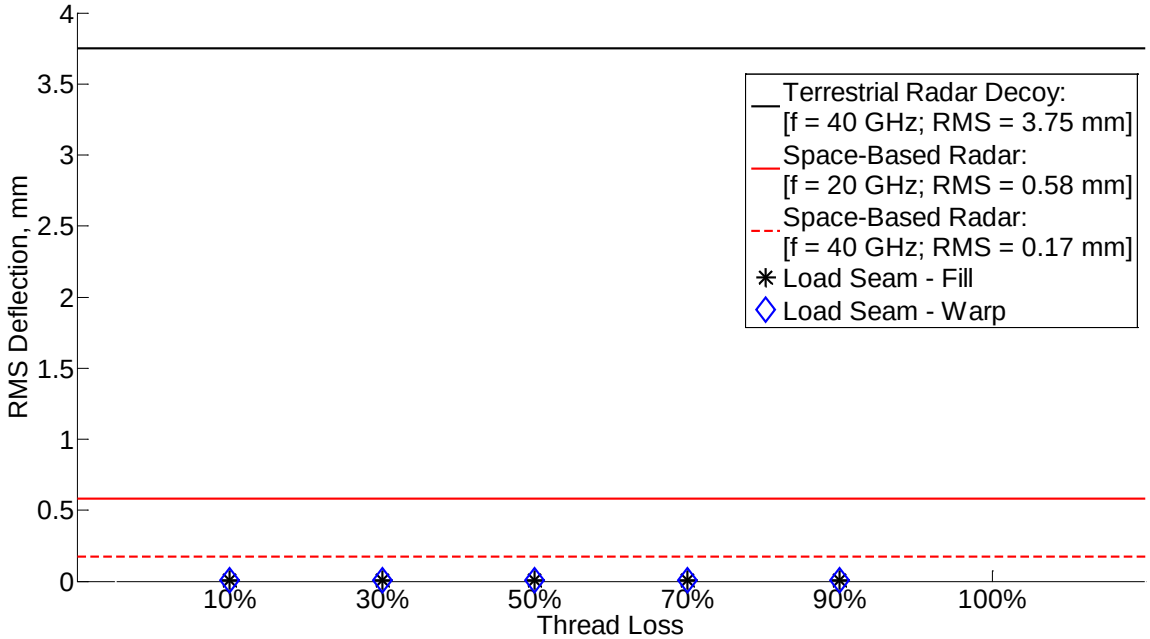

Figure 6.12. RMS deflections for thread loss along loading seams with expected performance requirements.

6.4 CHAPTER SUMMARY

Because the effect of damage in many applications, such as radar reflectors, could be important, a study was performed on the pathfinder system to illustrate the effect of imposing possible damage on the achievable geometric control. The damage analyzed in this study was thread loss along key seams in the fabric panel. Supporting seams aligned with the fill and warp material directions and loading seams were examined. Out-of-plane deflection contours and RMS deflections were used to define the relationship between thread loss and the level of geometric control.

Through examination of the deflection contours it was found that losing thread along the supporting seam aligned with the warp material direction affected the static response of the fabric panel the most. It was also seen that thread loss along the loading seams had the least effect on the static response of the fabric panel. However, compared to the expected performance requirements for radar reflector applications, the geometric control achieved for all levels of thread loss met or exceeded the standard for the pathfinder system.

CHAPTER SEVEN CONCLUSIONS AND FUTURE WORK

7.1 SUMMARY AND CONCLUSIONS

The research presented in this dissertation involved the development and design of an inflatable pathfinder system. The inflatable pathfinder was comprised of an octahedral set of tri-lateral corners (an assembly common to radar reflector and radar decoys) with an outer sphere that would be pressurized to tension the internal structure. Canonical geometries, common to inflatable structures, were incorporated to allow for universal insight into the design methodologies for the entire class of inflatable structures. The methodologies and techniques developed in this research are important foundations for the future design of inflatable systems.

Objectives of this dissertation included:

1. Developing an understanding of the material behavior of a high-performance coated woven nylon fabric.
    a. Correlate experimental static responses of the coated nylon fabric with non-linear finite element analyses.
    b. Design and develop a test rig for pre-tensioned fabric testing using precision photogrammetry techniques to increase accuracy of measured deflections.
2. Create accurate finite element (FE) models of a new pathfinder inflatable system using canonical structures.
    a. Evaluate the effect of boundary conditions, loading, and material properties on geometric controls (i.e. flatness).
    b. Design the pathfinder system to meet or exceed performance requirements related to radar reflectors and radar decoys.

Initially a material model had to be developed and verified for the commercially available poly-urethane coated woven nylon fabric. Coated nylon fabrics have been successfully used as construction materials for many inflatable systems. Nonlinear FEA and photogrammetry results were correlated to define a material model for the coated fabric. It was found that the shear modulus of the coated nylon fabric had a significant impact on the response of the coated fabric. Material model correlation was achieved for the coated nylon fabric under bi-axial tension and inflation loading. An effective shear

modulus was established as being 20% of the elastic modulus in the warp material direction (29.0 MPa for the current work).

An error analysis was performed on installation of the fabric panel into the inflation chamber. This analysis captured both installation error and photogrammetry measurement error. It was found that this error (3.28 mm) was more reflective of coated fabrics being highly flexible and having material nonlinearities compared to the study by Scherrer, 2012, where the flatness of a steel surface was measured using photogrammetry. Thus, the error associated with the photogrammetry results considers uncertainties in test article installation and photogrammetry measurement. However, some uncertainties remain undefined, such as application of loading (gauge accuracy for this work) and positioning of targets for photogrammetry measurement.

Once validated, the new FE material model was used to design the inflatable pathfinder system. The development of the pathfinder system was based upon analysis of sub-assemblies to create a final full model that would achieve the best performance. Standards for performance were based upon requirements for radar reflectors and radar decoys. Figure 7.1 shows the design process for the inflatable pathfinder system. First, a single panel was analyzed to evaluate the effect of support connections, panel geometry, and material orientation.

It was seen that the most efficient panel geometry was:

- Four support connections
- Circular free-center geometry
- 0° material orientation (the material directions of the woven fabric aligned with the legs of triangular panels)

All of these design decision were then incorporated into the inflatable pathfinder system as shown in Figure 7.1. With the final design of the inflatable pathfinder system complete, a damage analysis was performed. The damage analysis considered the effect of thread loss along prominent seams on the static response of the pathfinder system. It was seen that for extreme cases of thread loss (thread loss greater than 90%) the performance of the pathfinder system was degraded, but still met or exceeded the standards of performance for radar reflectors and radar decoys.

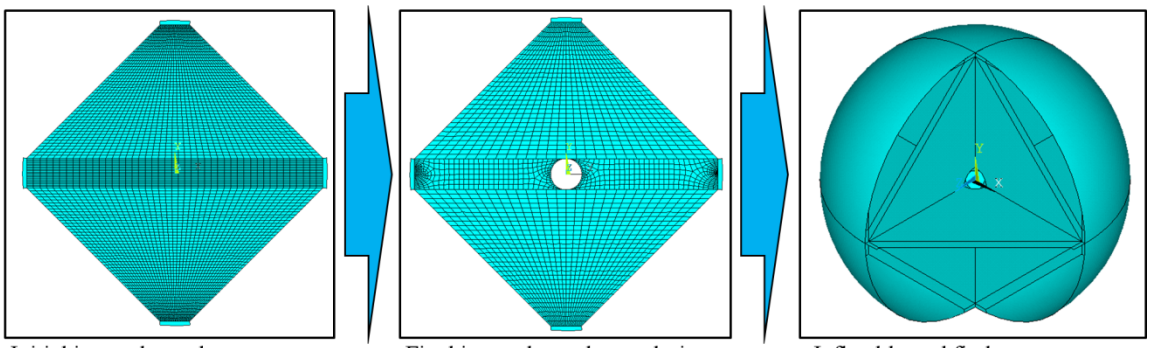

Figure 7.1. Phased design of inflatable pathfinder system.

7.2 FUTURE WORK

7.2.1 MATERIAL TESTING AND MODELING OF COATED NYLON

Correlation of the material model with photogrammetry and nonlinear FEA simulations was seen in the current research; however, some questions were raised. Future analysis of the behavior coated nylon could consider the effect of the coating on the behavior on the nylon fabric. The coating for fabrics used in inflatables are commonly hyperelastic materials and contribute a significant portion (if not all) of the nonlinear behavior.

Another area of interest to determine if the coated nylon is truly homogenous. It is expected that the coating should be applied consistently, but areas of high and low concentrations are to be expected. The coated fabric could be tested to determine how homogenous it is. Test articles could be cut form a yard of the coated fabric and analysis to determine how consistent the material properties and response are.

7.2.2 MANUFACTURING AND TESTING OF INFLATABLE PATHFINDER SYSTEM

The entirety of the current research used nonlinear FEA analysis to design the inflatable pathfinder system. It would be advantageous to build the actual pathfinder system and validate with the FE model developed in this research. It was seen that the stiffness of the FE model differed from the actual test articles in Chapter 3 and Chapter 4. With a physical pathfinder system built, analyses could be performed to verify the results of this work.

7.2.3 PACKING AND DEPLOYMENT OF INFLATABLE PATHFINDER SYSTEM

As part of the current work thread loss was defined as a possible mode of damage that could occur in the pathfinder system. Another area of interest would be the deformations caused by packing the deployable pathfinder system. Packing the coated nylon could produce creases and inconsistencies in the panels of the pathfinder system. Determining the effect of these creases and imperfections on the system performance would provide important information on the design of the next generation of inflatables.

Further investigation could be performed on the ideal packing scheme of the inflatable pathfinder system. Harris, 2011 performed analyses on packing of inflatable wings. As part of that study, the effect of creasing on strength of the fabric was examined. A similar analysis of pathfinder system would provide insight into packing, deployment, and creasing.

APPENDIX A: ANSYS APDL BATCH FILES

Bi-axial Tensioned Piece of Fabric

The following batch files were used for both the shear studies and final analysis of the bi-axial tensioned fabric specimen. Each of the twelve case's ANSYS APDL batch files are shown below. The shear studies were performed by varying the variable "G" in each of the input files. The value for "G" in each of the files below is the validated model shear modulus.

Test Case 1

```
finish
/clear
/filename,FabTriCase1
/prep7

!Material Properties
        EW=21055
        !(psi)
        EF=10682
        !(psi)
        G=0.19*EW
        !(psi)

 !Fabric
        mp,ey,1,EW
        mp,ex,1,EF
        mp,ez,1,EW
        mp,prxy,1,0.3
        mp,pryz,1,0.3
        mp,prxz,1,0.3
        mp,gxy,1,G
        mp,gyz,1,G
        mp,gxz,1,G
        mp,dens,1,0.037/386.4
        !(lb*s^2/in)

 !Clamp properties
        mp,ex,2,9860e3
        !(psi)
        mp,dens,2,0.0948697/386.4
        !(lb*s^2/in)
        mp,prxy,2,0.36

 !Fishing line properties
        mp,ex,3,223e3
        !(psi)
        mp,dens,3,0.046293/386.4
        !(lb*s^2/in)

!Elements

 !Fabric:
        et,1,shell181
        keyopt,1,3,2
        sectype,1,shell
        secdata,0.012
        !(in)

 !Clamp elements:
        et,2,shell181
        keyopt,2,3,2
        sectype,2,shell
        secdata,.261
        !(in)

 !Fishing line elements:
        et,3,beam188
        sectype,3,beam,csolid
        secdata,0.024/2
        !(in)

!Create Keypoints
        a=9
        !(in)
        b=0.75
        !(in)
```

```
d=0.25
c=sqrt(2)/2
L1=12.75
!(in)
L2=41.25
!(in)
L3=43.25
!(in)
*afun,deg
k,1,d,-d
k,2,c*(a-b),-c*(a-b)
k,3,c*(a-b/2),-c*(a-b/2)
k,4,c*a,-c*a
k,5,c*(a-b),-c*a
k,6,c*(a-2*b),-c*a
k,7,-c*(a-2*b),-c*a
k,8,-c*(a-b),-c*a
k,9,-c*a,-c*a
k,10,-c*(a-b/2),-c*(a-b/2)
k,11,-c*(a-b),-c*(a-b)
k,12,-d,-d
k,101,kx(3)+L2,ky(3),.345
k,102,kx(5),ky(5)-L1,.345
k,103,kx(8),ky(8)-L1,.345
k,104,kx(10)-L3,ky(10),.345

a,1,2,11,12
a,2,6,7,11

asel,s,area,,1,2
cm,FABRIC,area

a,2,3,5,6
a,3,4,5
!cm,RCLAMP,area

a,11,7,8,10
a,10,8,9
!cm,LCLAMP,area

allsel
aglue,all

ksel,s,kp,,1,2
lslk,s,1
ksel,s,kp,,11,12
lslk,a,1
ksel,s,kp,,6,7
lslk,a,1
ksel,s,kp,,2
ksel,a,kp,,11
lslk,a,1
lesize,all,,,50
allsel

ksel,s,kp,,1,2
ksel,a,kp,,6,7
ksel,a,kp,,11,12
lslk,s,1
asll,s,1
mshkey,1

!Material Orientation
local,11,0,0,0,0,0,45
esys,11
amesh,all
csys,0
esys,0

type,2
secnum,2
mat,2

asel,inve
mshkey,2
amesh,all
allsel


type,3
mat,3
secnum,3
l,3,101
l,5,102
l,10,104
l,8,103
ksel,s,kp,,3
ksel,a,kp,,101
lslk,s,1
ksel,s,kp,,5
ksel,a,kp,,102
lslk,a,1
```

```
        ksel,s,kp,,10
        ksel,a,kp,,104
        lslk,a,1
        ksel,s,kp,,8
        ksel,a,kp,,103
        lslk,a,1
        lesize,all,,,50

        lmesh,all

        allsel


/solu
        sstif,on
        nlgeom,on
        nsubst,100
        neqit,50



!Boundary Conditions (Clamps)

        ksel,s,kp,,1
        ksel,a,kp,,12
        lslk,s,1
        nsll,s
        d,all,all,0

        F1=0.68030
        !(lb)
        F2=0.40205
        !(lb)
        F3=0.40425
        !(lb)
        F4=0.68115
        !(lb)

        ksel,s,kp,,101
        nslk,s
        f,all,fx,F4
        d,all,uy,0
        d,all,uz,0
        d,all,rotx,0
        d,all,roty,0
        d,all,rotz,0

        ksel,s,kp,,102
        nslk,s
        f,all,fy,-F3
        d,all,ux,0
        d,all,uz,0
        d,all,rotx,0
        d,all,roty,0
        d,all,rotz,0

        ksel,s,kp,,103
        nslk,s
        f,all,fy,-F2
        d,all,ux,0
        d,all,uz,0
        d,all,rotx,0
        d,all,roty,0
        d,all,rotz,0

        ksel,s,kp,,104
        nslk,s
        f,all,fx,-F1
        d,all,uy,0
        d,all,uz,0
        d,all,rotx,0
        d,all,roty,0
        d,all,rotz,0

        allsel

        acel,,,386.4-(386.4*.00077)
        !(in/S^2)

        solve
```

Test Case 2

```
finish
/clear
/filename,FabTriCase2
/prep7

!Material Properties
        EW=21055
        !(psi)
        EF=10682
        !(psi)
        G=0.19*EW
        !(psi)

 !Fabric
        mp,ey,1,EW
        mp,ex,1,EF
        mp,ez,1,EW
        mp,prxy,1,0.3
        mp,pryz,1,0.3
        mp,prxz,1,0.3
        mp,gxy,1,G
        mp,gyz,1,G
        mp,gxz,1,G
        mp,dens,1,0.037/386.4
        !(lb*s^2/in)

 !Clamp properties
        mp,ex,2,9860e3
        !(psi)
        mp,dens,2,0.0948697/386.4
        !(lb*s^2/in)
        mp,prxy,2,0.36

 !Fishing line properties
        mp,ex,3,223e3
        !(psi)
        mp,dens,3,0.046293/386.4
        !(lb*s^2/in)

!Elements

 !Fabric:
        et,1,shell181
        keyopt,1,3,2
        sectype,1,shell
        secdata,0.012
        !(in)

 !Clamp elements:
        et,2,shell181
        keyopt,2,3,2
        sectype,2,shell
        secdata,.261
        !(in)

 !Fishing line elements:
        et,3,beam188
        sectype,3,beam,csolid
        secdata,0.024/2
        !(in)

!Create Keypoints
        a=9
        !(in)
        b=0.75
        !(in)
        d=0.25
        c=sqrt(2)/2
        L1=12.75
        !(in)
        L2=41.25
        !(in)
        L3=43.25
        !(in)
        *afun,deg
        k,1,d,-d
        k,2,c*(a-b),-c*(a-b)
        k,3,c*(a-b/2),-c*(a-b/2)
        k,4,c*a,-c*a
        k,5,c*(a-b),-c*a
        k,6,c*(a-2*b),-c*a
        k,7,-c*(a-2*b),-c*a
        k,8,-c*(a-b),-c*a
        k,9,-c*a,-c*a
        k,10,-c*(a-b/2),-c*(a-b/2)
        k,11,-c*(a-b),-c*(a-b)
        k,12,-d,-d
        k,101,kx(3)+L2,ky(3),.345
        k,102,kx(5),ky(5)-L1,.345
        k,103,kx(8),ky(8)-L1,.345
```

```
k,104,kx(10)-L3,ky(10),.345

a,1,2,11,12
a,2,6,7,11

asel,s,area,,1,2
cm,FABRIC,area

a,2,3,5,6
a,3,4,5
!cm,RCLAMP,area

a,11,7,8,10
a,10,8,9
!cm,LCLAMP,area

allsel
aglue,all

ksel,s,kp,,1,2
lslk,s,1
ksel,s,kp,,11,12
lslk,a,1
ksel,s,kp,,6,7
lslk,a,1
ksel,s,kp,,2
ksel,a,kp,,11
lslk,a,1
lesize,all,,,50
allsel

ksel,s,kp,,1,2
ksel,a,kp,,6,7
ksel,a,kp,,11,12
lslk,s,1
asll,s,1
mshkey,1

!Material Orientation
local,11,0,0,0,0,0,45
esys,11
amesh,all
csys,0
esys,0

type,2
secnum,2
mat,2

asel,inve
mshkey,2
amesh,all
allsel

type,3
mat,3
secnum,3
l,3,101
l,5,102
l,10,104
l,8,103
ksel,s,kp,,3
ksel,a,kp,,101
lslk,s,1
ksel,s,kp,,5
ksel,a,kp,,102
lslk,a,1
ksel,s,kp,,10
ksel,a,kp,,104
lslk,a,1
ksel,s,kp,,8
ksel,a,kp,,103
lslk,a,1
lesize,all,,,50

lmesh,all

allsel

/solu
sstif,on
nlgeom,on
nsubst,100
neqit,50

!Boundary Conditions (Clamps)

ksel,s,kp,,1
```

```
ksel,a,kp,,12
lslk,s,1
nsll,s
d,all,all,0

F1=0.98
!(lb)
F2=0.31845
!(lb)
F3=0.32185
!(lb)
F4=0.98065
!(lb)

ksel,s,kp,,101
nslk,s
f,all,fx,F4
d,all,uy,0
d,all,uz,0
d,all,rotx,0
d,all,roty,0
d,all,rotz,0

ksel,s,kp,,102
nslk,s
f,all,fy,-F3
d,all,ux,0
d,all,uz,0
d,all,rotx,0
d,all,roty,0
d,all,rotz,0

ksel,s,kp,,103
nslk,s
f,all,fy,-F2
d,all,ux,0
d,all,uz,0
d,all,rotx,0
d,all,roty,0
d,all,rotz,0

ksel,s,kp,,104
nslk,s
f,all,fx,-F1
d,all,uy,0
d,all,uz,0
d,all,rotx,0
d,all,roty,0
d,all,rotz,0

allsel

acel,,,386.4-(386.4*.00077)
!(in/s^2)

solve
```

Test Case 3

```
finish
/clear
/filename,FabTriCase3
/prep7

!Material Properties
	EW=21055
	!(psi)
	EF=10682
	!(psi)
	G=0.07*EW
	!(psi)

 !Fabric
	mp,ey,1,EW
	mp,ex,1,EF
	mp,ez,1,EW
	mp,prxy,1,0.3
	mp,pryz,1,0.3
	mp,prxz,1,0.3
	mp,gxy,1,G
	mp,gyz,1,G
	mp,gxz,1,G
	mp,dens,1,0.037/386.4
	!(lb*s^2/in)

 !Clamp properties
	mp,ex,2,9860e3
	!(psi)
	mp,dens,2,0.0948697/386.4
	!(lb*s^2/in)
	mp,prxy,2,0.36

 !Fishing line properties
	mp,ex,3,223e3
	!(psi)
	mp,dens,3,0.046293/386.4
	!(lb*s^2/in)

!Elements

 !Fabric:
	et,1,shell181
	keyopt,1,3,2
	sectype,1,shell
	secdata,0.012
	!(in)

 !Clamp elements:
	et,2,shell181
	keyopt,2,3,2
	sectype,2,shell
	secdata,.261
	!(in)

 !Fishing line elements:
	et,3,beam188
	sectype,3,beam,csolid
	secdata,0.024/2
	!(in)

!Create Keypoints
	a=9
	!(in)
	b=0.75
	!(in)
	d=0.25
	c=sqrt(2)/2
	L1=12.75
	!(in)
	L2=41.25
	!(in)
	L3=43.25
	!(in)
	*afun,deg
	k,1,d,-d
	k,2,c*(a-b),-c*(a-b)
	k,3,c*(a-b/2),-c*(a-b/2)
	k,4,c*a,-c*a
	k,5,c*(a-b),-c*a
	k,6,c*(a-2*b),-c*a
	k,7,-c*(a-2*b),-c*a
	k,8,-c*(a-b),-c*a
	k,9,-c*a,-c*a
	k,10,-c*(a-b/2),-c*(a-b/2)
	k,11,-c*(a-b),-c*(a-b)
	k,12,-d,-d
	k,101,kx(3)+L2,ky(3),.345
	k,102,kx(5),ky(5)-L1,.345
	k,103,kx(8),ky(8)-L1,.345
```

```
k,104,kx(10)-L3,ky(10),.345

a,1,2,11,12
a,2,6,7,11

asel,s,area,,1,2
cm,FABRIC,area

a,2,3,5,6
a,3,4,5
!cm,RCLAMP,area

a,11,7,8,10
a,10,8,9
!cm,LCLAMP,area

allsel
aglue,all

ksel,s,kp,,1,2
lslk,s,1
ksel,s,kp,,11,12
lslk,a,1
ksel,s,kp,,6,7
lslk,a,1
ksel,s,kp,,2
ksel,a,kp,,11
lslk,a,1
lesize,all,,,50
allsel

ksel,s,kp,,1,2
ksel,a,kp,,6,7
ksel,a,kp,,11,12
lslk,s,1
asll,s,1
mshkey,1

!Material Orientation
local,11,0,0,0,0,0,0
esys,11
amesh,all
csys,0
esys,0

type,2
secnum,2
mat,2

asel,inve
mshkey,2
amesh,all
allsel

type,3
mat,3
secnum,3
l,3,101
l,5,102
l,10,104
l,8,103
ksel,s,kp,,3
ksel,a,kp,,101
lslk,s,1
ksel,s,kp,,5
ksel,a,kp,,102
lslk,a,1
ksel,s,kp,,10
ksel,a,kp,,104
lslk,a,1
ksel,s,kp,,8
ksel,a,kp,,103
lslk,a,1
lesize,all,,,50

lmesh,all

allsel

/solu
sstif,on
nlgeom,on
nsubst,100
neqit,50

!Boundary Conditions (Clamps)

ksel,s,kp,,1
```

```
ksel,a,kp,,12
lslk,s,1
nsll,s
d,all,all,0

F1=0.68030
!(lb)
F2=0.40205
!(lb)
F3=0.40425
!(lb)
F4=0.68115
!(lb)

ksel,s,kp,,101
nslk,s
f,all,fx,F4
d,all,uy,0
d,all,uz,0
d,all,rotx,0
d,all,roty,0
d,all,rotz,0

ksel,s,kp,,102
nslk,s
f,all,fy,-F3
d,all,ux,0
d,all,uz,0
d,all,rotx,0
d,all,roty,0
d,all,rotz,0

ksel,s,kp,,103
nslk,s
f,all,fy,-F2
d,all,ux,0
d,all,uz,0
d,all,rotx,0
d,all,roty,0
d,all,rotz,0

ksel,s,kp,,104
nslk,s
f,all,fx,-F1
d,all,uy,0
d,all,uz,0
d,all,rotx,0
d,all,roty,0
d,all,rotz,0

allsel

acel,,,386.4-(386.4*.00077)
!(in/s^2)

solve
```

Test Case 4

```
finish
/clear
/filename,FabTriCase4
/prep7

!Material Properties
        EW=21055
        !(psi)
        EF=10682
        !(psi)
        G=0.07*EW
        !(psi)

 !Fabric
        mp,ey,1,EW
        mp,ex,1,EF
        mp,ez,1,EW
        mp,prxy,1,0.3
        mp,pryz,1,0.3
        mp,prxz,1,0.3
        mp,gxy,1,G
        mp,gyz,1,G
        mp,gxz,1,G
        mp,dens,1,0.037/386.4
        !(lb*s^2/in)

 !Clamp properties
        mp,ex,2,9860e3
        !(psi)
        mp,dens,2,0.0948697/386.4
        !(lb*s^2/in)
        mp,prxy,2,0.36

 !Fishing line properties
        mp,ex,3,223e3
        !(psi)
        mp,dens,3,0.046293/386.4
        !(lb*s^2/in)

!Elements

 !Fabric:
        et,1,shell181
        keyopt,1,3,2
        sectype,1,shell
        secdata,0.012
        !(in)

 !Clamp elements:
        et,2,shell181
        keyopt,2,3,2
        sectype,2,shell
        secdata,.261
        !(in)

 !Fishing line elements:
        et,3,beam188
        sectype,3,beam,csolid
        secdata,0.024/2
        !(in)

!Create Keypoints
        a=9
        !(in)
        b=0.75
        !(in)
        d=0.25
        c=sqrt(2)/2
        L1=12.75
        !(in)
        L2=41.25
        !(in)
        L3=43.25
        !(in)
        *afun,deg
        k,1,d,-d
        k,2,c*(a-b),-c*(a-b)
        k,3,c*(a-b/2),-c*(a-b/2)
        k,4,c*a,-c*a
        k,5,c*(a-b),-c*a
        k,6,c*(a-2*b),-c*a
        k,7,-c*(a-2*b),-c*a
        k,8,-c*(a-b),-c*a
        k,9,-c*a,-c*a
        k,10,-c*(a-b/2),-c*(a-b/2)
        k,11,-c*(a-b),-c*(a-b)
        k,12,-d,-d
        k,101,kx(3)+L2,ky(3),.345
        k,102,kx(5),ky(5)-L1,.345
        k,103,kx(8),ky(8)-L1,.345
```

```
k,104,kx(10)-L3,ky(10),.345

a,1,2,11,12
a,2,6,7,11

asel,s,area,,1,2
cm,FABRIC,area

a,2,3,5,6
a,3,4,5
!cm,RCLAMP,area

a,11,7,8,10
a,10,8,9
!cm,LCLAMP,area

allsel
aglue,all

ksel,s,kp,,1,2
lslk,s,1
ksel,s,kp,,11,12
lslk,a,1
ksel,s,kp,,6,7
lslk,a,1
ksel,s,kp,,2
ksel,a,kp,,11
lslk,a,1
lesize,all,,,50
allsel

ksel,s,kp,,1,2
ksel,a,kp,,6,7
ksel,a,kp,,11,12
lslk,s,1
asll,s,1
mshkey,1

!Material Orientation
local,11,0,0,0,0,0,0
esys,11
amesh,all
csys,0
esys,0

type,2
secnum,2
mat,2

asel,inve
mshkey,2
amesh,all
allsel

type,3
mat,3
secnum,3
l,3,101
l,5,102
l,10,104
l,8,103
ksel,s,kp,,3
ksel,a,kp,,101
lslk,s,1
ksel,s,kp,,5
ksel,a,kp,,102
lslk,a,1
ksel,s,kp,,10
ksel,a,kp,,104
lslk,a,1
ksel,s,kp,,8
ksel,a,kp,,103
lslk,a,1
lesize,all,,,50

lmesh,all

allsel

/solu
sstif,on
nlgeom,on
nsubst,100
neqit,50

!Boundary Conditions (Clamps)

ksel,s,kp,,1
```

```
ksel,a,kp,,12
lslk,s,1
nsll,s
d,all,all,0

F1=0.98065
!(lb)
F2=0.31845
!(lb)
F3=0.32185
!(lb)
F4=0.98
!(lb)

ksel,s,kp,,101
nslk,s
f,all,fx,F4
d,all,uy,0
d,all,uz,0
d,all,rotx,0
d,all,roty,0
d,all,rotz,0

ksel,s,kp,,102
nslk,s
f,all,fy,-F3
d,all,ux,0
d,all,uz,0
d,all,rotx,0
d,all,roty,0
d,all,rotz,0

ksel,s,kp,,103
nslk,s
f,all,fy,-F2
d,all,ux,0
d,all,uz,0
d,all,rotx,0
d,all,roty,0
d,all,rotz,0

ksel,s,kp,,104
nslk,s
f,all,fx,-F1
d,all,uy,0
d,all,uz,0
d,all,rotx,0
d,all,roty,0
d,all,rotz,0

allsel

acel,,,386.4-(386.4*.00077)
!(in/s^2)

solve
```

Test Case 5

```
finish
/clear
/filename,FabTriCase5
/prep7

!Material Properties
        EW=21055
        !(psi)
        EF=10682
        !(psi)
        G=0.15*EW
        !(psi)

 !Fabric
        mp,ey,1,EW
        mp,ex,1,EF
        mp,ez,1,EW
        mp,prxy,1,0.3
        mp,pryz,1,0.3
        mp,prxz,1,0.3
        mp,gxy,1,G
        mp,gyz,1,G
        mp,gxz,1,G
        mp,dens,1,0.037/386.4
        !(lb*s^2/in)

 !Clamp properties
        mp,ex,2,9860e3
        !(psi)
        mp,dens,2,0.0948697/386.4
        !(lb*s^2/in)
        mp,prxy,2,0.36

 !Fishing line properties
        mp,ex,3,223e3
        !(psi)
        mp,dens,3,0.046293/386.4
        !(lb*s^2/in)

!Elements

 !Fabric:
        et,1,shell181
        keyopt,1,3,2
        sectype,1,shell
        secdata,0.012
        !(in)

 !Clamp elements:
        et,2,shell181
        keyopt,2,3,2
        sectype,2,shell
        secdata,.261
        !(in)

 !Fishing line elements:
        et,3,beam188
        sectype,3,beam,csolid
        secdata,0.024/2
        !(in)

!Create Keypoints
        a=9
        !(in)
        b=0.75
        !(in)
        d=0.25
        c=sqrt(2)/2
        L1=12.75
        !(in)
        L2=41.25
        !(in)
        L3=43.25
        !(in)
        *afun,deg
        k,1,d,-d
        k,2,c*(a-b),-c*(a-b)
        k,3,c*(a-b/2),-c*(a-b/2)
        k,4,c*a,-c*a
        k,5,c*(a-b),-c*a
        k,6,c*(a-2*b),-c*a
        k,7,-c*(a-2*b),-c*a
        k,8,-c*(a-b),-c*a
        k,9,-c*a,-c*a
        k,10,-c*(a-b/2),-c*(a-b/2)
        k,11,-c*(a-b),-c*(a-b)
        k,12,-d,-d
        k,13,c*(a-b-1),-c*(a-b-1)
        k,14,kx(13)-0.1326,ky(13)-
0.1326
```

```
k,15,kx(13)-0.2210,ky(13)-
0.2210
k,16,kx(13)-0.3094,ky(13)-
0.3094
k,17,kx(13)-0.3977,ky(13)-
0.3977
k,18,kx(2)-0.1326,ky(2)-0.1326
k,19,kx(2)-0.2210,ky(2)-0.2210
k,20,kx(2)-0.3094,ky(2)-0.3094
k,21,kx(2)-0.3977,ky(2)-0.3977
k,22,-c*(a-b-1),-c*(a-b-1)
k,23,kx(22)+0.1326,ky(22)-
0.1326
k,24,kx(22)+0.2210,ky(22)-
0.2210
k,25,kx(22)+0.3094,ky(22)-
0.3094
k,26,kx(22)+0.3977,ky(22)-
0.3977
k,27,kx(11)+0.1326,ky(11)-
0.1326
k,28,kx(11)+0.2210,ky(11)-
0.2210
k,29,kx(11)+0.3094,ky(11)-
0.3094
k,30,kx(11)+0.3977,ky(11)-
0.3977

k,101,kx(3)+L2,ky(3),.345
k,102,kx(5),ky(5)-L1,.345
k,103,kx(8),ky(8)-L1,.345
k,104,kx(10)-L3,ky(10),.345

a,1,13,22,12
a,13,14,23,22
a,14,15,24,23
a,15,16,25,24
a,16,17,26,25
a,17,21,30,26
a,21,6,7,30
a,13,2,18,14
a,15,19,20,16
a,22,11,27,23
a,24,28,29,25

asel,s,area,,1,11
cm,FABRIC,area

a,2,3,5,6
a,3,4,5
cm,RCLAMP,area

a,11,7,8,10
a,10,8,9
cm,LCLAMP,area

allsel
aglue,all

ksel,s,kp,,1
ksel,a,kp,,13
lslk,s,1
ksel,s,kp,,12
ksel,a,kp,,22
lslk,a,1
ksel,s,kp,,13
ksel,a,kp,,22
lslk,a,1
ksel,s,kp,,14
ksel,s,kp,,23
lslk,a,1
ksel,s,kp,,15
ksel,s,kp,,24
lslk,a,1
ksel,s,kp,,16
ksel,s,kp,,25
lslk,a,1
ksel,s,kp,,17
ksel,s,kp,,26
lslk,a,1
ksel,s,kp,,21
ksel,a,kp,,30
lslk,a,1
ksel,s,kp,,6,7
lslk,a,1
lesize,all,,,50

asel,s,area,,1,11
mshkey,2

!Material Orientation
local,11,0,0,0,0,45
```

```
        esys,11
        amesh,all
        csys,0
        esys,0

        type,2
        secnum,2
        mat,2

        asel,s,area,,13,17
        mshkey,2
        amesh,all
        allsel

        type,3
        mat,3
        secnum,3
        l,3,101
        l,5,102
        l,10,104
        l,8,103
        ksel,s,kp,,3
        ksel,a,kp,,101
        lslk,s,1
        ksel,s,kp,,5
        ksel,a,kp,,102
        lslk,a,1
        ksel,s,kp,,10
        ksel,a,kp,,104
        lslk,a,1
        ksel,s,kp,,8
        ksel,a,kp,,103
        lslk,a,1
        lesize,all,,,50
        lmesh,all
        allsel

        nummrg,node

/solu
        sstif,on
        nlgeom,on
        nsubst,100
        neqit,50

!Boundary Conditions (Clamps)
        ksel,s,kp,,1
        ksel,a,kp,,12
        lslk,s,1
        nsll,s
        d,all,all,0

        F1=0.68030
        !(lb)
        F2=0.40205
        !(lb)
        F3=0.40425
        !(lb)
        F4=0.68115
        !(lb)

        ksel,s,kp,,101
        nslk,s
        f,all,fx,F4
        d,all,uy,0
        d,all,uz,0
        d,all,rotx,0
        d,all,roty,0
        d,all,rotz,0

        ksel,s,kp,,102
        nslk,s
        f,all,fy,-F3
        d,all,ux,0
        d,all,uz,0
        d,all,rotx,0
        d,all,roty,0
        d,all,rotz,0

        ksel,s,kp,,103
        nslk,s
        f,all,fy,-F2
        d,all,ux,0
        d,all,uz,0
        d,all,rotx,0
        d,all,roty,0
        d,all,rotz,0

        ksel,s,kp,,104
        nslk,s
        f,all,fx,-F1
        d,all,uy,0
```

```
d,all,uz,0
d,all,rotx,0
d,all,roty,0
d,all,rotz,0

allsel

acel,,,386.4-(386.4*.00077)
!(in/s^2)

solve
```

Test Case 6

```
finish
/clear
/filename,FabTriCase6
/prep7

!Material Properties
        EW=21055
        !(psi)
        EF=10682
        !(psi)
        G=3*EW
        !(psi)

 !Fabric
        mp,ey,1,EW
        mp,ex,1,EF
        mp,ez,1,EW
        mp,prxy,1,0.3
        mp,pryz,1,0.3
        mp,prxz,1,0.3
        mp,gxy,1,G
        mp,gyz,1,G
        mp,gxz,1,G
        mp,dens,1,0.037/386.4
        !(lb*s^2/in)

 !Clamp properties
        mp,ex,2,9860e3
        !(psi)
        mp,dens,2,0.0948697/386.4
        !(lb*s^2/in)
        mp,prxy,2,0.36

 !Fishing line properties
        mp,ex,3,223e3
        !(psi)
        mp,dens,3,0.046293/386.4
        !(lb*s^2/in)

!Elements

 !Fabric:
        et,1,shell181
        keyopt,1,3,2
        sectype,1,shell
        secdata,0.012
        !(in)

 !Clamp elements:
        et,2,shell181
        keyopt,2,3,2
        sectype,2,shell
        secdata,.261
        !(in)

 !Fishing line elements:
        et,3,beam188
        sectype,3,beam,csolid
        secdata,0.024/2
        !(in)

!Create Keypoints
        a=9
        !(in)
        b=0.75
        !(in)
        d=0.25
        c=sqrt(2)/2
        L1=12.75
        !(in)
        L2=41.25
        !(in)
        L3=43.25
        !(in)
        *afun,deg
        k,1,d,-d
        k,2,c*(a-b),-c*(a-b)
        k,3,c*(a-b/2),-c*(a-b/2)
        k,4,c*a,-c*a
        k,5,c*(a-b),-c*a
        k,6,c*(a-2*b),-c*a
        k,7,-c*(a-2*b),-c*a
        k,8,-c*(a-b),-c*a
        k,9,-c*a,-c*a
        k,10,-c*(a-b/2),-c*(a-b/2)
        k,11,-c*(a-b),-c*(a-b)
        k,12,-d,-d
        k,13,c*(a-b-1),-c*(a-b-1)
        k,14,kx(13)-0.1326,ky(13)-
0.1326
```

```
k,15,kx(13)-0.2210,ky(13)-
0.2210
k,16,kx(13)-0.3094,ky(13)-
0.3094
k,17,kx(13)-0.3977,ky(13)-
0.3977
k,18,kx(2)-0.1326,ky(2)-0.1326
k,19,kx(2)-0.2210,ky(2)-0.2210
k,20,kx(2)-0.3094,ky(2)-0.3094
k,21,kx(2)-0.3977,ky(2)-0.3977
k,22,-c*(a-b-1),-c*(a-b-1)
k,23,kx(22)+0.1326,ky(22)-
0.1326
k,24,kx(22)+0.2210,ky(22)-
0.2210
k,25,kx(22)+0.3094,ky(22)-
0.3094
k,26,kx(22)+0.3977,ky(22)-
0.3977
k,27,kx(11)+0.1326,ky(11)-
0.1326
k,28,kx(11)+0.2210,ky(11)-
0.2210
k,29,kx(11)+0.3094,ky(11)-
0.3094
k,30,kx(11)+0.3977,ky(11)-
0.3977

k,101,kx(3)+L2,ky(3),.345
k,102,kx(5),ky(5)-L1,.345
k,103,kx(8),ky(8)-L1,.345
k,104,kx(10)-L3,ky(10),.345

a,1,13,22,12
a,13,14,23,22
a,14,15,24,23
a,15,16,25,24
a,16,17,26,25
a,17,21,30,26
a,21,6,7,30
a,13,2,18,14
a,15,19,20,16
a,22,11,27,23
a,24,28,29,25

asel,s,area,,1,11
cm,FABRIC,area

a,2,3,5,6
a,3,4,5
cm,RCLAMP,area

a,11,7,8,10
a,10,8,9
cm,LCLAMP,area

allsel
aglue,all

ksel,s,kp,,1
ksel,a,kp,,13
lslk,s,1
ksel,s,kp,,12
ksel,a,kp,,22
lslk,a,1
ksel,s,kp,,13
ksel,a,kp,,22
lslk,a,1
ksel,s,kp,,14
ksel,s,kp,,23
lslk,a,1
ksel,s,kp,,15
ksel,s,kp,,24
lslk,a,1
ksel,s,kp,,16
ksel,s,kp,,25
lslk,a,1
ksel,s,kp,,17
ksel,s,kp,,26
lslk,a,1
ksel,s,kp,,21
ksel,a,kp,,30
lslk,a,1
ksel,s,kp,,6,7
lslk,a,1
lesize,all,,,50

asel,s,area,,1,11
mshkey,2

!Material Orientation
local,11,0,0,0,0,0,45
```

```
        esys,11
        amesh,all
        csys,0
        esys,0

        type,2
        secnum,2
        mat,2

        asel,s,area,,13,17
        mshkey,2
        amesh,all
        allsel

        type,3
        mat,3
        secnum,3
        l,3,101
        l,5,102
        l,10,104
        l,8,103
        ksel,s,kp,,3
        ksel,a,kp,,101
        lslk,s,1
        ksel,s,kp,,5
        ksel,a,kp,,102
        lslk,a,1
        ksel,s,kp,,10
        ksel,a,kp,,104
        lslk,a,1
        ksel,s,kp,,8
        ksel,a,kp,,103
        lslk,a,1
        lesize,all,,,50
        lmesh,all
        allsel

        nummrg,node

/solu
        sstif,on
        nlgeom,on
        nsubst,100
        neqit,50

!Boundary Conditions (Clamps)
        ksel,s,kp,,1
        ksel,a,kp,,12
        lslk,s,1
        nsll,s
        d,all,all,0

        F1=0.98185
        !(lb)
        F2=0.31835
        !(lb)
        F3=0.3191
        !(lb)
        F4=0.98145
        !(lb)

        ksel,s,kp,,101
        nslk,s
        f,all,fx,F4
        d,all,uy,0
        d,all,uz,0
        d,all,rotx,0
        d,all,roty,0
        d,all,rotz,0

        ksel,s,kp,,102
        nslk,s
        f,all,fy,-F3
        d,all,ux,0
        d,all,uz,0
        d,all,rotx,0
        d,all,roty,0
        d,all,rotz,0

        ksel,s,kp,,103
        nslk,s
        f,all,fy,-F2
        d,all,ux,0
        d,all,uz,0
        d,all,rotx,0
        d,all,roty,0
        d,all,rotz,0

        ksel,s,kp,,104
        nslk,s
        f,all,fx,-F1
        d,all,uy,0
```

```
d,all,uz,0
d,all,rotx,0
d,all,roty,0
d,all,rotz,0

allsel

acel,,,386.4-(386.4*.00077)
!(in/s^2)

solve
```

Test Case 7

```
finish
/clear
/filename,FabTriCase7
/prep7

!Material Properties
        EW=21055
        !(psi)
        EF=10682
        !(psi)
        G=0.06*EW
        !(psi)

 !Fabric
        mp,ey,1,EW
        mp,ex,1,EF
        mp,ez,1,EW
        mp,prxy,1,0.3
        mp,pryz,1,0.3
        mp,prxz,1,0.3
        mp,gxy,1,G
        mp,gyz,1,G
        mp,gxz,1,G
        mp,dens,1,0.037/386.4
        !(lb*s^2/in)

 !Clamp properties
        mp,ex,2,9860e3
        !(psi)
        mp,dens,2,0.0948697/386.4
        !(lb*s^2/in)
        mp,prxy,2,0.36

 !Fishing line properties
        mp,ex,3,223e3
        !(psi)
        mp,dens,3,0.046293/386.4
        !(lb*s^2/in)

!Elements

 !Fabric:
        et,1,shell181
        keyopt,1,3,2
        sectype,1,shell
        secdata,0.012
        !(in)

 !Clamp elements:
        et,2,shell181
        keyopt,2,3,2
        sectype,2,shell
        secdata,.261
        !(in)

 !Fishing line elements:
        et,3,beam188
        sectype,3,beam,csolid
        secdata,0.024/2
        !(in)

!Create Keypoints
        a=9
        !(in)
        b=0.75
        !(in)
        d=0.25
        c=sqrt(2)/2
        L1=12.75
        !(in)
        L2=41.25
        !(in)
        L3=43.25
        !(in)
        *afun,deg
        k,1,d,-d
        k,2,c*(a-b),-c*(a-b)
        k,3,c*(a-b/2),-c*(a-b/2)
        k,4,c*a,-c*a
        k,5,c*(a-b),-c*a
        k,6,c*(a-2*b),-c*a
        k,7,-c*(a-2*b),-c*a
        k,8,-c*(a-b),-c*a
        k,9,-c*a,-c*a
        k,10,-c*(a-b/2),-c*(a-b/2)
        k,11,-c*(a-b),-c*(a-b)
        k,12,-d,-d
        k,13,c*(a-b-1),-c*(a-b-1)
        k,14,kx(13)-0.1326,ky(13)-
0.1326
```

```
k,15,kx(13)-0.2210,ky(13)-
0.2210
k,16,kx(13)-0.3094,ky(13)-
0.3094
k,17,kx(13)-0.3977,ky(13)-
0.3977
k,18,kx(2)-0.1326,ky(2)-0.1326
k,19,kx(2)-0.2210,ky(2)-0.2210
k,20,kx(2)-0.3094,ky(2)-0.3094
k,21,kx(2)-0.3977,ky(2)-0.3977
k,22,-c*(a-b-1),-c*(a-b-1)
k,23,kx(22)+0.1326,ky(22)-
0.1326
k,24,kx(22)+0.2210,ky(22)-
0.2210
k,25,kx(22)+0.3094,ky(22)-
0.3094
k,26,kx(22)+0.3977,ky(22)-
0.3977
k,27,kx(11)+0.1326,ky(11)-
0.1326
k,28,kx(11)+0.2210,ky(11)-
0.2210
k,29,kx(11)+0.3094,ky(11)-
0.3094
k,30,kx(11)+0.3977,ky(11)-
0.3977

k,101,kx(3)+L2,ky(3),.345
k,102,kx(5),ky(5)-L1,.345
k,103,kx(8),ky(8)-L1,.345
k,104,kx(10)-L3,ky(10),.345

a,1,13,22,12
a,13,14,23,22
a,14,15,24,23
a,15,16,25,24
a,16,17,26,25
a,17,21,30,26
a,21,6,7,30
a,13,2,18,14
a,15,19,20,16
a,22,11,27,23
a,24,28,29,25

asel,s,area,,1,11
cm,FABRIC,area

a,2,3,5,6
a,3,4,5
cm,RCLAMP,area

a,11,7,8,10
a,10,8,9
cm,LCLAMP,area

allsel
aglue,all

ksel,s,kp,,1
ksel,a,kp,,13
lslk,s,1
ksel,s,kp,,12
ksel,a,kp,,22
lslk,a,1
ksel,s,kp,,13
ksel,a,kp,,22
lslk,a,1
ksel,s,kp,,14
ksel,s,kp,,23
lslk,a,1
ksel,s,kp,,15
ksel,s,kp,,24
lslk,a,1
ksel,s,kp,,16
ksel,s,kp,,25
lslk,a,1
ksel,s,kp,,17
ksel,s,kp,,26
lslk,a,1
ksel,s,kp,,21
ksel,a,kp,,30
lslk,a,1
ksel,s,kp,,6,7
lslk,a,1
lesize,all,,,50

asel,s,area,,1,11
mshkey,2

!Material Orientation
local,11,0,0,0,0,0
```

```
        esys,11
        amesh,all
        csys,0
        esys,0

        type,2
        secnum,2
        mat,2

        asel,s,area,,13,17
        mshkey,2
        amesh,all
        allsel

        type,3
        mat,3
        secnum,3
        l,3,101
        l,5,102
        l,10,104
        l,8,103
        ksel,s,kp,,3
        ksel,a,kp,,101
        lslk,s,1
        ksel,s,kp,,5
        ksel,a,kp,,102
        lslk,a,1
        ksel,s,kp,,10
        ksel,a,kp,,104
        lslk,a,1
        ksel,s,kp,,8
        ksel,a,kp,,103
        lslk,a,1
        lesize,all,,,50
        lmesh,all
        allsel

        nummrg,node

/solu
        sstif,on
        nlgeom,on
        nsubst,100
        neqit,50

!Boundary Conditions (Clamps)
        ksel,s,kp,,1
        ksel,a,kp,,12
        lslk,s,1
        nsll,s
        d,all,all,0

        F1=0.68030
        !(lb)
        F2=0.40205
        !(lb)
        F3=0.40425
        !(lb)
        F4=0.68115
        !(lb)

        ksel,s,kp,,101
        nslk,s
        f,all,fx,F4
        d,all,uy,0
        d,all,uz,0
        d,all,rotx,0
        d,all,roty,0
        d,all,rotz,0

        ksel,s,kp,,102
        nslk,s
        f,all,fy,-F3
        d,all,ux,0
        d,all,uz,0
        d,all,rotx,0
        d,all,roty,0
        d,all,rotz,0

        ksel,s,kp,,103
        nslk,s
        f,all,fy,-F2
        d,all,ux,0
        d,all,uz,0
        d,all,rotx,0
        d,all,roty,0
        d,all,rotz,0

        ksel,s,kp,,104
        nslk,s
        f,all,fx,-F1
        d,all,uy,0
```

```
d,all,uz,0
d,all,rotx,0
d,all,roty,0
d,all,rotz,0

allsel

acel,,,386.4-(386.4*.00077)
!(in/s^2)

solve
```

Test Case 8

```
finish
/clear
/filename,FabTriCase8
/prep7

!Material Properties
        EW=21055
        !(psi)
        EF=10682
        !(psi)
        G=10*EW
        !(psi)

 !Fabric
        mp,ey,1,EW
        mp,ex,1,EF
        mp,ez,1,EW
        mp,prxy,1,0.3
        mp,pryz,1,0.3
        mp,prxz,1,0.3
        mp,gxy,1,G
        mp,gyz,1,G
        mp,gxz,1,G
        mp,dens,1,0.037/386.4
        !(lb*s^2/in)

 !Clamp properties
        mp,ex,2,9860e3
        !(psi)
        mp,dens,2,0.0948697/386.4
        !(lb*s^2/in)
        mp,prxy,2,0.36

 !Fishing line properties
        mp,ex,3,223e3
        !(psi)
        mp,dens,3,0.046293/386.4
        !(lb*s^2/in)

!Elements

 !Fabric:
        et,1,shell181
        keyopt,1,3,2
        sectype,1,shell
        secdata,0.012
        !(in)

 !Clamp elements:
        et,2,shell181
        keyopt,2,3,2
        sectype,2,shell
        secdata,.261
        !(in)

 !Fishing line elements:
        et,3,beam188
        sectype,3,beam,csolid
        secdata,0.024/2
        !(in)

!Create Keypoints
        a=9
        !(in)
        b=0.75
        !(in)
        d=0.25
        c=sqrt(2)/2
        L1=12.75
        !(in)
        L2=41.25
        !(in)
        L3=43.25
        !(in)
        *afun,deg
        k,1,d,-d
        k,2,c*(a-b),-c*(a-b)
        k,3,c*(a-b/2),-c*(a-b/2)
        k,4,c*a,-c*a
        k,5,c*(a-b),-c*a
        k,6,c*(a-2*b),-c*a
        k,7,-c*(a-2*b),-c*a
        k,8,-c*(a-b),-c*a
        k,9,-c*a,-c*a
        k,10,-c*(a-b/2),-c*(a-b/2)
        k,11,-c*(a-b),-c*(a-b)
        k,12,-d,-d
        k,13,c*(a-b-1),-c*(a-b-1)
        k,14,kx(13)-0.1326,ky(13)-
0.1326
```

```
k,15,kx(13)-0.2210,ky(13)-
0.2210
k,16,kx(13)-0.3094,ky(13)-
0.3094
k,17,kx(13)-0.3977,ky(13)-
0.3977
k,18,kx(2)-0.1326,ky(2)-0.1326
k,19,kx(2)-0.2210,ky(2)-0.2210
k,20,kx(2)-0.3094,ky(2)-0.3094
k,21,kx(2)-0.3977,ky(2)-0.3977
k,22,-c*(a-b-1),-c*(a-b-1)
k,23,kx(22)+0.1326,ky(22)-
0.1326
k,24,kx(22)+0.2210,ky(22)-
0.2210
k,25,kx(22)+0.3094,ky(22)-
0.3094
k,26,kx(22)+0.3977,ky(22)-
0.3977
k,27,kx(11)+0.1326,ky(11)-
0.1326
k,28,kx(11)+0.2210,ky(11)-
0.2210
k,29,kx(11)+0.3094,ky(11)-
0.3094
k,30,kx(11)+0.3977,ky(11)-
0.3977

k,101,kx(3)+L2,ky(3),.345
k,102,kx(5),ky(5)-L1,.345
k,103,kx(8),ky(8)-L1,.345
k,104,kx(10)-L3,ky(10),.345

a,1,13,22,12
a,13,14,23,22
a,14,15,24,23
a,15,16,25,24
a,16,17,26,25
a,17,21,30,26
a,21,6,7,30
a,13,2,18,14
a,15,19,20,16
a,22,11,27,23
a,24,28,29,25

asel,s,area,,1,11
cm,FABRIC,area

a,2,3,5,6
a,3,4,5
cm,RCLAMP,area

a,11,7,8,10
a,10,8,9
cm,LCLAMP,area

allsel
aglue,all

ksel,s,kp,,1
ksel,a,kp,,13
lslk,s,1
ksel,s,kp,,12
ksel,a,kp,,22
lslk,a,1
ksel,s,kp,,13
ksel,a,kp,,22
lslk,a,1
ksel,s,kp,,14
ksel,s,kp,,23
lslk,a,1
ksel,s,kp,,15
ksel,s,kp,,24
lslk,a,1
ksel,s,kp,,16
ksel,s,kp,,25
lslk,a,1
ksel,s,kp,,17
ksel,s,kp,,26
lslk,a,1
ksel,s,kp,,21
ksel,a,kp,,30
lslk,a,1
ksel,s,kp,,6,7
lslk,a,1
lesize,all,,,50

asel,s,area,,1,11
mshkey,2

!Material Orientation
local,11,0,0,0,0,0
```

```
        esys,11
        amesh,all
        csys,0
        esys,0

        type,2
        secnum,2
        mat,2

        asel,s,area,,13,17
        mshkey,2
        amesh,all
        allsel

        type,3
        mat,3
        secnum,3
        l,3,101
        l,5,102
        l,10,104
        l,8,103
        ksel,s,kp,,3
        ksel,a,kp,,101
        lslk,s,1
        ksel,s,kp,,5
        ksel,a,kp,,102
        lslk,a,1
        ksel,s,kp,,10
        ksel,a,kp,,104
        lslk,a,1
        ksel,s,kp,,8
        ksel,a,kp,,103
        lslk,a,1
        lesize,all,,,50
        lmesh,all
        allsel

        nummrg,node

/solu
        sstif,on
        nlgeom,on
        nsubst,100
        neqit,50

!Boundary Conditions (Clamps)
        ksel,s,kp,,1
        ksel,a,kp,,12
        lslk,s,1
        nsll,s
        d,all,all,0

        F1=0.98185
        !(lb)
        F2=0.31835
        !(lb)
        F3=0.3191
        !(lb)
        F4=0.98145
        !(lb)

        ksel,s,kp,,101
        nslk,s
        f,all,fx,F4
        d,all,uy,0
        d,all,uz,0
        d,all,rotx,0
        d,all,roty,0
        d,all,rotz,0

        ksel,s,kp,,102
        nslk,s
        f,all,fy,-F3
        d,all,ux,0
        d,all,uz,0
        d,all,rotx,0
        d,all,roty,0
        d,all,rotz,0

        ksel,s,kp,,103
        nslk,s
        f,all,fy,-F2
        d,all,ux,0
        d,all,uz,0
        d,all,rotx,0
        d,all,roty,0
        d,all,rotz,0

        ksel,s,kp,,104
        nslk,s
        f,all,fx,-F1
        d,all,uy,0
```

```
d,all,uz,0
d,all,rotx,0
d,all,roty,0
d,all,rotz,0

allsel

acel,,,386.4-(386.4*.00077)
!(in/s^2)

solve
```

Test Case 9

```
finish
/clear
/filename,FabTriCase9
/prep7

!Material Properties
	EW=21055
	!(psi)
	EF=10682
	!(psi)
	G=0.11*EW
	!(psi)

 !Fabric
	mp,ey,1,EW
	mp,ex,1,EF
	mp,ez,1,EW
	mp,prxy,1,0.3
	mp,pryz,1,0.3
	mp,prxz,1,0.3
	mp,gxy,1,G
	mp,gyz,1,G
	mp,gxz,1,G
	mp,dens,1,0.037/386.4
	!(lb*s^2/in)

 !Clamp properties
	mp,ex,2,9860e3
	!(psi)
	mp,dens,2,0.0948697/386.4
	!(lb*s^2/in)
	mp,prxy,2,0.36

 !Fishing line properties
	mp,ex,3,223e3
	!(psi)
	mp,dens,3,0.046293/386.4
	!(lb*s^2/in)

!Elements

 !Fabric:
	et,1,shell181
	keyopt,1,3,2
	sectype,1,shell
	secdata,0.012
	!(in)

 !Clamp elements:
	et,2,shell181
	keyopt,2,3,2
	sectype,2,shell
	secdata,.261
	!(in)

 !Fishing line elements:
	et,3,beam188
	sectype,3,beam,csolid
	secdata,0.024/2
	!(in)

!Create Keypoints
	a=9
	!(in)
	b=0.75
	!(in)
	d=0.25
	c=sqrt(2)/2
	L1=12.75
	!(in)
	L2=41.25
	!(in)
	L3=43.25
	!(in)
	*afun,deg
	k,1,d,-d
	k,2,c*(a-b),-c*(a-b)
	k,3,c*(a-b/2),-c*(a-b/2)
	k,4,c*a,-c*a
	k,5,c*(a-b),-c*a
	k,6,c*(a-2*b),-c*a
	k,7,-c*(a-2*b),-c*a
	k,8,-c*(a-b),-c*a
	k,9,-c*a,-c*a
	k,10,-c*(a-b/2),-c*(a-b/2)
	k,11,-c*(a-b),-c*(a-b)
	k,12,-d,-d
	k,13,kx(2)-0.1326,ky(2)-0.1326
	k,14,Kx(6)+0.1768,ky(6)+0.1768
	k,15,Kx(7)-0.1768,ky(6)+0.1768
```

```
k,16,kx(11)+0.1326,ky(11)-.1326
k,17,kx(4)-0.4375,ky(4)+0.1768
k,18,kx(9)+0.4375,ky(9)+0.1768

k,101,kx(3)+L2,ky(3),.345
k,102,kx(5),ky(5)-L1,.345
k,103,kx(8),ky(8)-L1,.345
k,104,kx(10)-L3,ky(10),.345

a,1,2,11,12
a,2,13,16,11
a,13,14,15,16
a,13,17,14
a,15,16,18
a,14,6,7,15

asel,s,area,,1,4
cm,FABRIC,area

a,2,3,4,5,6,14,17,13
cm,RCLAMP,area

a,11,10,9,8,7,15,18,16
cm,LCLAMP,area

allsel
aglue,all

ksel,s,kp,,1,2
lslk,s,1
ksel,s,kp,,11,12
lslk,a,1
ksel,s,kp,,6,7
lslk,a,1
ksel,s,kp,,2
ksel,a,kp,,11
lslk,a,1
ksel,s,kp,,13
ksel,a,kp,,16
lslk,a,1
ksel,s,kp,,14
ksel,a,kp,,15
lslk,a,1
lesize,all,,,50
allsel
ksel,s,kp,,15
ksel,a,kp,,18
lslk,s,1
ksel,s,kp,,18
ksel,a,kp,,16
lslk,a,1
ksel,s,kp,,14
ksel,a,kp,,17
lslk,a,1
ksel,s,kp,,17
ksel,a,kp,,13
lslk,a,1
ksel,s,kp,,15
ksel,a,kp,,16
lslk,a,1
ksel,s,kp,,13
ksel,a,kp,,14
lslk,a,1
lesize,all,,,5

asel,s,area,,1,6
mshkey,2

!Material Orientation
local,11,0,0,0,0,45
esys,11
amesh,all
csys,0
esys,0

type,2
secnum,2
mat,2

asel,s,area,,7,8
mshkey,0
amesh,all
allsel

type,3
mat,3
secnum,3
l,3,101
l,5,102
l,10,104
l,8,103
```

```
        ksel,s,kp,,3
        ksel,a,kp,,101
        lslk,s,1
        ksel,s,kp,,5
        ksel,a,kp,,102
        lslk,a,1
        ksel,s,kp,,10
        ksel,a,kp,,104
        lslk,a,1
        ksel,s,kp,,8
        ksel,a,kp,,103
        lslk,a,1
        lesize,all,,,50

        lmesh,all

        allsel
        nummrg,node

/solu
        sstif,on
        nlgeom,on
        nsubst,100
        neqit,50

!Boundary Conditions (Clamps)
        ksel,s,kp,,1
        ksel,a,kp,,12
        lslk,s,1
        nsll,s
        d,all,all,0

        F1=0.67955
        !(lb)
        F2=0.4016
        !(lb)
        F3=0.40505
        !(lb)
        F4=0.68035
        !(lb)

        ksel,s,kp,,101
        nslk,s
        f,all,fx,F4
        d,all,uy,0
        d,all,uz,0
        d,all,rotx,0
        d,all,roty,0
        d,all,rotz,0

        ksel,s,kp,,102
        nslk,s
        f,all,fy,-F3
        d,all,ux,0
        d,all,uz,0
        d,all,rotx,0
        d,all,roty,0
        d,all,rotz,0

        ksel,s,kp,,103
        nslk,s
        f,all,fy,-F2
        d,all,ux,0
        d,all,uz,0
        d,all,rotx,0
        d,all,roty,0
        d,all,rotz,0

        ksel,s,kp,,104
        nslk,s
        f,all,fx,-F1
        d,all,uy,0
        d,all,uz,0
        d,all,rotx,0
        d,all,roty,0
        d,all,rotz,0

        allsel

        acel,,,386.4-(386.4*.00077)
        !(in/s^2)

        solve
```

Test Case 10

```
finish
/clear
/filename,FabTriCase10
/prep7

!Material Properties
	EW=21055
	!(psi)
	EF=10682
	!(psi)
	G=0.11*EW
	!(psi)

 !Fabric
	mp,ey,1,EW
	mp,ex,1,EF
	mp,ez,1,EW
	mp,prxy,1,0.3
	mp,pryz,1,0.3
	mp,prxz,1,0.3
	mp,gxy,1,G
	mp,gyz,1,G
	mp,gxz,1,G
	mp,dens,1,0.037/386.4
	!(lb*s^2/in)

 !Clamp properties
	mp,ex,2,9860e3
	!(psi)
	mp,dens,2,0.0948697/386.4
	!(lb*s^2/in)
	mp,prxy,2,0.36

 !Fishing line properties
	mp,ex,3,223e3
	!(psi)
	mp,dens,3,0.046293/386.4
	!(lb*s^2/in)

!Elements

 !Fabric:
	et,1,shell181
	keyopt,1,3,2
	sectype,1,shell
	secdata,0.012
	!(in)

 !Clamp elements:
	et,2,shell181
	keyopt,2,3,2
	sectype,2,shell
	secdata,.261
	!(in)

 !Fishing line elements:
	et,3,beam188
	sectype,3,beam,csolid
	secdata,0.024/2
	!(in)

!Create Keypoints
	a=9
	!(in)
	b=0.75
	!(in)
	d=0.25
	c=sqrt(2)/2
	L1=12.75
	!(in)
	L2=41.25
	!(in)
	L3=43.25
	!(in)
	*afun,deg
	k,1,d,-d
	k,2,c*(a-b),-c*(a-b)
	k,3,c*(a-b/2),-c*(a-b/2)
	k,4,c*a,-c*a
	k,5,c*(a-b),-c*a
	k,6,c*(a-2*b),-c*a
	k,7,-c*(a-2*b),-c*a
	k,8,-c*(a-b),-c*a
	k,9,-c*a,-c*a
	k,10,-c*(a-b/2),-c*(a-b/2)
	k,11,-c*(a-b),-c*(a-b)
	k,12,-d,-d
	k,13,kx(2)-0.1326,ky(2)-0.1326
	k,14,Kx(6)+0.1768,ky(6)+0.1768
	k,15,Kx(7)-0.1768,ky(6)+0.1768
```

```
k,16,kx(11)+0.1326,ky(11)-.1326
k,17,kx(4)-0.4375,ky(4)+0.1768
k,18,kx(9)+0.4375,ky(9)+0.1768

k,101,kx(3)+L2,ky(3),.345
k,102,kx(5),ky(5)-L1,.345
k,103,kx(8),ky(8)-L1,.345
k,104,kx(10)-L3,ky(10),.345

a,1,2,11,12
a,2,13,16,11
a,13,14,15,16
a,13,17,14
a,15,16,18
a,14,6,7,15

asel,s,area,,1,4
cm,FABRIC,area

a,2,3,4,5,6,14,17,13
cm,RCLAMP,area

a,11,10,9,8,7,15,18,16
cm,LCLAMP,area

allsel
aglue,all

ksel,s,kp,,1,2
lslk,s,1
ksel,s,kp,,11,12
lslk,a,1
ksel,s,kp,,6,7
lslk,a,1
ksel,s,kp,,2
ksel,a,kp,,11
lslk,a,1
ksel,s,kp,,13
ksel,a,kp,,16
lslk,a,1
ksel,s,kp,,14
ksel,a,kp,,15
lslk,a,1
lesize,all,,,50
allsel
ksel,s,kp,,15
ksel,a,kp,,18
lslk,s,1
ksel,s,kp,,18
ksel,a,kp,,16
lslk,a,1
ksel,s,kp,,14
ksel,a,kp,,17
lslk,a,1
ksel,s,kp,,17
ksel,a,kp,,13
lslk,a,1
ksel,s,kp,,15
ksel,a,kp,,16
lslk,a,1
ksel,s,kp,,13
ksel,a,kp,,14
lslk,a,1
lesize,all,,,5

asel,s,area,,1,6
mshkey,2

!Material Orientation
local,11,0,0,0,0,45
esys,11
amesh,all
csys,0
esys,0

type,2
secnum,2
mat,2

asel,s,area,,7,8
mshkey,0
amesh,all
allsel

type,3
mat,3
secnum,3
l,3,101
l,5,102
l,10,104
l,8,103
```

```
        ksel,s,kp,,3
        ksel,a,kp,,101
        lslk,s,1
        ksel,s,kp,,5
        ksel,a,kp,,102
        lslk,a,1
        ksel,s,kp,,10
        ksel,a,kp,,104
        lslk,a,1
        ksel,s,kp,,8
        ksel,a,kp,,103
        lslk,a,1
        lesize,all,,,50

        lmesh,all

        allsel
        nummrg,node

/solu
        sstif,on
        nlgeom,on
        nsubst,100
        neqit,50

!Boundary Conditions (Clamps)
        ksel,s,kp,,1
        ksel,a,kp,,12
        lslk,s,1
        nsll,s
        d,all,all,0

        F1=0.9816
        !(lb)
        F2=0.3184
        !(lb)
        F3=0.31915
        !(lb)
        F4=0.9822
        !(lb)

        ksel,s,kp,,101
        nslk,s
        f,all,fx,F4
        d,all,uy,0
        d,all,uz,0
        d,all,rotx,0
        d,all,roty,0
        d,all,rotz,0

        ksel,s,kp,,102
        nslk,s
        f,all,fy,-F3
        d,all,ux,0
        d,all,uz,0
        d,all,rotx,0
        d,all,roty,0
        d,all,rotz,0

        ksel,s,kp,,103
        nslk,s
        f,all,fy,-F2
        d,all,ux,0
        d,all,uz,0
        d,all,rotx,0
        d,all,roty,0
        d,all,rotz,0

        ksel,s,kp,,104
        nslk,s
        f,all,fx,-F1
        d,all,uy,0
        d,all,uz,0
        d,all,rotx,0
        d,all,roty,0
        d,all,rotz,0

        allsel

        acel,,,386.4-(386.4*.00077)
        !(in/s^2)

        solve
```

Test Case 11

```
finish
/clear
/filename,FabTriCase11
/prep7

!Material Properties
        EW=21055
        !(psi)
        EF=10682
        !(psi)
        G=0.04*EW
        !(psi)

 !Fabric
        mp,ey,1,EW
        mp,ex,1,EF
        mp,ez,1,EW
        mp,prxy,1,0.3
        mp,pryz,1,0.3
        mp,prxz,1,0.3
        mp,gxy,1,G
        mp,gyz,1,G
        mp,gxz,1,G
        mp,dens,1,0.037/386.4
        !(lb*s^2/in)

 !Clamp properties
        mp,ex,2,9860e3
        !(psi)
        mp,dens,2,0.0948697/386.4
        !(lb*s^2/in)
        mp,prxy,2,0.36

 !Fishing line properties
        mp,ex,3,223e3
        !(psi)
        mp,dens,3,0.046293/386.4
        !(lb*s^2/in)

!Elements

 !Fabric:
        et,1,shell181
        keyopt,1,3,2
        sectype,1,shell
        secdata,0.012
        !(in)

 !Clamp elements:
        et,2,shell181
        keyopt,2,3,2
        sectype,2,shell
        secdata,.261
        !(in)

 !Fishing line elements:
        et,3,beam188
        sectype,3,beam,csolid
        secdata,0.024/2
        !(in)

!Create Keypoints
        a=9
        !(in)
        b=0.75
        !(in)
        d=0.25
        c=sqrt(2)/2
        L1=12.75
        !(in)
        L2=41.25
        !(in)
        L3=43.25
        !(in)
        *afun,deg
        k,1,d,-d
        k,2,c*(a-b),-c*(a-b)
        k,3,c*(a-b/2),-c*(a-b/2)
        k,4,c*a,-c*a
        k,5,c*(a-b),-c*a
        k,6,c*(a-2*b),-c*a
        k,7,-c*(a-2*b),-c*a
        k,8,-c*(a-b),-c*a
        k,9,-c*a,-c*a
        k,10,-c*(a-b/2),-c*(a-b/2)
        k,11,-c*(a-b),-c*(a-b)
        k,12,-d,-d
        k,13,kx(2)-0.1326,ky(2)-0.1326
        k,14,Kx(6)+0.1768,ky(6)+0.1768
        k,15,Kx(7)-0.1768,ky(6)+0.1768
```

```
k,16,kx(11)+0.1326,ky(11)-.1326
k,17,kx(4)-0.4375,ky(4)+0.1768
k,18,kx(9)+0.4375,ky(9)+0.1768

k,101,kx(3)+L2,ky(3),.345
k,102,kx(5),ky(5)-L1,.345
k,103,kx(8),ky(8)-L1,.345
k,104,kx(10)-L3,ky(10),.345

a,1,2,11,12
a,2,13,16,11
a,13,14,15,16
a,13,17,14
a,15,16,18
a,14,6,7,15

asel,s,area,,1,4
cm,FABRIC,area

a,2,3,4,5,6,14,17,13
cm,RCLAMP,area

a,11,10,9,8,7,15,18,16
cm,LCLAMP,area

allsel
aglue,all

ksel,s,kp,,1,2
lslk,s,1
ksel,s,kp,,11,12
lslk,a,1
ksel,s,kp,,6,7
lslk,a,1
ksel,s,kp,,2
ksel,a,kp,,11
lslk,a,1
ksel,s,kp,,13
ksel,a,kp,,16
lslk,a,1
ksel,s,kp,,14
ksel,a,kp,,15
lslk,a,1
lesize,all,,,50
allsel
ksel,s,kp,,15
ksel,a,kp,,18
lslk,s,1
ksel,s,kp,,18
ksel,a,kp,,16
lslk,a,1
ksel,s,kp,,14
ksel,a,kp,,17
lslk,a,1
ksel,s,kp,,17
ksel,a,kp,,13
lslk,a,1
ksel,s,kp,,15
ksel,a,kp,,16
lslk,a,1
ksel,s,kp,,13
ksel,a,kp,,14
lslk,a,1
lesize,all,,,5

asel,s,area,,1,6
mshkey,2

!Material Orientation
local,11,0,0,0,0,0
esys,11
amesh,all
csys,0
esys,0

type,2
secnum,2
mat,2

asel,s,area,,7,8
mshkey,0
amesh,all
allsel

type,3
mat,3
secnum,3
l,3,101
l,5,102
l,10,104
l,8,103
```

```
        ksel,s,kp,,3
        ksel,a,kp,,101
        lslk,s,1
        ksel,s,kp,,5
        ksel,a,kp,,102
        lslk,a,1
        ksel,s,kp,,10
        ksel,a,kp,,104
        lslk,a,1
        ksel,s,kp,,8
        ksel,a,kp,,103
        lslk,a,1
        lesize,all,,,50

        lmesh,all

        allsel
        nummrg,node

/solu
        sstif,on
        nlgeom,on
        nsubst,100
        neqit,50

!Boundary Conditions (Clamps)
        ksel,s,kp,,1
        ksel,a,kp,,12
        lslk,s,1
        nsll,s
        d,all,all,0

        F1=0.67955
        !(lb)
        F2=0.4016
        !(lb)
        F3=0.40505
        !(lb)
        F4=0.68035
        !(lb)

        ksel,s,kp,,101
        nslk,s
        f,all,fx,F4
        d,all,uy,0
        d,all,uz,0
        d,all,rotx,0
        d,all,roty,0
        d,all,rotz,0

        ksel,s,kp,,102
        nslk,s
        f,all,fy,-F3
        d,all,ux,0
        d,all,uz,0
        d,all,rotx,0
        d,all,roty,0
        d,all,rotz,0

        ksel,s,kp,,103
        nslk,s
        f,all,fy,-F2
        d,all,ux,0
        d,all,uz,0
        d,all,rotx,0
        d,all,roty,0
        d,all,rotz,0

        ksel,s,kp,,104
        nslk,s
        f,all,fx,-F1
        d,all,uy,0
        d,all,uz,0
        d,all,rotx,0
        d,all,roty,0
        d,all,rotz,0

        allsel

        acel,,,386.4-(386.4*.00077)
        !(in/s^2)

        solve
```

Test Case 12

```
finish
/clear
/filename,FabTriCase12
/prep7

!Material Properties
	EW=21055
	!(psi)
	EF=10682
	!(psi)
	G=0.04*EW
	!(psi)

 !Fabric
	mp,ey,1,EW
	mp,ex,1,EF
	mp,ez,1,EW
	mp,prxy,1,0.3
	mp,pryz,1,0.3
	mp,prxz,1,0.3
	mp,gxy,1,G
	mp,gyz,1,G
	mp,gxz,1,G
	mp,dens,1,0.037/386.4
	!(lb*s^2/in)

 !Clamp properties
	mp,ex,2,9860e3
	!(psi)
	mp,dens,2,0.0948697/386.4
	!(lb*s^2/in)
	mp,prxy,2,0.36

 !Fishing line properties
	mp,ex,3,223e3
	!(psi)
	mp,dens,3,0.046293/386.4
	!(lb*s^2/in)

!Elements

 !Fabric:
	et,1,shell181
	keyopt,1,3,2
	sectype,1,shell
	secdata,0.012
	!(in)

 !Clamp elements:
	et,2,shell181
	keyopt,2,3,2
	sectype,2,shell
	secdata,.261
	!(in)

 !Fishing line elements:
	et,3,beam188
	sectype,3,beam,csolid
	secdata,0.024/2
	!(in)

!Create Keypoints
	a=9
	!(in)
	b=0.75
	!(in)
	d=0.25
	c=sqrt(2)/2
	L1=12.75
	!(in)
	L2=41.25
	!(in)
	L3=43.25
	!(in)
	*afun,deg
	k,1,d,-d
	k,2,c*(a-b),-c*(a-b)
	k,3,c*(a-b/2),-c*(a-b/2)
	k,4,c*a,-c*a
	k,5,c*(a-b),-c*a
	k,6,c*(a-2*b),-c*a
	k,7,-c*(a-2*b),-c*a
	k,8,-c*(a-b),-c*a
	k,9,-c*a,-c*a
	k,10,-c*(a-b/2),-c*(a-b/2)
	k,11,-c*(a-b),-c*(a-b)
	k,12,-d,-d
	k,13,kx(2)-0.1326,ky(2)-0.1326
	k,14,Kx(6)+0.1768,ky(6)+0.1768
	k,15,Kx(7)-0.1768,ky(6)+0.1768
```

```
k,16,kx(11)+0.1326,ky(11)-.1326
k,17,kx(4)-0.4375,ky(4)+0.1768
k,18,kx(9)+0.4375,ky(9)+0.1768

k,101,kx(3)+L2,ky(3),.345
k,102,kx(5),ky(5)-L1,.345
k,103,kx(8),ky(8)-L1,.345
k,104,kx(10)-L3,ky(10),.345

a,1,2,11,12
a,2,13,16,11
a,13,14,15,16
a,13,17,14
a,15,16,18
a,14,6,7,15

asel,s,area,,1,4
cm,FABRIC,area

a,2,3,4,5,6,14,17,13
cm,RCLAMP,area

a,11,10,9,8,7,15,18,16
cm,LCLAMP,area

allsel
aglue,all

ksel,s,kp,,1,2
lslk,s,1
ksel,s,kp,,11,12
lslk,a,1
ksel,s,kp,,6,7
lslk,a,1
ksel,s,kp,,2
ksel,a,kp,,11
lslk,a,1
ksel,s,kp,,13
ksel,a,kp,,16
lslk,a,1
ksel,s,kp,,14
ksel,a,kp,,15
lslk,a,1
lesize,all,,,50
allsel
ksel,s,kp,,15
ksel,a,kp,,18
lslk,s,1
ksel,s,kp,,18
ksel,a,kp,,16
lslk,a,1
ksel,s,kp,,14
ksel,a,kp,,17
lslk,a,1
ksel,s,kp,,17
ksel,a,kp,,13
lslk,a,1
ksel,s,kp,,15
ksel,a,kp,,16
lslk,a,1
ksel,s,kp,,13
ksel,a,kp,,14
lslk,a,1
lesize,all,,,5

asel,s,area,,1,6
mshkey,2

!Material Orientation
local,11,0,0,0,0,0
esys,11
amesh,all
csys,0
esys,0

type,2
secnum,2
mat,2

asel,s,area,,7,8
mshkey,0
amesh,all
allsel

type,3
mat,3
secnum,3
l,3,101
l,5,102
l,10,104
l,8,103
```

```
        ksel,s,kp,,3
        ksel,a,kp,,101
        lslk,s,1
        ksel,s,kp,,5
        ksel,a,kp,,102
        lslk,a,1
        ksel,s,kp,,10
        ksel,a,kp,,104
        lslk,a,1
        ksel,s,kp,,8
        ksel,a,kp,,103
        lslk,a,1
        lesize,all,,,50

        lmesh,all

        allsel
        nummrg,node

/solu
        sstif,on
        nlgeom,on
        nsubst,100
        neqit,50

!Boundary Conditions (Clamps)
        ksel,s,kp,,1
        ksel,a,kp,,12
        lslk,s,1
        nsll,s
        d,all,all,0

        F1=0.9816
        !(lb)
        F2=0.3184
        !(lb)
        F3=0.31915
        !(lb)
        F4=0.9822
        !(lb)

        ksel,s,kp,,101
        nslk,s
        f,all,fx,F4
        d,all,uy,0
        d,all,uz,0
        d,all,rotx,0
        d,all,roty,0
        d,all,rotz,0

        ksel,s,kp,,102
        nslk,s
        f,all,fy,-F3
        d,all,ux,0
        d,all,uz,0
        d,all,rotx,0
        d,all,roty,0
        d,all,rotz,0

        ksel,s,kp,,103
        nslk,s
        f,all,fy,-F2
        d,all,ux,0
        d,all,uz,0
        d,all,rotx,0
        d,all,roty,0
        d,all,rotz,0

        ksel,s,kp,,104
        nslk,s
        f,all,fx,-F1
        d,all,uy,0
        d,all,uz,0
        d,all,rotx,0
        d,all,roty,0
        d,all,rotz,0

        allsel

        acel,,,386.4-(386.4*.00077)
        !(in/s^2)

        solve
```

Inflated Circular Fabric Plate FE Batch File

The following ANSYS APDL batch file was used for the FE analysis of the inflated circular plate. Inflation pressure can be changed by adjusting the "int_press" variable in the batch file.

```
finish
/clear
/filename,FabricCircularPlate
/prep7

rad=0.1016
int_pres=21.5e3
steps=100

!Material Properties
 !Fabric:
        EW=145.17e6
        EF=73.65e6
        G=0.2*EW
        vwf=0.3

        mp,ey,1,EW
        mp,ex,1,EF
        mp,ez,1,EW
        mp,prxy,1,vwf
        mp,pryz,1,vwf
        mp,prxz,1,vwf
        mp,gxy,1,G
        mp,gyz,1,G
        mp,gxz,1,G
        mp,dens,1,1024.17

!Elements
        et,1,shell181
        !keyopt,1,3,2

        et,2,shell281
        !keyopt,2,2,1

        !Fabric Thickness
        sectype,1,shell
        secdata,0.000305

!Geometry
        pcirc,rad,,0,360

        !k,1,0,0,0
        !k,2,rad,0,0
        !k,3,rad,rad,0
        !k,4,0,rad,0
        !a,1,2,3,4

        asel,s,area,,1
        local,11,0,0,0,0,0,0
        esys,11


!Mesh
        type,2
        mshkey,1
        allsel
        amesh,all
        arefine,all,,,5

/solu
        nlgeom,on
        nsubst,steps

!Apply Boundary Conditions
        csys,2
        nsel,s,loc,x,rad
        d,all,all,0

!Apply Internal Pressure
        csys,0
        sfa,all,,pres,int_pres

!Apply Gravity Loading
        acel,,,9.81

allsel
solve
finish
```

Single Panel FE Batch Files

The first batch file below is the one created to estimate the deflection to be applied to the single panel models. A model was created using an isotropic material model and using eighth symmetry of the inflated sphere with internal membranes. Again the inflation pressure was adjusted by varying the "IntPres" variable.

Loading Study

```
finish
/clear
/filename,LoadStudyEighthSphere
/prep7
seltol,0.5e-6

!Non-Linear Controls
        steps=50

!Mesh Control
        refine=3

!Geometry Contorls
        FabThick=0.000305
        !(m)

        rad=0.125
        !(m)

  !FBS Boundary
        l=0.025
        !(m)
        t=0.003
        !(m)

        theta=(180/3.1415)*(l/rad)
        !(degrees)

!Loading Controls
        IntPres=70e3
        !(Pa)

!Material Properties
        EW=145.17e6
        !(Pa)
        EF=1.1*73.65e6
        !(Pa)
        EAVG=(EW+EF)/2
        !(Pa)

!Fabric
        mp,ex,1,EAVG
        !(Pa)
        mp,prxy,1,0.3
        mp,dens,1,1024.16
        !(kg/m^3)


!Elements

!Fabric:
        et,1,shell181
        et,2,shell281

        sectype,1,shell
        secdata,FabThick/2

        sectype,2,shell
        secdata,FabThick

!Creat Keypoints

        k,100,0,0,0

        csys,2
        k,1,rad,0,0
        k,2,rad,theta/2,0
        k,3,rad,(90-theta/2),0
        k,4,rad,90,0

        k,5,rad-t,theta/2,0
```

```
k,6,rad-t,90-theta/2,0

csys,0
k,7,0,ky(6),0
k,8,kx(5),0,0

csys,2
k,9,rad,0,90
k,10,rad,90,theta/2
k,11,rad-t,90,theta/2
k,12,rad,90,(90-theta/2)
k,13,rad-t,90,(90-theta/2)

csys,0
k,14,0,0,kz(13)

csys,2
k,15,rad,0,theta/2
k,16,rad,0,(90-theta/2)
k,17,rad-t,0,theta/2
k,18,rad-t,0,(90-theta/2)
csys,0
nkpt,1,1
nkpt,2,2
nkpt,3,3
nkpt,4,4
nkpt,5,5
nkpt,6,6
nkpt,7,7
nkpt,8,8
nkpt,9,9
nkpt,10,10
nkpt,11,11
nkpt,12,12
nkpt,13,13
nkpt,14,14
nkpt,15,15
nkpt,16,16
nkpt,17,17
nkpt,18,18
nkpt,100,100

!FBS Boundary
larc,1,2,100,rad
larc,3,4,100,rad
larc,4,10,100,rad
larc,12,9,100,rad
larc,1,15,100,rad
larc,9,16,100,rad

a,1,2,5,8
a,3,4,7,6
a,4,10,11,7
a,12,9,14,13
a,8,17,15,1
a,9,16,18,14

!Internal Membrane
a,5,6,7,8
a,7,100,8
a,11,13,14,7
a,14,100,7
a,18,17,8,14
a,8,100,14

!Spherical Membrane
csys,2
l,1,4
arotat,31,,,,,,100,4,-90
csys,0

allsel
aglue,all
!Mesh
mshkey,1
type,1
secnum,1
asel,s,area,,1,12
amesh,all

mshkey,2
type,1
secnum,2
asel,s,area,,14
amesh,all

allsel
nummrg,all

arefine,all,,,refine

!Boundary Conditions (Sym.)
```

```
nsel,s,loc,x,0
d,all,ux,0
d,all,rotx,0
d,all,roty,0
d,all,rotz,0

nsel,s,loc,y,0
d,all,uy,0
d,all,rotx,0
d,all,roty,0
d,all,rotz,0

nsel,s,loc,z,0
d,all,uz,0
d,all,rotx,0
d,all,roty,0
d,all,rotz,0

!Applied Internal Pressure
asel,s,area,,14
sfa,all,,pres,-IntPres

/solu
nlgeom,on
nsubst,steps

allsel

solve
```

The next set of batch files are the single panel file used for the majority of the single panel design study. In order below are the complete center geometry file, the complete center geometry with multiple loading connections file, the rectangular free center geometry file, the diamond free center geometry file, and the circular free center geometry file. The loading was varied by changing the deflection magnitude, the "deflect" variable in the batch file.

Free Center Geometry Full Model

```
finish
/clear
/filename,CompleteMiddle_FullModel
/prep7

!Non-Linear Controls
steps=50

!Mesh Controls
FabMesh=150
FBSLMesh=100
FBSTMesh=10
LoadMesh=200

!Geometry Controls
FabThick=0.000305
!(m)
rad=0.125
!(m)

!FBS Boundary
l=0.025
!(m)
t=0.003
!(m)

theta=(180/3.1415)*(l/rad)
!(degrees)

!Loading Controls
deflect=0.004311
!(m)

!Material Properties
!Fabric:
```

```
EW=145.17e6
!(Pa)
EF=73.65e6
!(Pa)
G=0.2*EW
!(Pa)
vwf=0.3
FabDensity=1024.16
!(kg/m^3

mp,ey,1,EF
mp,ex,1,EW
mp,ez,1,EW
mp,prxy,1,vwf
mp,pryz,1,vwf
mp,prxz,1,vwf
mp,gxy,1,G
mp,gyz,1,G
mp,gxz,1,G
mp,dens,1,FabDensity

!FBS Boundary:
mp,ey,2,EF
mp,ex,2,EW
mp,ez,2,EW
mp,prxy,2,vwf
mp,pryz,2,vwf
mp,prxz,2,vwf
mp,gxy,2,G
mp,gyz,2,G
mp,gxz,2,G
mp,dens,2,FabDensity

!Circular Membrane
mp,ex,3,EW
mp,dens,3,FabDensity
mp,prxy,3,vwf

!Aluminum Properties
mp,ex,4,68e9
!(Pa)
mp,dens,4,2711.52
!(kg/m^3)
mp,prxy,4,0.36

!Elements
et,1,shell181
et,2,shell281
et,3,beam188

!Fabric Thickness
sectype,1,shell
secdata,FabThick

!Keypoint Geometry
csys,1

k,100,0,0,0
k,1,rad,-theta/2
k,2,rad,theta/2
k,3,rad,(-theta/2)+90
k,4,rad,(theta/2)+90
k,5,rad,(-theta/2)+180
k,6,rad,(theta/2)+180
k,7,rad,(-theta/2)-90
k,8,rad,(theta/2)-90

k,9,rad-t,-theta/2
k,10,rad-t,theta/2
k,11,rad-t,(-theta/2)+90
k,12,rad-t,(theta/2)+90
k,13,rad-t,(-theta/2)+180
k,14,rad-t,(theta/2)+180
k,15,rad-t,(-theta/2)-90
k,16,rad-t,(theta/2)-90

nkpt,1,1
nkpt,2,2
nkpt,3,3
nkpt,4,4
nkpt,5,5
nkpt,6,6
nkpt,7,7
nkpt,8,8
nkpt,9,9
nkpt,10,10
nkpt,11,11
nkpt,12,12
nkpt,13,13
nkpt,14,14
nkpt,15,15
nkpt,16,16
```

```
        nkpt,100,100

!FBS Boundary Areas
        larc,1,2,100,rad
        larc,3,4,100,rad
        larc,5,6,100,rad
        larc,7,8,100,rad

        csys,0
        a,9,1,2,10
        a,11,3,4,12
        a,13,5,6,14
        a,15,7,8,16

!Fabric Area
        a,10,11,12,13
        a,9,10,13,14
        a,16,15,14,9

!Mesh Size Fabric Area
        ksel,s,kp,,10,11
        lslk,s,1
        ksel,s,kp,,12,13
        lslk,a,1
        ksel,s,kp,,14,15
        lslk,a,1
        ksel,s,kp,,1
        ksel,a,kp,,16
        lslk,a,1
        lesize,all,,,FabMesh

!Mesh Size FBS Boundary Areas
        ksel,s,kp,,1,2
        lslk,s,1
        ksel,s,kp,,3,4
        lslk,a,1
        ksel,s,kp,,5,6
        lslk,a,1
        ksel,s,kp,,7,8
        lslk,a,1
        ksel,s,kp,,10
        ksel,a,kp,,13
        lslk,a,1
        ksel,s,kp,,9
        ksel,a,kp,,14
        lslk,a,1
        lesize,all,,,FBSLMesh

        ksel,s,kp,,1
        ksel,a,kp,,9
        lslk,s,1
        ksel,s,kp,,3
        ksel,a,kp,,11
        lslk,a,1
        ksel,s,kp,,5
        ksel,a,kp,,13
        lslk,a,1
        ksel,s,kp,,7
        ksel,a,kp,,15
        lslk,a,1
        lesize,all,,,FBSTMesh

!Meshing
        type,1
        mshkey,1
        mat,1
        secnum,1

        asel,s,area,,1,4

        local,11,0,0,0,0,0
        esys,11
        amesh,all
        esys,0

        type,1
        mshkey,1
        mat,1

        asel,s,area,,5,7

        local,11,0,0,0,0,0
        esys,11
        amesh,all
        esys,0

        allsel
        nummrg,node

        csys,1
        nsel,s,loc,x,rad
        nrotat,all
```

```
        allsel
        csys,0

        nsel,s,loc,x,-1e-4,1e-4
        nsel,r,loc,y,-1e-4,1e-4
        d,all,uz,1e-3

        allsel
/solu
nlgeom,on
nsubst,steps

!Boundary Conditions
        csys,1
        csys,1
        lsel,s,line,,1,4
        esll,s,all
        nsll,s,all
        nsel,a,node,,1,8
        d,all,uy,0
        d,all,uz,0
        d,all,rotx,0
        d,all,roty,0
        d,all,rotz,0
        csys,0

!Apply Deflection
        csys,1
        lsel,s,line,,1,4
        esll,s,all
        nsll,s,all
        nsel,a,node,,1,8
        d,all,ux,deflect
        allsel

!Gravity Loading
        !acel,,,9.81

allsel
solve
finish
```

Complete Center Geometry Quarter Symmetry Model

```
finish
/clear
/filename,CompleteMiddle_SymModel
/prep7

!Non-Linear Controls
        steps=50

!Mesh Controls
        FabMesh=200
        FBSLMesh=40
        FBSTMesh=12

!Geometry Controls
        FabThick=0.000305
        !(m)

        rad=0.125
        !(m)

  !FBS Boundary
        l=0.025
        !(m)
        t=0.003
        !(m)

        theta=(180/3.1415)*(l/rad)
        !(degrees)

!Loading Controls
        deflect=0.004311
        !(m)

!Material Properties
  !Fabric:
        EW=145.17e6
        !(Pa)
        EF=73.65e6
        !(Pa)
        G=0.2*EW
        !(Pa)
        vwf=0.3
        FabDensity=1024.16
        !(kg/m^3
        mp,ey,1,EF
        mp,ex,1,EW
        mp,ez,1,EW
        mp,prxy,1,vwf
        mp,pryz,1,vwf
        mp,prxz,1,vwf
        mp,gxy,1,G
        mp,gyz,1,G
        mp,gxz,1,G
        mp,dens,1,FabDensity

  !FBS Boundary:
        mp,ey,2,EF
        mp,ex,2,EW
        mp,ez,2,EW
        mp,prxy,2,vwf
        mp,pryz,2,vwf
        mp,prxz,2,vwf
        mp,gxy,2,G
        mp,gyz,2,G
        mp,gxz,2,G
        mp,dens,2,FabDensity

  !Circular Membrane
        mp,ex,3,EW
        mp,dens,3,FabDensity
        mp,prxy,3,vwf

    !Aluminum Properties
        mp,ex,4,68e9
        !(Pa)
        mp,dens,4,2711.52
        !(kg/m^3)
        mp,prxy,4,0.36


!Elements
        et,1,shell181
        et,2,shell281
        et,3,beam188

        !Fabric Thickness
        sectype,1,shell
        secdata,FabThick
```

```
!Keypoint Geometry
        csys,1

        k,100,0,0,0
        k,1,rad,0
        k,2,rad,theta/2
        k,3,rad,(-theta/2)+90
        k,4,rad,90

        k,5,rad-t,theta/2
        k,6,rad-t,(-theta/2)+90

        csys,0
        k,7,kx(5),0
        k,8,0,ky(6)

        nkpt,1,1
        nkpt,2,2
        nkpt,3,3
        nkpt,4,4
        nkpt,5,5
        nkpt,6,6
        nkpt,7,7
        nkpt,8,8
        nkpt,100,100

!FBS Boundary Areas
        larc,1,2,100,rad
        larc,3,4,100,rad

        a,7,1,2,5
        a,6,3,4,8

!Fabric Area
        a,5,6,8,7
        a,100,7,8

!Mesh Size Fabric Area
        ksel,s,kp,,5,6
        lslk,s,1
        ksel,s,kp,,7
        ksel,a,kp,,100
        lslk,a,1
        ksel,s,kp,,8
        ksel,a,kp,,100
        lslk,a,1
        lesize,all,,,FabMesh

!Mesh Size FBS Boundary Areas
        ksel,s,kp,,1,2
        lslk,s,1
        ksel,s,kp,,3,4
        lslk,a,1
        lesize,all,,,FBSLMesh

        ksel,s,kp,,1
        ksel,a,kp,,7
        lslk,s,1
        ksel,s,kp,,3
        ksel,a,kp,,6
        lslk,a,1
        lesize,all,,,FBSTMesh

!Meshing

        type,1
        mshkey,1
        mat,1
        secnum,1

        asel,s,area,,1,2

        local,11,0,0,0,0,0
        esys,11
        amesh,all
        esys,0

        type,1
        mshkey,1
        mat,1

        asel,s,area,,3,4

        local,11,0,0,0,0,0
        esys,11
        amesh,all
        esys,0

        allsel
        nummrg,node

        csys,1
```

```
        nsel,s,loc,x,rad
        nsel,a,loc,y,0
        nsel,a,loc,y,90
        nrotat,all
        allsel
        csys,0

/solu
nlgeom,on
nsubst,steps

!Boundary Conditions
        csys,1
        lsel,s,line,,1,2
        !lsel,a,line,,13
        esll,s,all
        nsll,s,all
        nsel,a,node,,1,4
        d,all,uy,0
        d,all,uz,0
        d,all,rotx,0
        d,all,roty,0
        d,all,rotz,0
        csys,0

 !Sym Boundary Conditions
        csys,1
        nsel,s,loc,y,0
        nsel,a,loc,y,90
        d,all,uy,0
        csys,0
        allsel

!Apply Deflection
        csys,1
        lsel,s,line,,1,2
        esll,s,all
        nsll,s,all
        nsel,a,node,,1,4
        d,all,ux,deflect

        allsel

!Gravity Loading
        acel,,,9.81

allsel
solve
finish
```

Complete Center Geometry with Multiple Connections

```
finish
/clear
/filename,MC_CompleteMiddle
/prep7

pi=3.14159265359

!Non-Linear Controls
        steps=50

!Mesh Controls
        FabMesh=120
        FBSLMesh=Fabmesh/3
        FBSTMesh=10

!Geometry Controls
        FabThick=0.000305
        !(m)

        rad=0.125
        !(m)

  !FBS Boundary
        l=0.025
        !(m)
        t=0.003
        !(m)
        theta=(180/pi)*(l/rad)
        !(degrees)

    !Mid FBS Boundary
        lm=l
        !(m)
        t=t
        !(m)
        thetam=(180/pi)*(lm/rad)
        !(degrees)

!Loading Controls
        deflect=0.000143
        !(m)

!Material Properties
  !Fabric:
        EW=145.17e6
        !(Pa)
        EF=73.65e6
        !(Pa)
        G=0.2*EW
        !(Pa)
        vwf=0.3
        FabDensity=1024.16
        !(kg/m^3

        mp,ey,1,EF
        mp,ex,1,EW
        mp,ez,1,EW
        mp,prxy,1,vwf
        mp,pryz,1,vwf
        mp,prxz,1,vwf
        mp,gxy,1,G
        mp,gyz,1,G
        mp,gxz,1,G
        mp,dens,1,FabDensity

!FBS Boundary:
        mp,ey,2,EF
        mp,ex,2,EW
        mp,ez,2,EW
        mp,prxy,2,vwf
        mp,pryz,2,vwf
        mp,prxz,2,vwf
        mp,gxy,2,G
        mp,gyz,2,G
        mp,gxz,2,G
        mp,dens,2,FabDensity

!Circular Membrane
        mp,ex,3,EW
        mp,dens,3,FabDensity
        mp,prxy,3,vwf

    !Aluminum Properties
        mp,ex,4,68e9
        !(Pa)
        mp,dens,4,2711.52
        !(kg/m^3)
        mp,prxy,4,0.36
```

```
!Elements
        et,1,shell181
        et,2,shell281
        et,3,beam188

        !Fabric Thickness
        sectype,1,shell
        secdata,FabThick

!Keypoint Geometry
        csys,1

        k,100,0,0,0
        k,1,rad,0
        k,2,rad,theta/2
        k,3,rad,(-theta/2)+90
        k,4,rad,90

        k,5,rad-t,theta/2
        k,6,rad-t,(-theta/2)+90

        csys,0
        k,7,kx(5),0
        k,8,0,ky(6)

        csys,1
        k,9,rad,45-(thetam/2),0
        k,10,rad,45+(thetam/2),0
        k,11,rad-t,45-(thetam/2),0
        k,12,rad-t,45+(thetam/2),0

        csys,0
        a=sqrt((kx(5)-kx(7))*(kx(5)-
kx(7))+(ky(5)-ky(7))*(ky(5)-ky(7)))

        a1=sqrt((kx(100)-
kx(7))*(kx(100)-kx(7))+(ky(100)-
ky(7))*(ky(100)-ky(7)))

        dist=a1-a

        dist1=sqrt((kx(11)-
kx(12))*(kx(11)-kx(12))+((ky(11)-
        ky(12)))*((ky(11)-ky(12))))

        a1=dist1/(sqrt(2)*2)

        k,13,(a+dist/2)+a1,(a+dist/2)-a1
        k,14,(a+dist/2)-a1,(a+dist/2)+a1

        nkpt,1,1
        nkpt,2,2
        nkpt,3,3
        nkpt,4,4
        nkpt,5,5
        nkpt,6,6
        nkpt,7,7
        nkpt,8,8
        nkpt,9,9
        nkpt,10,10
        nkpt,11,11
        nkpt,12,12
        nkpt,13,13
        nkpt,14,14
        nkpt,100,100

!FBS Boundary Areas
        larc,1,2,100,rad
        larc,3,4,100,rad
        larc,9,10,100,rad

        a,7,1,2,5
        a,6,3,4,8
        a,9,10,12,11
        a,11,12,14,13

!Fabric Area
        a,5,13,14,6,8,7
        a,100,7,8

        aglue,all
!Mesh Size Fabric Area
        ksel,s,kp,,7,8
        lslk,s,1
        ksel,s,kp,,7
        ksel,a,kp,,100
        lslk,a,1
        ksel,s,kp,,8
        ksel,a,kp,,100
        lslk,a,1
        lesize,all,,,FabMesh
```

```
        ksel,s,kp,,5
        ksel,a,kp,,13
        lslk,s,1
        ksel,s,kp,,6
        ksel,a,kp,,14
        lslk,a,1
        lesize,all,,,FabMesh/3



!Mesh Size FBS Boundary Areas
        ksel,s,kp,,1,2
        lslk,s,1
        ksel,s,kp,,3,4
        lslk,a,1
        ksel,s,kp,,9,10
        lslk,a,1
        lesize,all,,,FBSLMesh

        ksel,s,kp,,1
        ksel,a,kp,,7
        lslk,s,1
        ksel,s,kp,,3
        ksel,a,kp,,6
        lslk,a,1
        ksel,s,kp,,9
        ksel,a,kp,,11
        lslk,a,1
        ksel,s,kp,,11
        ksel,a,kp,,13
        lslk,a,1
        lesize,all,,,FBSTMesh

!Meshing

        type,0
        mshkey,1
        mat,1
        secnum,1

        asel,s,area,,1,4

        local,11,0,0,0,0,0
        esys,11
        amesh,all
        esys,0

        type,1
        mshkey,0
        mat,1

        asel,s,area,,5,6

        local,11,0,0,0,0,0
        esys,11
        amesh,all
        esys,0

        allsel

        nummrg,node

        csys,1
        nsel,s,loc,x,rad
        nsel,a,loc,y,0
        nsel,a,loc,y,90
        nrotat,all
        allsel
        csys,0

/solu
nlgeom,on
nsubst,steps

!Boundary Conditions
        csys,1
        lsel,s,line,,1,3
        esll,s,all
        nsll,s,all
        nsel,a,node,,1,4
        nsel,a,node,,9,10
        d,all,uy,0
        d,all,uz,0
        d,all,rotx,0
        d,all,roty,0
        d,all,rotz,0
        csys,0

 !Sym Boundary Conditions
        csys,1
        nsel,s,loc,y,0
```

```
        nsel,a,loc,y,90
        d,all,uy,0
        csys,0
        allsel

!Apply Deflection
        csys,1
        lsel,s,line,,1
        esll,s,all
        nsll,s,all
        nsel,a,node,,1,2
        d,all,ux,deflect

        lsel,s,line,,2
        esll,s,all
        nsll,s,all
        nsel,a,node,,3,4
        d,all,ux,deflect

        lsel,s,line,,3
        esll,s,all
        nsll,s,all
        nsel,a,node,,9,10
        d,all,ux,deflect
        allsel

!Gravity Loading
        acel,,,9.81

allsel
solve
finish
```

Rectangular Free Center Geometry Quarter Symmetry Model

```
finish
/clear
/filename,FreeRect_SymModel
/prep7

!Non-Linear Controls
        steps=50

!Mesh Controls
        FabMesh=200
        FBSLMesh=50
        FBSTMesh=10

!Geometry Controls
        FabThick=0.000305
        !(m)

        rad=0.125
        !(m)

  !FBS Boundary
        l=0.025
        !(m)
        t=0.003
        !(m)
        theta=(180/3.1415)*(l/rad)
        !(degrees)

  !Center
        b=l/2
        !(m)
        h=l/2
        !(m)

!Loading Controls
        deflect=0.004311
        !(m)

!Material Properties
  !Fabric:
        EW=145.17e6
        !(Pa)
        EF=73.65e6
        !(Pa)
        G=0.2*EW
        !(Pa)
        vwf=0.3
        FabDensity=1024.16
        !(kg/m^3

        mp,ey,1,EF
        mp,ex,1,EW
        mp,ez,1,EW
        mp,prxy,1,vwf
        mp,pryz,1,vwf
        mp,prxz,1,vwf
        mp,gxy,1,G
        mp,gyz,1,G
        mp,gxz,1,G
        mp,dens,1,FabDensity

  !FBS Boundary:
        mp,ey,2,EF
        mp,ex,2,EW
        mp,ez,2,EW
        mp,prxy,2,vwf
        mp,pryz,2,vwf
        mp,prxz,2,vwf
        mp,gxy,2,G
        mp,gyz,2,G
        mp,gxz,2,G
        mp,dens,2,FabDensity

  !Circular Membrane
        mp,ex,3,EW
        mp,dens,3,FabDensity
        mp,prxy,3,vwf

    !Aluminum Properties
        mp,ex,4,68e9
        !(Pa)
        mp,dens,4,2711.52
        !(kg/m^3)
        mp,prxy,4,0.36

!Elements
        et,1,shell181
        et,2,shell281
```

```
et,3,beam188

!Fabric Thickness
sectype,1,shell
secdata,FabThick

!Circular Membrane
sectype,2,beam,rect
secdata,FabThick,FabThick

!Keypoint Geometry
k,1000,b,0
k,2000,b,h
k,3000,0,h


csys,1
k,100,0,0,0
k,1,rad,0
k,2,rad,theta/2
k,3,rad,(-theta/2)+90
k,4,rad,90

k,5,rad-t,theta/2
k,6,rad-t,(-theta/2)+90

csys,0
k,7,kx(5),0
k,8,0,ky(6)

nkpt,1,1
nkpt,2,2
nkpt,3,3
nkpt,4,4
nkpt,5,5
nkpt,6,6
nkpt,7,7
nkpt,8,8
nkpt,100,100
nkpt,1000,1000
nkpt,2000,2000
nkpt,3000,3000

!FBS Boundary Areas
larc,1,2,100,rad
larc,3,4,100,rad
csys,0
a,1,2,5,7
a,3,4,8,6

!Fabric Area
a,1000,7,5,2000
a,2000,6,8,3000
a,2000,5,6


!Circular Membrane
!larc,2,3,100,rad
!larc,4,5,100,rad
!larc,6,7,100,rad
!larc,8,1,100,rad

!Mesh Size Fabric Area
ksel,s,kp,,5,6
lslk,s,1
ksel,s,kp,,6
ksel,a,kp,,2000
lslk,a,1
ksel,s,kp,,5
ksel,a,kp,,2000
lslk,a,1
lesize,all,,,FabMesh

!Mesh Size FBS Boundary Areas
ksel,s,kp,,1,2
lslk,s,1
ksel,s,kp,,3,4
lslk,a,1
ksel,s,kp,,1000,2000
lslk,a,1
ksel,s,kp,,2000,3000
lslk,a,1
lesize,all,,,FBSLMesh

ksel,s,kp,,1
ksel,a,kp,,7
lslk,s,1
ksel,s,kp,,3
ksel,a,kp,,6
lslk,a,1
lesize,all,,,FBSTMesh
```

```
!Meshing

    !Mesh Circular Membrane
    !ksel,s,kp,,2,3
    !lslk,s,1
    !ksel,s,kp,,4,5
    !lslk,a,1
    !ksel,s,kp,,6,7
    !lslk,a,1
    !ksel,s,kp,,1
    !ksel,a,kp,,8
    !lslk,a,1
    !lesize,all,,,LoadMesh

    !type,3
    !mat,4
    !secnum,2

    !lsel,s,line,,1,4
    !lsel,a,line,,23,26
    !lmesh,all

    type,1
    mshkey,1
    mat,1
    secnum,1

    asel,s,area,,1,2

    local,11,0,0,0,0,0,0
    esys,11
    amesh,all
    esys,0

    type,1
    mshkey,1
    mat,1

    asel,s,area,,3,5

    local,11,0,0,0,0,0,0
    esys,11
    amesh,all
    esys,0

    allsel
    nummrg,node

    csys,1
    nsel,s,loc,x,rad
    nsel,a,loc,y,0
    nsel,a,loc,y,90
    nrotat,all
    allsel
    csys,0

/solu
nlgeom,on
nsubst,steps

!Boundary Conditions
    csys,1
    lsel,s,line,,1,2
    esll,s,all
    nsll,s,all
    nsel,a,node,,1,4
    d,all,uy,0
    d,all,uz,0
    d,all,rotx,0
    d,all,roty,0
    d,all,rotz,0
    csys,0

 !Sym Boundary Conditions
    csys,1
    nsel,s,loc,y,0
    nsel,a,loc,y,90
    d,all,uy,0
    csys,0
    allsel

!Apply Loading
    !lsel,s,line,,1,4
    !lsel,a,line,,23,26
    !esll,s,all
    !sfbeam,all,2,pres,IntPres

    csys,1
    lsel,s,line,,1,2
    esll,s,all
    nsll,s,all
```

```
        nsel,a,node,,1,4
        d,all,ux,deflect
        allsel

!Gravity Loading
        acel,,,9.81

allsel
solve
finish
```

Diamond Free Center Geometry Quarter Symmetry Model

```
finish
/clear
/filename,FreeDiamond_SymModel
/prep7

!Non-Linear Controls
        steps=50

!Mesh Controls
        FabMesh=200
        FBSLMesh=40
        FBSTMesh=10

!Geometry Controls
        FabThick=0.000305
        !(m)

        rad=0.125
        !(m)

  !FBS Boundary
        l=0.025
        !(m)
        t=0.003
        !(m)
        theta=(180/3.1415)*(l/rad)
        !(degrees)

  !Center
        b=l/2
        !(m)

!Loading Controls
        deflect=0.004311
        !(m)

!Material Properties
  !Fabric:
        EW=145.17e6
        !(Pa)
        EF=73.65e6
        !(Pa)
        G=0.2*EW
        !(Pa)
        vwf=0.3
        FabDensity=1024.16
        !(kg/m^3

        mp,ey,1,EF
        mp,ex,1,EW
        mp,ez,1,EW
        mp,prxy,1,vwf
        mp,pryz,1,vwf
        mp,prxz,1,vwf
        mp,gxy,1,G
        mp,gyz,1,G
        mp,gxz,1,G
        mp,dens,1,FabDensity

  !FBS Boundary:
        mp,ey,2,EF
        mp,ex,2,EW
        mp,ez,2,EW
        mp,prxy,2,vwf
        mp,pryz,2,vwf
        mp,prxz,2,vwf
        mp,gxy,2,G
        mp,gyz,2,G
        mp,gxz,2,G
        mp,dens,2,FabDensity

  !Circular Membrane
        mp,ex,3,EW
        mp,dens,3,FabDensity
        mp,prxy,3,vwf

    !Aluminum Properties
        mp,ex,4,68e9
        !(Pa)
        mp,dens,4,2711.52
        !(kg/m^3)
        mp,prxy,4,0.36

!Elements
        et,1,shell181
        et,2,shell281
        et,3,beam188
```

```
        !Fabric Thickness
        sectype,1,shell
        secdata,FabThick

        !Circular Membrane
        sectype,2,beam,rect
        secdata,FabThick,FabThick

!Keypoint Geometry
        k,1000,b,0
        k,2000,0,b



        csys,1
        k,100,0,0,0
        k,1,rad,0
        k,2,rad,theta/2
        k,3,rad,(-theta/2)+90
        k,4,rad,90

        k,5,rad-t,theta/2
        k,6,rad-t,(-theta/2)+90

        csys,0
        k,7,kx(5),0
        k,8,0,ky(6)

        nkpt,1,1
        nkpt,2,2
        nkpt,3,3
        nkpt,4,4
        nkpt,5,5
        nkpt,6,6
        nkpt,7,7
        nkpt,8,8
        nkpt,100,100
        nkpt,1000,1000
        nkpt,2000,2000



!FBS Boundary Areas
        larc,1,2,100,rad
        larc,3,4,100,rad

        csys,0
        a,1,2,5,7
        a,3,4,8,6

!Fabric Area
        a,7,5,6,8
        a,1000,7,8,2000



!Mesh Size Fabric Area
        ksel,s,kp,,5,6
        lslk,s,1
        ksel,s,kp,,7,8
        lslk,a,1
        ksel,s,kp,,1000
        ksel,a,kp,,7
        lslk,a,1
        ksel,s,kp,,2000
        ksel,a,kp,,8
        lslk,a,1
        lesize,all,,,FabMesh

!Mesh Size FBS Boundary Areas
        ksel,s,kp,,1,2
        lslk,s,1
        ksel,s,kp,,3,4
        lslk,a,1
        ksel,s,kp,,1000,2000
        lslk,a,1
        lesize,all,,,FBSLMesh

        ksel,s,kp,,1
        ksel,a,kp,,7
        lslk,s,1
        ksel,s,kp,,3
        ksel,a,kp,,6
        lslk,a,1
        lesize,all,,,FBSTMesh

!Meshing
        type,1
        mshkey,0
        mat,1
        secnum,1

        asel,s,area,,1,2
```

```
        local,11,0,0,0,0,0
        esys,11
        amesh,all
        esys,0

        type,1
        mshkey,0
        mat,1

        asel,s,area,,3,4

        local,11,0,0,0,0,0
        esys,11
        amesh,all
        esys,0

        allsel
        nummrg,node

        csys,1
        nsel,s,loc,x,rad
        nsel,a,loc,y,0
        nsel,a,loc,y,90
        nrotat,all
        allsel
        csys,0

/solu
nlgeom,on
nsubst,steps

!Boundary Conditions
        csys,1
        lsel,s,line,,1,2
        esll,s,all
        nsll,s,all
        nsel,a,node,,1,4
        d,all,uy,0
        d,all,uz,0
        d,all,rotx,0
        d,all,roty,0
        d,all,rotz,0
        csys,0

  !Sym Boundary Conditions
        csys,1
        nsel,s,loc,y,0
        nsel,a,loc,y,90
        d,all,uy,0
        csys,0
        allsel

!Apply Loading
        !lsel,s,line,,1,4
        !lsel,a,line,,23,26
        !esll,s,all
        !sfbeam,all,2,pres,IntPres

        csys,1
        lsel,s,line,,1,2
        esll,s,all
        nsll,s,all
        nsel,a,node,,1,4
        d,all,ux,deflect
        allsel

!Gravity Loading
        acel,,,9.81

allsel
solve
finish
```

Circular Free Center Geometry Quarter Symmetry Model

```
finish
/clear
/filename,FreeCirc_SymModel
/prep7

!Non-Linear Controls
        steps=50

!Mesh Controls
        FabMesh=200
        FBSLMesh=20
        FBSTMesh=10

!Geometry Controls
        FabThick=0.000305
        !(m)

        rad=0.125
        !(m)

  !FBS Boundary
        l=0.025
        !(m)
        t=0.003
        !(m)
        theta=(180/3.1415)*(l/rad)
        !(degrees)

  !Center
        b=l/2
        !(m)

!Loading Controls
        deflect=0.000143
        !(m)

!Material Properties
  !Fabric:
        EW=145.17e6
        !(Pa)
        EF=73.65e6
        !(Pa)
        G=0.2*EW
        !(Pa)
        vwf=0.3
        FabDensity=1024.16
        !(kg/m^3

        mp,ey,1,EF
        mp,ex,1,EW
        mp,ez,1,EW
        mp,prxy,1,vwf
        mp,pryz,1,vwf
        mp,prxz,1,vwf
        mp,gxy,1,G
        mp,gyz,1,G
        mp,gxz,1,G
        mp,dens,1,FabDensity

  !FBS Boundary:
        mp,ey,2,EF
        mp,ex,2,EW
        mp,ez,2,EW
        mp,prxy,2,vwf
        mp,pryz,2,vwf
        mp,prxz,2,vwf
        mp,gxy,2,G
        mp,gyz,2,G
        mp,gxz,2,G
        mp,dens,2,FabDensity

  !Circular Membrane
        mp,ex,3,EW
        mp,dens,3,FabDensity
        mp,prxy,3,vwf

    !Aluminum Properties
        mp,ex,4,68e9
        !(Pa)
        mp,dens,4,2711.52
        !(kg/m^3)
        mp,prxy,4,0.36

!Elements
        et,1,shell181
        et,2,shell281
        et,3,beam188
```

```
        !Fabric Thickness
        sectype,1,shell
        secdata,FabThick

        !Circular Membrane
        sectype,2,beam,rect
        secdata,FabThick,FabThick

!Keypoint Geometry
        k,1000,b,0
        k,2000,0,b



        csys,1
        k,100,0,0,0
        k,1,rad,0
        k,2,rad,theta/2
        k,3,rad,(-theta/2)+90
        k,4,rad,90

        k,5,rad-t,theta/2
        k,6,rad-t,(-theta/2)+90

        csys,0
        k,7,kx(5),0
        k,8,0,ky(6)

        nkpt,1,1
        nkpt,2,2
        nkpt,3,3
        nkpt,4,4
        nkpt,5,5
        nkpt,6,6
        nkpt,7,7
        nkpt,8,8
        nkpt,100,100
        nkpt,1000,1000
        nkpt,2000,2000


!FBS Boundary Areas
        larc,1,2,100,rad
        larc,3,4,100,rad
        larc,1000,2000,100,b

        csys,0
        a,1,2,5,7
        a,3,4,8,6

!Fabric Area
        a,7,5,6,8
        a,1000,7,8,2000


!Mesh Size Fabric Area
        ksel,s,kp,,5,6
        lslk,s,1
        ksel,s,kp,,7,8
        lslk,a,1
        ksel,s,kp,,1000
        ksel,a,kp,,7
        lslk,a,1
        ksel,s,kp,,2000
        ksel,a,kp,,8
        lslk,a,1
        lesize,all,,,FabMesh

!Mesh Size FBS Boundary Areas
        ksel,s,kp,,1,2
        lslk,s,1
        ksel,s,kp,,3,4
        lslk,a,1
        ksel,s,kp,,1000,2000
        lslk,a,1
        lesize,all,,,FBSLMesh

        ksel,s,kp,,1
        ksel,a,kp,,7
        lslk,s,1
        ksel,s,kp,,3
        ksel,a,kp,,6
        lslk,a,1
        lesize,all,,,FBSTMesh

!Meshing
        type,1
        mshkey,0
        mat,1
        secnum,1

        asel,s,area,,1,2
```

```
        local,11,0,0,0,0,0
        esys,11
        amesh,all
        esys,0

        type,1
        mshkey,0
        mat,1

        asel,s,area,,3,4

        local,11,0,0,0,0,0
        esys,11
        amesh,all
        esys,0

        allsel
        nummrg,node

        csys,1
        nsel,s,loc,x,rad
        nsel,a,loc,y,0
        nsel,a,loc,y,90
        nrotat,all
        allsel
        csys,0

/solu
nlgeom,on
nsubst,steps

!Boundary Conditions
        csys,1
        lsel,s,line,,1,2
        esll,s,all
        nsll,s,all
        nsel,a,node,,1,4
        d,all,uy,0
        d,all,uz,0
        d,all,rotx,0
        d,all,roty,0
        d,all,rotz,0
        csys,0

 !Sym Boundary Conditions
        csys,1
        nsel,s,loc,y,0
        nsel,a,loc,y,90
        d,all,uy,0
        csys,0
        allsel

!Apply Deflection Constraint
        csys,1
        lsel,s,line,,1,2
        esll,s,all
        nsll,s,all
        nsel,a,node,,1,4
        d,all,ux,deflect
        allsel

!Gravity Loading
        acel,,,9.81

allsel
solve
finish
```

Inflatable Pathfinder System FE Batch Files

The following batch files are for the complete final design of the inflatable pathfinder system. A model incorporating the full linear orthotropic material model is presented first. The second batch file is for an inflatable system with an isotropic outer sphere. Again the inflation pressure is changed by editing the "IntPres" variable for both of the pathfinder system models.

Inflatable Pathfinder System – Linear Orthotropic Outer Sphere

```
finish
/clear
/filename,Fabricrev4
/prep7

!Non-Linear Controls
        steps=50

!Mesh Control
        refine=3

!Geometry Contorls
        FabThick=0.000305
        !(m)

        rad=0.125
        !(m)

 !FBS Boundary
        l=0.025
        !(m)
        t=0.003
        !(m)

        theta=(180/3.1415)*(l/rad)
        !(degrees)

!Loading Controls
        IntPres=20e3
        !(Pa)

!Center Geometry
        b=l/2
```

```
!Material Properties
        EW=145.17e6
        !(Pa)
        EF=73.65e6
        !(Pa)
        G=0.2*EW
        !(Pa)
        vwf=0.3
        FabDensity=1024.16
        !(kg/m^3
        EAVG=(EW+EF)/2
        !(Pa)

 !Fabric Linear Orthotropic
        mp,ey,1,EF
        mp,ex,1,EW
        mp,ez,1,EW
        mp,prxy,1,vwf
        mp,pryz,1,vwf
        mp,prxz,1,vwf
        mp,gxy,1,G
        mp,gyz,1,G
        mp,gxz,1,G
        mp,dens,1,FabDensity

 !Fabric Isotropic
        mp,ex,2,EW
        mp,prxy,2,0.3
        mp,dens,2,FabDensity

!Elements

!Fabric:
        et,1,shell181
```

```
et,2,shell281

sectype,1,shell
secdata,FabThick

!Creat Keypoints

k,1000,0,0,0

csys,2
k,100,b,0,0
k,200,b,90,0
k,300,b,0,90
k,400,b,-90,0
k,500,b,0,180
k,600,b,0,270

k,1,rad,0,0
k,2,rad,theta/2,0
k,3,rad,(90-theta/2),0
k,4,rad,90,0

k,5,rad-t,theta/2,0
k,6,rad-t,90-theta/2,0

csys,0
k,7,0,ky(6),0
k,8,kx(5),0,0

csys,2
k,9,rad,0,90
k,10,rad,90,theta/2
k,11,rad-t,90,theta/2
k,12,rad,90,(90-theta/2)
k,13,rad-t,90,(90-theta/2)

csys,0
k,14,0,0,kz(13)

csys,2
k,15,rad,0,theta/2
k,16,rad,0,(90-theta/2)
k,17,rad-t,0,theta/2
k,18,rad-t,0,(90-theta/2)

csys,0
k,19,kx(3),-ky(3),kz(3)
k,20,kx(4),-ky(4),kz(4)
k,21,kx(6),-ky(6),kz(6)
k,22,kx(7),-ky(7),kz(7)
k,23,kx(10),-ky(10),kz(10)
k,24,kx(11),-ky(11),kz(11)
k,25,kx(2),-ky(2),kz(2)
k,26,kx(5),-ky(5),kz(5)
k,27,kx(12),-ky(12),kz(12)
k,28,kx(13),-ky(13),kz(13)
k,29,-kx(16),ky(16),kz(16)
k,30,-kx(18),kY(18),kz(18)
k,31,-kx(1),ky(1),kz(1)
k,32,-kx(2),ky(2),kz(2)
k,33,-kx(5),ky(5),kz(5)
k,34,-kx(8),ky(8),kz(8)
k,35,-kx(26),ky(26),kz(26)
k,36,-kx(25),ky(25),kz(25)
k,37,-kx(19),ky(19),kz(19)
k,38,-kx(21),ky(21),kz(21)
k,39,-kx(17),kY(17),kz(17)
k,40,-kx(15),ky(15),kz(15)
k,41,-kx(6),ky(6),kz(6)
k,42,-kx(3),ky(3),kz(3)

csys,0
k,43,kx(9),ky(9),-kz(9)
k,44,kx(10),ky(10),-kz(10)
k,45,kx(11),ky(11),-kz(11)
k,46,kx(12),ky(12),-kz(12)
k,47,kx(13),ky(13),-kz(13)
k,48,kx(14),ky(14),-kz(14)
k,49,kx(15),ky(15),-kz(15)
k,50,kx(16),ky(16),-kz(16)
k,51,kx(17),ky(17),-kz(17)
k,52,kx(18),ky(18),-kz(18)
k,53,kx(24),ky(24),-kz(24)
k,54,kx(23),ky(23),-kz(23)
k,55,kx(39),ky(39),-kz(39)
k,56,kx(40),ky(40),-kz(40)
k,57,kx(29),ky(29),-kz(29)
k,58,kx(30),ky(30),-kz(30)
k,59,kx(27),ky(27),-kz(27)
k,60,kx(28),ky(28),-kz(28)

nkpt,1,1
```

```
nkpt,2,2
nkpt,3,3
nkpt,4,4
nkpt,5,5
nkpt,6,6
nkpt,7,7
nkpt,8,8
nkpt,9,9
nkpt,10,10
nkpt,11,11
nkpt,12,12
nkpt,13,13
nkpt,14,14
nkpt,15,15
nkpt,16,16
nkpt,17,17
nkpt,18,18
nkpt,19,19
nkpt,20,20
nkpt,21,21
nkpt,22,22
nkpt,23,23
nkpt,24,24
nkpt,25,25
nkpt,26,26
nkpt,27,27
nkpt,28,28
nkpt,29,29
nkpt,30,30
nkpt,31,31
nkpt,32,32
nkpt,33,33
nkpt,34,34
nkpt,35,35
nkpt,36,36
nkpt,37,37
nkpt,38,38
nkpt,39,39
nkpt,40,40
nkpt,41,41
nkpt,42,42
nkpt,43,43
nkpt,44,44
nkpt,45,45
nkpt,46,46
nkpt,47,47
nkpt,48,48
nkpt,49,49
nkpt,50,50
nkpt,51,51
nkpt,52,52
nkpt,53,53
nkpt,54,54
nkpt,55,55
nkpt,56,56
nkpt,57,57
nkpt,58,58
nkpt,100,100
nkpt,200,200
nkpt,300,300
nkpt,400,400
nkpt,500,500
nkpt,600,600
nkpt,1000,1000

!FBS Boundary
larc,1,2,1000,rad
larc,3,4,1000,rad
larc,4,10,1000,rad
larc,12,9,1000,rad
larc,1,15,1000,rad
larc,9,16,1000,rad
larc,19,20,1000,rad
larc,20,23,1000,rad
larc,1,25,1000,rad
larc,9,27,1000,rad
larc,9,29,1000,rad
larc,31,36,1000,rad
larc,31,40,1000,rad
larc,31,32,1000,rad
larc,31,56,1000,rad
larc,20,37,1000,rad
larc,4,42,1000,rad
larc,4,44,1000,rad
larc,43,50,1000,rad
larc,43,46,1000,rad
larc,43,57,1000,rad
larc,43,59,1000,rad
larc,1,49,1000,rad
larc,20,54,1000,rad

a,25,1,2,5,8,26
```

```
a,15,1,49,51,8,17
a,50,43,57,58,48,52
a,59,43,46,47,48,60
a,44,4,10,11,7,45
a,3,4,42,41,7,6
a,56,31,40,39,34,55
a,32,31,36,35,34,33
a,29,9,16,18,14,30
a,12,9,27,28,14,13
a,23,20,54,53,22,24
a,37,38,22,21,19,20

asel,all
aovlap,all


!Internal Membrane
larc,100,200,1000,b
larc,200,300,1000,b
larc,100,300,1000,b
larc,300,400,1000,b
larc,100,400,1000,b
larc,300,500,1000,b
larc,400,500,1000,b
larc,200,500,1000,b
larc,100,600,1000,b
larc,500,600,1000,b
larc,200,600,1000,b
larc,600,400,1000,b

a,300,100,8,14
a,8,17,18,14
a,100,200,7,8
a,7,6,5,8
a,300,200,7,14
a,7,11,13,14
a,400,100,8,22
a,26,8,22,21
a,400,300,14,22
a,22,24,28,14

a,500,300,14,34
a,34,39,30,14
a,500,200,7,34
a,7,41,33,34
a,500,400,22,34
a,22,38,35,34

a,600,200,7,48
a,7,45,47,48
a,600,100,8,48
a,48,52,51,8
a,600,500,34,48
a,48,58,55,34

a,400,600,48,22
a,22,53,60,48

asel,all
aglue,all
!Spherical Membrane
csys,2
l,1,4
arotat,121,,,,,,1000,4,-360
l,20,1
arotat,129,,,,,,1000,20,360
csys,0

allsel
aglue,all
!Mesh
mshkey,1
type,1
secnum,1

!Mesh FBS Boundary
asel,s,area,,13,36
amesh,all

!Mesh Internal Membrane
asel,s,area,,1,12
asel,a,area,,37,48
amesh,all

!!!!!!!!Material Orientation!!!!!!!!!!
!Rotate XZ-Plane
local,11,0,0,0,0,90
esys,11
asel,s,area,,1,2
asel,a,area,,11,12
asel,a,area,,43,46
esla,s,all
```

```
        nsla,s,all
        nrotat,all
        esys,0

    !Mesh Outer Sphere
        mshkey,0
        asel,a,area,,57,64
        amesh,all
        allsel
        nummrg,all

        arefine,all,,,refine

!Boundary Conditions (Sym.)

        nsel,s,node,,1
        nsel,a,node,,4
        nsel,a,node,,9
        nsel,a,node,,20
        nsel,a,node,,31
        nsel,a,node,,43

        !nsel,s,node,,1,4
        !nsel,a,node,,9,10
        !nsel,a,node,,12
        !nsel,a,node,,15,16
        !nsel,a,node,,19,20
        !nsel,a,node,,23
        !nsel,a,node,,25
        !nsel,a,node,,27
        !nsel,a,node,,29
        !nsel,a,node,,31,32
        !nsel,a,node,,36,37
        !nsel,a,node,,40
        !nsel,a,node,,42,44
        !nsel,a,node,,46
        !nsel,a,node,,49,50
        !nsel,a,node,,54
        !nsel,a,node,,56,57
        !nsel,a,node,,59
        !lsel,s,line,,1,24
        !esll,s
        !nsll,a
        csys,2
        nrotat,all
        d,all,uy,0
        d,all,uz,0
        d,all,rotx,0
        d,all,roty,0
        d,all,rotz,0
        csys,0

!Solution
        /solu
        nlgeom,on
        sstiff,on
        !nsubst,steps

!Applied Internal Pressure
        asel,s,area,,57,64
        sfa,all,,pres,-IntPres

!Apply Gravity
        allsel
        acel,,9.81

        solve
```

Inflatable Pathfinder System – Linear Isotropic Outer Sphere

```
finish
/clear
/filename,Fabricrev4
/prep7

!Non-Linear Controls
        steps=50

!Mesh Control
        refine=3

!Geometry Contorls
        FabThick=0.000305
        !(m)

        rad=0.125
        !(m)

  !FBS Boundary
        l=0.025
        !(m)
        t=0.003
        !(m)

        theta=(180/3.1415)*(l/rad)
        !(degrees)

!Loading Controls
        IntPres=70e3
        !(Pa)

!Center Geometry
        b=l/2

!Material Properties
        EW=145.17e6
        !(Pa)
        EF=73.65e6
        !(Pa)
        G=0.2*EW
        !(Pa)
        vwf=0.3
        FabDensity=1024.16
        !(kg/m^3
        EAVG=(EW+EF)/2
        !(Pa)

  !Fabric Linear Orthotropic
        mp,ey,1,EF
        mp,ex,1,EW
        mp,ez,1,EW
        mp,prxy,1,vwf
        mp,pryz,1,vwf
        mp,prxz,1,vwf
        mp,gxy,1,G
        mp,gyz,1,G
        mp,gxz,1,G
        mp,dens,1,FabDensity

  !Fabric Isotropic
        mp,ex,2,EW
        mp,prxy,2,0.3
        mp,dens,2,FabDensity

!Elements

!Fabric:
        et,1,shell181
        et,2,shell281

        sectype,1,shell
        secdata,FabThick

!Creat Keypoints

        k,1000,0,0,0

        csys,2
        k,100,b,0,0
        k,200,b,90,0
        k,300,b,0,90
        k,400,b,-90,0
        k,500,b,0,180
        k,600,b,0,270

        k,1,rad,0,0
        k,2,rad,theta/2,0
        k,3,rad,(90-theta/2),0
```

```
k,4,rad,90,0

k,5,rad-t,theta/2,0
k,6,rad-t,90-theta/2,0

csys,0
k,7,0,ky(6),0
k,8,kx(5),0,0

csys,2
k,9,rad,0,90
k,10,rad,90,theta/2
k,11,rad-t,90,theta/2
k,12,rad,90,(90-theta/2)
k,13,rad-t,90,(90-theta/2)

csys,0
k,14,0,0,kz(13)

csys,2
k,15,rad,0,theta/2
k,16,rad,0,(90-theta/2)
k,17,rad-t,0,theta/2
k,18,rad-t,0,(90-theta/2)

csys,0
k,19,kx(3),-ky(3),kz(3)
k,20,kx(4),-ky(4),kz(4)
k,21,kx(6),-ky(6),kz(6)
k,22,kx(7),-ky(7),kz(7)
k,23,kx(10),-ky(10),kz(10)
k,24,kx(11),-ky(11),kz(11)
k,25,kx(2),-ky(2),kz(2)
k,26,kx(5),-ky(5),kz(5)
k,27,kx(12),-ky(12),kz(12)
k,28,kx(13),-ky(13),kz(13)
k,29,-kx(16),ky(16),kz(16)
k,30,-kx(18),kY(18),kz(18)
k,31,-kx(1),ky(1),kz(1)
k,32,-kx(2),ky(2),kz(2)
k,33,-kx(5),ky(5),kz(5)
k,34,-kx(8),ky(8),kz(8)
k,35,-kx(26),ky(26),kz(26)
k,36,-kx(25),ky(25),kz(25)
k,37,-kx(19),ky(19),kz(19)
k,38,-kx(21),ky(21),kz(21)
k,39,-kx(17),kY(17),kz(17)
k,40,-kx(15),ky(15),kz(15)
k,41,-kx(6),ky(6),kz(6)
k,42,-kx(3),ky(3),kz(3)

csys,0
k,43,kx(9),ky(9),-kz(9)
k,44,kx(10),ky(10),-kz(10)
k,45,kx(11),ky(11),-kz(11)
k,46,kx(12),ky(12),-kz(12)
k,47,kx(13),ky(13),-kz(13)
k,48,kx(14),ky(14),-kz(14)
k,49,kx(15),ky(15),-kz(15)
k,50,kx(16),ky(16),-kz(16)
k,51,kx(17),ky(17),-kz(17)
k,52,kx(18),ky(18),-kz(18)
k,53,kx(24),ky(24),-kz(24)
k,54,kx(23),ky(23),-kz(23)
k,55,kx(39),ky(39),-kz(39)
k,56,kx(40),ky(40),-kz(40)
k,57,kx(29),ky(29),-kz(29)
k,58,kx(30),ky(30),-kz(30)
k,59,kx(27),ky(27),-kz(27)
k,60,kx(28),ky(28),-kz(28)

nkpt,1,1
nkpt,2,2
nkpt,3,3
nkpt,4,4
nkpt,5,5
nkpt,6,6
nkpt,7,7
nkpt,8,8
nkpt,9,9
nkpt,10,10
nkpt,11,11
nkpt,12,12
nkpt,13,13
nkpt,14,14
nkpt,15,15
nkpt,16,16
nkpt,17,17
nkpt,18,18
nkpt,19,19
nkpt,20,20
nkpt,21,21
```

```
nkpt,22,22
nkpt,23,23
nkpt,24,24
nkpt,25,25
nkpt,26,26
nkpt,27,27
nkpt,28,28
nkpt,29,29
nkpt,30,30
nkpt,31,31
nkpt,32,32
nkpt,33,33
nkpt,34,34
nkpt,35,35
nkpt,36,36
nkpt,37,37
nkpt,38,38
nkpt,39,39
nkpt,40,40
nkpt,41,41
nkpt,42,42
nkpt,43,43
nkpt,44,44
nkpt,45,45
nkpt,46,46
nkpt,47,47
nkpt,48,48
nkpt,49,49
nkpt,50,50
nkpt,51,51
nkpt,52,52
nkpt,53,53
nkpt,54,54
nkpt,55,55
nkpt,56,56
nkpt,57,57
nkpt,58,58
nkpt,100,100
nkpt,200,200
nkpt,300,300
nkpt,400,400
nkpt,500,500
nkpt,600,600
nkpt,1000,1000

!FBS Boundary
```

```
larc,1,2,1000,rad
larc,3,4,1000,rad
larc,4,10,1000,rad
larc,12,9,1000,rad
larc,1,15,1000,rad
larc,9,16,1000,rad
larc,19,20,1000,rad
larc,20,23,1000,rad
larc,1,25,1000,rad
larc,9,27,1000,rad
larc,9,29,1000,rad
larc,31,36,1000,rad
larc,31,40,1000,rad
larc,31,32,1000,rad
larc,31,56,1000,rad
larc,20,37,1000,rad
larc,4,42,1000,rad
larc,4,44,1000,rad
larc,43,50,1000,rad
larc,43,46,1000,rad
larc,43,57,1000,rad
larc,43,59,1000,rad
larc,1,49,1000,rad
larc,20,54,1000,rad

a,25,1,2,5,8,26
a,15,1,49,51,8,17
a,50,43,57,58,48,52
a,59,43,46,47,48,60
a,44,4,10,11,7,45
a,3,4,42,41,7,6
a,56,31,40,39,34,55
a,32,31,36,35,34,33
a,29,9,16,18,14,30
a,12,9,27,28,14,13
a,23,20,54,53,22,24
a,37,38,22,21,19,20

asel,all
aovlap,all


!Internal Membrane
larc,100,200,1000,b
larc,200,300,1000,b
larc,100,300,1000,b
```

```
larc,300,400,1000,b
larc,100,400,1000,b
larc,300,500,1000,b
larc,400,500,1000,b
larc,200,500,1000,b
larc,100,600,1000,b
larc,500,600,1000,b
larc,200,600,1000,b
larc,600,400,1000,b

a,300,100,8,14
a,8,17,18,14
a,100,200,7,8
a,7,6,5,8
a,300,200,7,14
a,7,11,13,14
a,400,100,8,22
a,26,8,22,21
a,400,300,14,22
a,22,24,28,14

a,500,300,14,34
a,34,39,30,14
a,500,200,7,34
a,7,41,33,34
a,500,400,22,34
a,22,38,35,34

a,600,200,7,48
a,7,45,47,48
a,600,100,8,48
a,48,52,51,8
a,600,500,34,48
a,48,58,55,34

a,400,600,48,22
a,22,53,60,48

asel,all
aglue,all
!Spherical Membrane
csys,2
l,1,4
arotat,121,,,,,,1000,4,-360
l,20,1
arotat,129,,,,,,1000,20,360
csys,0

allsel
aglue,all
!Mesh
mshkey,1
type,1
secnum,1

!Mesh FBS Boundary
asel,s,area,,13,36
amesh,all

!Mesh Internal Membrane
asel,s,area,,1,12
asel,a,area,,37,48
amesh,all

!!!!!!!!Material Orientation!!!!!!!!!!
!Rotate XZ-Plane
local,11,0,0,0,0,0,90
esys,11
asel,s,area,,1,2
asel,a,area,,11,12
asel,a,area,,43,46
esla,s,all
nsla,s,all
nrotat,all
esys,0

!Mesh Outer Sphere
mat,2
mshkey,0
asel,a,area,,57,64
amesh,all
allsel
nummrg,all

arefine,all,,,refine

!Boundary Conditions (Sym.)

nsel,s,node,,1
nsel,a,node,,4
nsel,a,node,,9
nsel,a,node,,20
```

```
nsel,a,node,,31
nsel,a,node,,43

!nsel,s,node,,1,4
!nsel,a,node,,9,10
!nsel,a,node,,12
!nsel,a,node,,15,16
!nsel,a,node,,19,20
!nsel,a,node,,23
!nsel,a,node,,25
!nsel,a,node,,27
!nsel,a,node,,29
!nsel,a,node,,31,32
!nsel,a,node,,36,37
!nsel,a,node,,40
!nsel,a,node,,42,44
!nsel,a,node,,46
!nsel,a,node,,49,50
!nsel,a,node,,54
!nsel,a,node,,56,57
!nsel,a,node,,59
!lsel,s,line,,1,24
!esll,s
!nsll,a
        csys,2
        nrotat,all
        d,all,uy,0
        d,all,uz,0
        d,all,rotx,0
        d,all,roty,0
        d,all,rotz,0
        csys,0

!Solution
        /solu
        nlgeom,on
        sstiff,on
        !nsubst,steps

!Applied Internal Pressure
        asel,s,area,,57,64
        sfa,all,,pres,-IntPres

!Apply Gravity
        allsel
        acel,,9.81

        solve
```

APPENDIX B: ADDITIONAL ANALYSIS PLOTS

Shear Study Plots

The first set of plots is a complete set of the shear studies used to define the validated-model shear modulus.

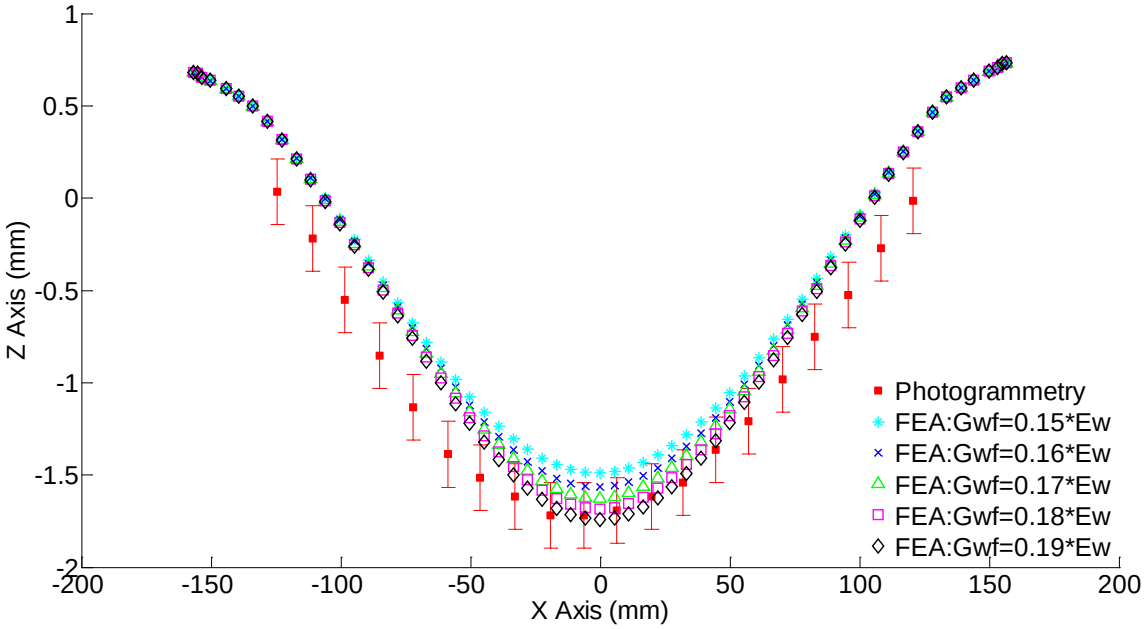

Figure B.1. Shear study for Test Case 1.

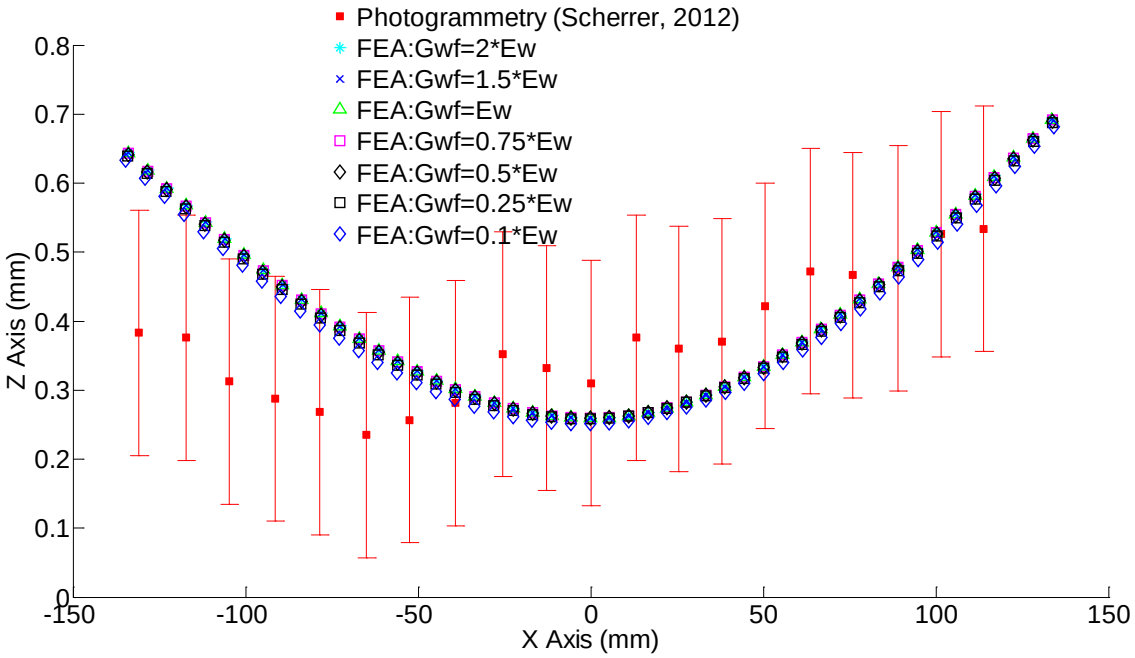

Figure B.2. Shear study for Test Case 2.

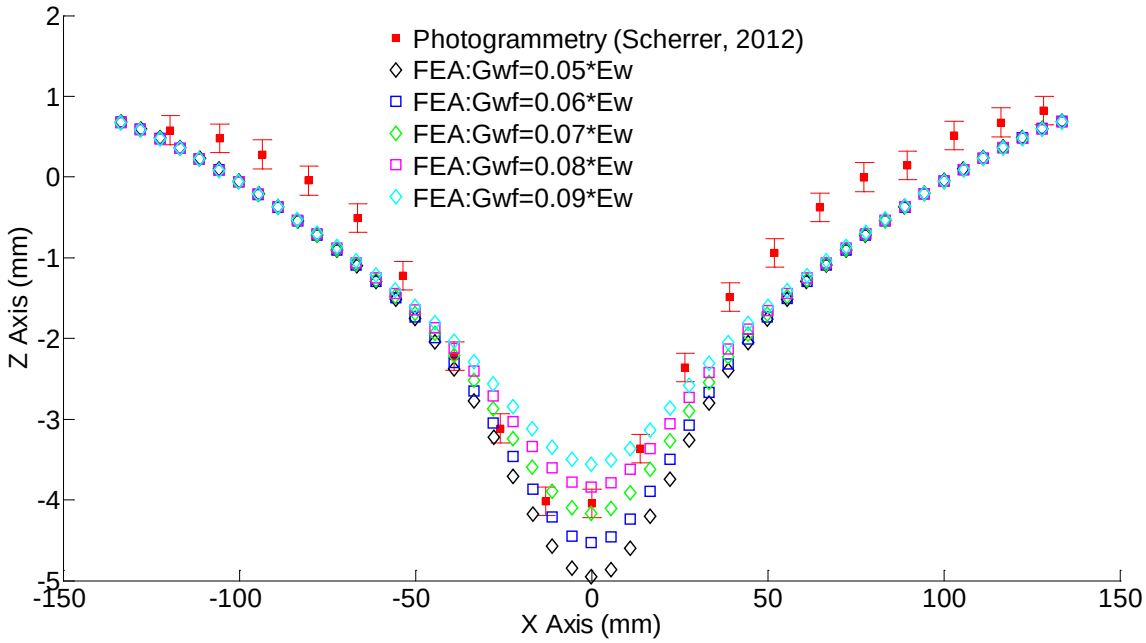

Figure B.3. Shear study for Test Case 3.

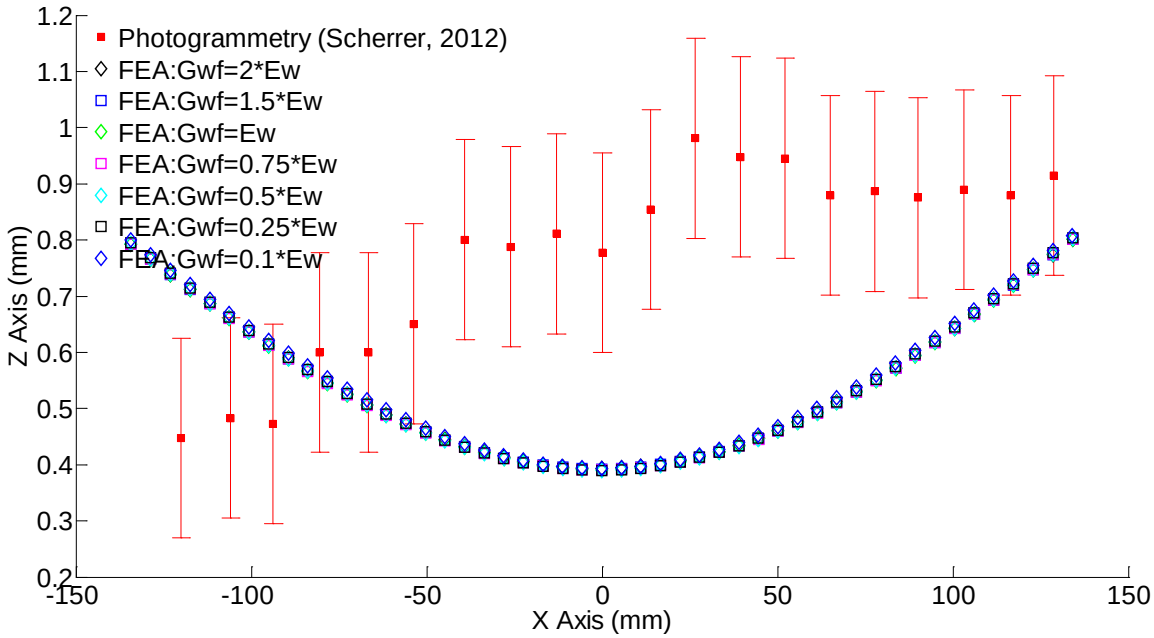

Figure B.4. Shear study for Test Case 4.

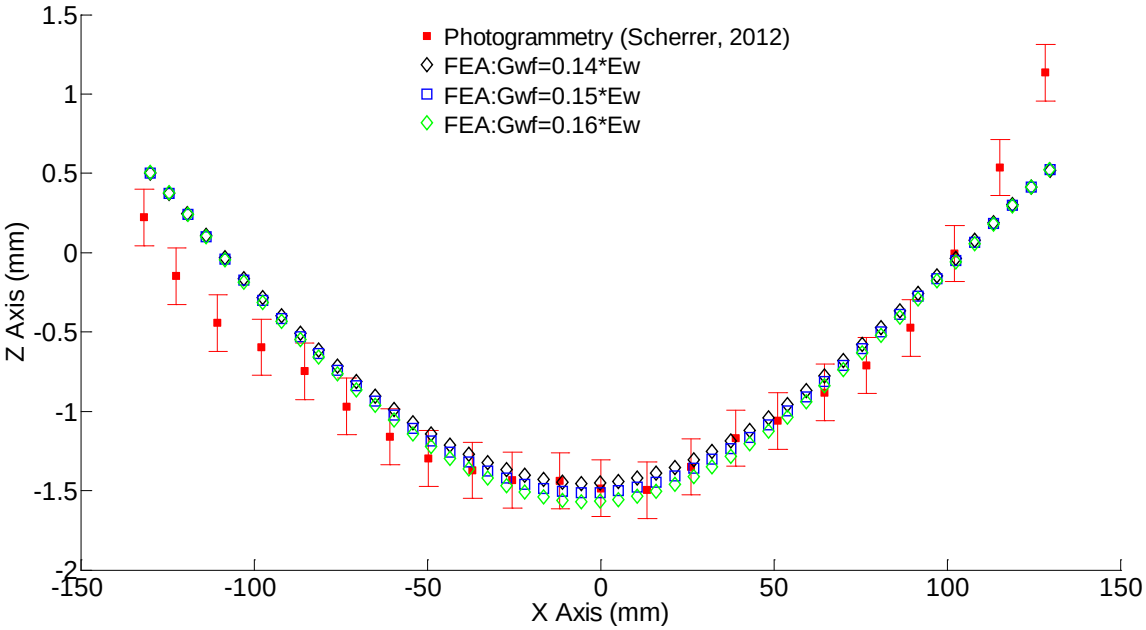

Figure B.5. Shear study for Test Case 5.

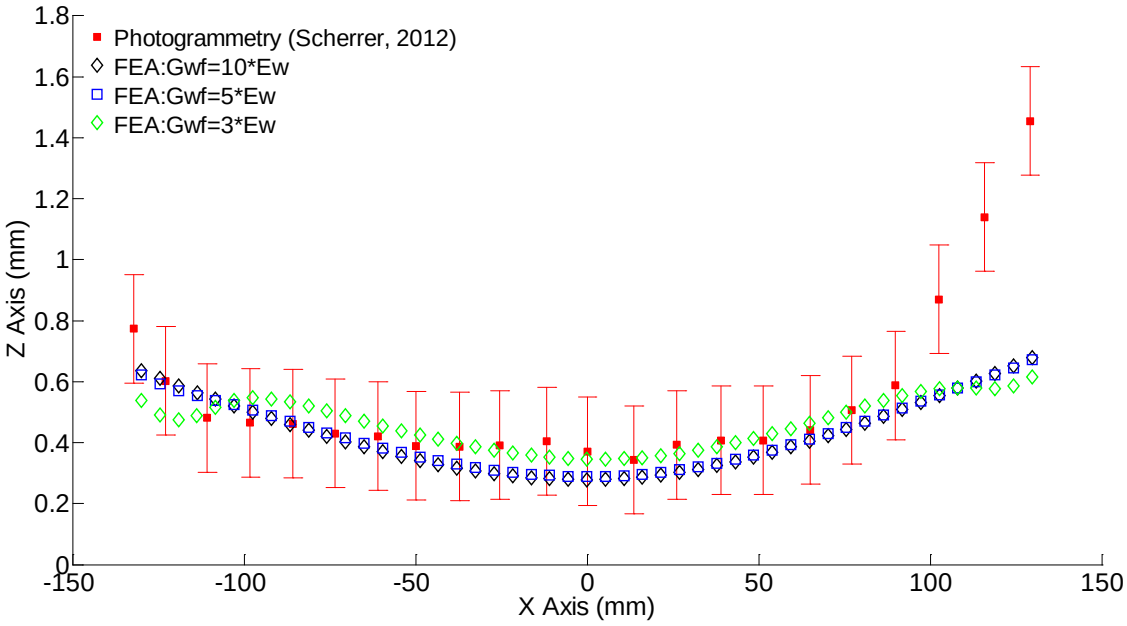

Figure B.6. Shear study for Test Case 6.

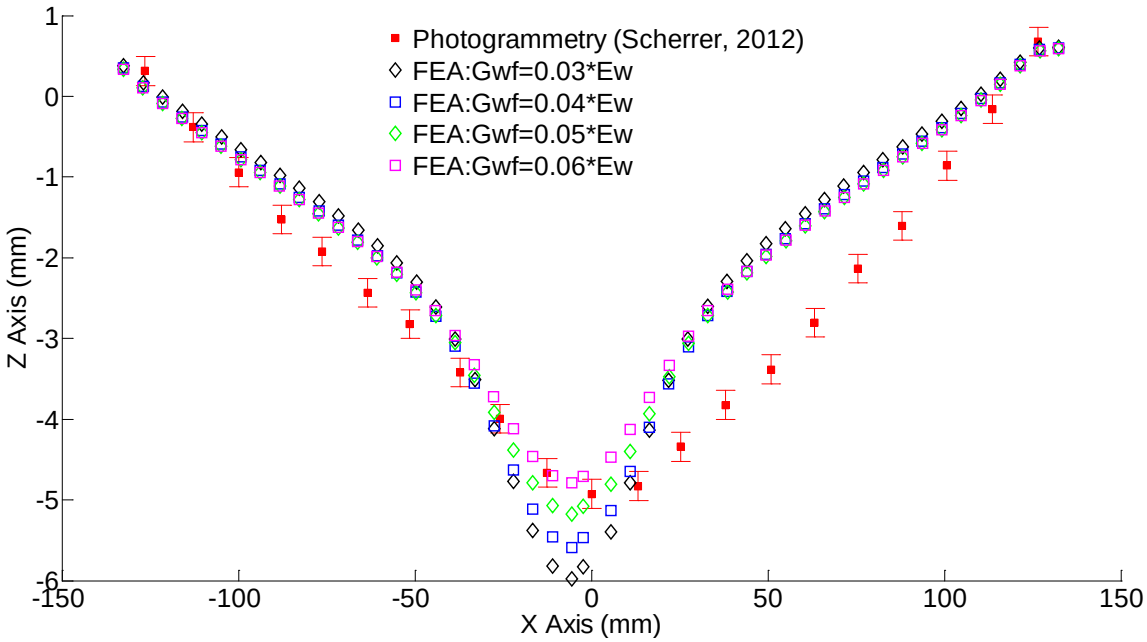

Figure B.7. Shear study for Test Case 7.

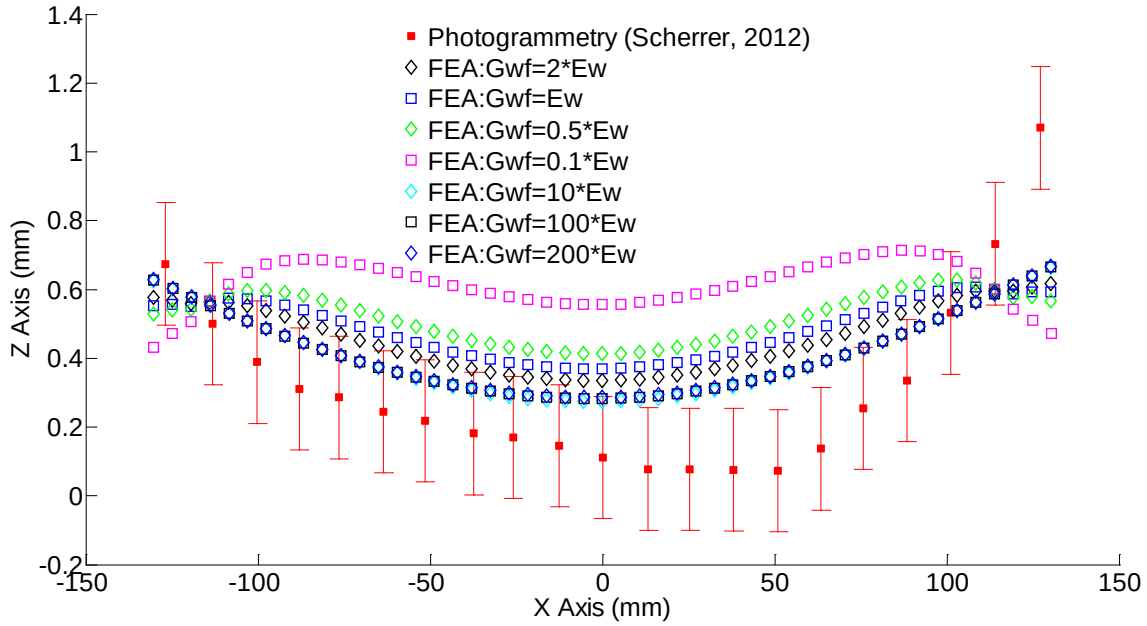

Figure B.8. Shear study for Test Case 8.

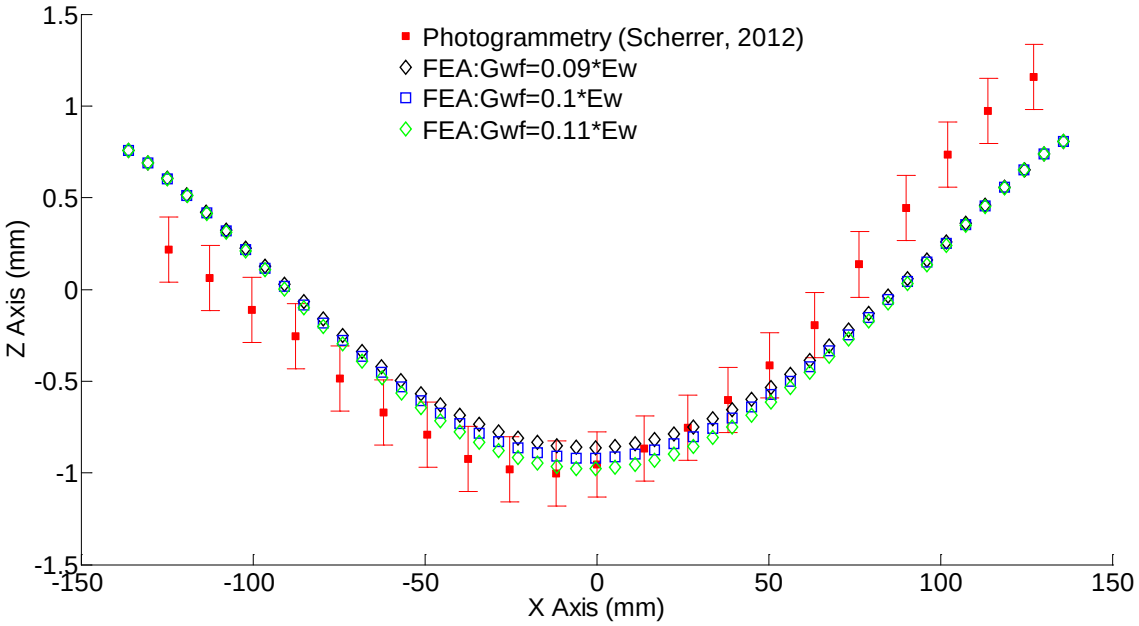

Figure B.9. Shear study for Test Case 9.

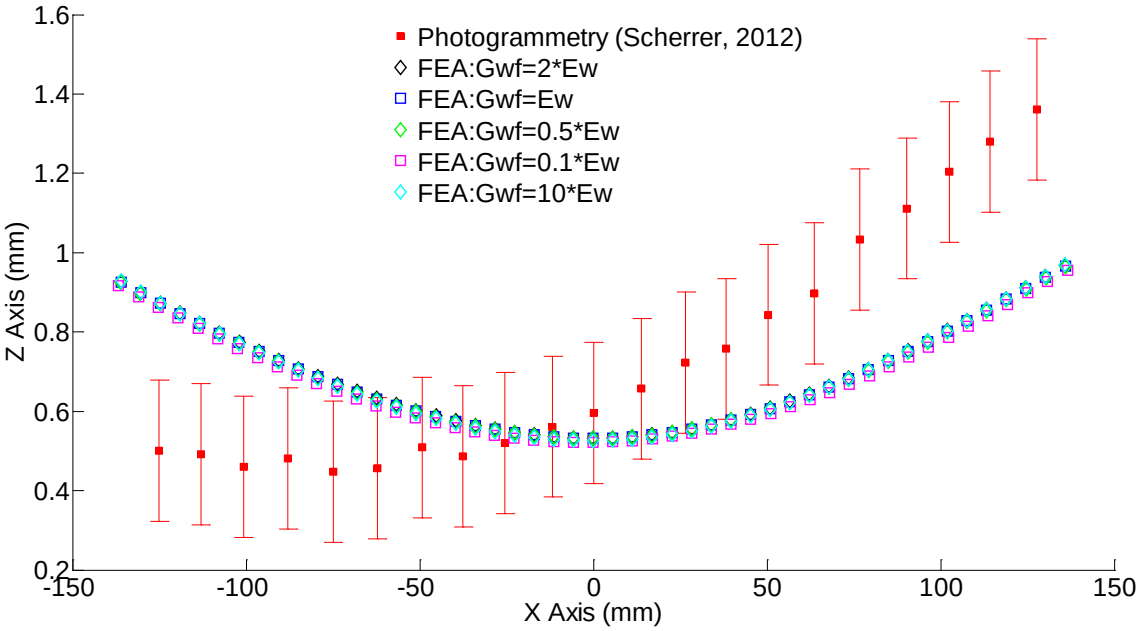

Figure B.10. Shear study for Test Case 10.

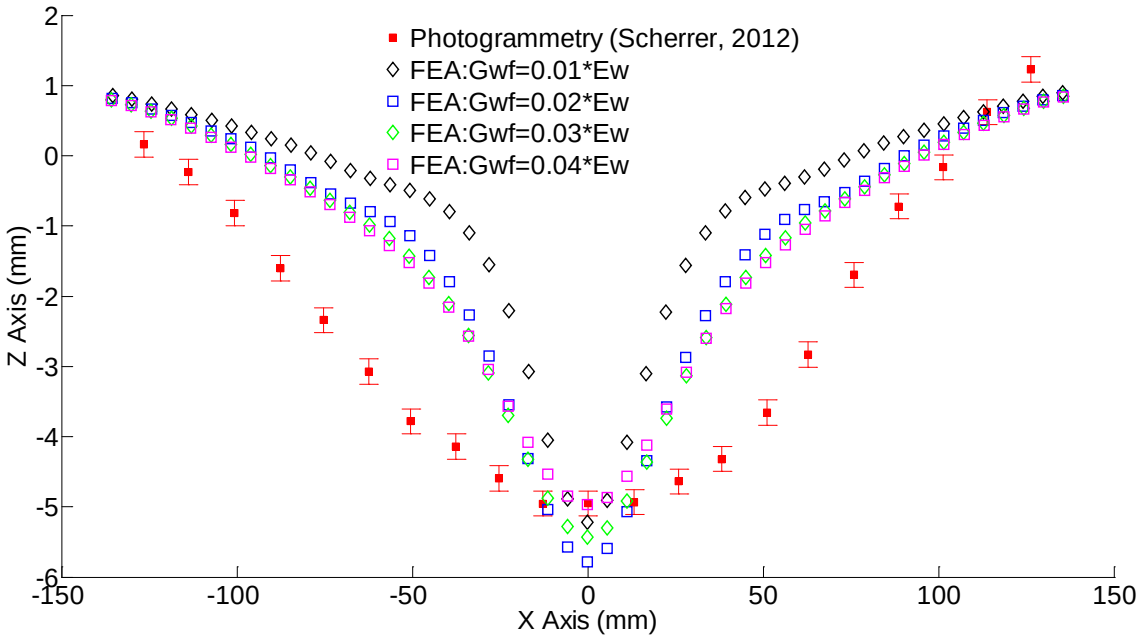

Figure B.11. Shear study for Test Case 11.

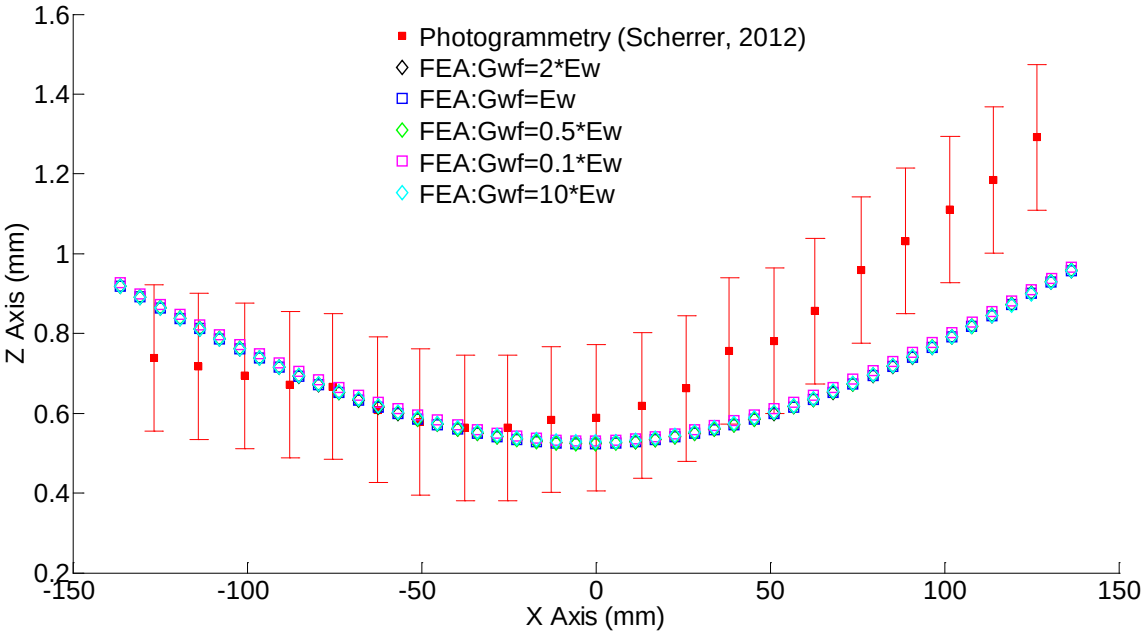

Figure B.12. Shear study for Test Case 12.

Hypotenuse, Center Line, and 3-D Contours

The following plots are the static deflection contours for each of the test cases studied in the bi-axial tension fabric analysis. Center and hypotenuse contours are compared, as well as, full 3-D contours of the triangular fabric specimen.

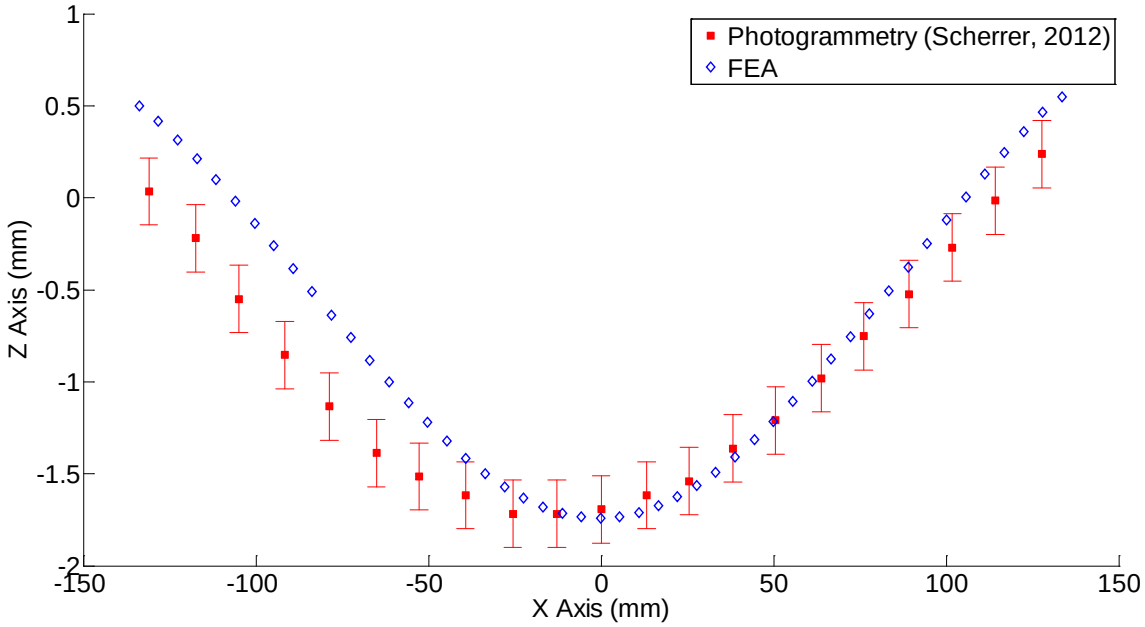

Figure B.13. Hypotenuse deflection contour for Test Case 1.

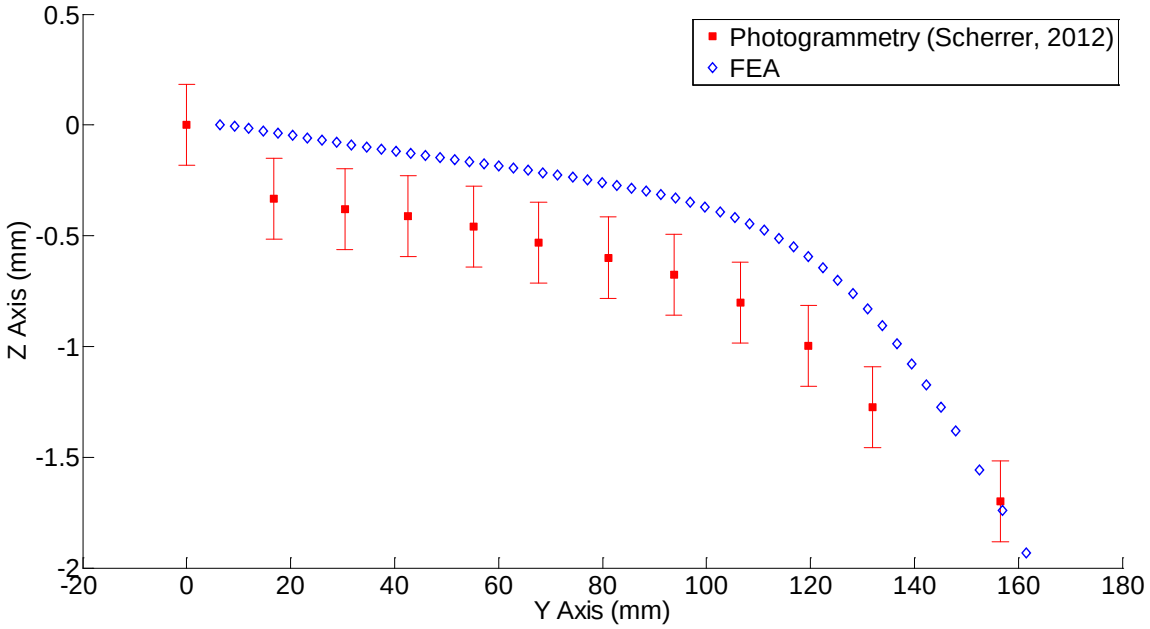

Figure B.14. Center deflection contour for Test Case 1.

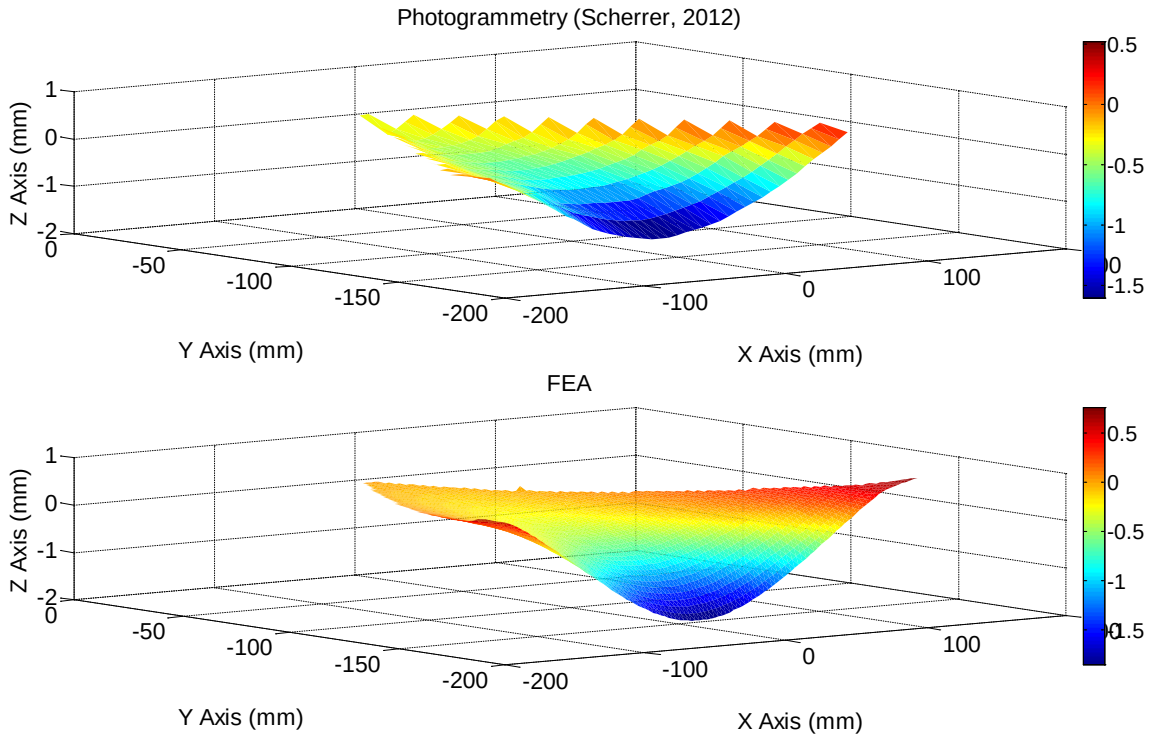

Figure B.15. 3-D deflection contour for Test Case 1.

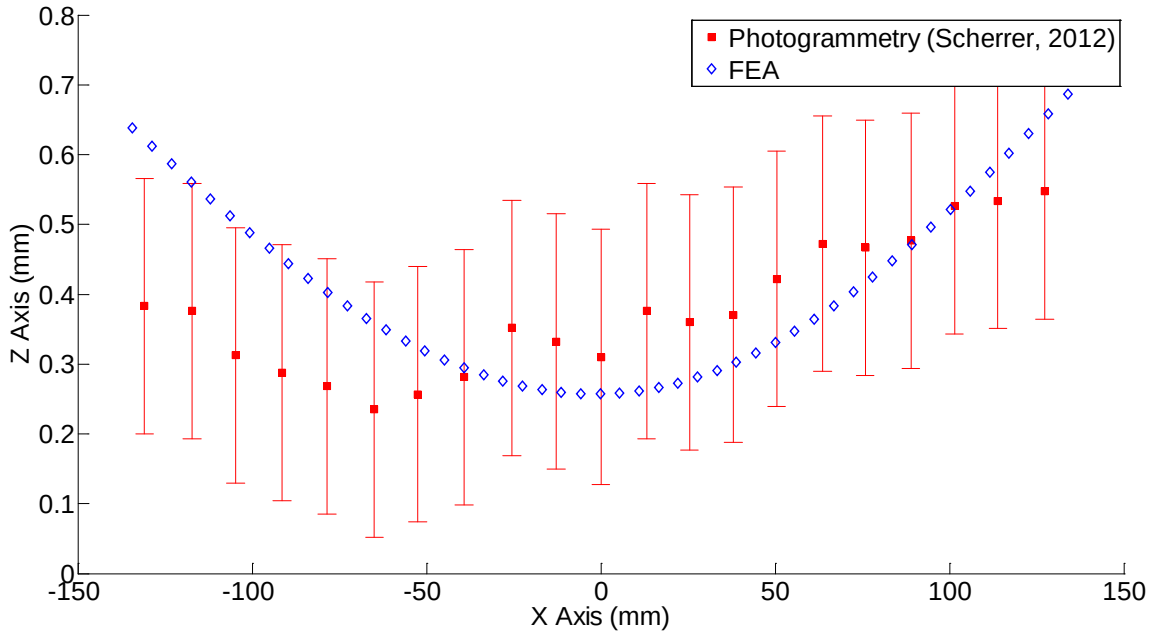

Figure B.16. Hypotenuse deflection contour for Test Case 2.

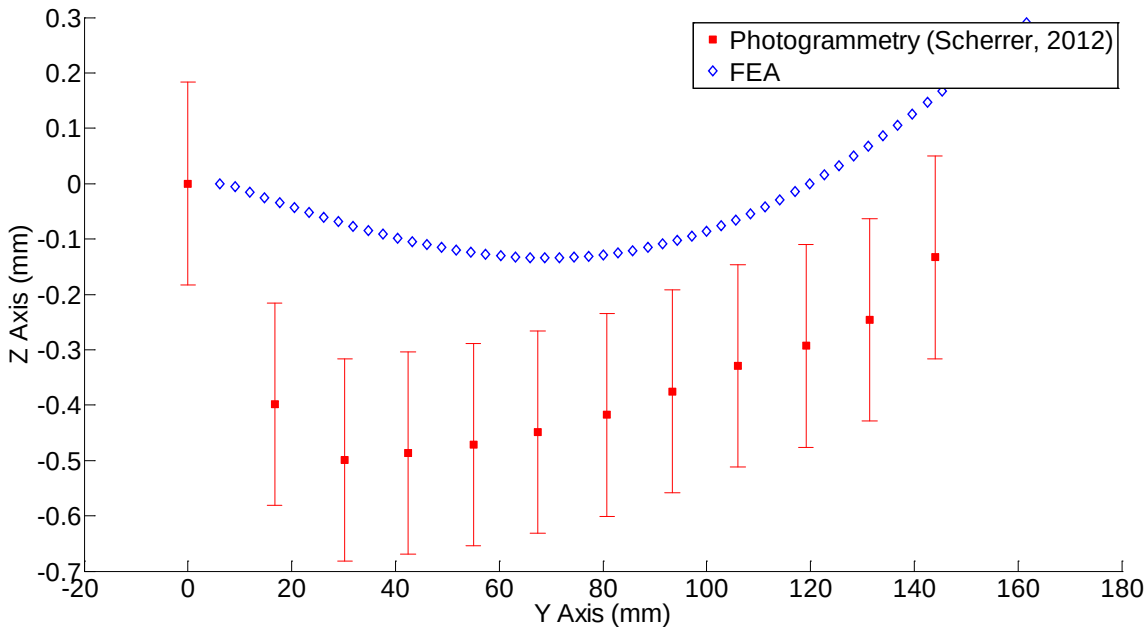

Figure B.17. Center deflection contour for Test Case 2.

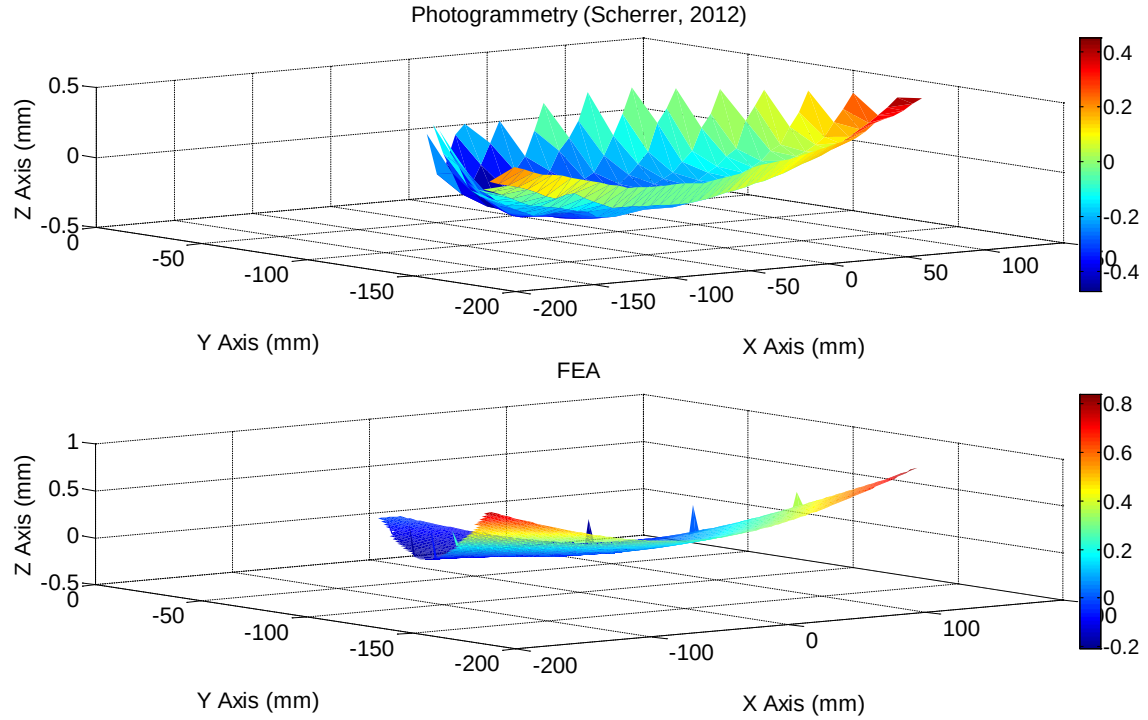

Figure B.18. 3-D deflection contour for Test Case 2.

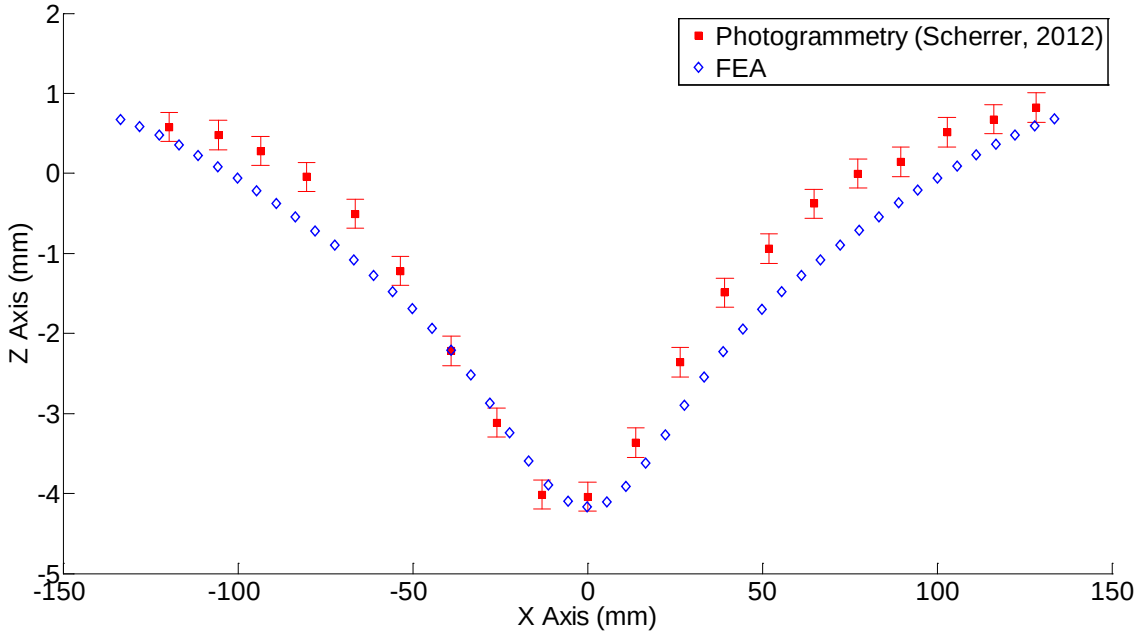

Figure B.19. Hypotenuse deflection contour for Test Case 3.

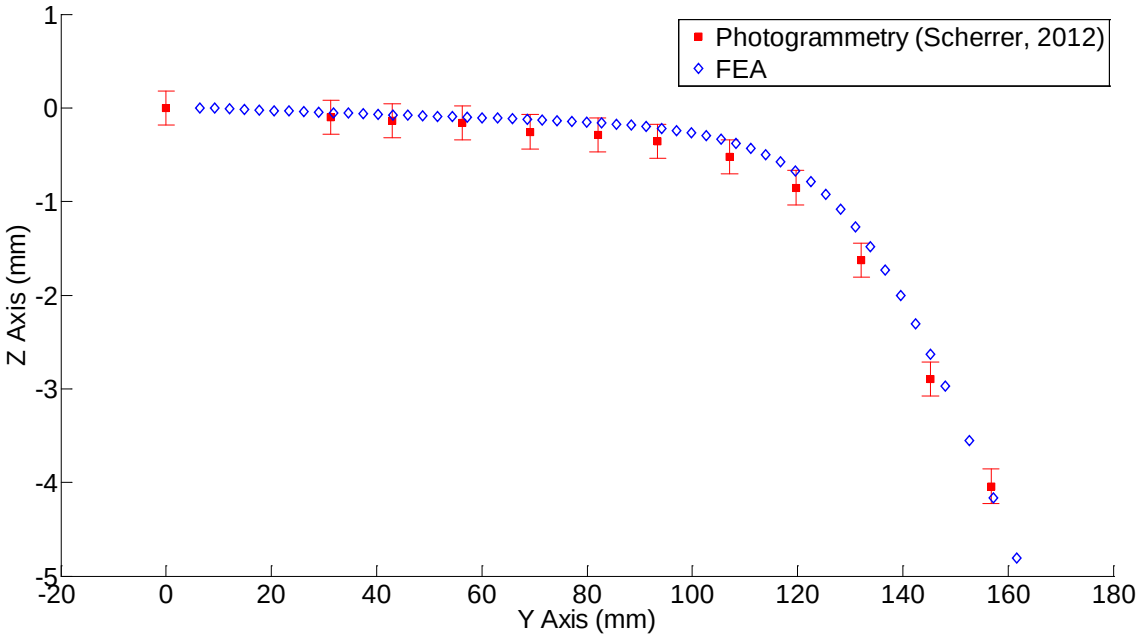

Figure B.20. Center deflection contour for Test Case 3.

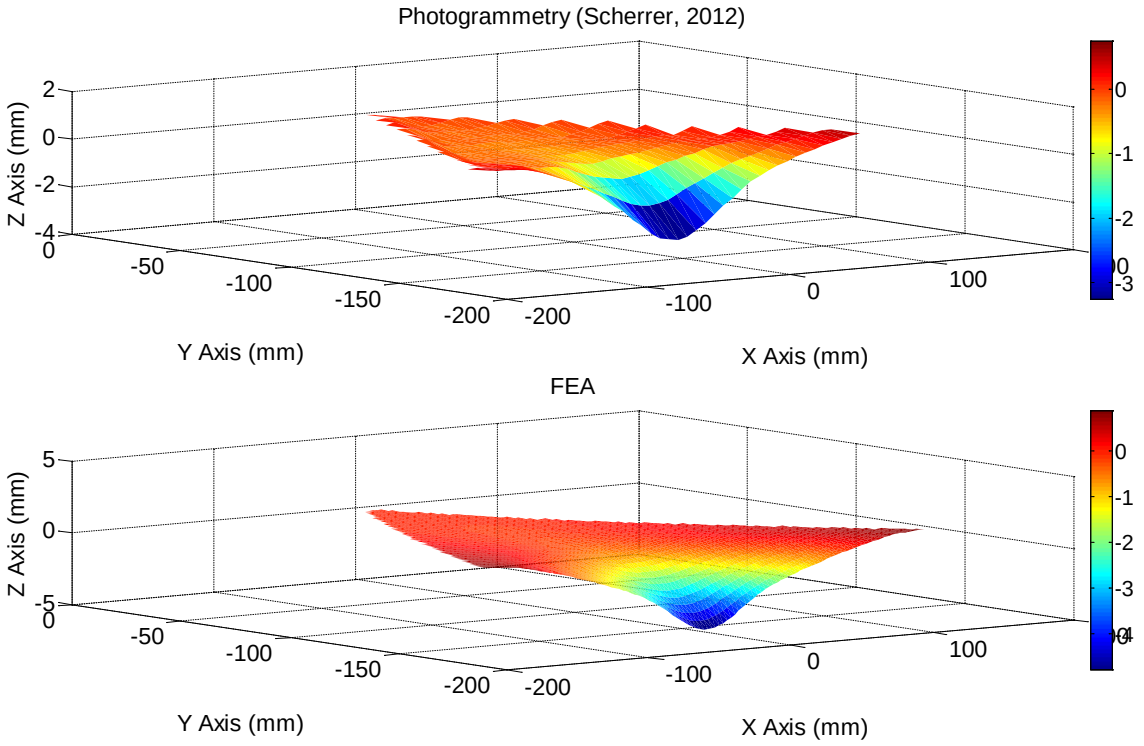

Figure B.21. 3-D deflection contour for Test Case 3.

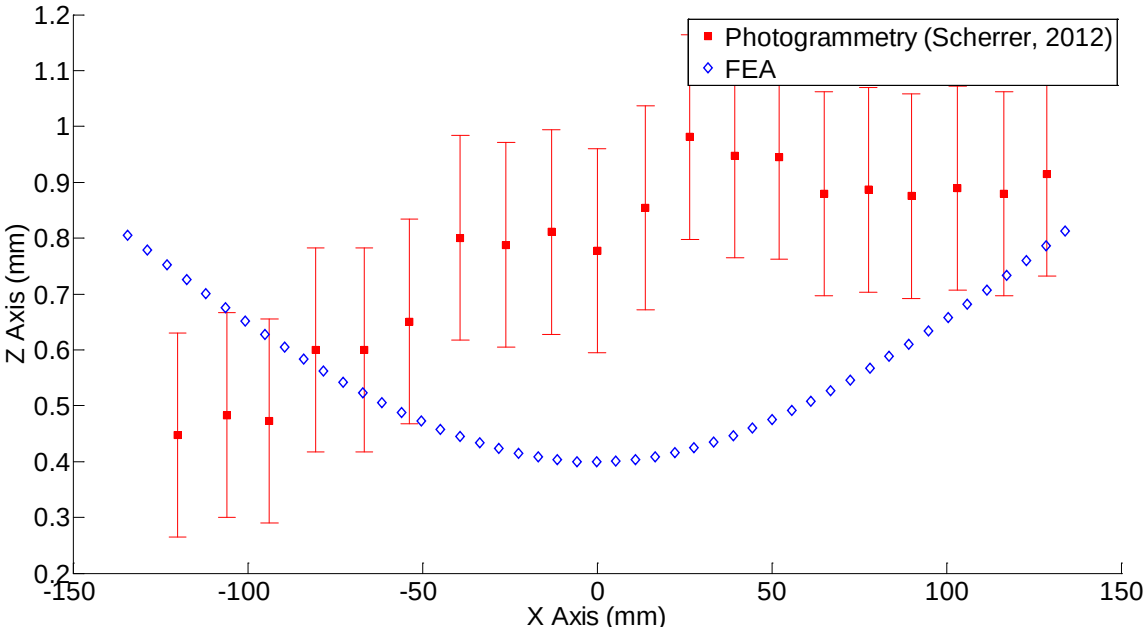

Figure B.22. Hypotenuse deflection contour for Test Case 4.

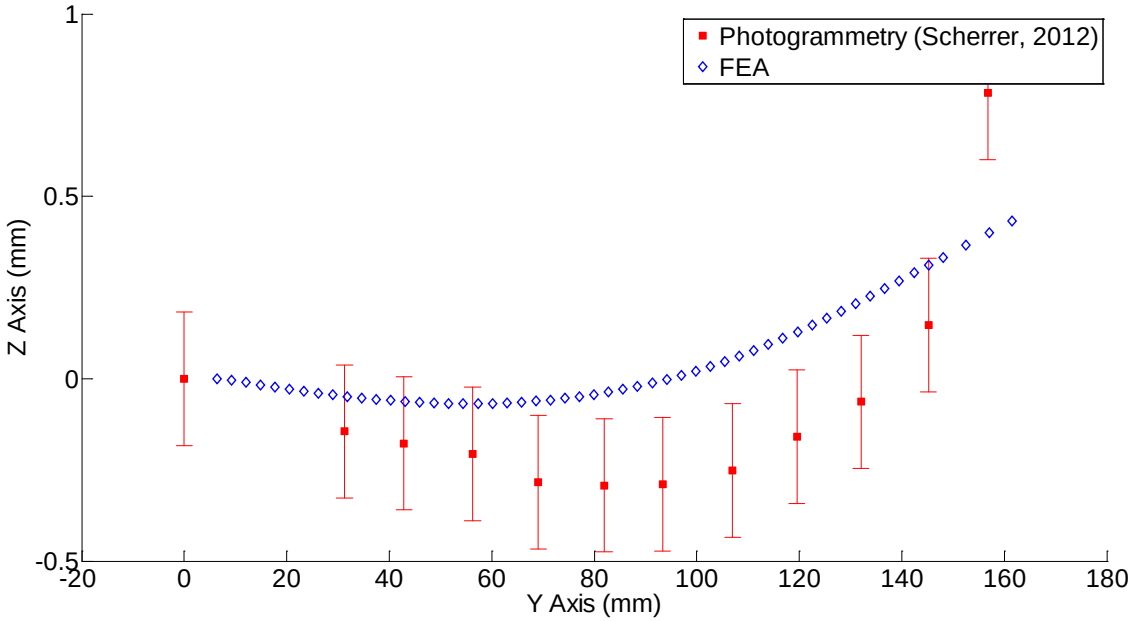

Figure B.23. Center deflection contour for Test Case 4.

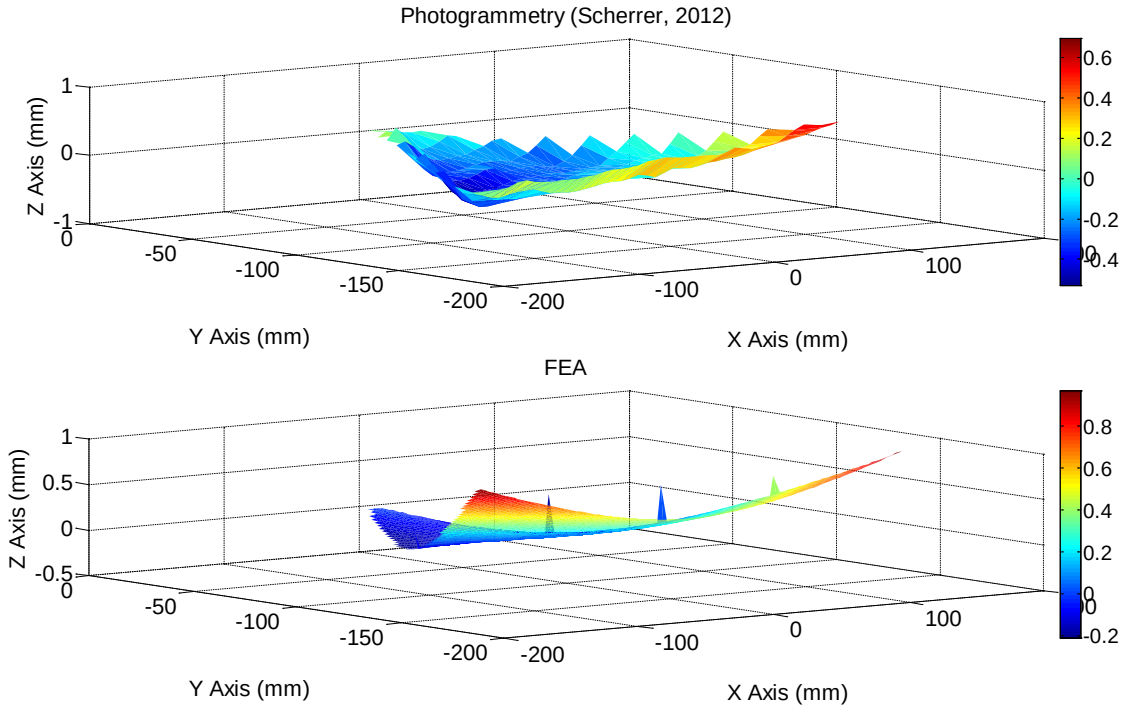

Figure B.24. 3-D deflection contour for Test Case 4.

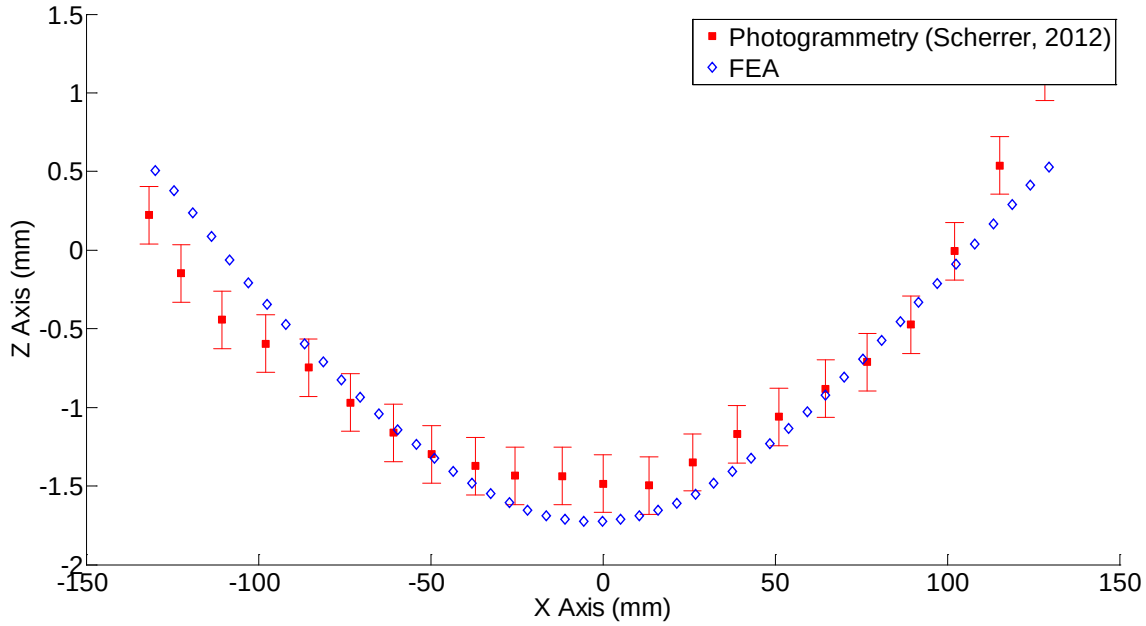

Figure B.25. Hypotenuse deflection contour for Test Case 5.

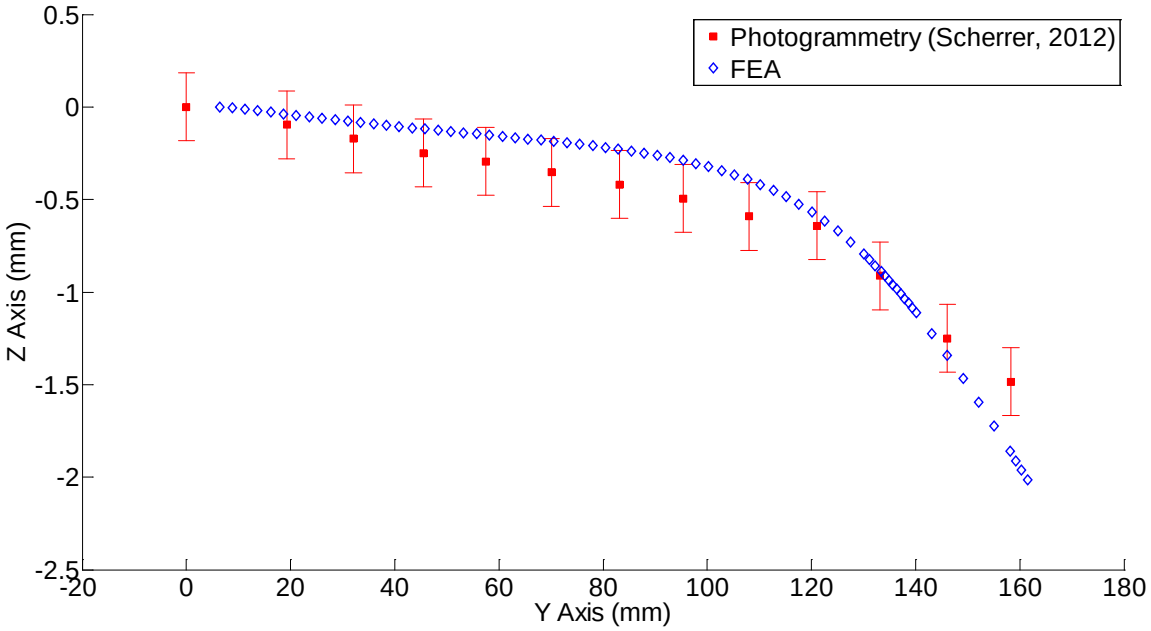

Figure B.26. Center deflection contour for Test Case 5.

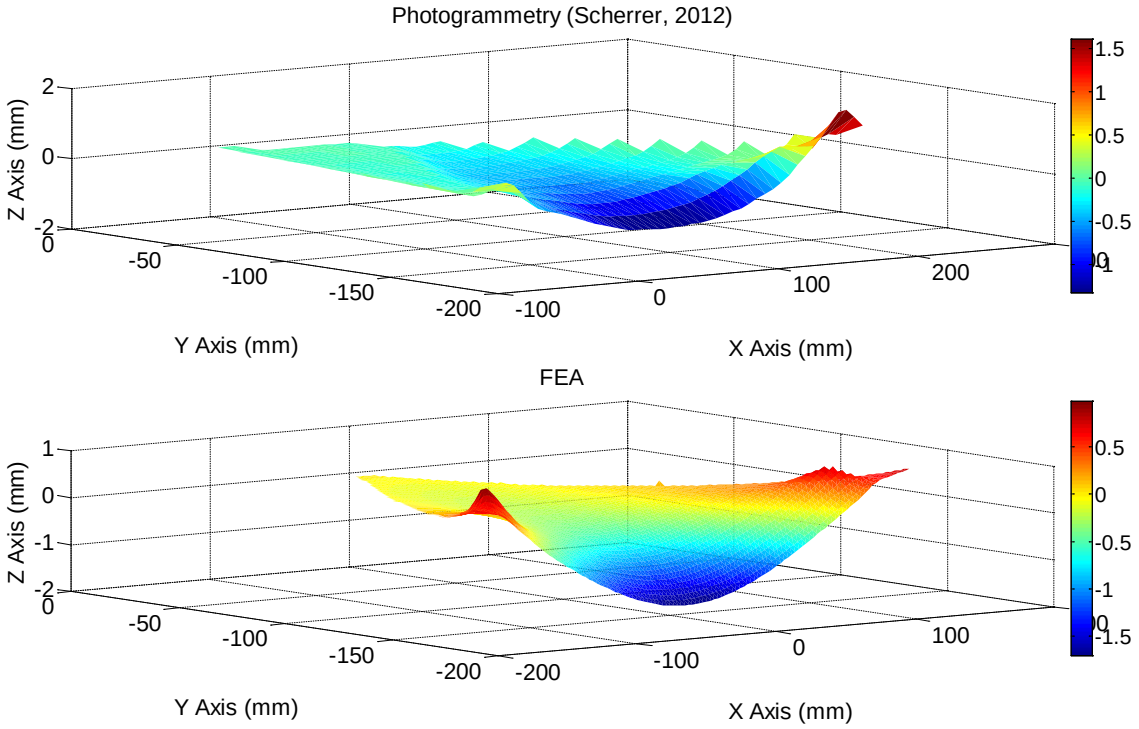

Figure B.27. 3-D deflection contour for Test Case 5.

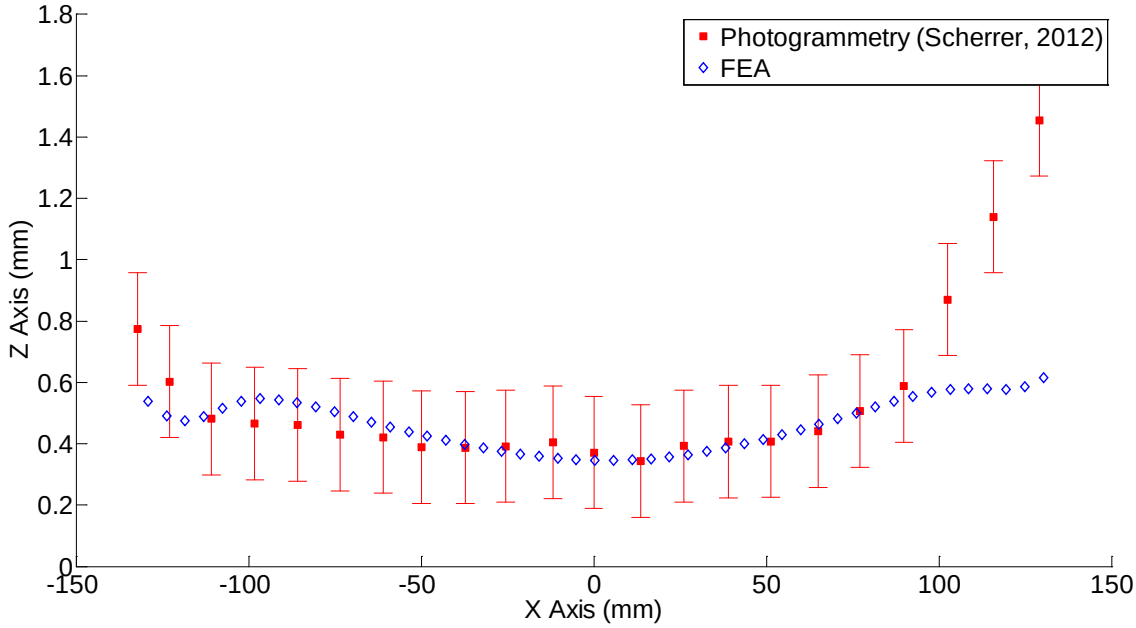

Figure B.28. Hypotenuse deflection contour for Test Case 6.

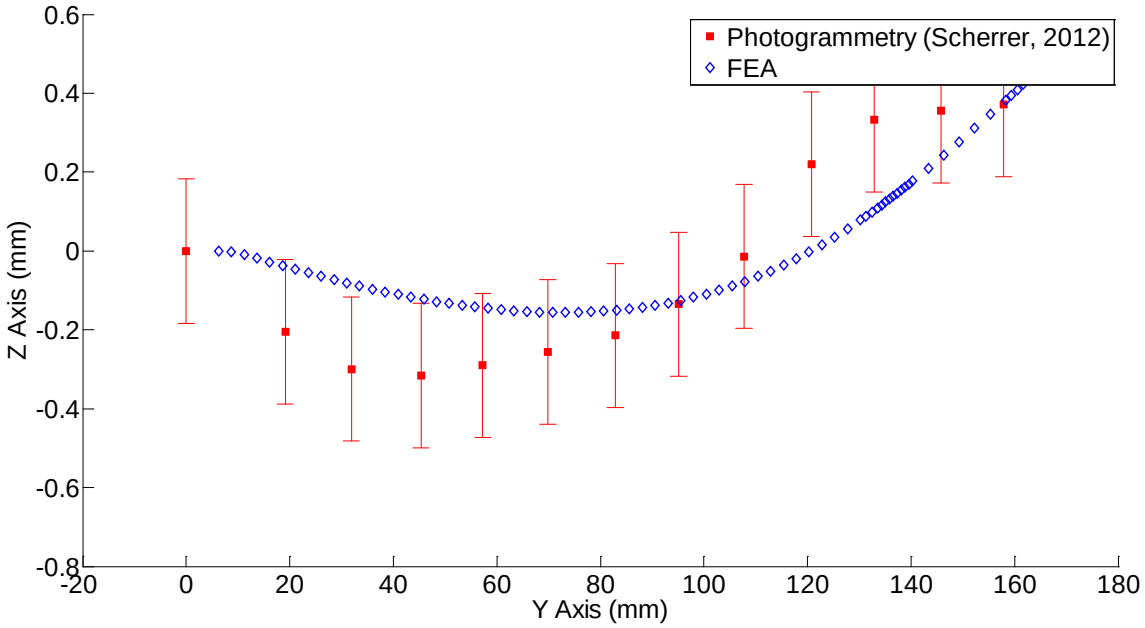

Figure B.29. Center deflection contour for Test Case 6.

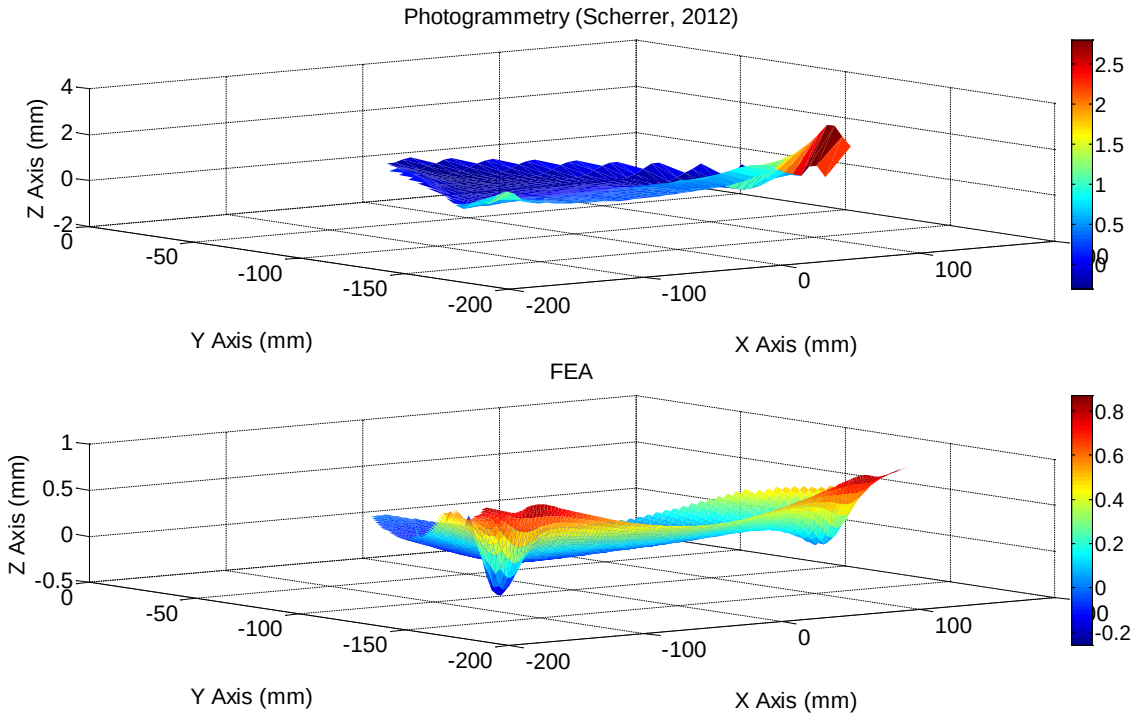

Figure B.30. 3-D deflection contour for Test Case 6.

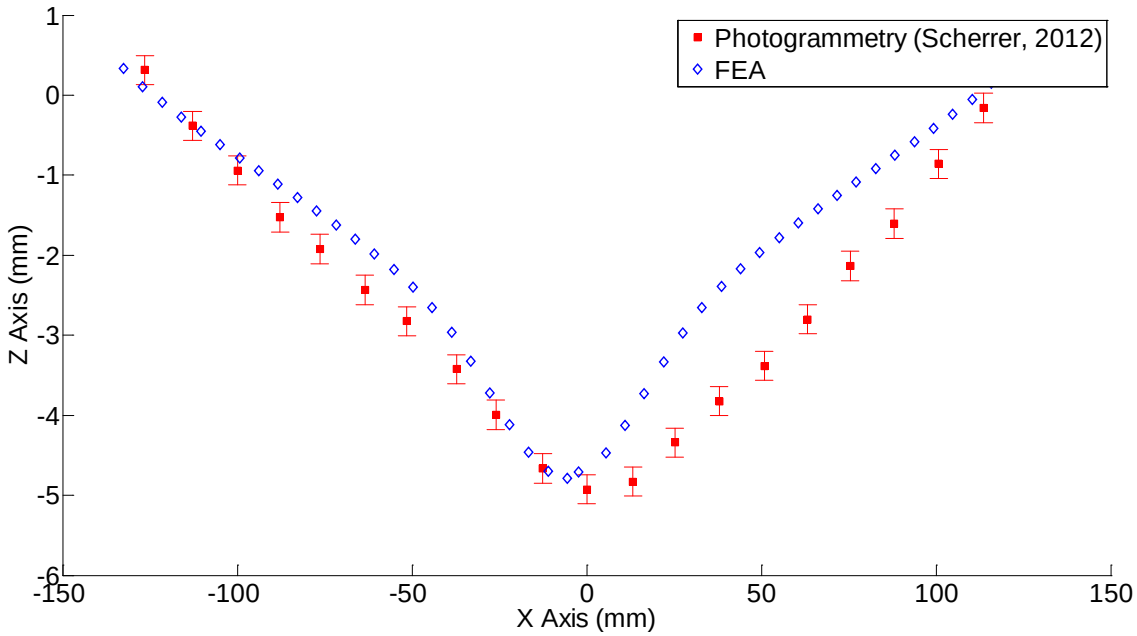

Figure B.31. Hypotenuse deflection contour for Test Case 7.

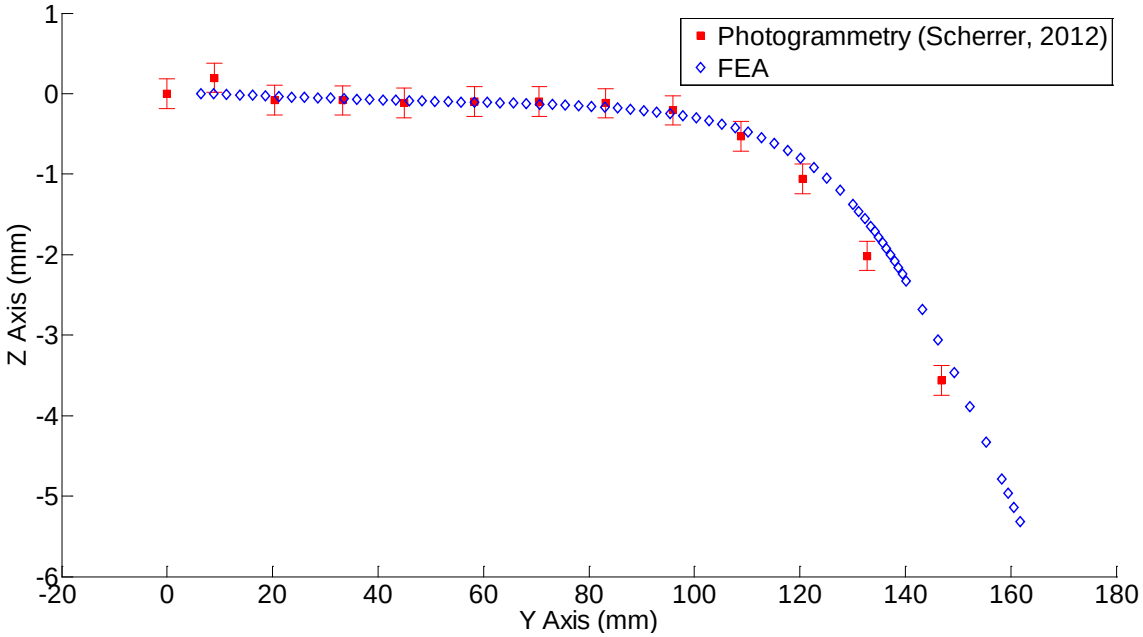

Figure B.32. Center deflection contour for Test Case 7.

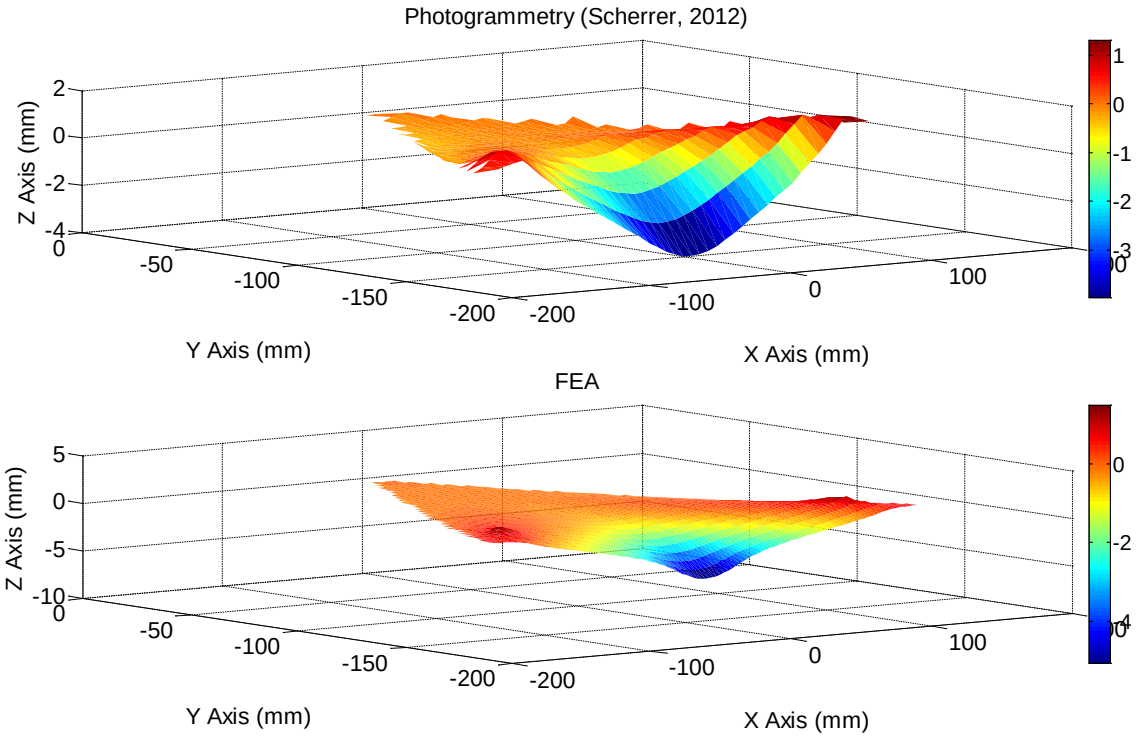

Figure B.33. 3-D deflection contour for Test Case 7.

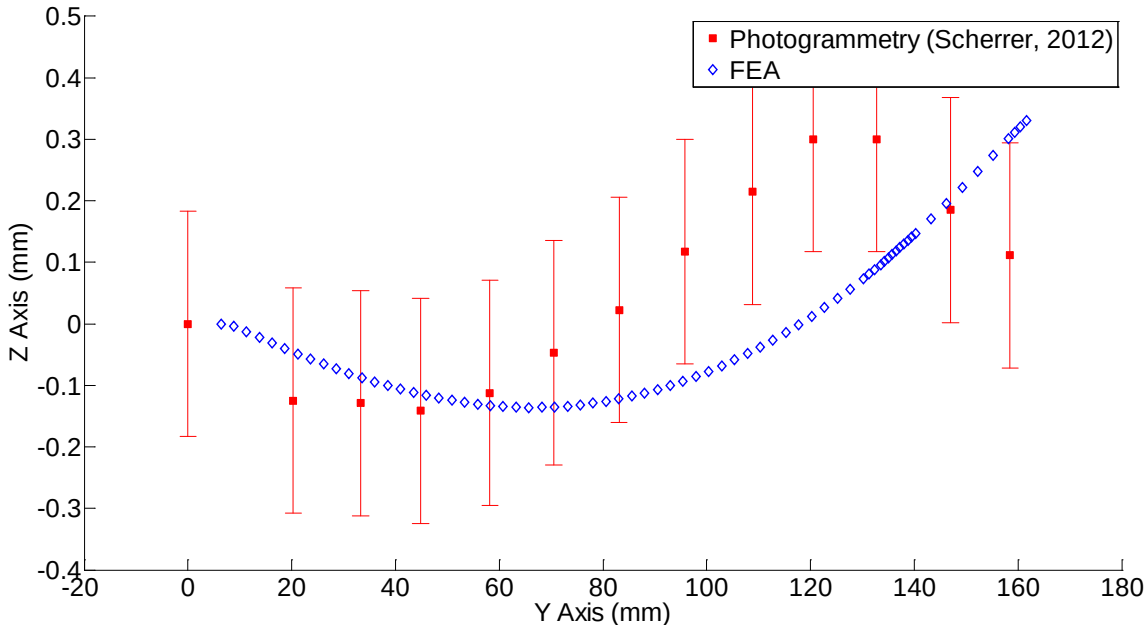

Figure B.34. Hypotenuse deflection contour for Test Case 8.

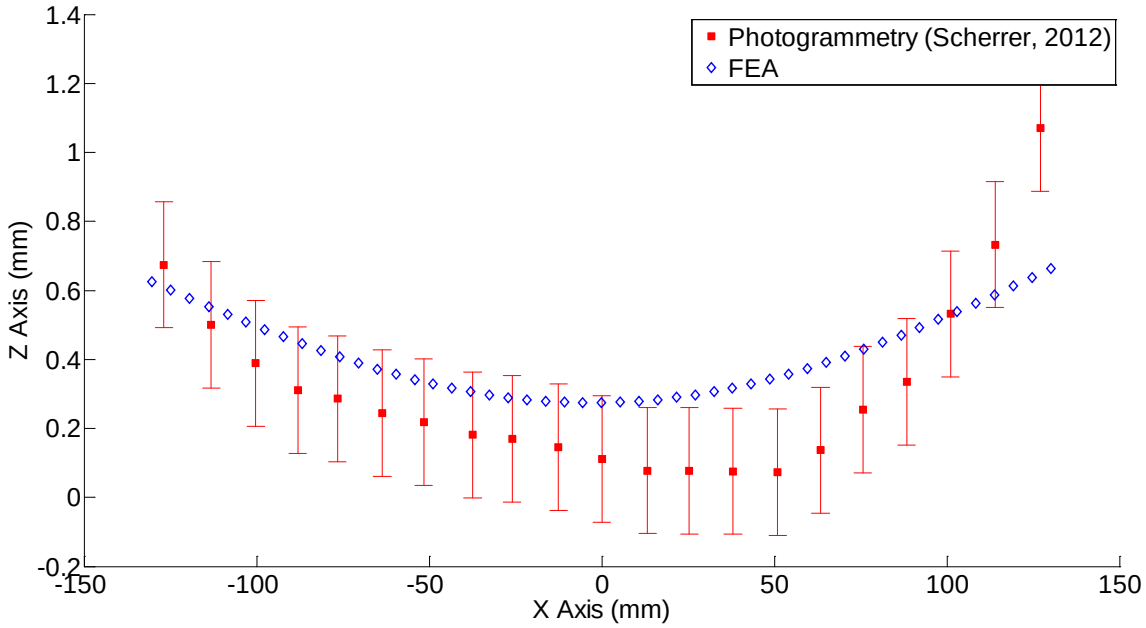

Figure B.35. Center deflection contour for Test Case 8.

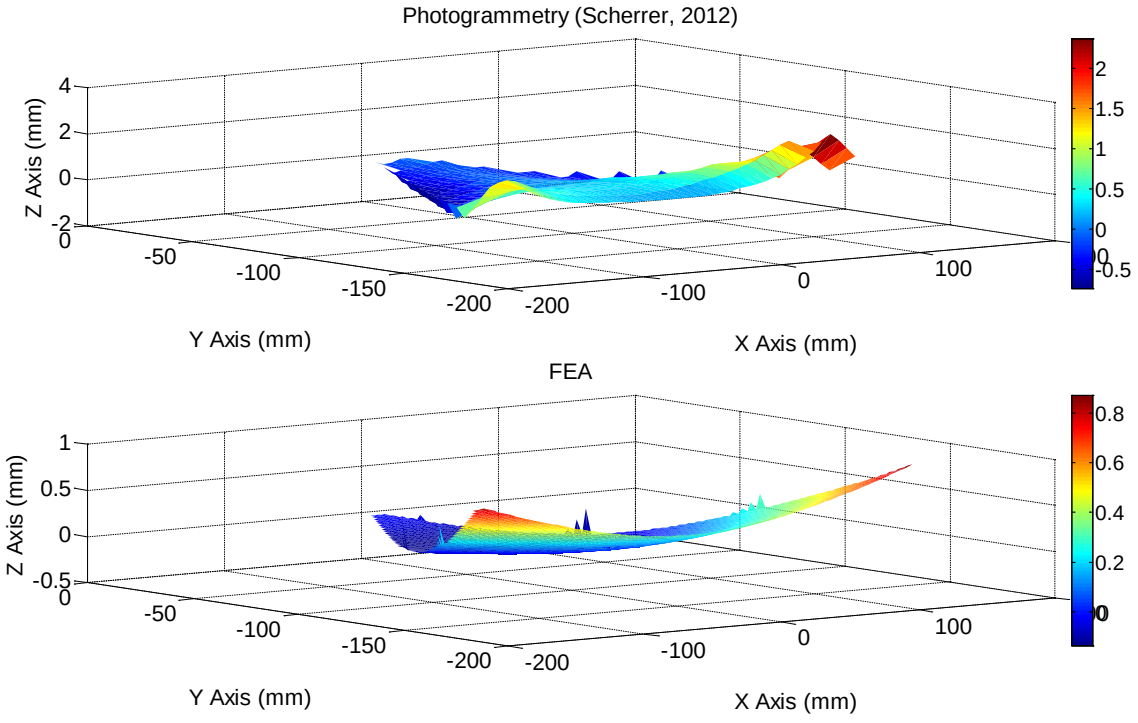

Figure B.36. 3-D deflection contour for Test Case 8.

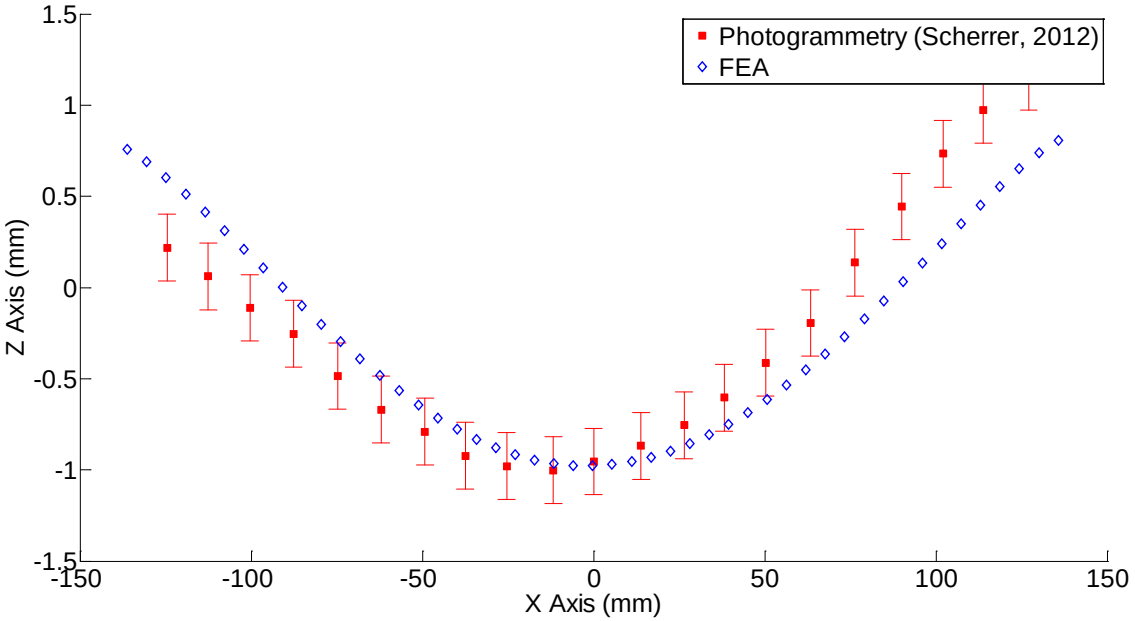

Figure B.37. Hypotenuse deflection contour for Test Case 9.

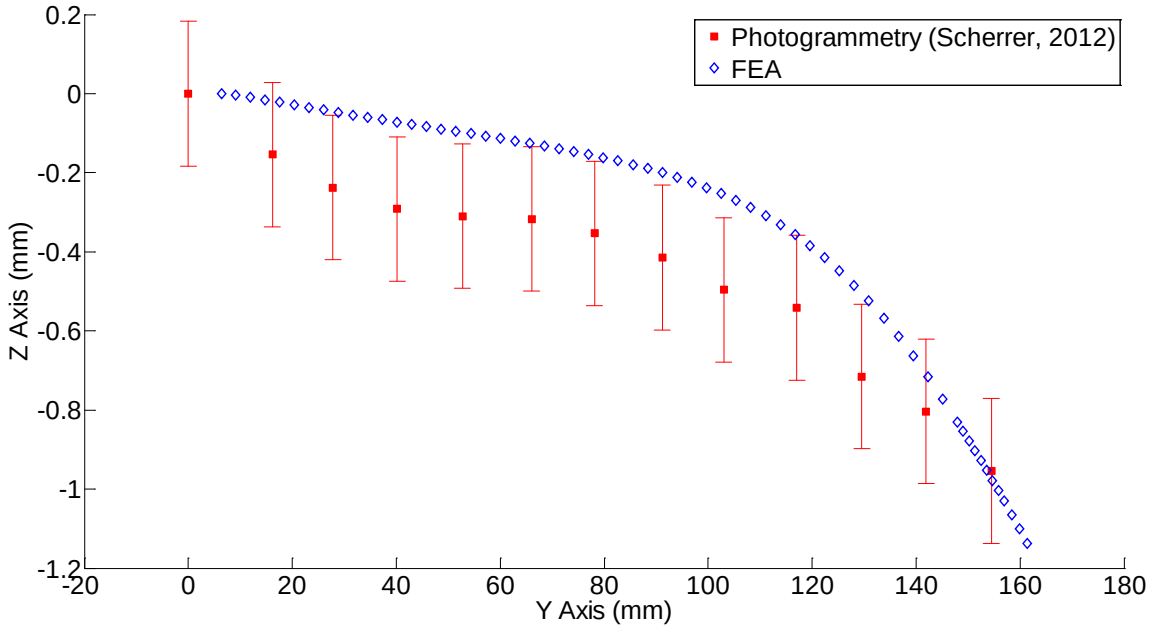

Figure B.38. Center deflection contour for Test Case 9.

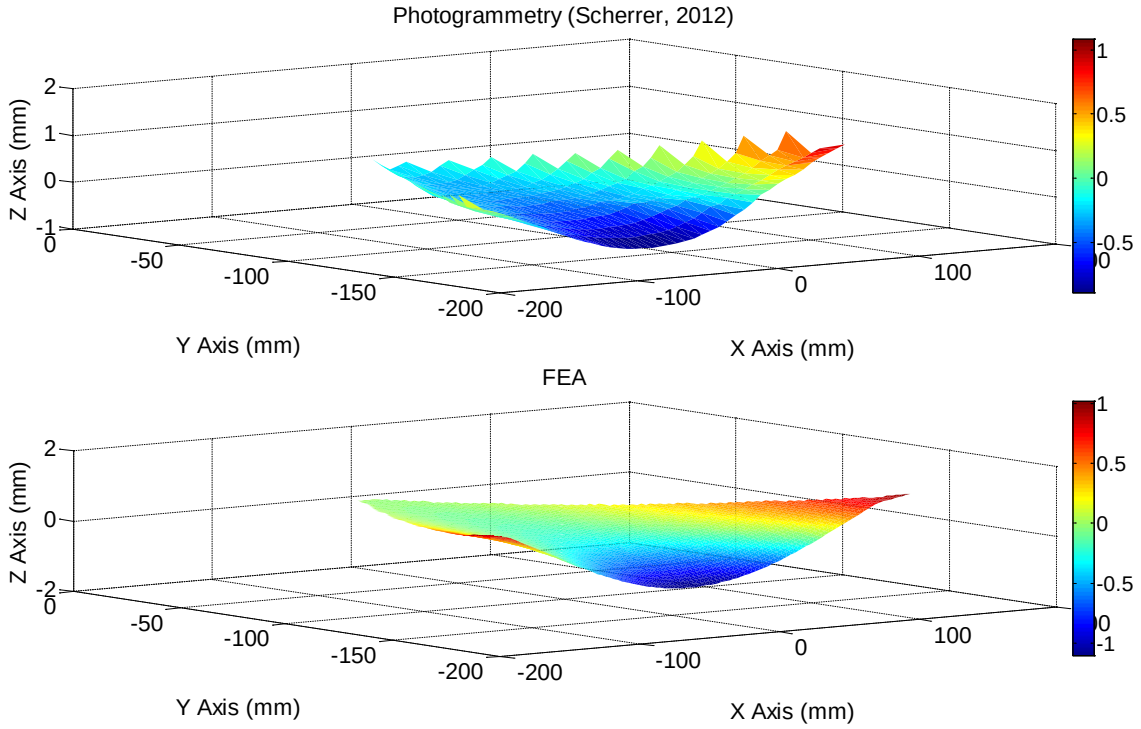

Figure B.39. 3-D deflection contour for Test Case 9.

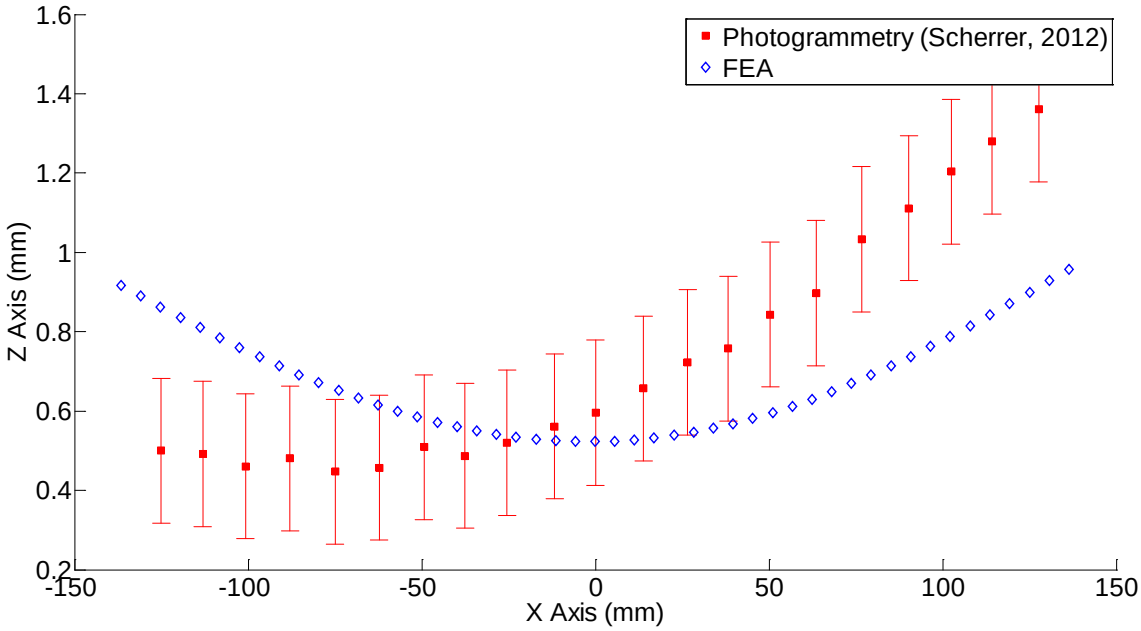

Figure B.40. Hypotenuse deflection contour for Test Case 10.

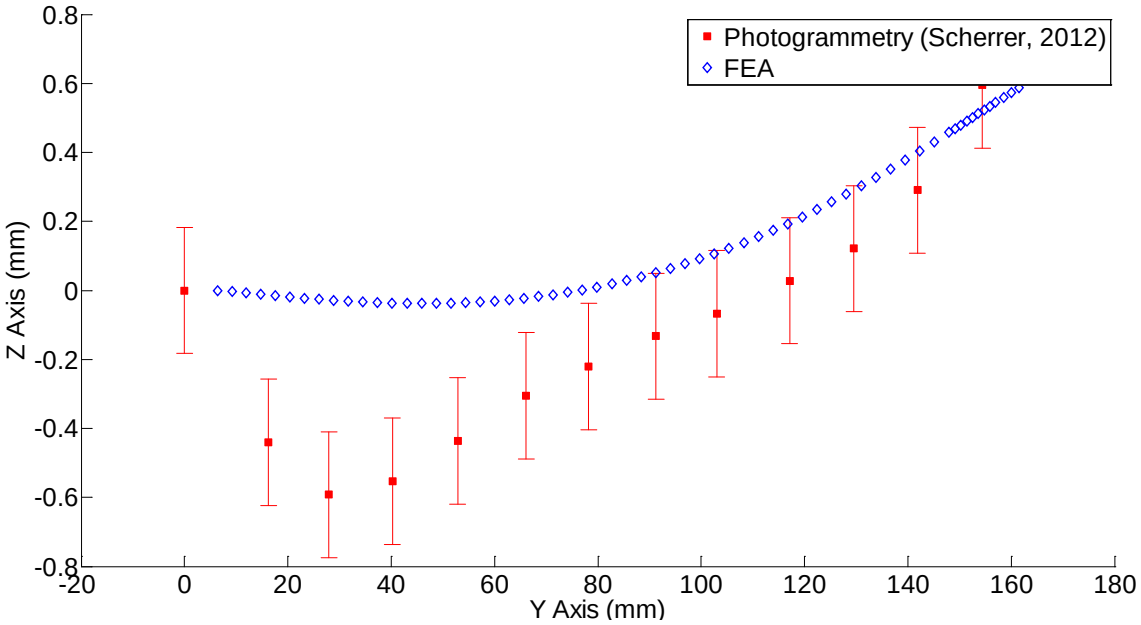

Figure B.41. Center deflection contour for Test Case 10.

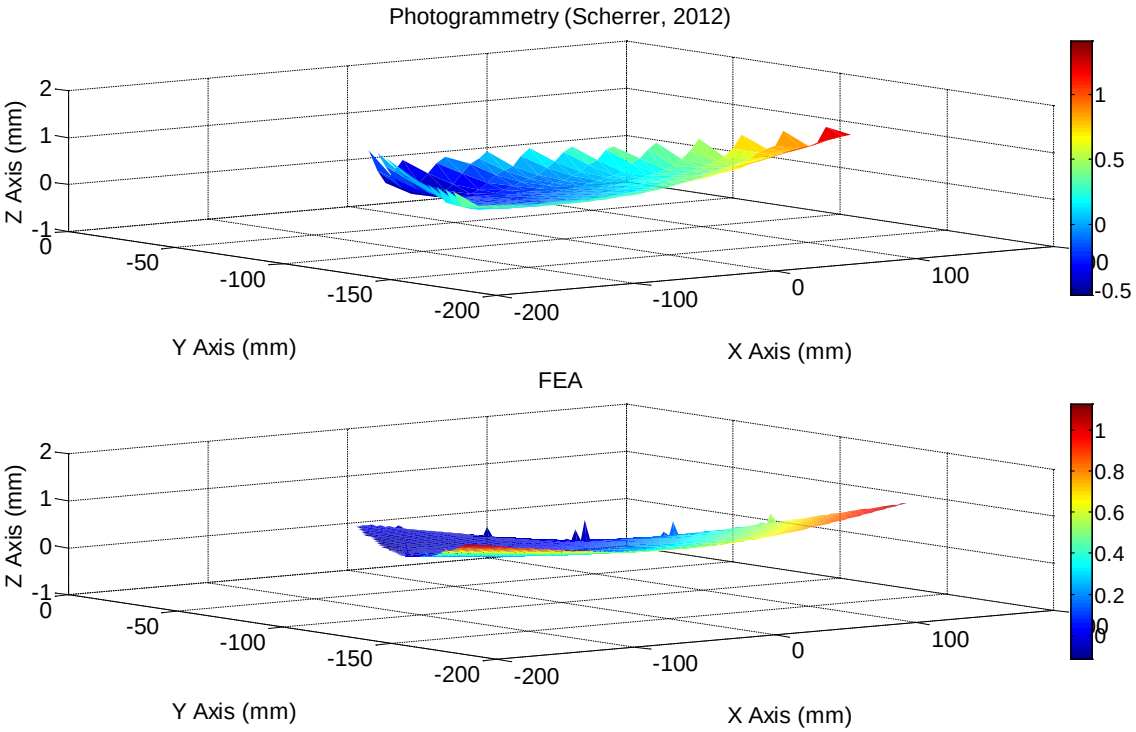

Figure B.42. 3-D deflection contour for Test Case 10.

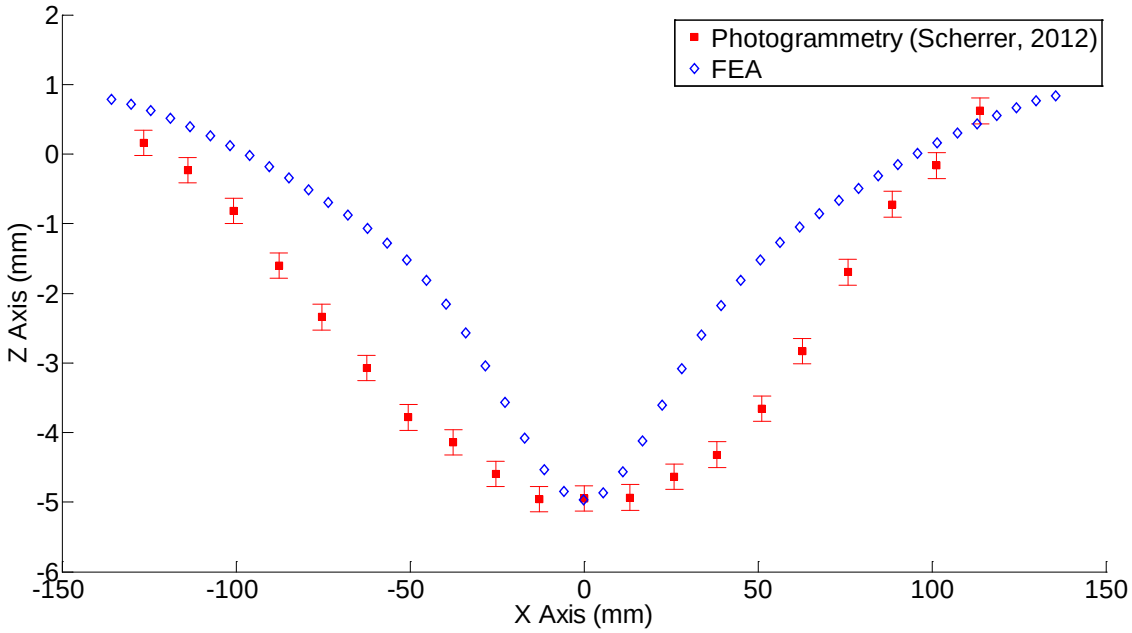

Figure B.43. Hypotenuse deflection contour for Test Case 11.

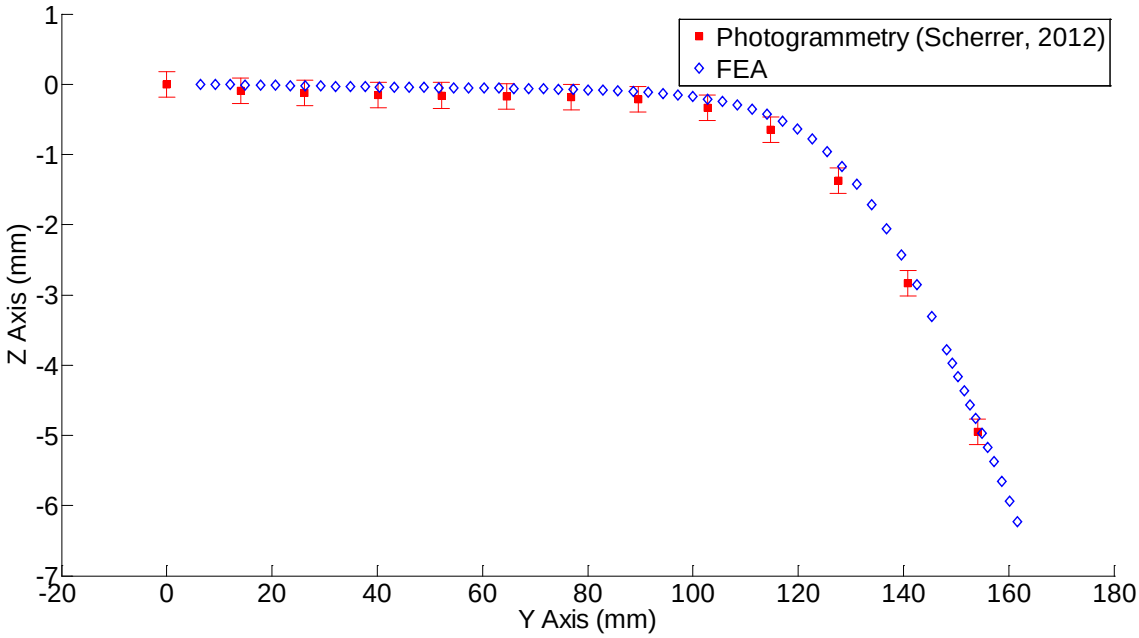

Figure B.44. Center deflection contour for Test Case 11.

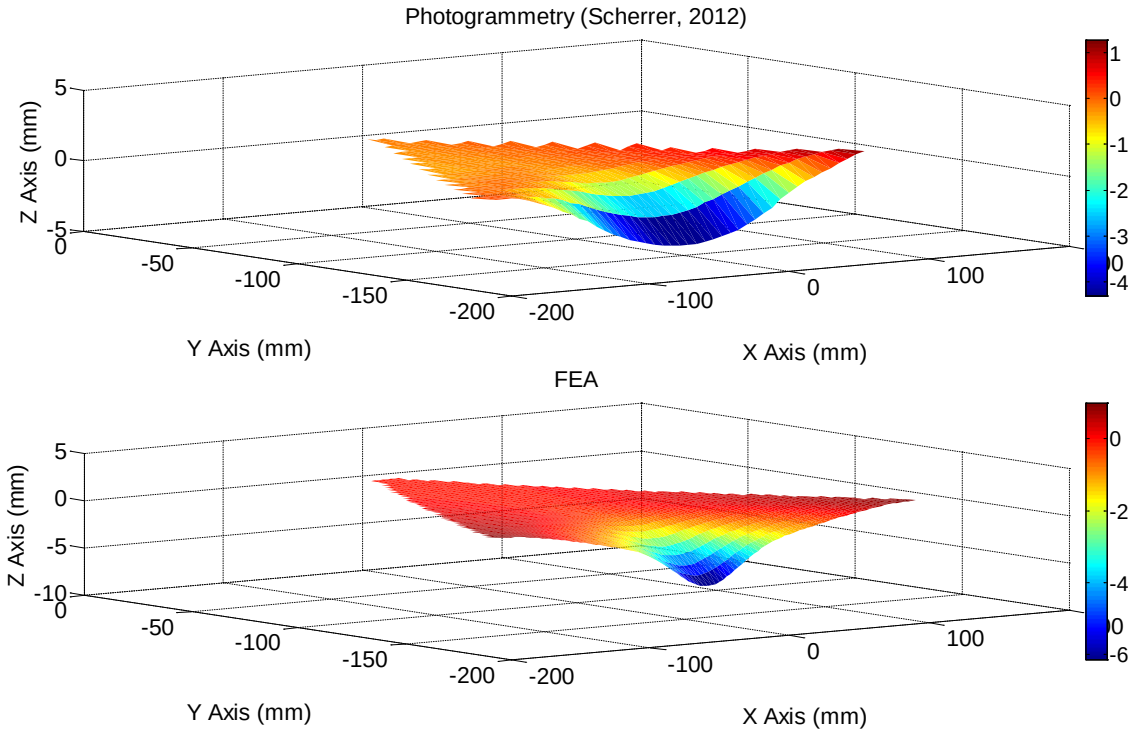

Figure B.45. 3-D deflection contour for Test Case 11.

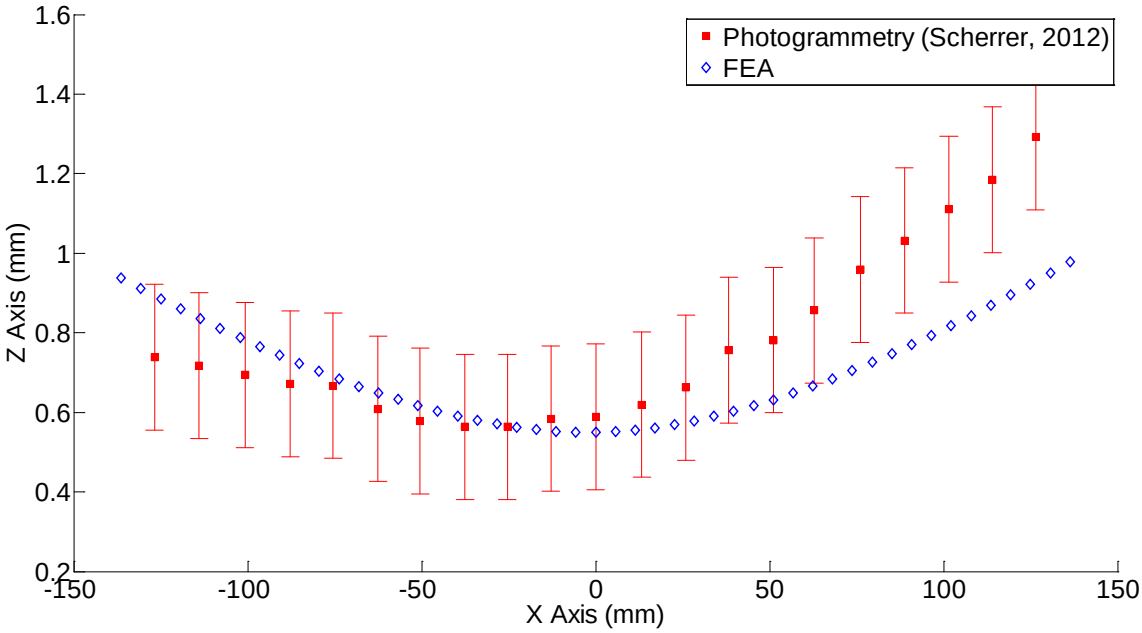

Figure B.46. Hypotenuse deflection contour for Test Case 12.

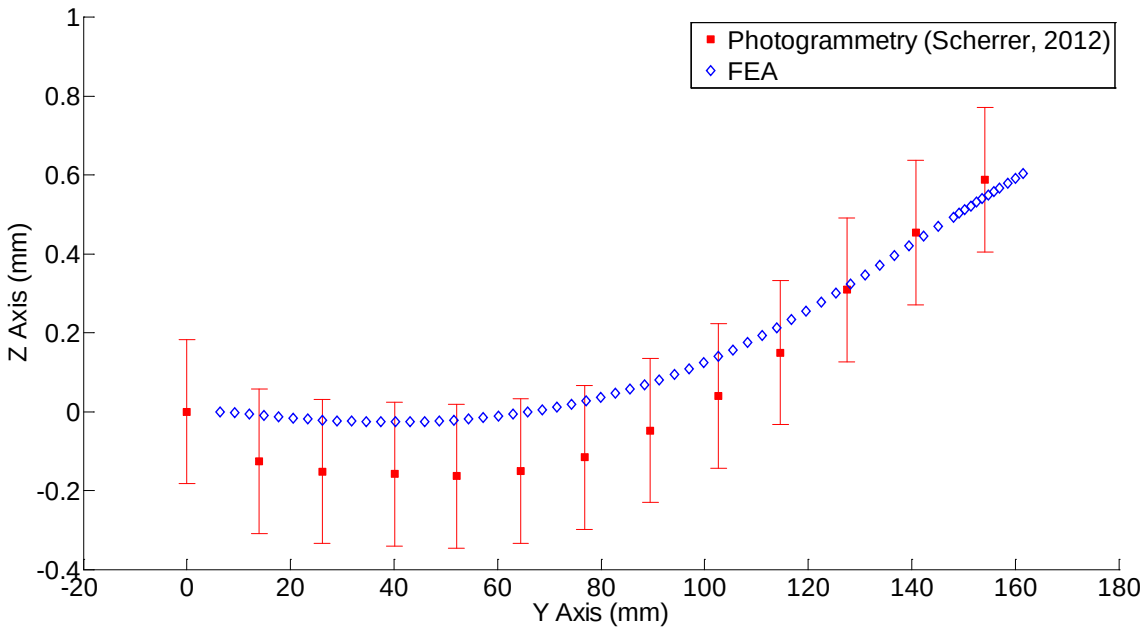

Figure B.47. Center deflection contour for Test Case 12.

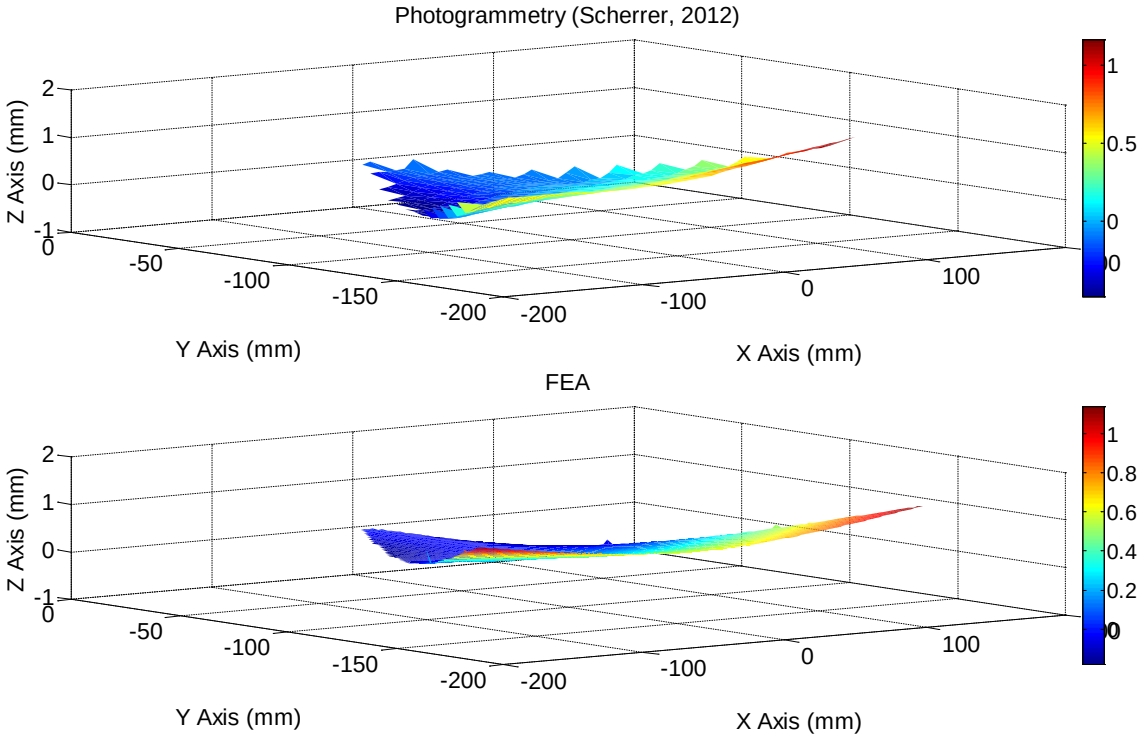

Figure B.48. 3-D deflection contour for Test Case 12.

Single Panel Design: Final Panel Geometry Deflection Contours

The following plots are the out-of-plane deflection contours for the circular free center geometry. These contours are the ones compared to the results from the final full inflatable pathfinder model.

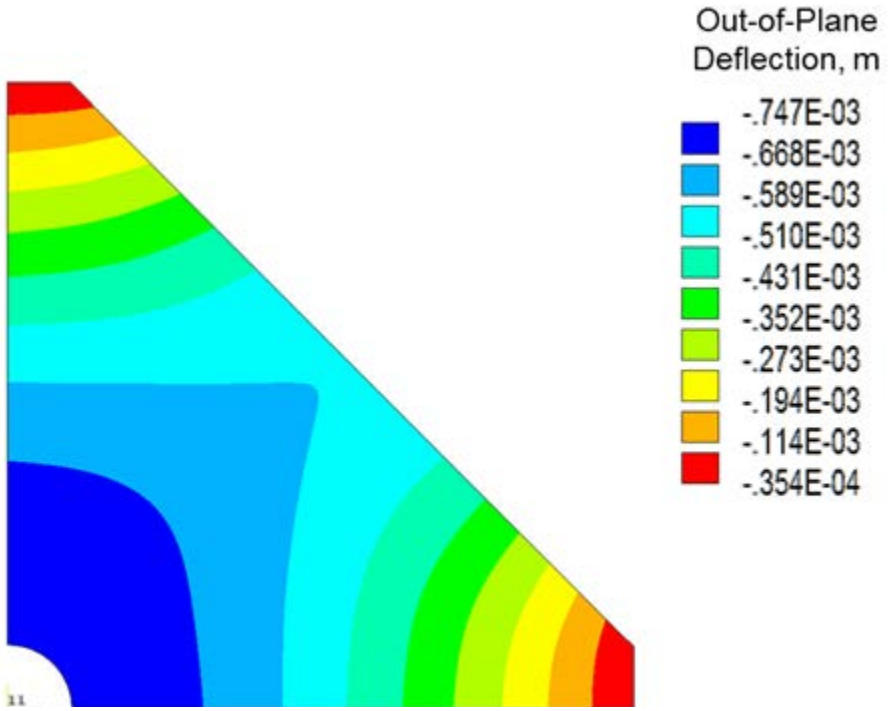

Figure B.49. Out-of-plane deflection contour for single panel loaded at the 7 kPa pressure level.

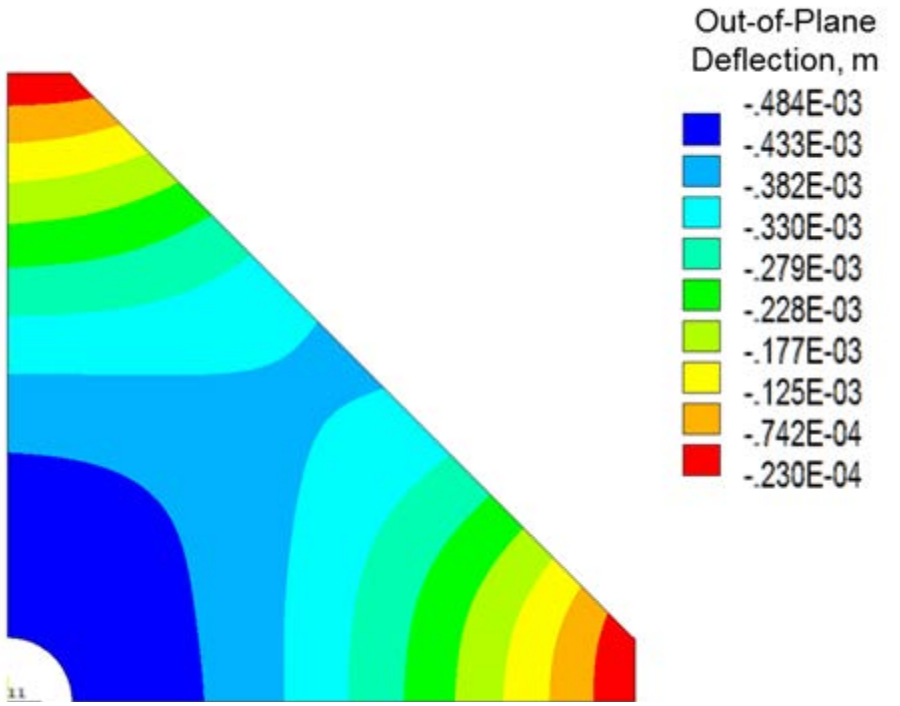

Figure B.50. Out-of-plane deflection contour for single panel loaded at the 10 kPa pressure level.

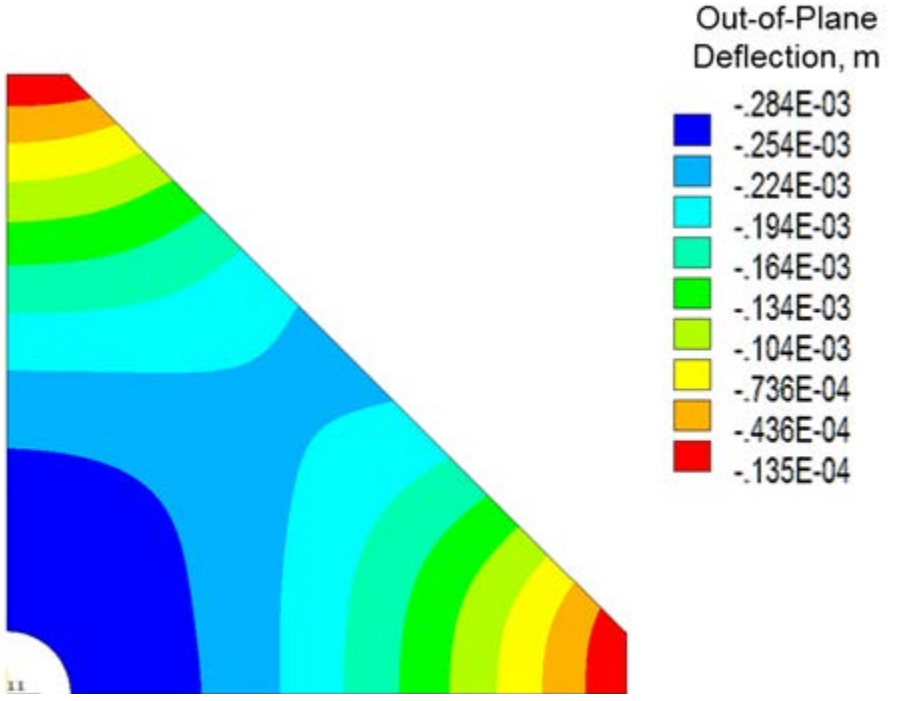

Figure B.51. Out-of-plane deflection contour for single panel loaded at the 15 kPa pressure level.

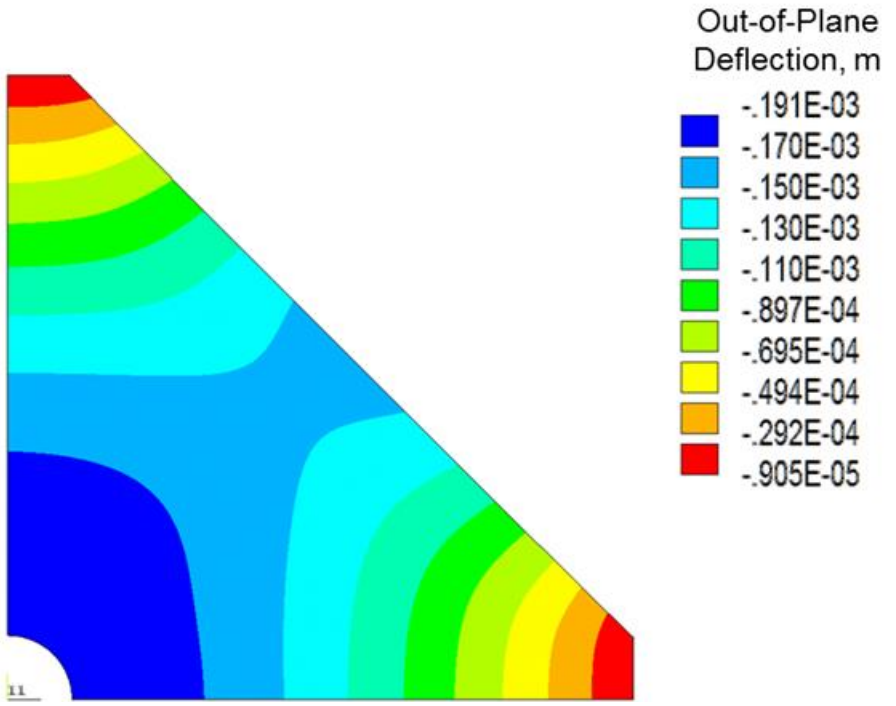

Figure B.52. Out-of-plane deflection contour for single panel loaded at the 20 kPa pressure level.

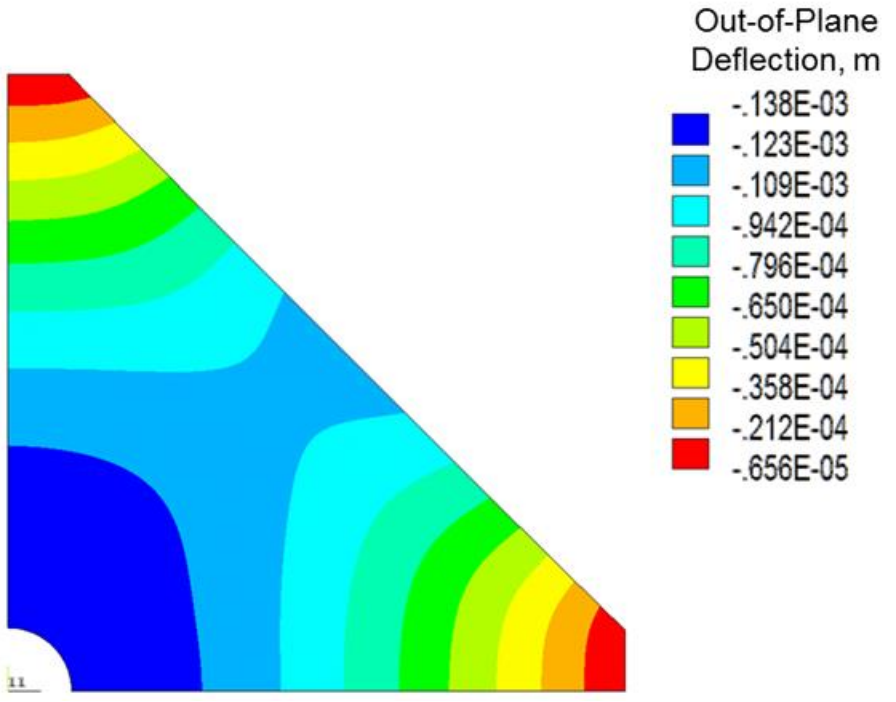

Figure B.53. Out-of-plane deflection contour for single panel loaded at the 25 kPa pressure level.

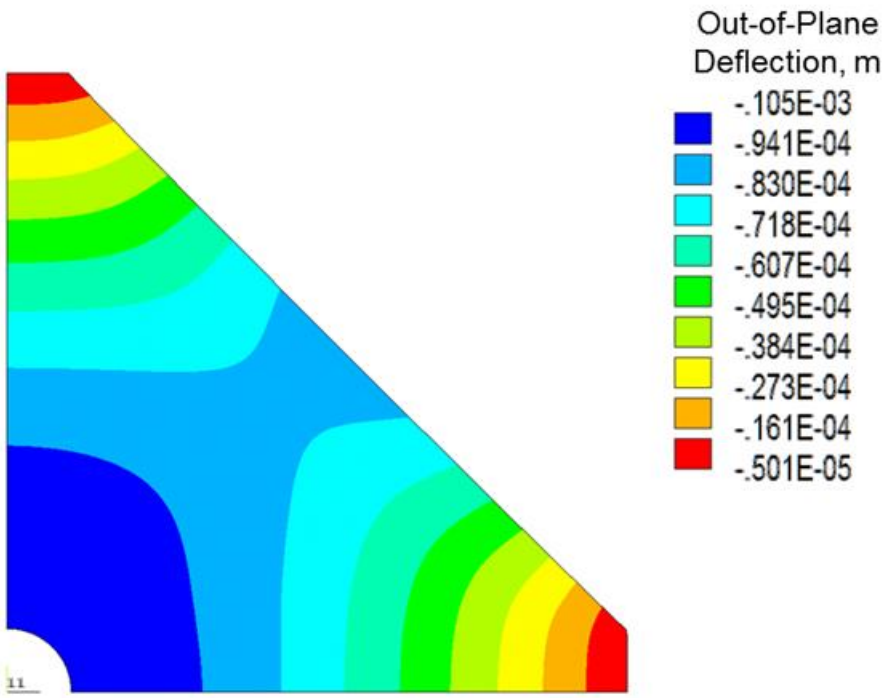

Figure B.54. Out-of-plane deflection contour for single panel loaded at the 30 kPa pressure level.

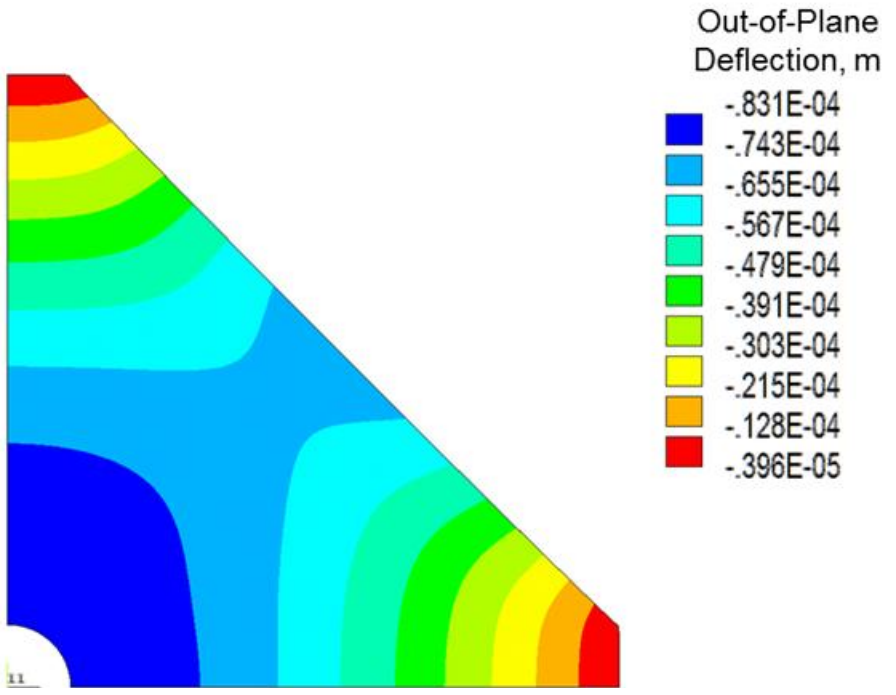

Figure B.55. Out-of-plane deflection contour for single panel loaded at the 35 kPa pressure level.

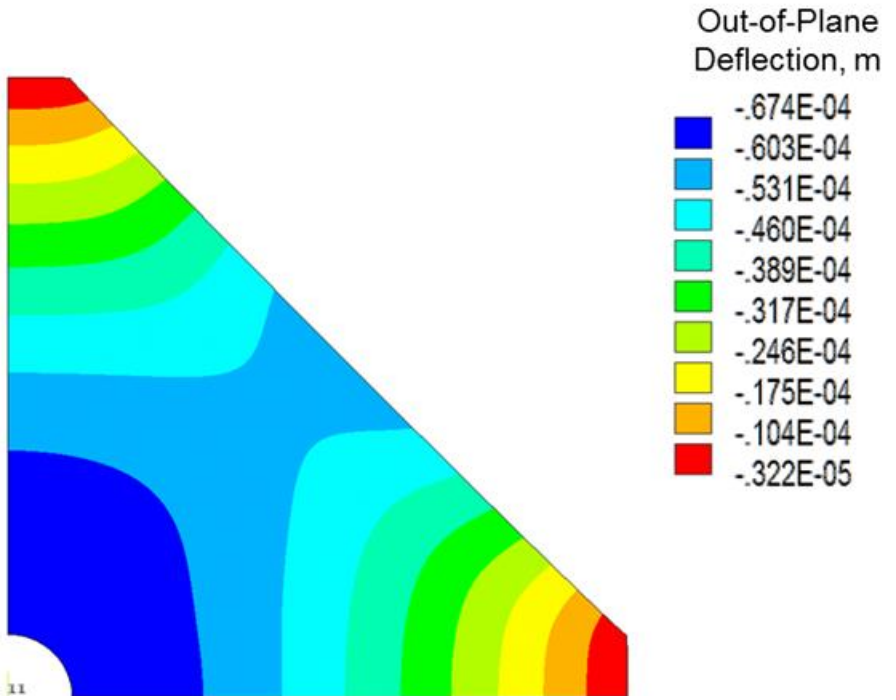

Figure B.56. Out-of-plane deflection contour for single panel loaded at the 40 kPa pressure level.

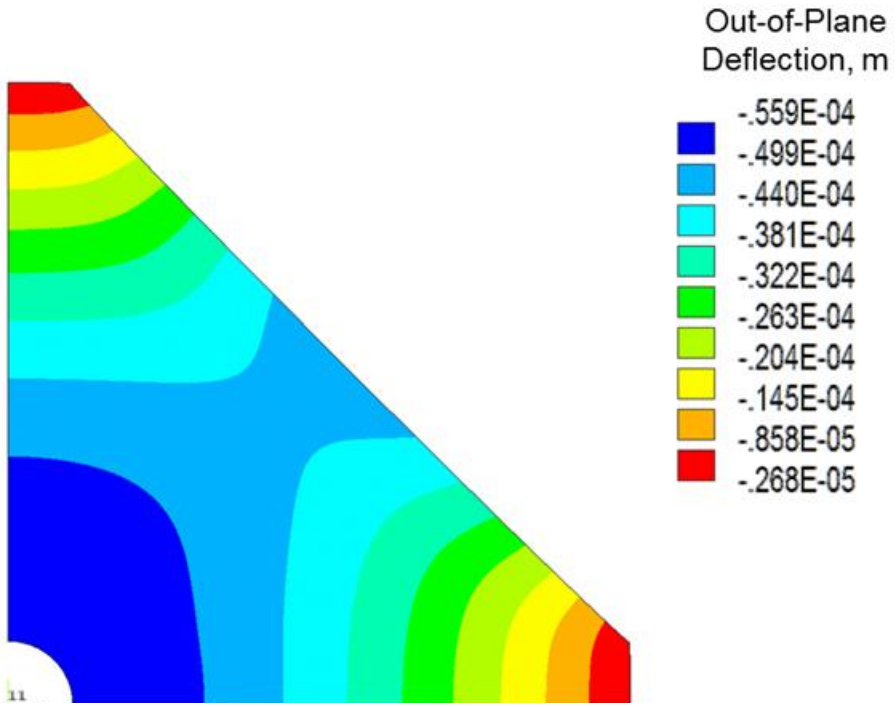

Figure B.57. Out-of-plane deflection contour for single panel loaded at the 45 kPa pressure level.

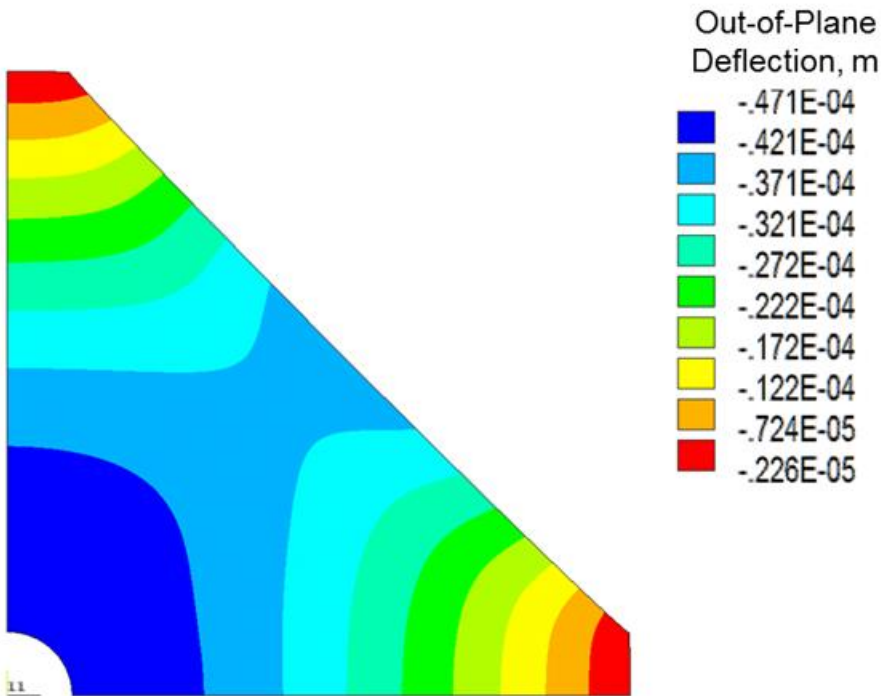

Figure B.58. Out-of-plane deflection contour for single panel loaded at the 50 kPa pressure level.

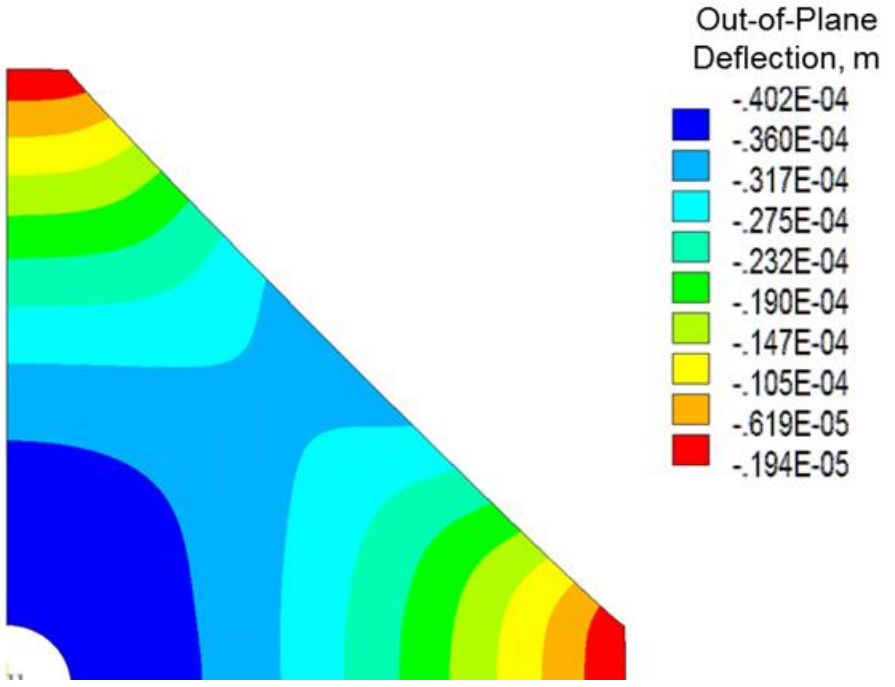

Figure B.59. Out-of-plane deflection contour for single panel loaded at the 55 kPa pressure level.

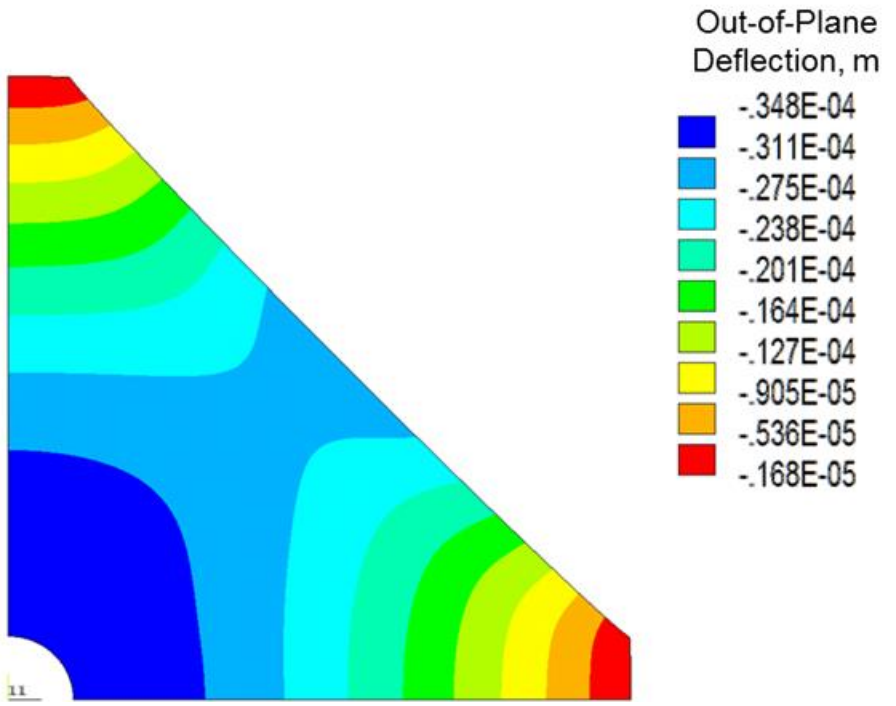

Figure B.60. Out-of-plane deflection contour for single panel loaded at the 60 kPa pressure level.

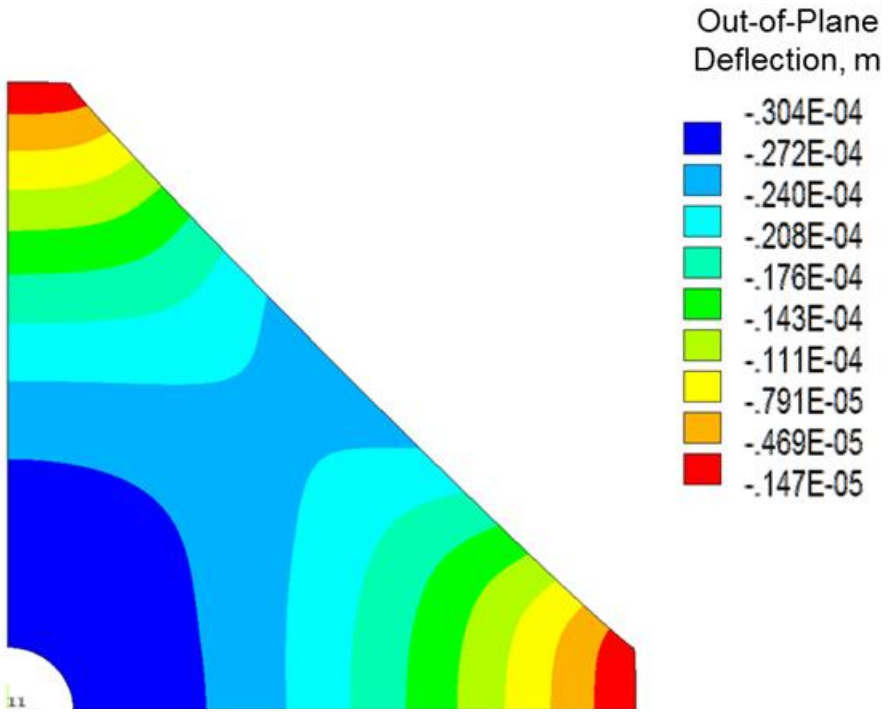

Figure B.61. Out-of-plane deflection contour for single panel loaded at the 65 kPa pressure level.

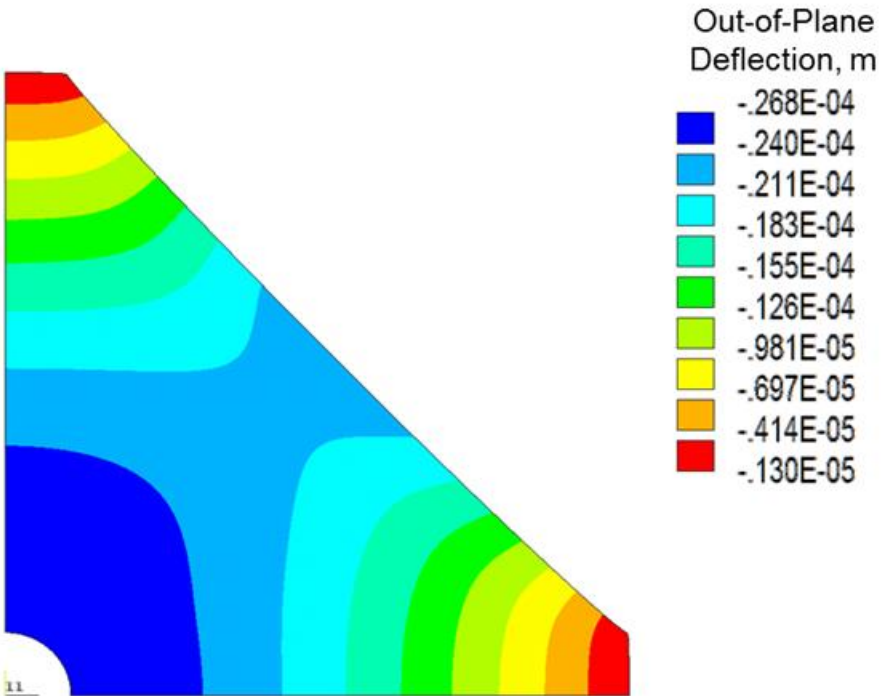

Figure B.62. Out-of-plane deflection contour for single panel loaded at the 70 kPa pressure level.

Pathfinder Inflatable System: Out-of-Plane Deflection Contours

The following contours are the out-of-plane deflection contours for a select panel from the octahedral set of tri-lateral corners. These contours were used for comparison with the single panel model. The first set of contours is the full model with an outer sphere modeled with a linear orthotropic material model. Contours for the full model with an outer sphere modeled with a linear isotropic material model are presented in the second set.

Deflection Contours with Linear Orthotropic Outer Sphere

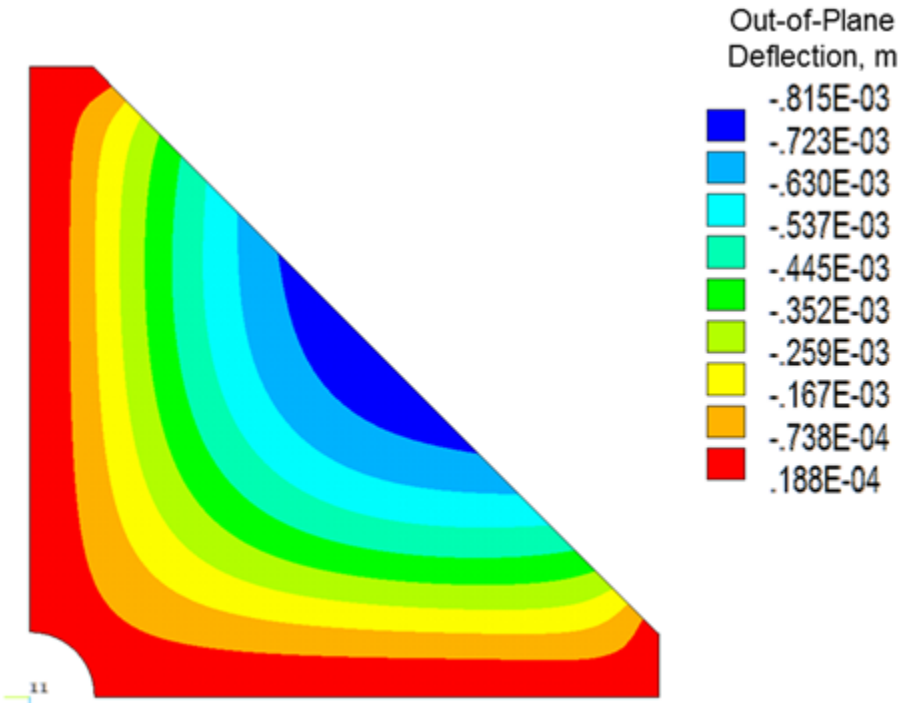

Figure B.63. Out-of-plane deflection contour for the select panel modeled with the linear orthotropic outer sphere inflated at 7 kPa.

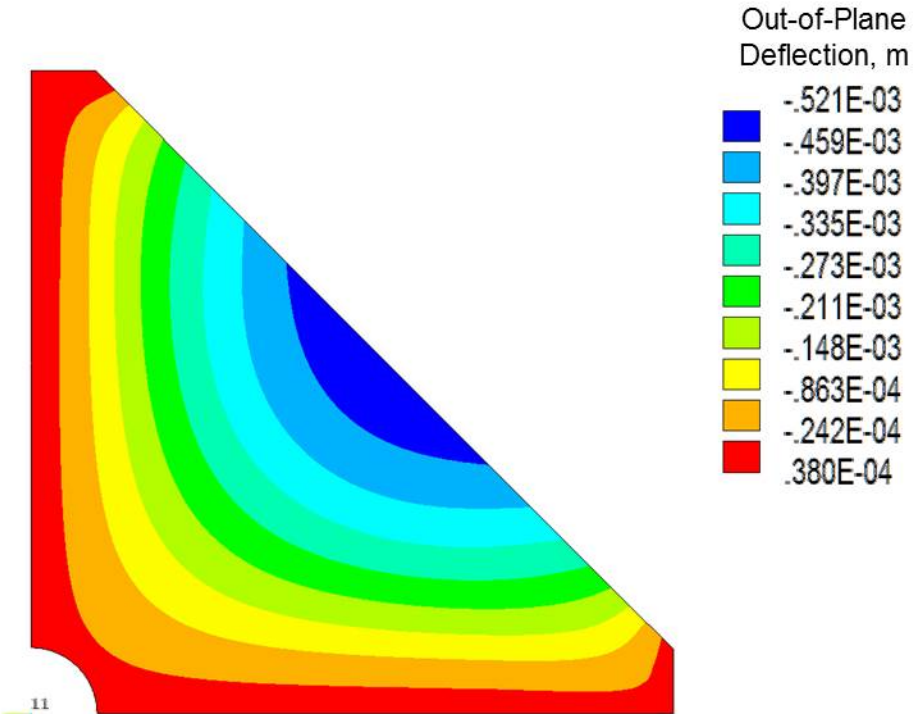

Figure B.64. Out-of-plane deflection contour for the select panel modeled with the linear orthotropic outer sphere inflated at 10 kPa.

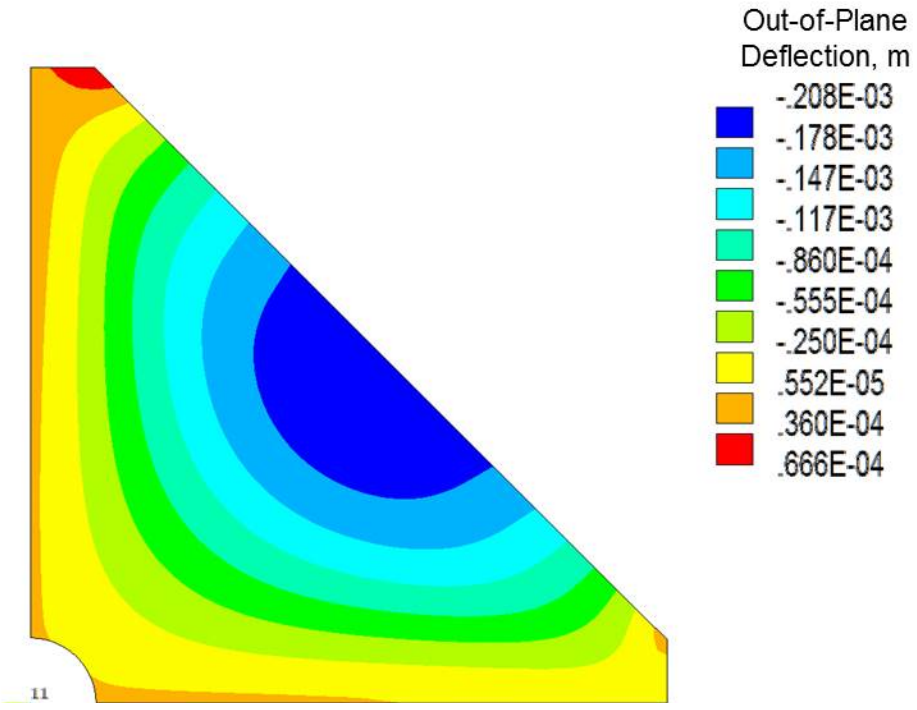

Figure B.65. Out-of-plane deflection contour for the select panel modeled with the linear orthotropic outer sphere inflated at 15 kPa.

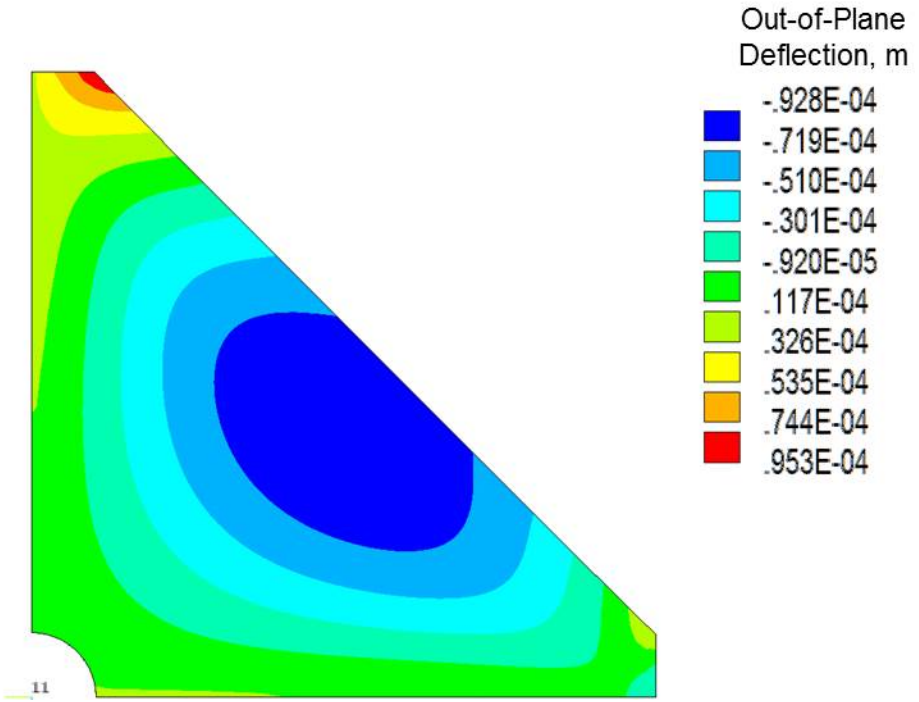

Figure B.66. Out-of-plane deflection contour for the select panel modeled with the linear orthotropic outer sphere inflated at 20 kPa.

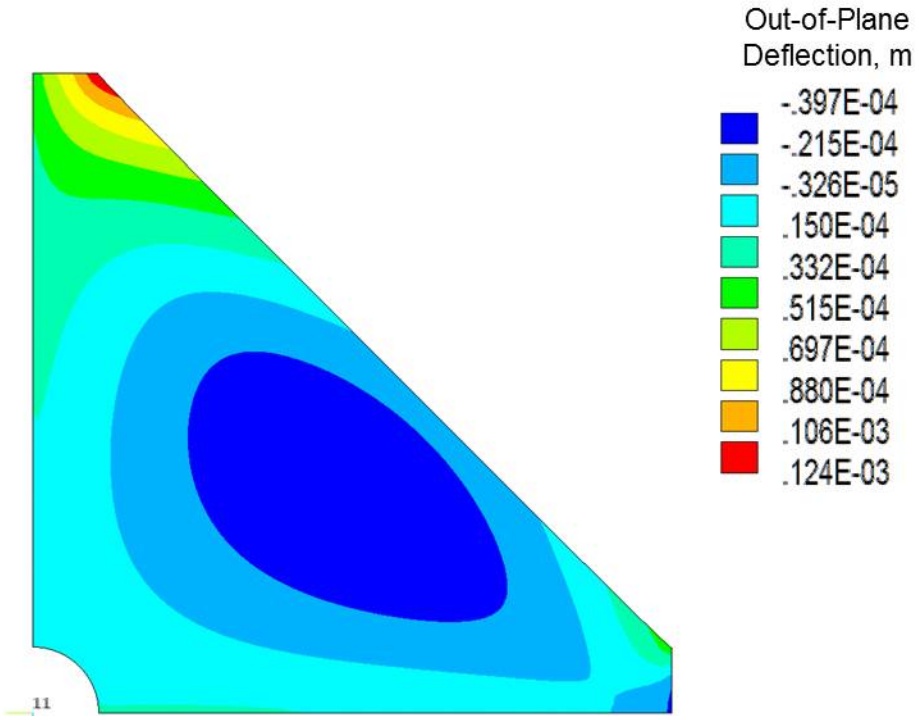

Figure B.67. Out-of-plane deflection contour for the select panel modeled with the linear orthotropic outer sphere inflated at 25 kPa.

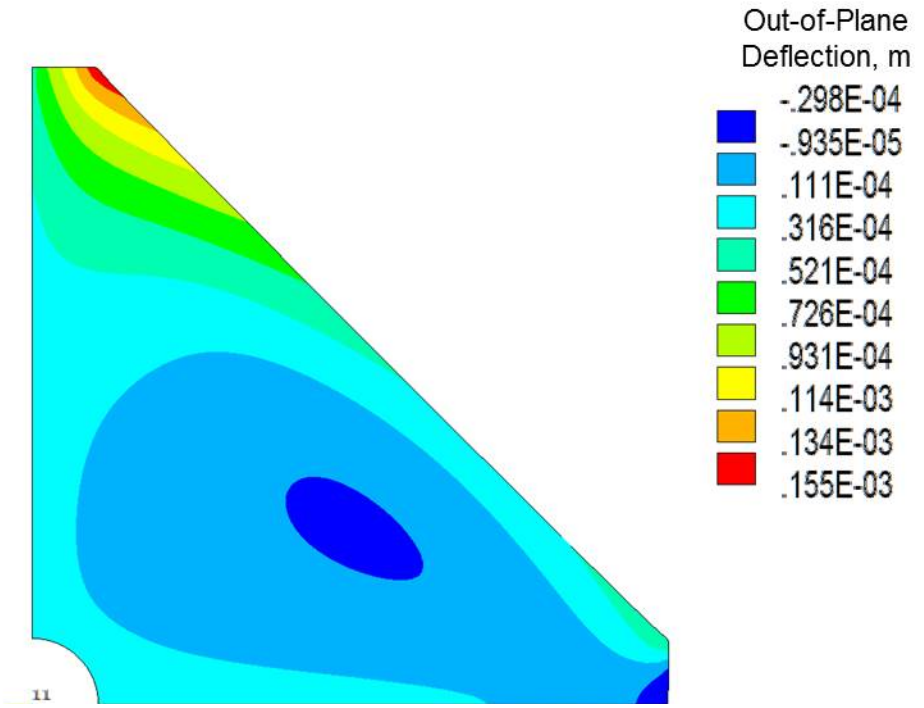

Figure B.68. Out-of-plane deflection contour for the select panel modeled with the linear orthotropic outer sphere inflated at 30 kPa.

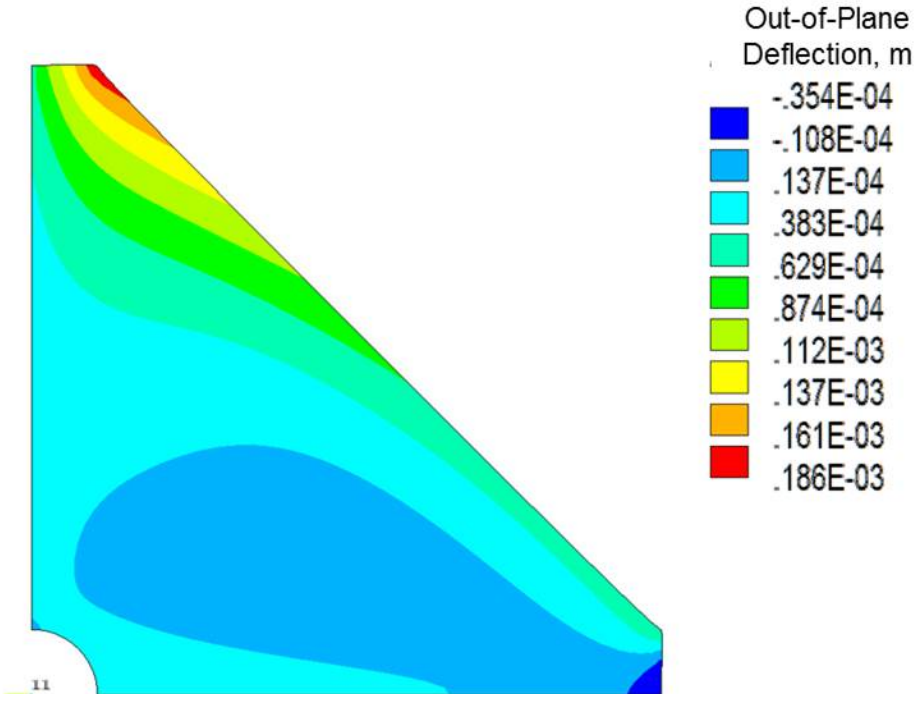

Figure B.69. Out-of-plane deflection contour for the select panel modeled with the linear orthotropic outer sphere inflated at 35 kPa.

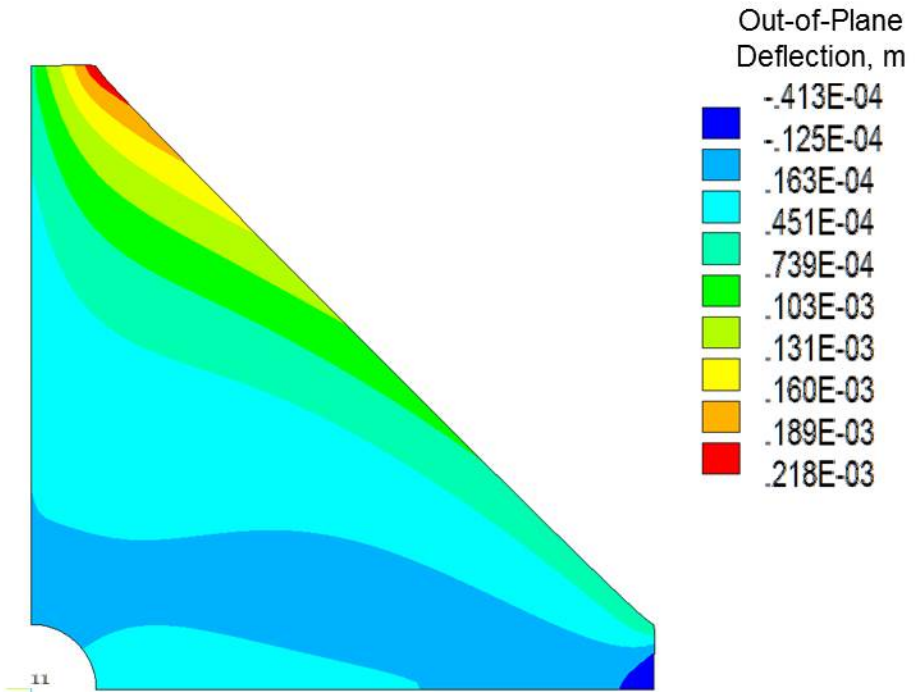

Figure B.70. Out-of-plane deflection contour for the select panel modeled with the linear orthotropic outer sphere inflated at 40 kPa.

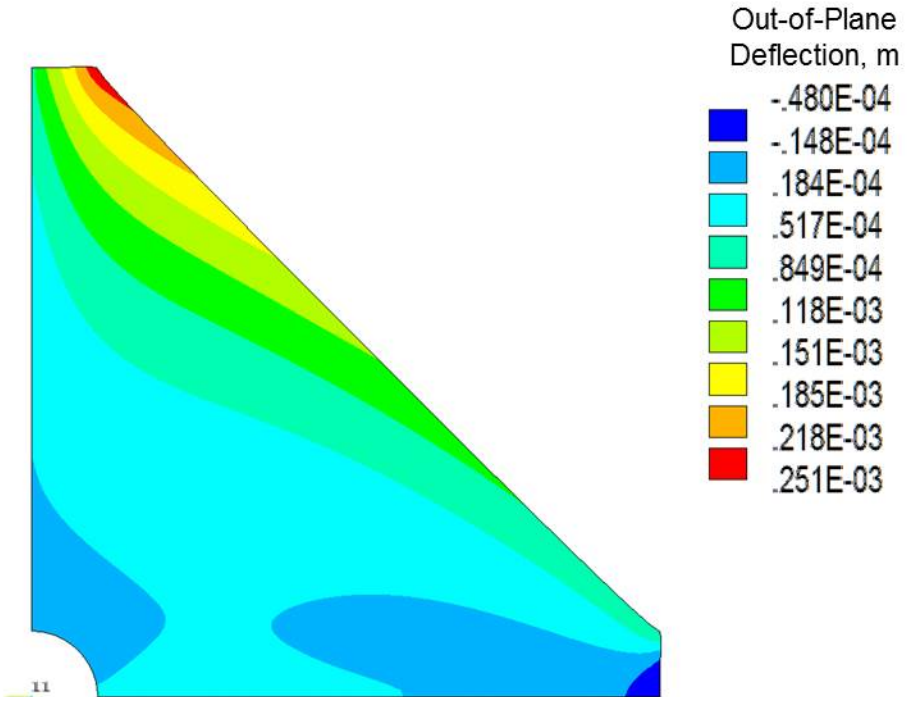

Figure B.71. Out-of-plane deflection contour for the select panel modeled with the linear orthotropic outer sphere inflated at 45 kPa.

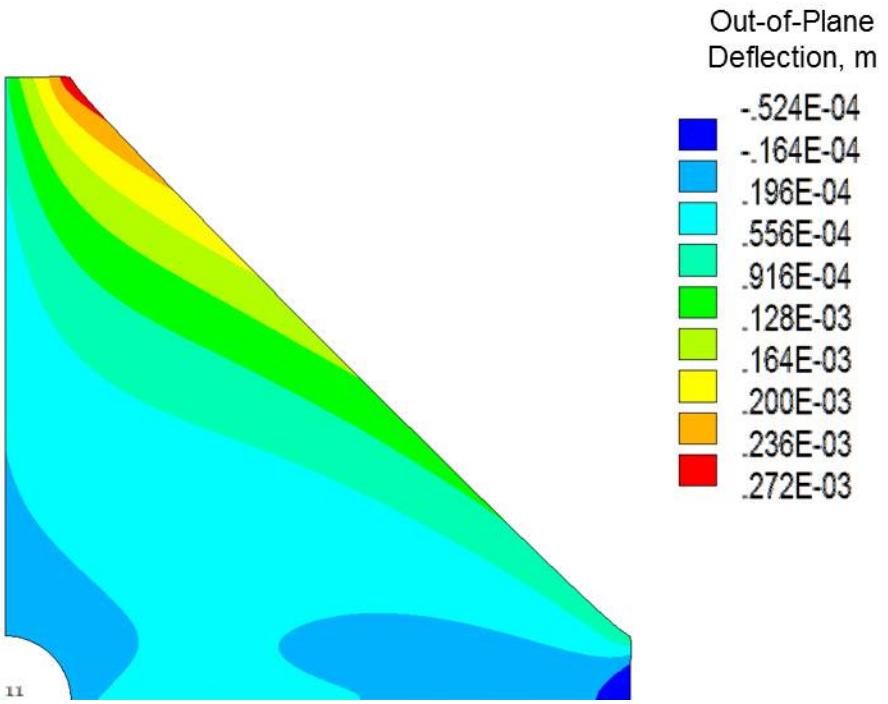

Figure B.72. Out-of-plane deflection contour for the select panel modeled with the linear orthotropic outer sphere inflated at 48 kPa.

Deflection Contours with Linear Isotropic Outer Sphere

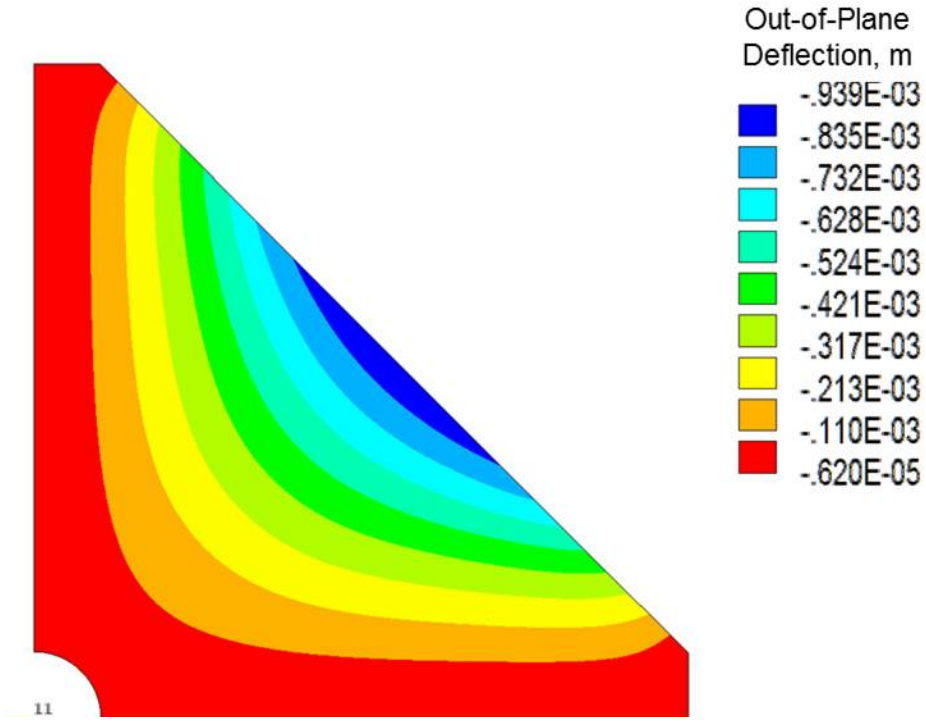

Figure B.73. Out-of-plane deflection contour for the select panel

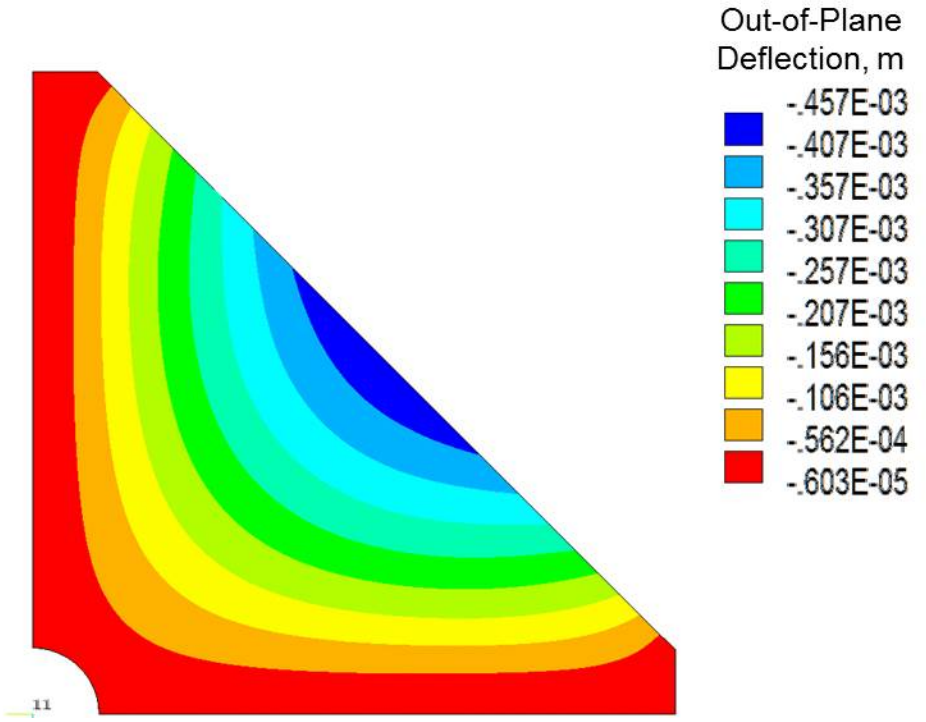

Figure B.74. Out-of-plane deflection contour for the select panel modeled with the linear isotropic outer sphere inflated at 10 kPa.

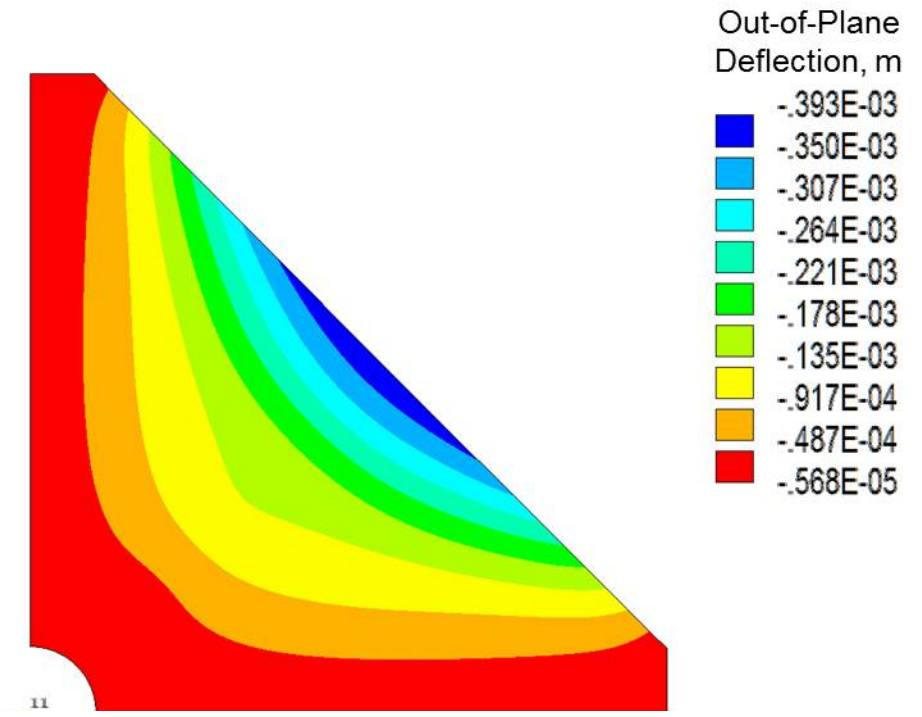

Figure B.75. Out-of-plane deflection contour for the select panel modeled with the linear isotropic outer sphere inflated at 15 kPa.

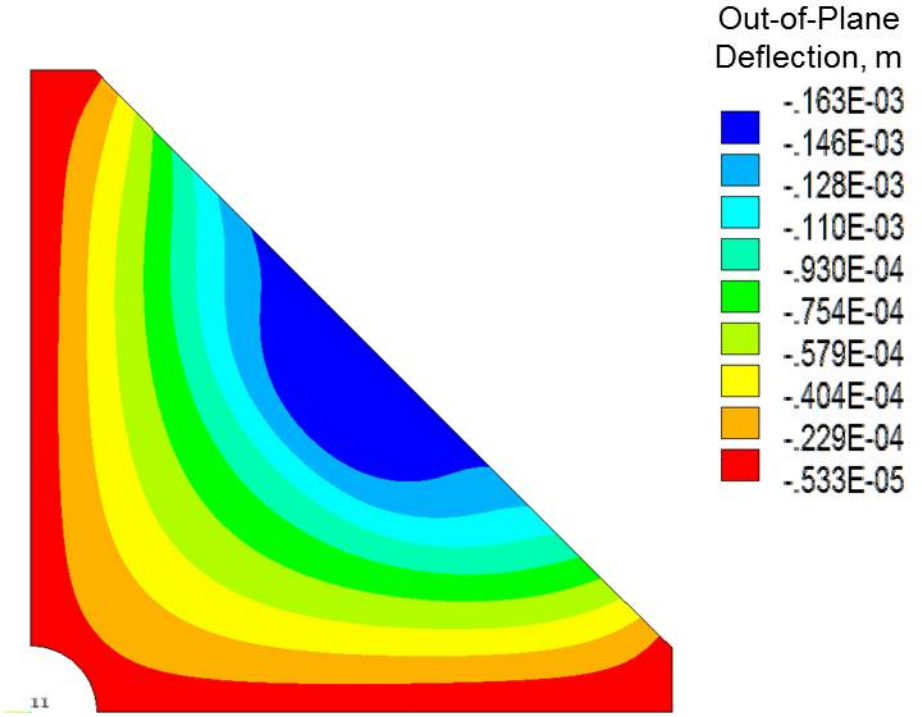

Figure B.76. Out-of-plane deflection contour for the select panel modeled with the linear isotropic outer sphere inflated at 20 kPa.

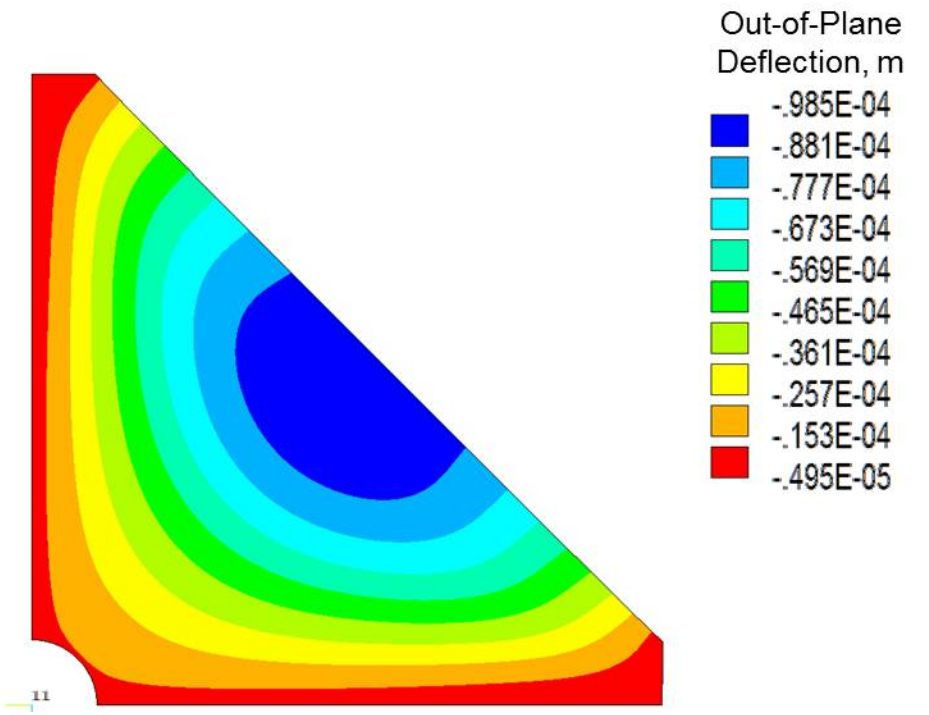

Figure B.77. Out-of-plane deflection contour for the select panel modeled with the linear isotropic outer sphere inflated at 25 kPa.

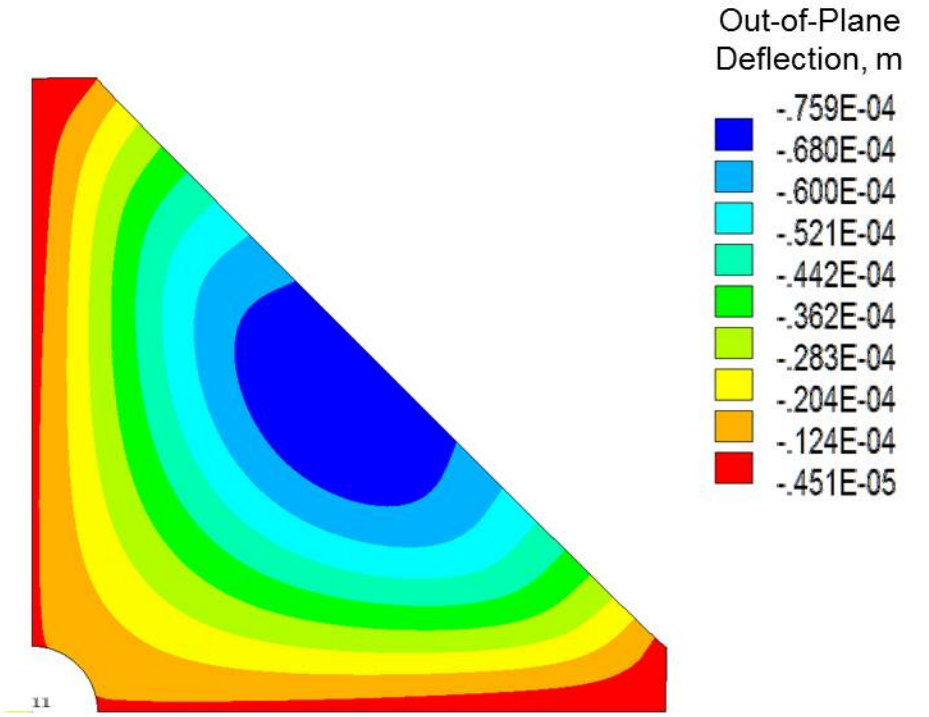

Figure B.78. Out-of-plane deflection contour for the select panel modeled with the linear isotropic outer sphere inflated at 30 kPa.

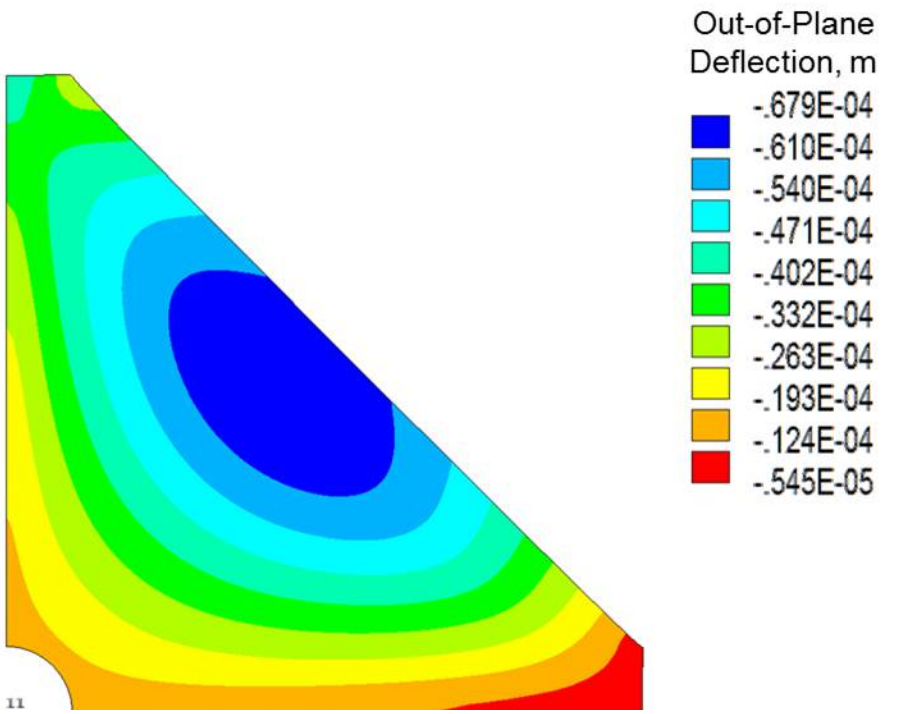

Figure B.79. Out-of-plane deflection contour for the select panel modeled with the linear isotropic outer sphere inflated at 35 kPa.

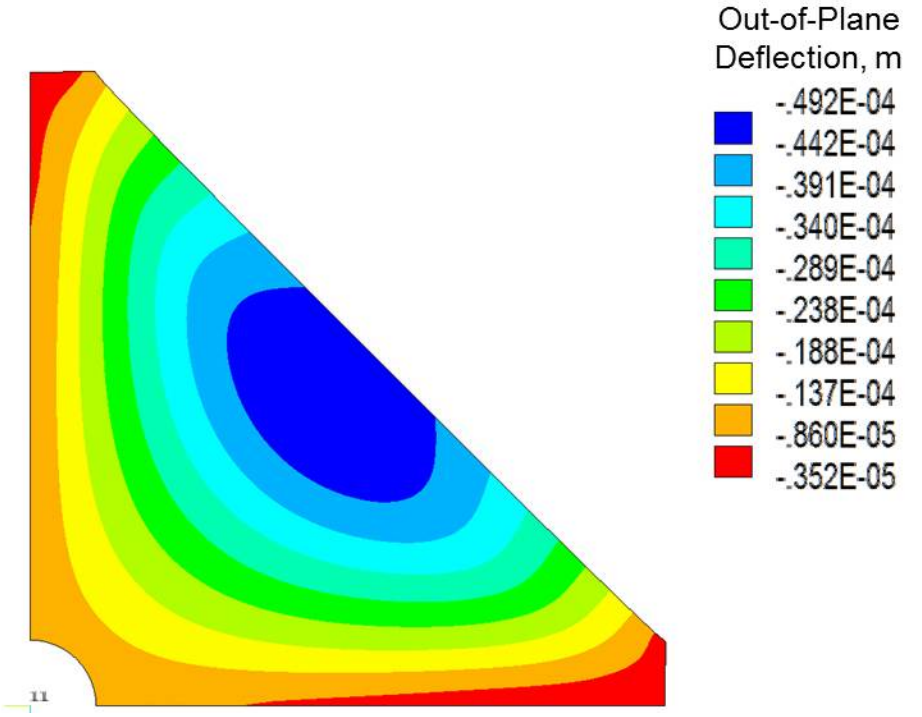

Figure B.80. Out-of-plane deflection contour for the select panel modeled with the linear isotropic outer sphere inflated at 40 kPa.

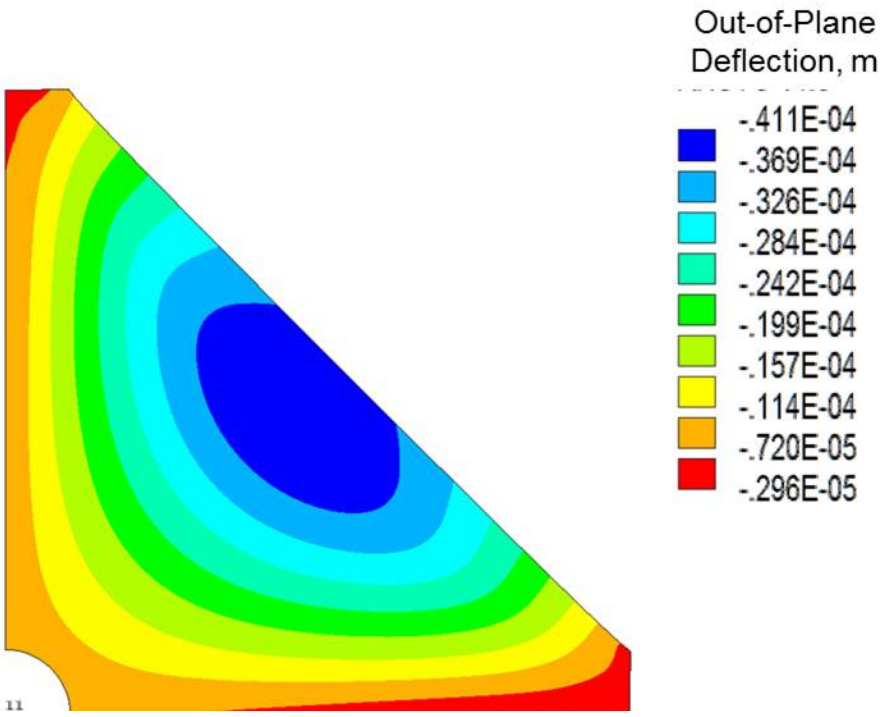

Figure B.81. Out-of-plane deflection contour for the select panel modeled with the linear isotropic outer sphere inflated at 45 kPa.

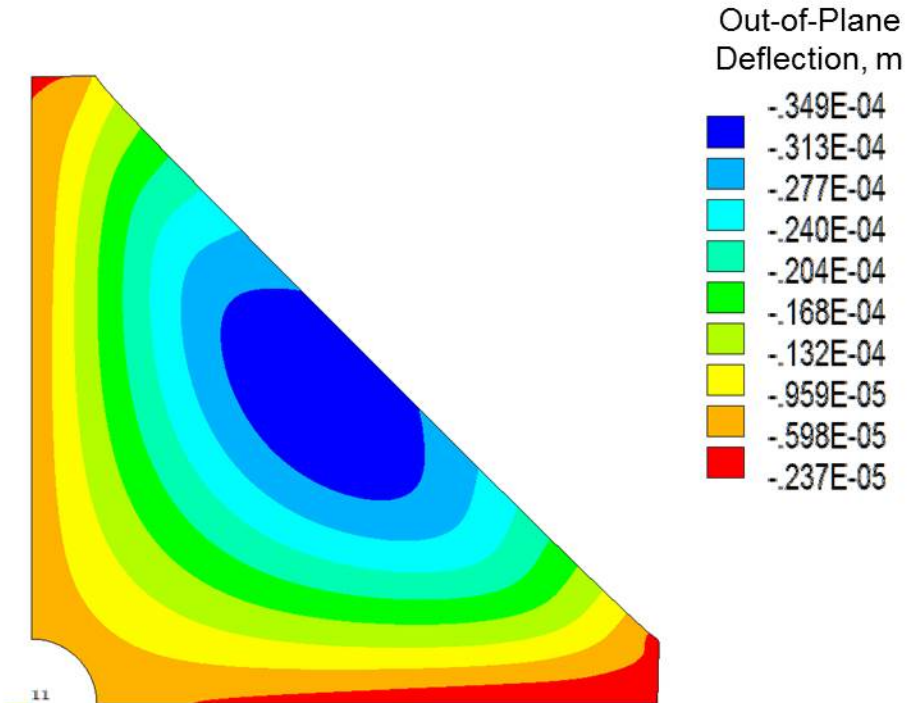

Figure B.82. Out-of-plane deflection contour for the select panel modeled with the linear isotropic outer sphere inflated at 50 kPa.

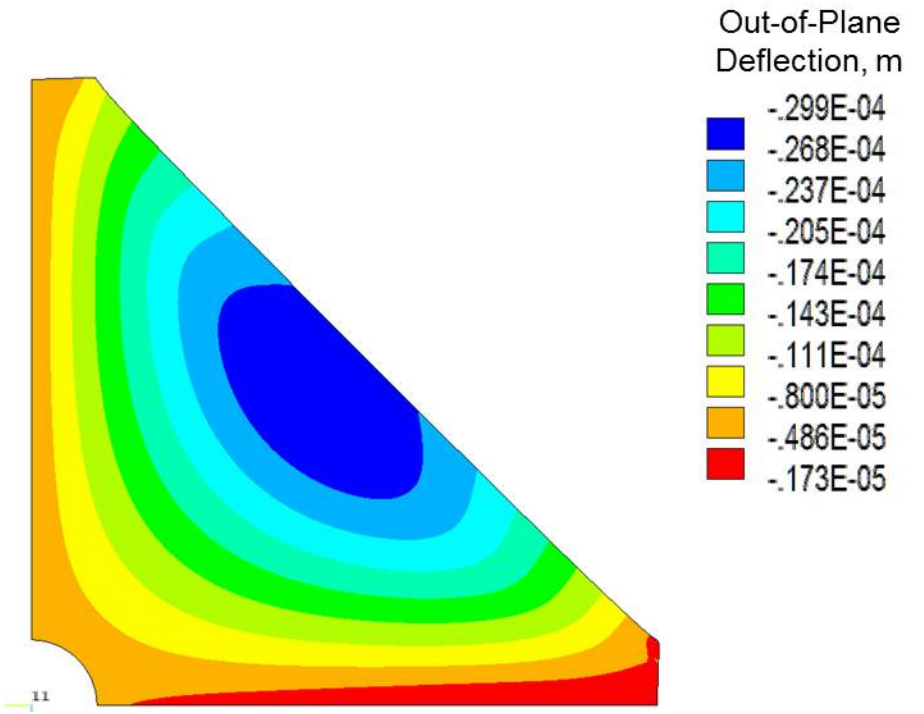

Figure B.83. Out-of-plane deflection contour for the select panel modeled with the linear isotropic outer sphere inflated at 55 kPa.

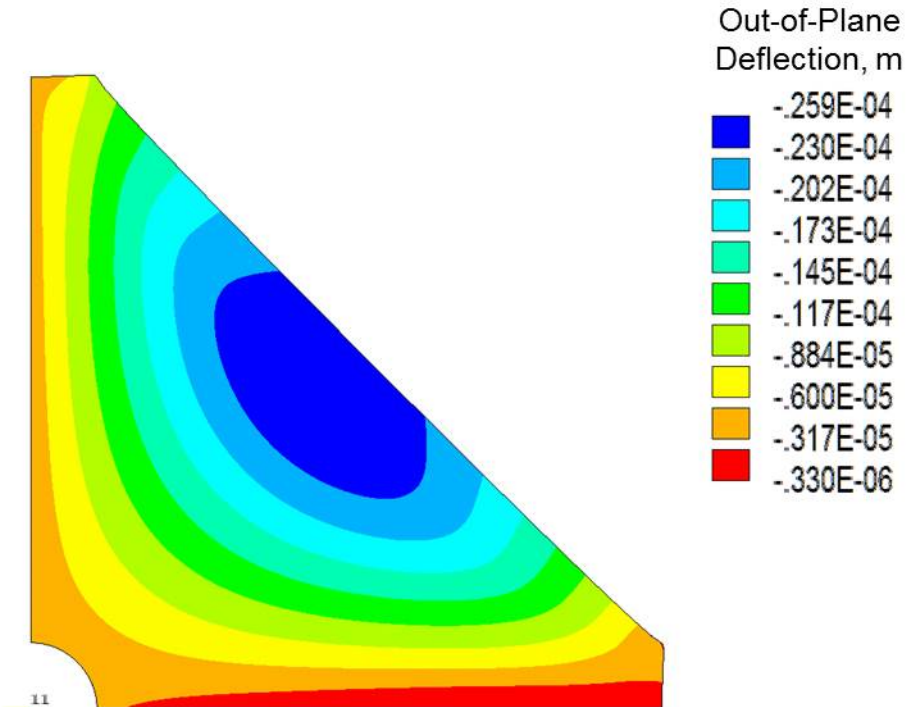

Figure B.84. Out-of-plane deflection contour for the select panel modeled with the linear isotropic outer sphere inflated at 60 kPa.

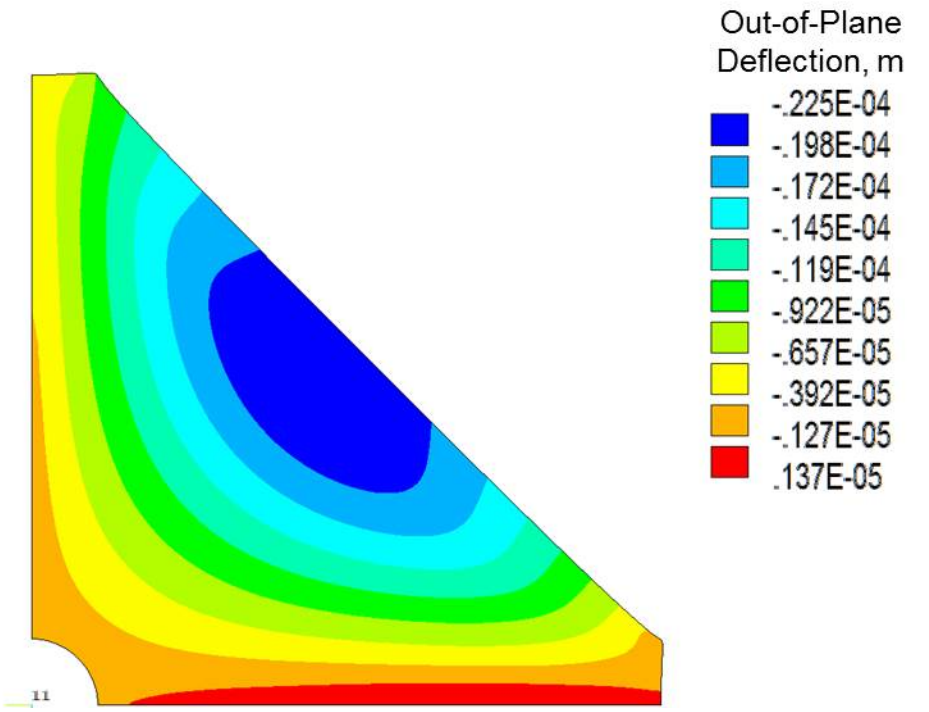

Figure B.85. Out-of-plane deflection contour for the select panel modeled with the linear isotropic outer sphere inflated at 65 kPa.

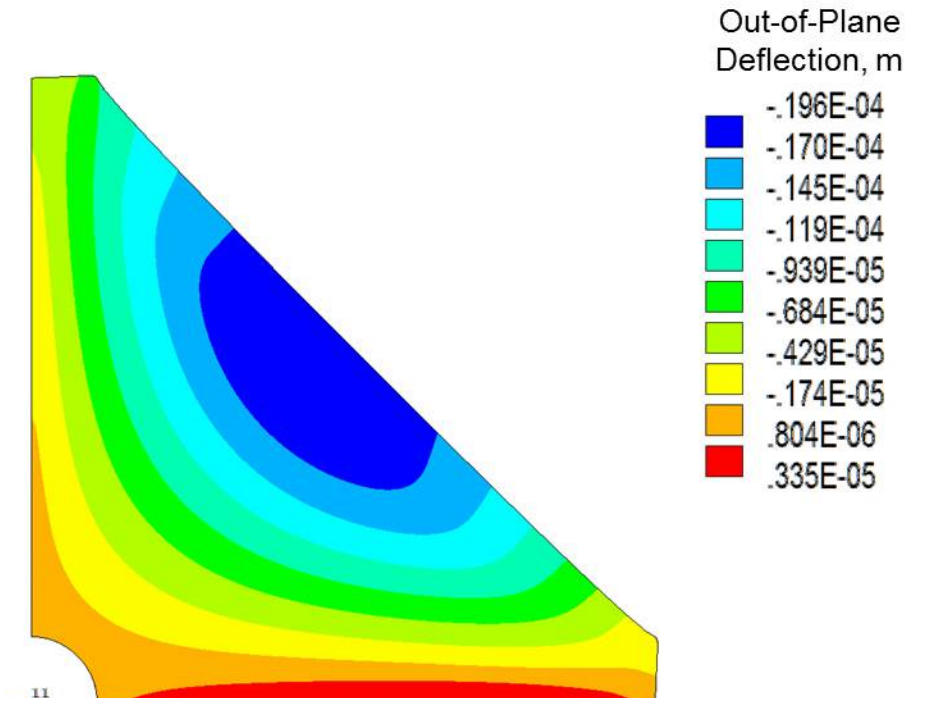

Figure B.86. Out-of-plane deflection contour for the select panel modeled with the linear isotropic outer sphere inflated at 70 kPa.

REFERENCES

[1] Cadogan, D., Grahne, M. and Mikulas, M., "Inflatable Space Structures: A New Paradigm for Space Structure Design", *49th International Astronautical Congress*, IAF.98.I.1.02, International Astronautical Federation, Melbourne, Australia, 1998.

[2] Darooka, D. K. and Jensen, D. W., "Advanced Space Structures Concepts and Their Development", *42nd AIAA/ASME/ASCE/AHS/ASC Structures, Structural Dynamics and Materials Conference and Exhibit*, AIAA-2001-1257, AIAA, Seattle, WA, 2001.

[3] Freeland, R. E., Bilyeu, G. D., Veal, G. R. and Mikulas, M. M., "Inflatable Deployable Space Structures Technology Summary", *49th International Astronautical Congress*, IAF-98-I.5.01, International Astronautical Federation, Melbourne, Australia, 1998.

[4] Harris, T., "Constrained Volume Packing Of Deployable Wings For Unmanned Aircraft", Master's Thesis, Mechanical Engineering, University of Kentucky, Lexington, KY, 2011.

[5] Jacob, J., Smith, S. W., Cadogan, D. and Scarborough, S., "Expanding the Small UAV Design Space with Inflatable Wings", *Society of Automotive Engineers AeroTech Congress and Exhibition*, 07ATC-217, SAE, Los Angeles, CA, 2007.

[6] Pai, P. F., *Highly Flexible Structures: Modeling, Computation, and Experimentation*, 1st ed., American Institute of Aeronautics and Astronautics, Inc., Reston, VA, 2007,

[7] Ambroziak, A. and Klosowshi, P., "Example of Tension Fabric Structure Analysis", *Task Quarterly*, Vol. 14, No. 1-2, 2010, pp. 5-14.

[8] Veldman, S. L., "Design and Analysis Methodologies for Inflated Beams", Ph.D. Dissertation, Aerospace Engineering, Delft University Press, Technische Universiteit Delft, Delft, The Netherlands, 2005.

[9] Freeland, R. E. and Veal, G. R., "Significance of the Inflatable Antenna Experiment Technology", *39th AIAA/ASME/ASCE/AHS/ASC Structures, Structural Dynamics, and Materials Conference, AIAA/ASME/AHS Adaptive Structures Forum*, AIAA-98-2104, AIAA, Long Beach, CA, 1998.

[10] Jenkins, C. H. and Marker, D. K., "Surface Precision of Inflatable Membrane Reflectors", *ASME Journal of Solar Energy Engineering*, Vol. 120, 1998, pp. 298-305.

[11] Scherrer, I., "Geometric Control of Inflatable Structures", Master's Thesis, Mechanical Engineering, University of Kentucky, Lexington, KY, 2012.

[12] Talley, C., Clayton, W., Gierow, P., Laue, G., McGee, J. and Moore, J., "Advanced Membrane Materials for Improved Solar Sail Capabilities", *43rd AIAA/ASME/ASCE/AHS/ASC Structures, Structural Dynamics, and Material Conference: 3rd AIAA Gossamer Spacecraft Forum*, AIAA 2002-1561, AIAA, Denver, CO, 2002.

[13] Luchsinger, R. H., Pedretti, M. and Reinhard, A., "Pressure Induced Stability: From Pneumatic Structures to Tensairity®", *Journal of Bionics Engineering*, Vol. 1, No. 3, 2004, pp. 141-148.

[14] Thomas, J. C. and Wielgosz, C., "Deflections of highly inflated fabric tubes", *Thin-Walled Structures*, Vol. 42, 2004, pp. 1049-1066.

[15] Cavallaro, P. V., Johnson, M. E. and Sadegh, A. M., "Mechanics of plain-woven fabrics for inflated structures", *Composite Structures*, Vol. 61, 2003, pp. 375-393.
[16] Kabche, J. P., Peterson, M. L. and Davids, W. G., "Effect of inflation pressure on the constitutive response of coated woven fabrics used in airbeams", *Composites: Part B*, Vol. 42, 2011, pp. 526-537.
[17] Zahm, A. F., "Relation of Rib Spacing to Stress in Wing Planes", National Advisory Committee for Aeronautics, Technical Notes, 5, Washington D.C., 1920.
[18] Ward, K. E., "Characteristics of an Airfoil as Affected by Fabric Sag", National Advisory Committee for Aeronautics, Technical Notes, 428, Washington D.C., 1932.
[19] Prőll, A., "Testing Airplane Fabrics", National Advisory Committee for Aeronautics, Technical Notes, 186, Washington, D.C., 1924.
[20] Simpson, A. D., "Design and Performance of UAVs With Inflatable Wings", Ph.D. Dissertation, Mechanical Engineering, University of Kentucky, Lexington, KY, 2008.
[21] Simpson, A., Coulombe, N., Jacob, J. D. and Smith, S. W., "Morphing of Inflatable Wings", *AIAA SDM Adaptive Structures Conference*, AIAA 2005-2110, AIAA, Austin, TX, 2005.
[22] Rowe, J. M., Smith, S. W., Simpson, A., Jacob, J. and Scarborough, S., "Development of a Finite Element Model of Warping Inflatable Wings", *47th AIAA/ASME/ASCE/AHS/ASC Structures, Structural Dynamics and Materials Conference, 7th Gossamer Spacecraft Forum*, AIAA-2006-1697, AIAA, Newport, RI, 2006.
[23] Rowe, J. M., "Finite Element Modeling of an Inflatable Wing", Master's Thesis, Mechanical Engineering, University of Kentucky, Lexington, KY, 2007.
[24] Cadogan, D., Smith, T., Lee, R., Scarborough, S. and Graziosi, D., "Inflatable and Rigidizable Wing Components for Unmanned Aerial Vehicles", *44th AIAA/ASME/ASCE/AHS/ASC*, AIAA-2003-6630, AIAA, Norfolk, VA, 2003.
[25] Simpson, A. D., Usui, M., Smith, S. W. and Jacob, J. D., "Development and Flight Testing of a UAV with Inflatable-Rigidizable Wings", *42nd AIAA Aerospace Sciences Meeting and Exhibit*, AIAA-2004-1373, AIAA, Reno, NV, 2004.
[26] Allred, R., Hoyt, A., Harrah, L., McElroy, P., Scarborough, S. and Cadogan, D., "Light Curing Rigidizable Inflatable Wing", *45th AIAA/ASME/ASCE/AHS/ASC Structures, Structural Dynamics and Materials Conference*, AIAA 2004-1809, AIAA, Palm Springs, CA, 2004.
[27] Smith, S. C., Hahn, A. S., Johnson, W. R., Kinney, D. J., Pollitt, J. A. and Reuther, J. J., "The Design of the Canyon Flyer, an Airplane for Mars Exploration", *38th AIAA Aerospace Sciences Meeting and Exhibit*, AIAA-2000-0514, AIAA, Reno, NV, 2000.
[28] Kerns, J., Usui, M., Smith, S., Scarborough, S., Smith, T. and Cadogan, D., "Development of UV-Curable Inflatable Wings for Low Density Flight Applications", *5th AIAA Gossamer Spacecraft Forum*, Palm Springs, CA, 2004.

[29] Smith, S. W., Jacob, J. D., Jone, R., Scarborough, S. and Cadogan, D., "A High-Alitude Test of Inflatable Wings for Low-Density Flight Applications", *7th AIAA SDM Gossamer Spacecraft Forum*, AIAA-2006-1696, AIAA, Newport, RI, 2006.

[30] Lin, J. K. H., Knoll, C. F. and Willey, C. E., "Shape Memory Rigidizable Inflatable (RI) Structures for Large Space Systems Applications", *47th AIAA/ASME/ASCE/AHS/ASC Structures, Structural Dynamics, and Materials Conference*, AIAA 2006-1986, AIAA, Newport, RI, 2006.

[31] Pappa, R. S., Black, J. T., Blandino, J. R., Jones, T. W., Danehy, P. M. and Dorrington, A. A., "Dot-Projection Photogrammetry and Videogrammetry of Gossamer Space Structures", *Journal of Spacecraft and Rockets*, Vol. 40, No. 6, 2003, pp. 858-867.

[32] Salama, M., Lou, M. and Fang, H., "Deployment of Inflatable Space Structures: A Review of Recent Developments", *AIAA Structures, Structural Dynamics and Materials Conference*, AIAA-2000-1730, AIAA, Atlanta, GA, 2000.

[33] Mathers, N., "Inflatable Antennas for Portable Direct Satellite Communication", Bachelor of Engineering, Electrical and Computer Engineering, RMIT Univeristy Melbourne, Australia, 2010.

[34] Zhao, J., Tian, Q. and Hu, H. Y., "Deployment dynamics of a simplified spinning IKAROS solar sail via absolute coordinate based method", *Acta Mechanica Sinica*, Vol. 29, 1, 2013, pp. 132-142.

[35] Lichodziejewski, D., Derbes, B., Reinert, R., Belvin, K., Slade, K. and Mann, T., "Development and Ground Testing of a Compactly Stowed Scalable Inflatably Deployed Solar Sail", *45th AIAA/ASME/ASCE/AHS/ASC Structures, Structural Dynamics & Material Conference*, AIAA-2004-1507, AIAA, Palm Springs, CA, 2004.

[36] Black, J. T., Leifer, J., DeMoss, J. A. and Walker, E. N., "Experimental and Numerical Correlation of Gravity Sag in Solar-Sail-Quality Membranes", *Journal of Spacecraft and Rockets*, Vol. 44, No. 3, 2007, pp. 522-527.

[37] Leifer, J., "Simplified Computational Models for Shear-Compliant Borders in Solar Sails", *Journal of Spacecraft and Rockets*, Vol. 44, No. 3, 2007, pp. 571-581.

[38] Leifer, J. and Belvin, W. K., "Prediction of Wrinkle Amplitudes in Thin Film Membranes Using Finite Element Modeling", *44th AIAA/ASME/ASCE/AHS Structures, Structural Dynamics, and Materials Conference* AIAA-2003-1983, AIAA, Norfolk, VA, 2003.

[39] Leifer, J., Black, J. T., Belvin, W. K. and Behun, V., "Evaluation of Shear Compliant Borders for Wrinkle Reduction in Thin Film Membrane Structures", *44th AIAA/ASME/ASCE/AHS Structures, Structural Dynamics, and Materials Conference*, AIAA 2003-1984, AIAA, Norfolk, VA, 2003.

[40] Leifer, J., Jones, D. C. and Cook, A. M., "Gravity-Induced Wrinkling in Subscale, Singly Curved Parabolic Gossamer Membrane", *Journal of Spacecraft and Rockets*, Vol. 47, No. 1, 2010, pp. 214-219.

[41] Welch, J. V., Wang, S., Blandino, J. R. and McEvoy, K., "Super Pressure Balloon Non-linear Structural Analysis and Correlation Using Photogrammetric Measurements", *AIAA 5th Aviation, Technology, Integration, and Operations*

Conference(ATIO) 16th Lighter-Than-Air Systems Technology Conference and Balloon Systems Conference, AIAA 2005-7447, AIAA, Arlington, VA, 2005.

[42] Thota, P., Leifer, J., Smith, S. W. and Lumpp, J. K., "Initial Pattern Evaluation for Inplane Displacement Measurement of Thin Films", *Experimental Mechanics*, Vol. 45, No. 1, 2005, pp.

[43] Pappa, R. S., Black, J. T. and Blandino, J. R., "Photogrammetric Measurement of Gossamer Spacecraft Membrane Wrinkling", *SEM Annual Conference and Exposition on Experimental and Applied Mechanics*, 20030065917, SEM, Charlotte, NC, 2003.

[44] Foch, R. J., "Omni-Directional Inflatable Radar Reflector", Naval Research Lab, Washington D.C., 2010.

[45] Palisoc, A., Veal, G., Cassapakis, C., Greschik, G. and Mikulas, M., "Geometry attained by pressurized membranes", *Space Telescopes and Instruments V*, SPIE 3356, SPIE, Kona, HI, 1998.

[46] Im, E., Thomson, M., Fang, H., Pearson, J. C., Moore, J. and Lin, J. K., "Prospects of Large Deployable Reflector Antennas for a New Generation of Geostationary Doppler Weather Radar Satellites", *AIAA SPACE 2007 Conference and Exposition*, AIAA 2007-9917, AIAA, Long Beach, CA, 2007.

[47] Moncrieff, E., "Systems for Lightweight Structure Design: the State-of-the-Art and Current Developments", *Textile Composites and Inflatable Structures*, Vol. 2005, pp. 17-28.

[48] Ishikawa, T. and Cho, T. W., "Nonlinear Behavior of Woven Fabric Composites", *Journal of Composite Materials*, Vol. 17, 1983, pp. 399-413.

[49] Gautier, K. B., Gasser, A., Launay, J. and Boisse, P., "Meso-Macro Mechanical Behaviour of Dry Fiber Fabrics", *12th International Conference on Composites Materials*, Paris, France, 1999.

[50] Pan, N., "Analysis of Woven Fabric Strengths: Prediction of Fabric Strength Under Uniaxial and Biaxial Extensions", *Composites Science and Technology*, Vol. 56, 1996, pp. 311-327.

[51] Behre, B., "Mechanical Properties of Textile Fabrics Part I: Shearing", *Textile Research Journal*, Vol. 31, No. 2, 1961, pp. 87-93.

[52] Grosberg, P. and Park, B. J., "The Mechanical Properties of Woven Fabrics: Part V: The Initial Modulus and the Frictional Restraint in shearing of Plain Weave Fabrics", *Textile Research Journal*, Vol. 36, No. 5, 1966, pp. 420-431.

[53] Skelton, J., "Fundamentals of Fabric Shear", *Textile Research Journal*, Vol. 46, No. 12, 1976, pp. 862-869.

[54] Mohammed, U., Lekakou, C., Dong, L. and Bader, M. G., "Shear deformation and micromechanics of woven fabrics", *Composites Part A: Applied Science and Manufacturing*, Vol. 31, 2000, pp. 299-308.

[55] Nguyen, M., Herszber, I. and Paton, R., "The shear properties of woven carbon fabric", *Composite Structures* Vol. 47, 1999, pp. 767-779.

[56] Liu, L., Chen, J., Li, X. and Sherwood, J., "Two-dimensional macro-mechanics shear models of woven fabrics", *Composites Part A: Applied Science and Manufacturing*, Vol. 36, 2005, pp. 105-114.

[57] Cao, J., Cheng, H. S., Yu, T. X., Zhu, B., Tao, X. M., Lomov, S. V., Stoilova, T., Verpoest, I., Boisse, P., Launay, J., Hivet, G., Liu, L., Chen, J., de Graaf, E. F.

and Akkerman, R., "A Cooperative Benchmark Effort on Testing of Woven Composites", *ESAFORM Conference*, 2004, pp. 305.

[58] Wu, J. and Pan, N., "Grab and Strip Tensile Strengths for Woven Fabrics: An Experimental Verification", *Textile Research Journal*, Vol. 75, No. 11, 2005, pp. 789-796.

[59] Corbin, C., "The Design of Cruciform Test Specimens for Planar Biaxial Testing of Fabrics for Inflatable Aerodynamic Decelerators", *ASCE Earth and Space 2012 Conference*, NF1676L-13347, NASA, Pasadena, CA, 2012.

[60] Zhu, B., "Picture Frame Test - A report on benchmark test", Hong Kong University of Science and Technology, Clear Water Bay, Kowloon, Hong Kong,

[61] Harrison, P., Clifford, M. J. and Long, A. C., "Shear characterisation of viscous woven textile composites: a comparison between picture frame and bias extension experiments", *Composites Science and Technology*, Vol. 64, 2004, pp. 1453-1465.

[62] Peil, K. L., Barbero, E. J. and Sosa, E. M., "Experimental Evaluation of Shear Strength of Woven Webbings", *SAMPE 2012 Conference and Exhibition*, Baltimore, MD, 2012, pp.

[63] Galliot, C. and Luchsinger, R. H., "The shear ramp: A new test method for the investigation of coated fabric shear behaviour - Part I: Theory", *Composites Part A: Applied Sciences and Manufacturing*, Vol. 41, No. 12, 2010, pp. 1743-1749.

[64] Galliot, C. and Luchsinger, R. H., "The shear ramp: A new test method for investigation of coated fabric shear behaviour - Part II: Experimental", *Composites Part A: Applied Science and Manufacturing*, Vol. 41, No. 12, 2010, pp. 1750-1759.

[65] Skelton, J. and Freeston, W. D., "Mechanics of Elastic Performance of Textile Materials: Part XIX: The Shear Behavior of Fabrics Under Biaxial Loads 1", *Textile Research Journal*, Vol. 41, 1971, pp. 871-880.

[66] Santee, K., "Finite Element Modeling of Army Airbeam Structures", U.S. Army RDECOM - Natick Soldier Center Collective, Protection Directorate, Fabric Structures Team, Port Hueneme, CA, 2005.

[67] Boisse, P., Borr, M., Buet, K. and Cherouat, A., "Finite element simulations of textile composite forming including the biaxial fabric behaviour", *Composites Part B*, Vol. 28B, 1997, pp. 453-464.

[68] Tan, P., Tong, L. and Steven, G. P., "Modelling for predicting the mechanical properties of textile composites - A review", *Composites Part A*, Vol. 28A, 1997, pp. 903-922.

[69] Tan, P., Tong, L. and Steven, G. P., "A three-dimensional modelling technique for predicting the linear elastic property of opened-packing woven fabric unit cells", *Composite Structures*, Vol. 38, No. 1-4, 1997, pp. 261-271.

[70] Lin, H., Clifford, M. J., Long, A. C. and Sherburn, M., "Finite element modelling of fabric shear", *Modeling and Simulation in Materials Science and Engineering*, Vol. 17, 2009, pp. 1-16.

[71] Kato, S., Yoshino, T. and Minami, H., "Formulation of Constitutive Equations for Fabric Membranes Based on the Concept of Fabric Lattice Model", *Engineering Structures*, Vol. 21, No. 8, 1999, pp. 691-708.

[72] Kyriacou, S. K., Schwab, C. and Humphrey, J. D., "Finite element analysis of nonlinear orthotropic hyperelastic membranes", *Computational Mechanics*, Vol. 18, 1996, pp. 269-278.
[73] Manach, P. Y. and Rio, G., "Analysis of orthotropic behavior in convected coordinate frames", *Computational Mechanics*, Vol. 23, 1999, pp. 510-518.
[74] Tessler, A., Sleight, D. W. and Wang, J. T., "Nonlinear Shell Modeling of Thin Membranes with Emphasis on Structural Wrinkling", *44th AIAA/ASME/ASCE/AHS/ASC Structures, Structural Dynamics, and Material Conference and Exhibit*, AIAA 2003-1931, AIAA, Norfolk, VA, 2003.
[75] Jones, R. M., *Mechanics of Composite Materials*, 2nd Edition ed., Taylor & Francis Group, New York, NY, 1999, 55-120.
[76] Allemang, R. J., "The Modal Assurance Criterioin - Twenty Years of Use and Abuse", *Sound and Vibration*, Vol. 2003, pp. 14-21.

VITA

JARED T. FULCHER

Education

MS, Mechanical Engineering, University of Kentucky, Lexington, KY (May 2011)
BS, Summa cum Laude, Mechanical Engineering, University of Kentucky, Paducah, KY (May 2009)
AS, High Distinction, West Kentucky Community and Technical College, Paducah, KY (May 2007)

Professional Experience

Graduate Teaching Assistant – 01/2011-Present

- University of Kentucky – College of Engineering, Lexington, KY

Dynamic Systems and Controls Research Lab Manager – 08/2012-Present

- University of Kentucky – College of Engineering Lexington, KY

Graduate Research Assistant

- Air Force Research Laboratory (AFRL) – Materials and Manufacturing Decorate, WPAFB, Dayton, OH
- NASA KY Space Grant Fellow - University of Kentucky – College of Engineering, Lexington, KY

Lab Technician – 02/2006-05/2009

- UK College of Engineering Extended Campus Program, Paducah, KY

Design Engineer Intern – 05/2008-08/2008

- United States Enrichment Corporation, Inc., Paducah, KY

Plant Engineer Intern – 05/2007-07/2007

- Arkema, Inc., Calvert City, KY

Honors

- Outstanding Graduate Student in Mechanical Engineering – University of Kentucky, Lexington, KY (2014)
- American Institute of Aeronautics and Astronautics – University of Kentucky, Lexington, KY
    - Member – 2012-2014

- American Society of Mechanical Engineers – University of Kentucky-Paducah, Paducah, KY
    - President – 2007-2009
    - Treasurer – 2006/2007
    - Design Competition Participant – 2007-2009

- Society of Automotive Engineers – University of Kentucky-Paducah, Paducah, KY
    - Reporter – 2008/2009
    - Baja SAE Crew Member – 2007-2009

- Pi Tau Sigma, National Mechanical Engineering Honor Society, Inducted Fall 2007

- Tau Beta Pi, National Engineering Honor Society, Inducted Fall 2007

- 3rd Place Undergraduate Research Division – American Society for Engineering Education, ASEE SE Annual Meeting, Southern Polytechnic State University, Marietta, GA (2009)

- Donn E. Hancher Senior Leadership Award – UK College of Engineering, Lexington, KY (Inaugural Recipient 2009)

- Outstanding Mechanical Engineering Student – UK College of Engineering Extended Campus, Paducah, KY (2009)

- Paducah Rotary Senior Scholar – UK College of Engineering Extended Campus, Paducah, KY (2009)

- J.M. Harper Memorial Engineering Scholarship – UK College of Engineering Extended Campus, Paducah, KY (Fall 2008/Spring 2009)

- White, E. Field Memorial Scholarship – UK College of Engineering, Lexington, KY (2008/2009)

- Dean's List – University of Kentucky, Lexington, KY (Fall 2007/Spring 2009)
- Hites Family Scholarship – West Kentucky Community and Technical College, Paducah, KY (Fall 2007/Spring 2009)

- Marvin Family Scholarship – UK College of Engineering Extended Campus, Paducah, KY (Fall 2007/Spring 2009)
- Trustees Scholarship – University of Kentucky, Lexington, KY (Fall 2007/Spring 2009)

- Paducah Kiwanis Sophomore Scholar- UK College of Engineering Extended Campus, Paducah, KY (2007)

- Dean's List – West Kentucky Community and Technical College, Paducah, KY (Fall 2005/Spring 2007)

Publications/Presentations

Fulcher, J. T., Smith, S. W., Baker, J. R., “Effect of Boundary Conditions on Geometric Control for an Inflatable Pathfinder System”, Presented at 2014 AIAA SciTech Conference AIAA Spacecraft Structures Conference, National Harbor, MD, 01/14.

Fulcher, J. T., Scherrer, I. J., Smith, S. W., Baker, J. R., "Using Nonlinear FE Modeling to Understand the Effect of Boundary Conditions on Precise Surfaces of Inflatable Structures", Presented at 54th AIAA/ASME/ASCE/AHS/ASC Structures, Structural Dynamics, and Materials Conference 14th AIAA Gossamer Systems Forum, Boston, MA, 04/13.

Fulcher, J.T., Karaca, H.E., Tandon, G.P., Lu, Y.C., “Thermomechanical and shape memory properties of thermosetting shape memory polymer under compressive loadings”, *Journal of Applied Polymer Science,* Published Online, DOI: 10.1002/app.38791, 11/2012.

Fulcher, J.T., Scherrer, I., Smith, S. W., Baker, J., “Development of Modeling Approach for Design of Precision Inflatable Structures”, Presented at the 37th Dayton-Cincinnati Aerospace Sciences Symposium, Dayton, OH, 03/12.

Lu, Y.C., Fulcher, J.T., Tandon, G.P., Foster, D.C., “Microscale thermomechanical characterization of environmentally conditioned shape memory polymers”, *Polymer Testing*, Volume 30, 563-570, 8/2011.

Fulcher, J.T., Karaca, H.E., Tandon, G.P., Foster, D.C., Lu, Y.C., “Multiscale Thermomechanical Characterization of Environmentally Conditioned Shape Memory Polymers”, Proceedings of 2011 SEM Annual Conference and Exposition on Experimental and Applied Mechanics, Mohegan Sun, Uncasville, Connecticut, 06/11.

Fulcher, J.T., 2011, “Mechanical characterizations of environmentally conditioned shape memory polymers for reconfigurable aerospace structures”, Master’s thesis, University of Kentucky.

Fulcher, J.T., Lu, Y.C., Tandon, G.P., Foster, D.C., "Thermomechanical characterization of shape memory polymers using high temperature nanoindentation", *Polymer Testing*, Volume 29, Issue 5, 08/10.

Fulcher, J.T., Lu, Y.C., Tandon, G.P., Foster, D.C., "Mechanical Characterization of Environmentally Conditioned Shape Memory Polymers by High Temperature Indentation", Presented at 2010 SEM Annual Conference & Exposition on Experimental and Applied Mechanics, Indianapolis, IN, 06/10.

Fulcher, J.T., Lu, Y.C., Tandon, G.P., Foster, D.C., "Shape Memory Effects of Environmentally Conditioned Shape Memory Polymers Studied by Nanoindentation", Presented at SAMPE 2010, Seattle, WA, 05/10.

Fulcher, J.T., Lu, Y.C., Tandon, G.P., Foster, D.C., "Thermomechanical Characterization of Environmentally Conditioned Shape Memory Polymer Using Nanoindentation", Presented at Proceedings of the SPIE Smart Structures / NDE Conference, San Diego, CA, 03/10.

Beadles, W. J., Fulcher, J. T., "Modal Analysis of an Engine Valve Cover: Experimental Testing and Finite Element Modeling", Technical Poster presented at ASEE SE Annual Meeting, Marietta, GA, 04/09.